Promoted ZnO Sorbents for Wide Temperature Range H_2S/COS Removal for Applications in Fuel Cells

by

Priyanka P. Dhage

A dissertation submitted to the Graduate Faculty of
Auburn University
in partial fulfillment of the
requirements for the Degree of
Doctor of Philosophy

Auburn, Alabama
August 6, 2011

Keywords: desulfurization, hydrogen sulfide, carbonyl sulfide, doped sorbents, Hydrolysis

Approved by

Bruce J. Tatarchuk, Chair, Professor of Chemical Engineering
Yoon Y. Lee, Professor of Chemical Engineering
William Ashurst, Professor of Chemical Engineering
Aleksandr Simonian, Professor of Materials Engineering

Abstract

High efficiency desulfurization is critical to maintain the activity of fuel processing catalysts and high-value membrane electrode assemblies in logistic fuel cell systems. On-board fuel processing of liquid hydrocarbon fuel is being investigated to supply hydrogen for fuel cell-based auxiliary power units. For such a system, if sulfur is not removed from the liquid phase, the removal of sulfur as H_2S from the reformate becomes a key-step since downstream catalysts and the fuel cell itself can be poisoned by a small amount of H_2S in the feed. Hydrogen sulfide is present in many high temperature gas streams during extraction and processing of fossil fuels, natural gas and geothermal brines. Steam reforming catalysts, PEM anode catalysts and also the shift catalysts are intolerant to sulfur and to ensure adequate lifetime of fuel processors the desulfurization step is very important.

This dissertation presents results of R&D efforts to develop novel sorbents for efficient gas phase desulfurization. Promoted ZnO sorbents with formulation $M_{0.05}Zn_{0.95}O$ (M = Mn, Fe, Co, Ni, Cu) were supported on silica and effect of support, various operating parameters and microfibrous entrapment was studied. The results of desulfurization tests on these sorbents at room temperature indicate that a copper doped ZnO (15% w/w)/MCM-41 sorbent ($Cu_{0.05}Zn_{0.95}O$/MCM-41) has the highest saturation sulfur capacity at 0.9 mol S/mol ($Cu_{0.05}Zn_{0.95}O$), which is approximately twice that of ZnO/SiO_2 sorbent at similar loadings. the utilization of the reactant ($M_{0.05}Zn_{0.95}O$) toward H_2S removal depended on the support employed

in the order MCM-41 > MCM-48 > silica gel. This dependence was investigated in terms of the support: surface area, pore volume, and pore size; using N_2 adsorption-desorption isotherms (Chapter III).

The Cu-ZnO/SiO_2 sorbent for ultradeep adsorptive removal of H_2S from the reformate streams at room temperature was prepared, tested, and characterization of the active sites was performed. The Cu dopant significantly enhances desulfurization capacity of ZnO/SiO_2 sorbent at room temperature (up to 92 % utilization of ZnO), and maintains a high sulfur uptake capacity upon multiple cycles (up to 10) of regeneration by a simple thermal oxidation in air. XRD suggests that both zinc and copper compounds of the CuO-ZnO/SiO_2 sorbent are nano-dispersed. The ESR spectroscopy found that the "calcined" and "sulfided" CuO-ZnO/SiO_2 sorbents contain Cu^{2+} in the single dispersion and coordination state and during H_2S adsorption, partial reduction of Cu^{2+} to Cu^{1+} occurs (Chapter IV)

The Fe- and Mn-promoted H_2S sorbents Fe_x-Mn_y-$Zn_{1-x-y}O/SiO_2$ (x, y=0, 0.025) for the ultradeep desulfurization of model reformates at room temperature were prepared, tested and characterized. The role of Mn and Fe promoter cations in the 'calcined' and 'sulfided' forms of the $Fe_xMn_yZnO_{(1-x-y)}/SiO_2$ sorbent has been studied by the in-situ ESR, temperature dependent XPS. Operando ESR is used for the first time to study dynamics of reduction of Mn^{3+}promoter sites simultaneously with measuring sulfidation dynamics of the Fe_x–Mn_y–$Zn_{1-x-y}O/SiO_2$ sorbent. Fe cations are believed to occupy the surface of supported ZnO nanocrystallites, while Mn cations are distributed within ZnO (Chapter V)

Removal of both H_2S and COS from reformate streams is critical for maintaining the activity of fuel processing catalysts. At temperatures < 250 C, COS formation is effectively inhibited, but at temperatures above 250 C, significant amount of COS is formed in presence of

CO_2/CO and H_2S. A layered bed approach was used with layer of Al_2O_3/Carbon for COS hydrolysis over the followed by a layer high efficiency H_2S removal over bimetallic-promoted supported ZnO sorbent (Chapter VI). The objective of our work is developing the sorbents for an efficient, cost-effective and scalable removal of H_2S and COS over the broad temperature range, without significant activity loss upon multiple regeneration cycles, and understanding the mechanism of sulfur sorption by the metal oxide-promoted ZnO-based sorbents.

Acknowledgements

I would like to acknowledge the guidance and encouragement of my advisor Dr. Bruce Tatarchuk. I would like to express my sincere gratitude to Dr. Yoon Lee, Dr. Robert Ashurst and Dr. Aleksandr Simonian and Dr. Evert Duin for serving on my committee. This dissertation would not have been possible without the unwavering support of Dr. Hongyun Yang from Intramicron Inc. Also without the cooperation and support of my colleagues at the Center for Microfibrous Materials Manufacturing, especially Dwight Cahela, Dr. Don Cahela, Dr. Alexander Samokhvalov, Megan Schumacher, Kimberly Dennis, Benjamin Doty, Matt and Wendall from Glass Shop Sachin Nair, Hussain, Amogh Karwa, Abhijeet Phalle, Robert Henderdon, Min Sheng, Achintya Sujant and many other, this work would not have been possible. I am also grateful to Sue Abner and Karen Cochran for their administrative support throughout my tenure at Auburn.

Most importantly, I would like to thank my family and especially my parents, sister- Supriya & brother - Pratik for their support and trust in my abilities. My sincere thanks goes to my friends especially Jola Jayselene and Saurabh Wadwalkar who made my stay at Auburn, one of the most memorable of all times.

Table of Contents

List of Tables

List of Figures

Nomenclature

C_o - Initial H_2S concentration, ppmv

C_{Ao} - Initial challenge H_2S molar concentration, mol/cc

C_b - breakthrough concentration mol/cc

K - Lumped shape factor of breakthrough curve, s^{-1}

U -Face velocity, cm/s

X - ZnO utilization of the accessible ZnO, dimensionless

t -time, s

$t_{1/2}$ -time to reach 50% Cao, s

τ -saturation time s

φ - Void fraction, dimensionless

Chapter I: Introduction and Literature Survey

I.1 Introduction

With the very growing demands for fuels, and depleting natural resources it is the need of the day to find alternative fuel or equipments for futuristic technologies. Fuel cells are emerging technology with applications in transportation, stationary and portable power generation. Hydrogen is the real fuel for fuel cells, which can be obtained by fuel reformulation on-site for stationary applications or on-board for automotive applications.

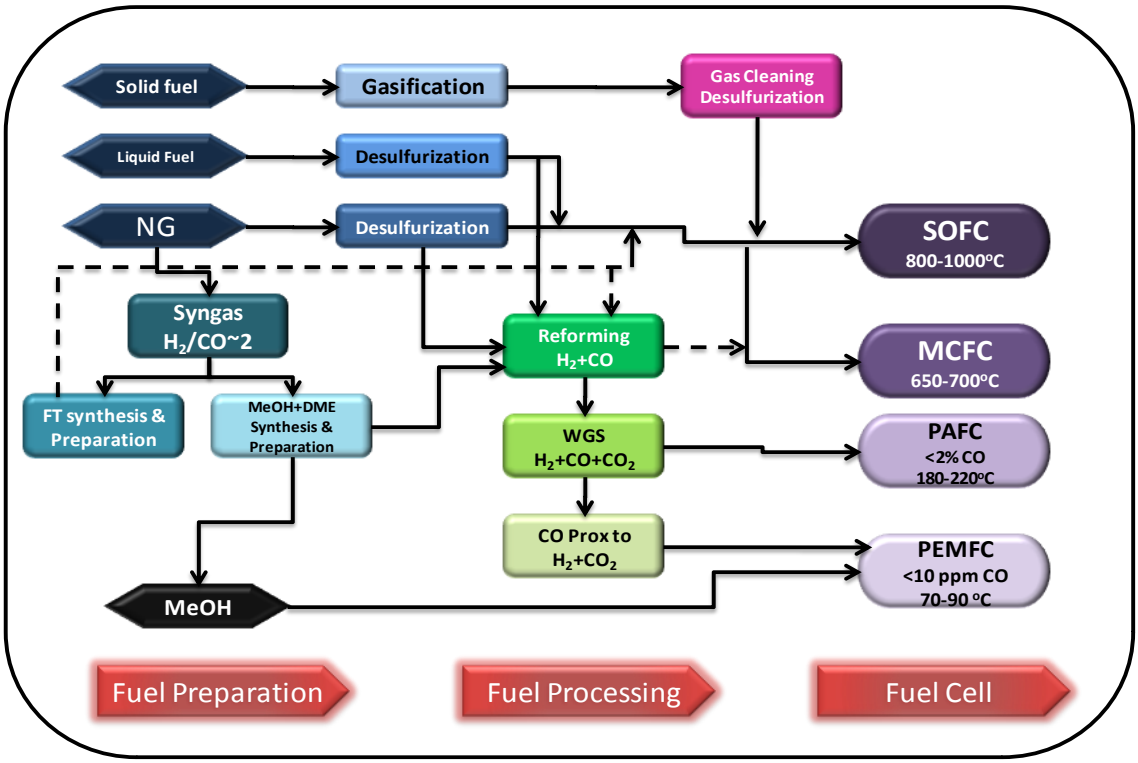

Figure I.1: The concepts and steps for fuel processing for gaseous , liquid and solid fuels for high temperature and low temperature fuel cell applications

Fig I.1. illustrates the general concept of processing gaseous, liquid and solid fuels for fuel cell applications. Reformate (syngas and other components such as steam and carbon dioxide) can be used as fuel for high temperature fuel cells such as Solid Oxide Fuel Cell (SOFC) and Molten Carbonate Fuel Cell (MCFC), for which the fuel needs to be reformulated. When natural gas or other hydrocarbon is used in Phosphoric Acid Fuel Cell (PAFC) system, reformate must be processed by water-gas-shift (WGS) reaction.

Table I. 1 : The fuel requirements for the principal fuel cells

Gas species	**PEMFC**	**AFC**	**PAFC**	**MCFC**	**SOFC**
H_2	Fuel	Fuel	Fuel	Fuel	Fuel
CO	Poison (>10ppm)	Poison	Poison (> 0.5%)	Fuel[a]	Fuel[a]
CH_4	Diluent	Diluent	Diluent	Diluent[b]	Diluent[b]
CO_2 and H_2O	Diluent	Poison[c]	Diluent	Diluent	Diluent
S **(as H_2S and COS)**	Few studies	Unknown	Poison (>50ppm)	Poison (>0.5ppm)	Poison (>0.1 ppm)

a. In reality CO reacts with H_2O producing H_2 and CO_2 viz the shift reaction and CH_4 and H_2O reforms to H_2 and CO faster than reacting as a fuel at the electrode

b. A fuel in the internal reforming MCFC and SOFC

c. The fact that CO_2 is a poison for the AFC more or less rules out its use with reformed fuels.

The lower the operating temperature of the stack, the more stringent are the requirements, and greater the demand placed on fuel processing as shown in Table I.1. The most promising and most widely researched, developed and demonstrated type of fuel cells is the proton exchange membrane (PEM) fuel cell, which operates at low temperatures (~ 80^oC) [1]. Hydrogen as a fuel is not readily available, particularly not for residential applications, except if the system is to be used as a backup power system, in which case it may be equipped with an electrolytic hydrogen generator. To facilitate market acceptance, fuel cell developers are forced to add a fuel

processing section to the fuel cell system. For residential and commercial applications, natural gas is a logical fuel choice because its distribution channel is widely developed. The majority of the stationary power fuel cell systems developed to date use natural gas as fuel[2].

High efficiency desulfurization is critical to maintain the activity of fuel processing catalysts and high-value membrane electrode assemblies in logistic fuel cell systems. On-board fuel processing of liquid hydrocarbon fuel is being investigated to supply hydrogen for fuel cell-based auxiliary power units. For such a system, if sulfur is not removed from the liquid phase, the removal of sulfur as H_2S from the reformate becomes a key-step since downstream catalysts and the fuel cell itself can be poisoned by a small amount of H_2S in the feed [3]. Hydrogen sulfide is present in many high temperature gas streams during extraction and processing of fossil fuels, natural gas and geothermal brines. H_2S is also found in many industrial process gases, particularly in the mineral and metallurgical process industries. Because it is highly toxic, and corrosive, H_2S must be removed completely as early in a process as possible. Depending on the fuel selection additional ancillary components are required for processing the fuel to meet the fuel requirement for fuel cell. Steam reforming catalysts, PEM anode catalysts and also the shift catalysts are intolerant to sulfur and to ensure adequate lifetime of fuel processors the desulfurization step is very important.

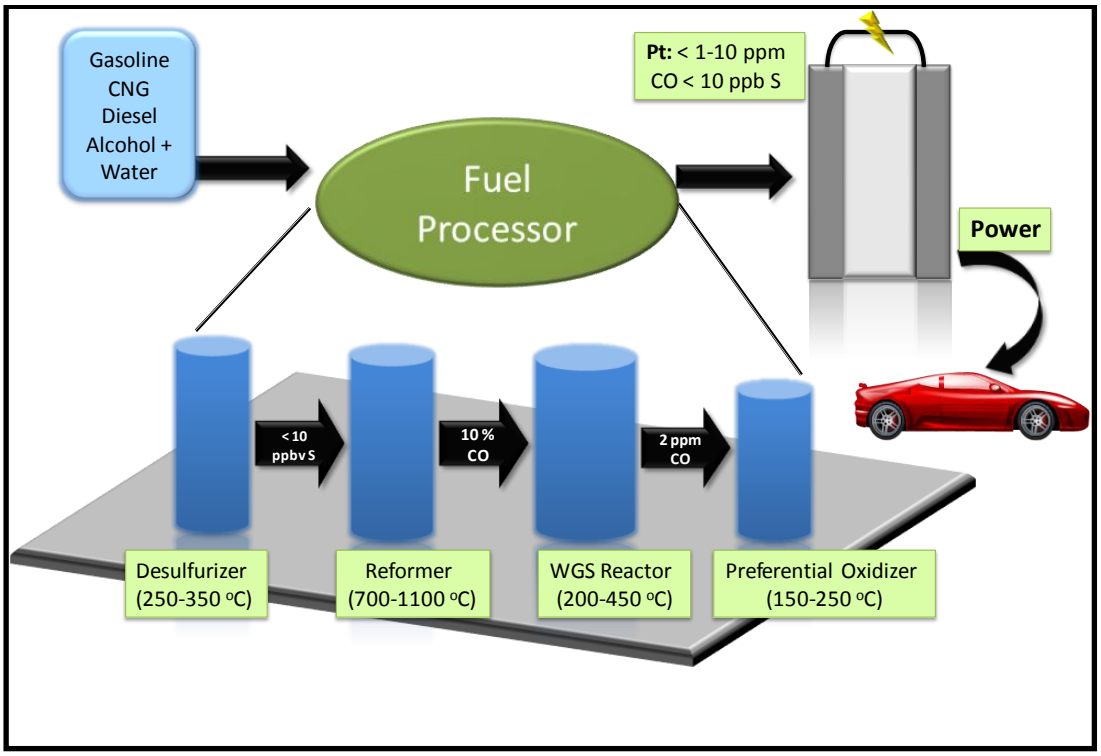

Figure I.2: Fuel processing steps with amounts of poisons tolerable for operation in PEMFCs

Irrespective of the approach adopted to remove sulfur, following are some of the common requirements for sorbents used for logistical fuel cell applications:

a. Achieving high levels of sulfur removal. Packed beds are used commercially for desulfurization to attain lower breakthrough concentration, higher bed utilization. These packed beds have larger size due to possible channeling and lower intra-particle mass/heat transfer.

b. Regenerability of the sorbent: temperature, energy requirement, purging gas, safety concern, valves and other utilities

c. Scalability of the sorbent, ease of availability and cost

d. Minimization of the system mass/volume and complexity

This work is focused on development of sorbents which are regenerable, scalable over wide temperature ranges with uses in fuel cell systems. Attempts have been made to device

appropriate strategies to reduce sulfur concentration to ppb levels in the reformate streams. Use of microfibrous entrapped sorbents as employed for benefits in the composite bed design is used to help miniaturize the desulfurization unit; this design has added benefit of higher breakthrough time without adding to pressure drop.

I.2 Literature Review

I.2.1 Desulfurization Technologies

Sulfur removal from feed stocks usually takes place in two stages. The first stage involves the hydro desulfurization of organic compounds in the presence of hydrogen typically at 370 ^{o}C, 40 Bars over $CoO/MoO_3/Al_2O_3$ catalyst to generate H_2S. The H_2S is then absorbed in a bed of highly porous zinc oxide catalyst at 350-450 ^{o}C.

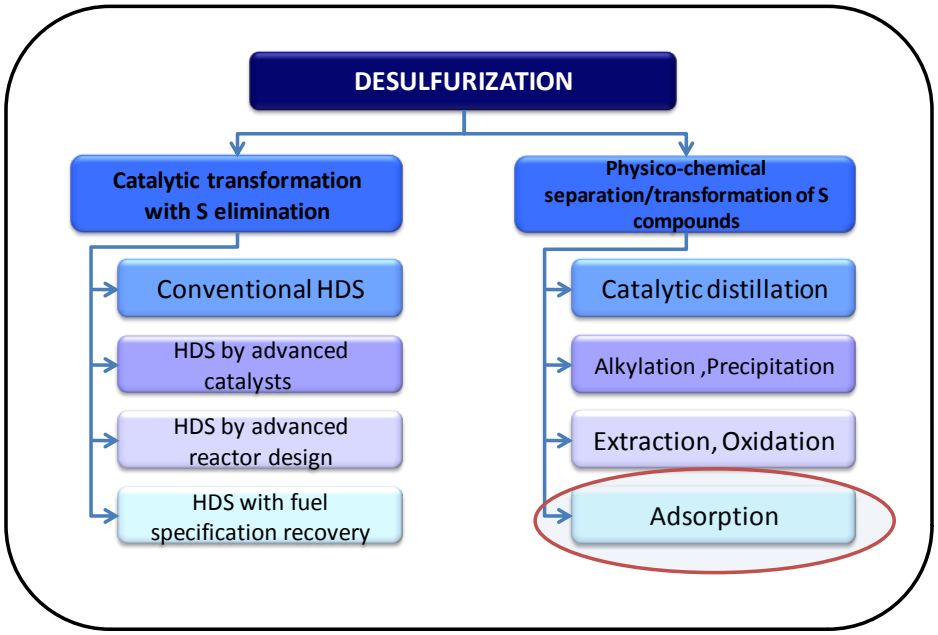

Figure I.3: Desulfurization technologies classified by the nature of the key process to remove sulfur

Desulfurization by adsorption (ADS) is based on the ability of the solid sorbent to selectively adsorb sulfur compound from refinery streams. ADS is divided in two groups: Adsorptive desulfurization and Reactive adsorption desulfurization. Adsorptive desulfurization is based on physical adsorption of sulfur compounds on a solid sorbent surface. Regeneration of the sorbent is usually done by flushing the spent sorbent with a desorbent, resulting in a high sulfur compound concentration flow. Reactive adsorption desulfurization employs chemical interaction of the sulfur compound and the sorbent. Sulfur is fixed in the sorbent, usually as sulfide, and the S-free hydrocarbon is released into the purified fuel stream. Regeneration of the spent sorbent results in sulfur elimination as H_2S, S, or SOx depending on the process applied. Efficiency of desulfurization is mainly determined by the sorbent properties: its adsorption capacity, selectivity for the sulfur compounds, durability and regenerability [4].

I.2.2 ZnO based sorbents

The removal of H_2S can be performed by different routes such as adsorption in liquid alkanolamine, ammonia solution and alkaline salt solution, oxidation with Fe (III) oxide and activated carbon. ZnO has been in use for H_2S removal for more than 30 years. Among the tested metal oxides ZnO has the highest equilibrium constant for sulfidation, yielding H_2S removal down to a fraction of 1 ppmv. Its principal limitation is that in the highly reducing atmosphere of synthesis gas it is partially reduced to elemental Zinc. It is volatile above 600 ^oC, with consequent sorbent loss. For achieving maximum useful life of the PEMFCs, it is crucial to reduce the H_2S concentration to < 0.1 ppmv. Zinc Oxide is highly efficient desulfurizer due to favorable thermodynamics in the temperature range of 350-550 ^oC. ZnO shows low equilibrium H_2S concentration. H_2S absorption by ZnO is considered to be controlled by the following reaction:

$$ZnO(s) + H_2S(g) \Leftrightarrow ZnS(s) + H_2O(g)$$

This is an exothermic reaction and the equilibrium H_2S concentration is determined by the temperature, the H_2S partial pressure and to a lesser extent the phase of the zinc oxide. Equilibrium H_2S concentration for ZnO with no H_2O is shown in Fig I.4. The data is generated using the HSC software. Thermodynamically, it is impossible to reduce the sulfur concentration to less than 100 ppbv at temperatures above 300 ^oC. At lower temperatures of (< 250 ^oC), absorption kinetics are slower but the ZnS equilibrium is more favorable. The data in the table indicates that if the kinetics of H_2S absorption is sufficiently rapid, concentrations well below 100 ppb should be achievable.

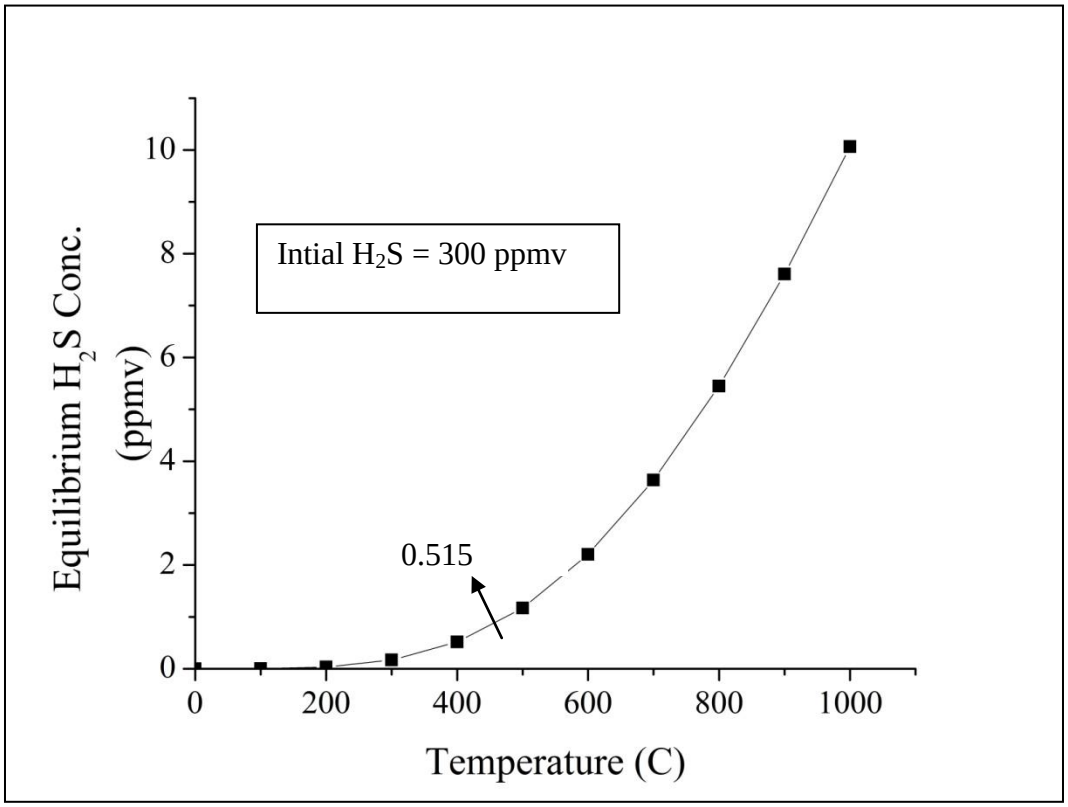

Figure I. 4: Equilibrium H_2S concentration (ppmv) using HSC software.

*HSC Chemistry Ver.3.0 Copyright © Outokumpu Research Oy Pori Finland A.Roine.

Table I. 2 : Equilibrium data for $ZnO+H_2S = ZnS+H_2O$ by HSC* software

T (^oC)	Equilibrium constant (K)	H_2S outlet (ppmv)
0	5.32E+13	4.11E-05
200	7.60E+07	3.44E-02
400	3.39E+05	5.15E-01
600	1.82E+04	2.20E+00
800	2.92E+03	5.45E+00
1000	8.30E+02	1.01E+01

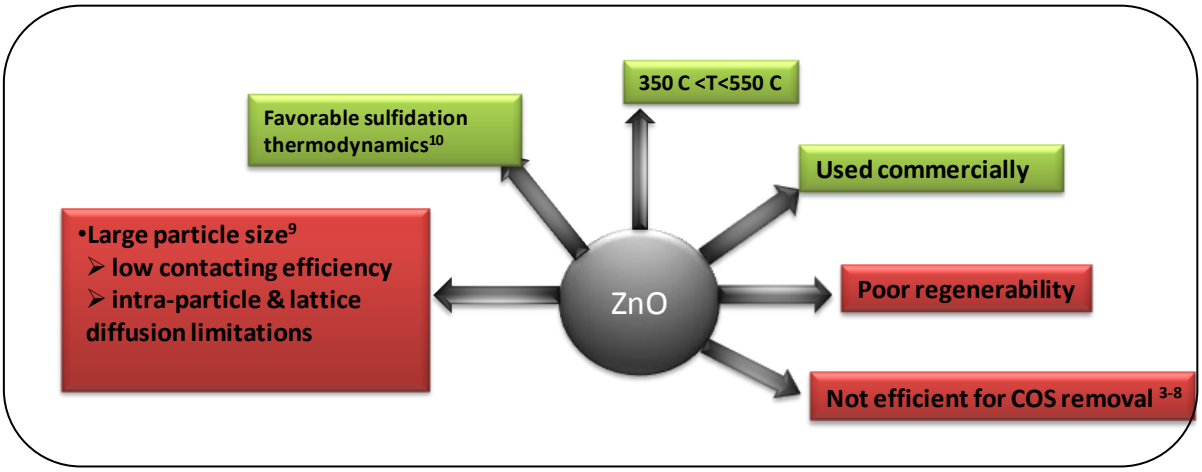

Figure I. 5: Background on commercial ZnO sorbent based on literature search

Based on the Fig I.5, there is a need of sorbents that can effectively remove sulfur in the lower temperature regime (T < 350C), high temperature regime (T > 550 C), regenerable over multiple cycles, COS tolerant. The following sections present the literature review on the low temperature desulfurization, COS removal, high temperature desulfurization and Microfibrous entrapment for enhanced contacting efficiency in a packed bed.

I.3 Low Temperature Desulfurization

There is an increasing need to purify gases at low temperatures (< 200 C) to improve the energy efficiency. Although this requirement has been partially met by the recent development of a high-surface area ZnO, there is still a scope for improvement[5]. Proton Exchange membrane fuel cells (PEMFC) have become the focus of significant interest for the stationary and portable power systems. A recent challenge is the development of the on-board fuel processing technologies utilizing high energy density commercial grade hydrocarbon fuels. For Natural gas, Liquefied Petroleum Gas (LPG), which is the *most suited for PEMFC applications* (due to the highly developed infrastructure that exists for their distribution), ambient temperature removal of sulfur compounds using a solid adsorbent is technically attractive. There has been little work done on the H_2S removal by metal oxides at room temperature. Activated carbons are also used for the H_2S removal from natural gas or municipal sewage treatment facilities, because of their developed high surface area and large pore volumes. At room temperature, activated carbon was found to be a better adsorbent after extensive humidification of its surface[6].

Stirling et al [7] investigated different adsorbents such a ZnO and ZnO doped with 5% oxides of Cu, Fe and Co, high surface are Zn/Co/Al oxides and ZnCo oxides with different Co/Zn ratios for the H_2S removal at room temperature. Among the oxides studied, they reported the Co_2O_4 oxide to be the best one because it showed almost stoichiometric reaction with H_2S. Davidson et al [8] studied the rate of reaction of H_2S with high surface area of undoped and doped ZnO samples at 0-45 ^oC and they reported the fast rates appeared to depend upon the crystallite size, morphology and coexisting water. Addition of the dopant not only stabilizes the active sorbent by increasing active surface area and decreasing crystallite size, but may introduce defects with promoter behavior [5, 7]. Small particle size (100-200 microns) allows entrapment in the

microfibrous media viable for composite bed design. The microfibrous media (developed in Auburn University) offer enhanced contacting efficiency and mass transfer without significant pressure drop [9-11]. This approach towards small-scale regenerable continuous batch fuel processing in PEMFC applications is commercially feasible by using micro structured particulate carriers.

I.4 COS Removal/Inhibition

With the introduction of the strong legislation to reduce sulfur emissions, fresh impetus is being given to modifying improving existing desulfurization technology. However, dehydrodesulfurization does not remove or significantly affect sulfur containing compound, namely, Carbonyl Sulfide (COS). Various researches for H_2S removal have been reported in details for the purification of gasified products derived from various feedstocks [12]; however, removal of COS is not a big concern yet, because it is not the major sulfur compounds produced from gasification. The absorption of H_2S by ZnO is stoichiometric above 350 ^oC but it falls rapidly at lower temperatures. The removal of COS has been reported to be more difficult at low temperatures in the range from room temperature to 200 ^oC than H_2S. ZnO is a preferred metal oxide because of favorable sulfidation thermodynamics, [13] but is not efficient to remove COS [7]. Most commercial H_2 is produced form natural gas via steam methane reformation (SMR) followed by a water gas shift (WGR) reaction in which CO is oxidized to CO_2 while water is reduced to H_2. The gas effluent from the WGS varies from a few ppmv to 2% by volume of CO in excess of H_2. This low concentration of CO in the H_2 outlet stream from the WGS can be avoided. However, eliminating the CO is beneficial in increasing the PEM fuel cell performance. Over the last two decades it has become increasingly apparent that emissions of sulfur

compounds, including COS, into atmosphere have been unacceptably high. Since COS is rather inactive compared to H_2S probably due to its neutrality and similarity to CO_2, COS is sometimes produced through the reaction of H_2S with CO_2, although the reaction can be reversible to produce again H_2S and CO_2 from the reaction of COS and H_2O depending upon the adsorption conditions[14].

The formation of COS is primarily governed by the reversible hydrolysis reaction and equilibrium conditions present:

$$COS + H_2O \Leftrightarrow H_2S + CO_2$$

Removal of sulfur-containing compounds is one of the most important technologies for the utilization of the gasified products derived from various feedstocks such as biomass, waste and solid fossil fuels. Gaseous sulfur compounds of H_2S and COS are severe catalyst poisons against the following processes of steam reforming for hydrogen. COS can be formed by the conversion of H_2S and CO_2 in the absence of water. Natural gas is saturated with water and therefore COS does not usually occur in those streams. A relatively small volume of COS can combine with water to form H_2S if suitable equilibrium conditions exist[14].

I.5 High Temperature Desulfurization

The removal of hydrogen sulfide to sufficiently low levels from coal derived fuel gases at elevated temperatures is crucial for efficient and economic coal utilization in emerging advanced

power generation systems such as integrated gasification-combined cycle (IGCC) and the gasification molten carbonate fuel cell (MCFC). Gasification is expected to be among the most promising conversion processes to produce synthesis gases[15]. Integrated coal gasification combined cycle (IGCC) is one of the most prospective coal-based power generation technologies in this century because of its high efficiency and low emission. Before the gas goes into the gas turbine combustor, the polluting species and other contaminants in the raw gas must be removed, including dust, sulfur species, nitrogen species (ammonia and cyanides), halides and trace metals, the high temperature gas cleanup system is then introduced and the gas sensible heat can be fully utilized with and increase in the efficiency by 0.5-1.5%.[16]

The important factors of hot gas desulfurization sorbent are

1. The sorbent should have good sulfur removal capacity and fast adsorption kinetics
2. The sorbent should be chemically stable, i.e., it should not evaporate or sinter during regeneration
3. The sorbent should be physically stable, i.e., it should withstand any attrition.
4. The sorbent should catalyze formation of elemental sulfur upon reductive regeneration, hydrolyze carbonyl sulfide (COS), and react with other contaminants such as tars
5. The sorbent should be regenerable and it should maintain its sulfur removal capacity for many cycles
6. The sorbent replacement cost should be affordable.

Hot gas desulfurization can be accomplished by using metal oxide based sorbents like zinc, manganese, iron and copper. Typically, metal oxides are converted to sulfides during a sulfur loading stage under reducing hot gas conditions.

For optimal IGCC performance, high temperature coal gas purification technology is necessary. The sulfur present in the coal is converted primarily to H_2S in the gasifier with a small amount of COS. Several liquid scrubbing processes are available for H_2S removal to achieve the 20-ppmv target. These processes, however, do not integrate well with IGCC due to large temperature differences. There will be energy losses associated with cooling to scrubbing temperatures, which is almost ambient temperature. Therefore, hot gas desulfurization is critical to the optimal development of the IGCC and the other advanced coal gas processes.

ZnS can be regenerated if sufficiently high temperatures or low oxygen concentrations are used to avoid zinc sulfate formation. Zinc loss in the form of vapors limits the application of the ZnO at higher temperature. Mixed metal oxides allow raising the operating temperature for fuel gas desulfurization as a result of their lower ZnO reduction rate. Zinc-based and ferrite based sorbents show superior reactivity to H_2S. Structural stability and good mechanical strength are additional desired features of the sorbents.

Process requirements taken as a basis for determining metal oxides suitability for high temperature desulfurization:

1. Rate of desulfurization and stability of the sulfide under reducing gas conditions
2. Potential for detrimental secondary reactions on the solid under reducing coal gases (e.g. metal carbides, reduction to zero-oxidation state, formation of chlorides from HCl)
3. Rate of regeneration and production of SO_2 or elemental sulfur under oxidizing gas conditions

4. Potential for detrimental secondary reactions on the solid under oxidizing gases (e.g. sulfates) and hydrothermal stability during regeneration.

I.6 Microfibrous Entrapped Sorbents

Microfibrous technology developed at the Center of Microfibrous Materials Manufacturing (CM3) at Auburn University [17-26] provides a novel approach for a versatile design of small, efficient, and lightweight fuel processors. This approach can also enhance heat/mass transfer, improve contacting efficiency and promote regenerability. Packed beds that provide enough volume to remove sulfur from several 1000 ppmv to sub-ppmv levels generally use sorbent particles sizes, ca. 1-5 mm. These demonstrate low sorbent utilization and poor regenerability, owing to low contacting efficiency, intra-particle and lattice diffusion limitations [27]. Small particle size (100-200 μm) allows entrapment in the microfibrous media viable for composite bed design. These microfibrous media offer enhanced contacting efficiency and mass transfer without significant pressure drop [11].

The fabrication of the microfibrous media is based on reliable, proven, high speed roll to roll papermaking and sintering processes, which substantially reduces the production costs and improves the product quality. This approach utilizes micro-sized fibers to entrap sorbent and/or catalyst particulates into a sinter-locked microfibrous structures with a high voidage and high contacting efficiency. With improved contacting efficiency, these materials can reduce both the reactor weight and volume, which is very important for logistic fuel processors[28]. For example, microfibrous entrapped Ni/Al_2O_3 catalysts for toluene hydrogenation in a trickle bed reactor demonstrated 2-6 times higher specific activities than conventional packed bed catalysts

on a gravimetric basis, while volumetric activities of 40 vol% composite catalysts were 80% higher than conventional extrudates[29] . Microfibrous entrapped promoted Pt /Al_2O_3 catalysts for PrOx provided 3 times higher bed utilization efficiency compared to packed beds of 2-3 mm (dia.) pellets [25, 30] at same CO conversion. Two-phase mass-transfer experiments indicated that microfibrous composite catalysts take advantage of both high gas-liquid contacting and bulk mixing at low pressure drop with the potential to provide enhanced catalyst utilization. *Additionally, the microfibrous media can be made into thin sheets of large area and/or pleated to control pressure drop and contacting efficiency*. As for H_2S removal, Ni fiber entrapped ZnO/SiO_2 was prepared and demonstrated 3 times longer breakthrough time than a commercial ZnO extrudates [31],[24]. However, Ni fiber cannot sustain the high oxidizing atmosphere during ZnO regeneration. Therefore, new microfibrous entrapped sorbents with microfibrous structures that are able to work in both reducing and oxidizing environments were developed using the sintered ceramic/glass carriers with micro-sized ZnO entrapped for regenerable use to scavenge bulk H_2S from reformate streams in a continuous batch mode at 400 ^oC [20]. Based on the thermal properties of various types of glass fibers available (Advanced glass fiber yarns LLC) S2 fiber and E type fiber were chosen as shown in Table I.3 and the SEM image of the glass fibers entrapped silica is shown in Fig. I.8.

Table I. 3: Properties of the Glass fibers

Glass fiber type	**Dimensions Dia (um) x length (mm)**	**Density ($g\ cm^{-3}$)**	**Softening point (^oC)**	**Annealing point (^oC)**	**Strain point (^oC)**
S2	8 x 6	2.46	1056	810	760
E	10 x 6	2.58	846	657	615

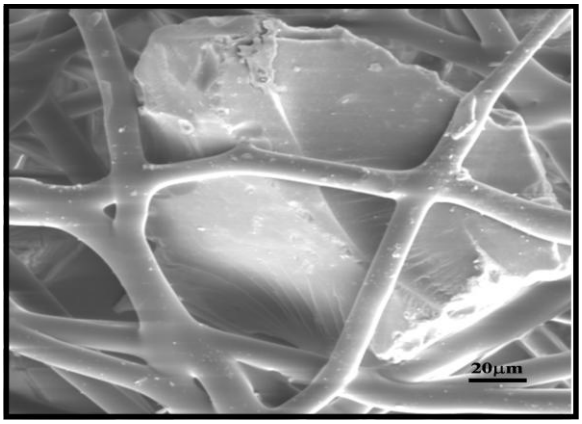

Figure I. 6: SEM Image of the S2 glass fiber entrapped SiO_2 particle. [20]

I.7 Advantages of supported sorbents

Supported types of sorbents are generally preferred for their mechanical strength because sufficient amount of cycles of sulfidation and regeneration are desirable in either fixed-bed form or fluidized bed systems. The support materials of sorbent applied for hot coal gas desulfurization is presently composed primarily of Al_2O_3 and SiO_2, activated carbon, or other materials.

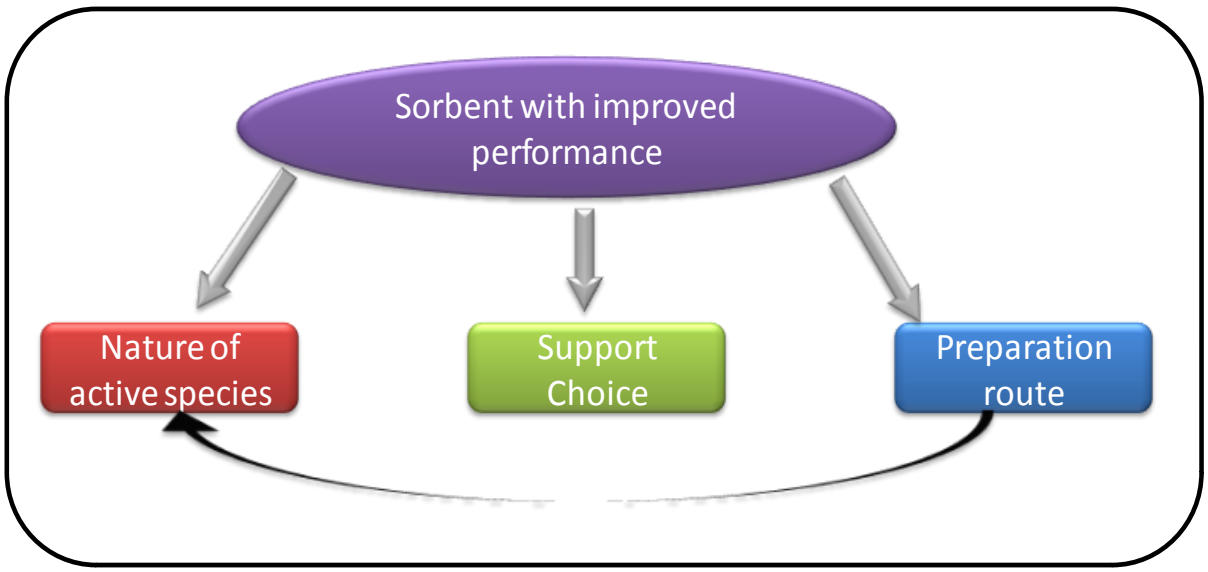

Figure I. 7: Important properties for sorbent formulation

1. In order to improve desulfurization performance, sorbents with high porosity and small grain sizes are preferred. In this regard, metal oxide sorbents on inert supports are widely used for desulfurization.
2. In supported sorbents, active sorbent substances are supported on secondary oxides to form high surface area and high porosity sorbent particles/extrudates. These secondary compounds are mainly inert to sulfur.
3. Supports are utilized to enhance the structural stability for the active sorbent and to adhere/hold the sorbent crystallites within the micropores of the support in the absence of grain size, agglomeration and sintering.
4. Supports also serve to stabilize the active metal oxide component against chemical reduction and vaporization. The supported sorbent design also facilitates the incorporation of the sorbent into process system hardware.

5. Due to the above noted advantages provided by supported sorbents, these systems provide stable performance with extended service lives.

The most extensively used porous adsorbent materials for desulfurization include activated carbon, γ-alumina, modified zeolites, etc. [32, 33]. However, these materials suffer several drawbacks in practical application as shown in Fig.I.7.

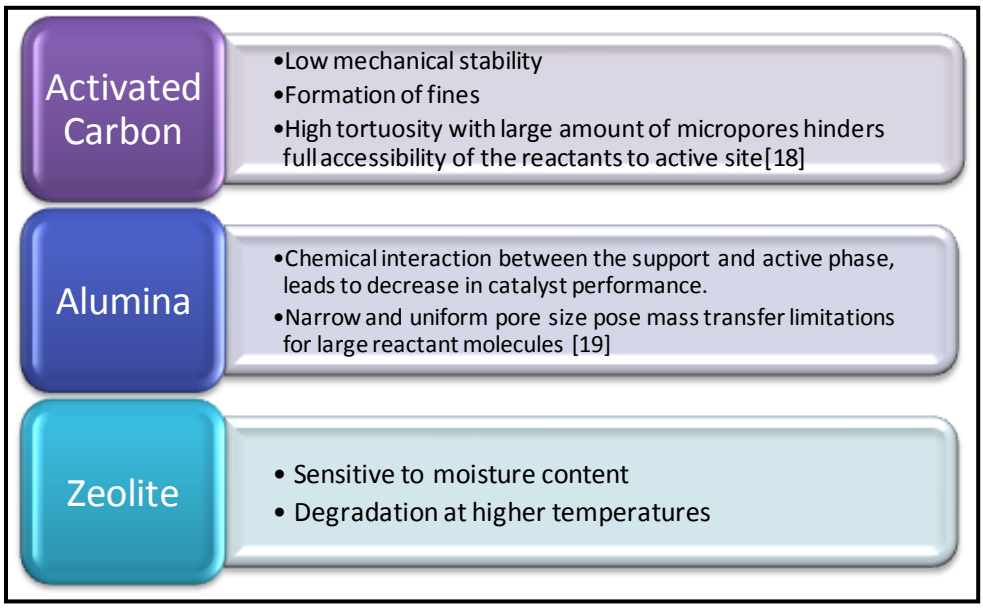

Figure I. 8: Overview of literature review on various supports

Silica supported ZnO sorbents are preferred because of better ZnO utilization and thermal stability [1-4]. Recent developments on improvement in the diffusion of reactants to the catalyst sites have been focused on the increase in Zeolite pore sizes decrease in zeolite crystal size and providing an additional mesoporous system within the microporous crystals.

The discovery of highly ordered mesoporous materials has received considerable attention in heterogeneous catalysis. These materials have much promise for the development of novel solid catalyst due to their structural characteristics such as ordered pore structure, high specific surface area (1000-2000 m^2/g), uniform pore size distribution (varying from 1.5-10 nm), and high specific pore volume (1.0-2.0 cc/g) [34]-[35]. The mesoporous silica supports including

MCM-41, MCM-48, SBA-15 are found to be the superior base matrix for various surface modifications with amines and their subsequent application in the low temperature removal of acidic gases like H_2S and CO_2 [36, 37]. Mesoporous silica has been recently used as a support for metal catalysts, resulting in significant improvements when compared to commercial and conventional amorphous silica-alumina catalysts. For example, Corma et al. [38] have reported a superior hydrogenation activity and sulfur tolerance for Pt/MCM-41 in comparison to Pt/Zeolite, Pt/SiO_2, and Pt/Al_2O_3. Song and Reddy [39] reported that Co-Mo/MCM-41 showed higher hydrogenation and hydrocracking activities than conventional Co-Mo/γ-Al_2O_3. Fe_2O_3/MCM-41 was found to exhibit a superior performance for the conversion of SO_2 into SO_3 compared to Fe_2O_3/silica [40]. *However, on reviewing literature, it is worth to mention that only little information is reported so far on the MCM-41 and MCM-48 application for H_2S uptake.* It is in this context only that in this study the commercially procured MCM-41 and laboratory synthesized MCM-48 were selected as H_2S sorbent and their performances were compared with conventional silica gel. MCM-41 is the most extensively studied member of the mesoporous silica materials family. It exhibits a hexagonal array of one dimensional mesoporous which can be tuned from 2-10 nm by the suitable choice of the structure directing agent and synthesis conditions [41]. The mesoporous materials are in general synthesized by supra-molecular self-assembly process in the presence of (cat-) ionic surfactants as templates during the mesophase formation.

I.7.1 Novel Support – *Mobil composition of Matter*- MCM-41

The Table I.4 lists the comparison of the various method used for preparation of the supported metal oxide on MCM.

Table I. 4. Comparison of the literature Review on preparation of MCM- 41

Sorbent /Catalyst	**Method**	**Application**	**Remarks**	**Author/Year**
Cr-MCM-41	In-situ	Olefin Oligomerization to produce lube oil	Pour points and Viscosity index improved	Pelrine et al.,1992[42]
Co- MCM-41	In-situ	HDS and HDN	High activity at Si/Al= 60	Souza etal., 1995[43]
MCM-41	N/A	Acid catalyst for Friedal Crafts alkylation	Good catalytic activity	Kloeststra et al.,1995[44, 45]
Ti (V, Cr)-MCM-41	In-situ	Oxidation in presence of hydrogen peroxide	Excellent catalytic oxidation	Tanev et al., 1994[46]
Ti,V-MCM-41	In-situ	Selective catalytic reduction of NO	Higher NOx conversion than for silica based catalyst	Beck et al., 1992[47]
Cu-MCM-41	Organofunctionalization	Not studied	Characterization for metal loading	Hao etal., 2006[48, 49]
Fe-MCM-41	Incipient wetness, solid state impregnation, in-situ	SO_2 oxidation at high temp (>600K)	Wetness impregnation was better (conversions~60-70%)	Wingen et al., 2000[50]
Ag-MCM-41	Direct Hydrothermal & thermal ion exchange	CO oxidation	Reduction at 500$^oC\rightarrow$ oxidation at RT(~95%conversion)	Gac et al., 2007[51]
Zn-MCM-41	HIP	Hydrogenation of MB	At 300-400^oC-100% conversion	Lu et al., 2002[52]
ZnO, CuO MCM-41, MCM-48	***Incipient wetness method***	***Low temperature H_2S Adsorption-desorption***	***NOT EXPLORED MUCH***	***NOT REPORTED***

.Incipient wetness impregnation method as used to make metal oxide supported on MCM sorbent. Very few studies are reported on the metal incorporation in mesoporous silica by incipient wetness impregnation. Incipient wetness impregnation[53] is a simple method with fewer steps; an adequate amount of active metal can be loaded on the support by changing the precursor concentration, the oxide formed after calcination is stable. The sorbents supports can disperse the active components and increase the surface area of sorbents. Some support materials such as carbon material may also play roles in converting sulfur species. The quantity of support

materials is large in industry scale systems; therefore, the support material must be economic and easy to be obtained.

I.8 Scope and Objective of the work:

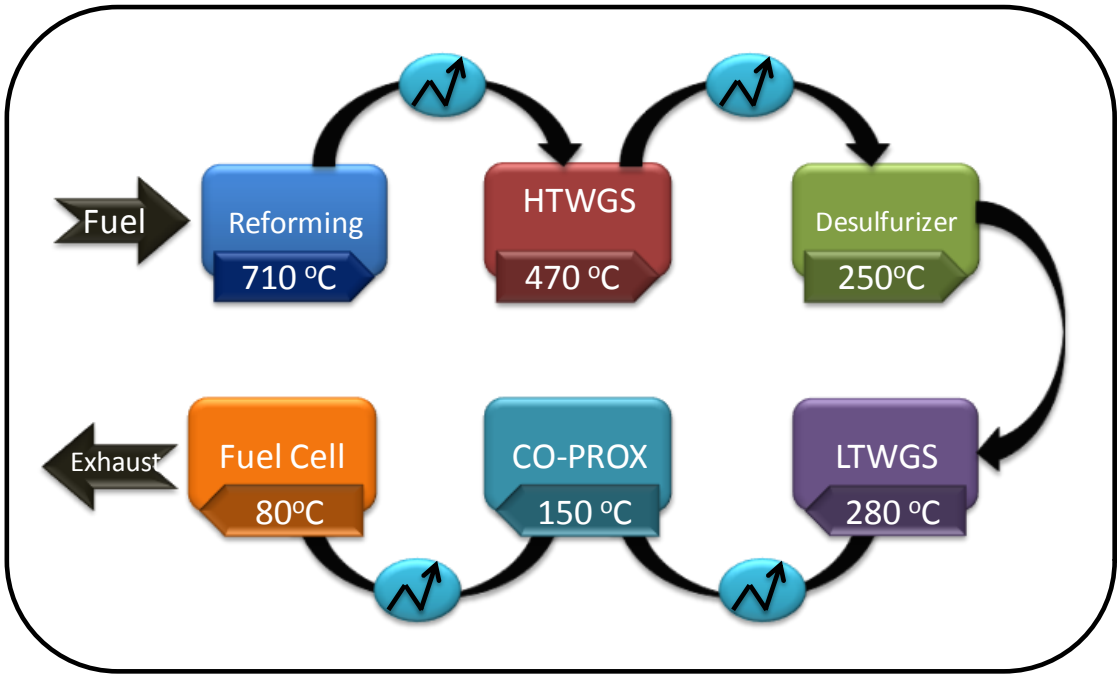

Figure I. 9: Schematic diagram of the fuel processing for PEMFCs with average operating temperatures

Fig.I.9 shows the fuel processor system with average operating temperatures, the desulfurizer can be located either before or after the HTWGS unit[54]. In the first case, high temperature sorbent will be required for protection of the HTWGS catalysts against sulfur poisoning. However for the second case, a low temperature ZnO based sorbent for protection against the most sulfur sensitive catalysts of the fuel processor (LTWGS and CO-PROX catalysts). Typical sulfur compound include RSH, R_2S, H_2S and COS. COS is particularly problematic to remove as commercial sulfur adsorbents generally show poor adsorption capacities for COS at ambient temperature, and thermodynamic constraints limit COS removal via conventional hydrotreating. Sulfur impurities can reduce the effectiveness of fuel-processor

catalysts and can poison the anode catalysts of both high- and low-temperature fuel cells. The problem is most severe in polymer electrolyte fuel cells (PEMFC); because they operate at low temperature and their Pt group catalysts are susceptible to sulfur poisoning. The poisoning effects of sulfur are irreversible. PEMFCs operate at low temperatures ~80^{o}C, an inline filter can be developed which takes care of removal of sulfur from several ppmv level to sub-ppmv level. During the cold start-ups of FC system, the temperature drops to less than 30^{o}C, at this time we need an efficient sorbent which can operate over wide temperature range. Regardless of initial H_2S concentration, subsequent replacement of the contaminated fuel stream with pure H_2 does not allow full recovery of the catalyst. Sulfur also degrades the performance of the high-temperature solid oxide fuel cells (SOFC). The performance of the SOFC drops about 15% in the presence of 1 ppmv sulfur. The cell voltage increases, and performance is recovered once the sulfur flow is stopped[55]. Although this poisoning effect is reversible in SOFCs, long-term stable electrochemical performance of both high- and low temperature fuel cells requires that the sulfur concentration to be reduced to sub-ppmv levels.

Accordingly the objective of this work is divided in four major parts:

1) Low temperature Desulfurization
2) COS Removal
3) High Temperature Desulfurization
4) Microfibrous entrapped sorbents

I.9 Objective of this work

- To develop a sorbent for wide temperature range ($20 \leq T \leq 550$ C) gas phase sulfur removal (H_2S & COS)
- To develop a process that is efficient, cost-effective and scalable.
- To develop sorbents that work efficiently without significant activity loss upon multiple regeneration cycles for logistic Fuel Cell systems.
- To attain high levels of sulfur removal by employing various support characteristics
- To test the sorbent efficiency for use in hot gas desulfurization for applications in SOFCs
- To remove COS by employing various strategies
    - hydrolysis of COS
    - inhibition of COS by varying test conditions
- To propose various schemes to eliminate sulfur from the fuel stream by developing sorbents that are
    - regenerable
    - non –regenerable
- To characterize the sorbents synthesized in lab to understand the reaction mechanisms To study the effect of kinetic parameters on MFES
- To establish a composite bed design for miniaturization of the desulfurization unit

I.10 Outline of this work

- Chapter II describes the general experimental section and the characterization techniques used in this study.
- Chapter III discusses the study on the wide temperature range promoted ZnO/SiO_2 sorbents and effect of various parameters like type of support, promoters, promoter concentration, temperature, moisture content, presence of reformate streams (with CO, CO_2) and advantages of microfibrous entrapment over packed bed and study of kinetic parameters for the same[56].
- Chapter IV discusses the adsorption and multiple cycle regeneration performance of $Cu_{0.05}Zn_{0.95}O/SiO_2$ and its characterization to understand the role of active sites using techniques like XPS, ESR and N_2 adsorption-desorption isotherms[57].
- Chapter V focuses on the preparation and performance of the novel bimetallic doped $Mn_{0.025}Fe_{0.025}Zn_{0.95}O/SiO_2$ for wide temperature range H_2S removal from the fuel reformate streams coupled with the XPS and Operando ESR studies to better understand the role of the dopants in ZnO/SiO_2 [58]
- Chapter VI discusses the strategies to mitigate COS present/formed in reformate streams. The chapter focuses on preparation and performance on carbon and alumina based sorbents to remove, inhibit and hydrolyze COS over wide temperature range. It also discusses the room temperature hydrolysis and removal of COS from fuel reformates using Al_2O_3/carbon and $Mn_{0.025}Fe_{0.025}Zn_{0.95}O/SiO_2$ layered beds [59].

Chapter II: Experimental Setup and Characterization Techniques

II.1 Sorbent Preparation

II.1.1 Sorbent for Packed Bed

II.1.1.1 Preparation of doped supported sorbent

The doped ZnO-based sorbents with the formula $M_{0.05}ZnO_{0.95}/SiO_2$ (M=Mn, Fe, Co, Ni, Cu) were prepared by an incipient impregnation of the commercial high surface area silica (Fischer Scientific Inc., surface area ~550 m^2/g, powder 100-200 μm), with metal nitrates as the 2 M solutions in water used as precursors. Total metal loading was 15, 21 or 25 wt. %. The metal oxide loading was confirmed by Inductively Coupled Plasma Spectrometer (ICP) analysis. After impregnation and drying, the samples were calcined in air at 350 ^oC; these are referred to as the "calcined" samples. Different types of silica supports including MCM-41, MCM-48 silica and conventional silica gel were used. The un-promoted and promoted silica supported catalysts were prepared by incipient wetness method. The metal nitrate solutions of different transition metals were used as precursors for impregnating the MCM (-41 and -48) and silica support with different ZnO and doped ZnO loadings. The impregnated supports samples were dried at 100^oC

for 6h and subsequently calcined at 350^{o}C for 1 h under air flow. All the samples were stored in desiccators for further use.

The promoted ZnO-based desulfurization sorbents of the nominal formula $Fe_xMn_yZnO_{1-x-y}/SiO_2$ (x, y=0; 0.025) were prepared by incipient co-impregnation of high surface area (300-550 m^2/g) silica (Fischer Scientific Inc.) of grain size 100-200 μm with solutions of nitrates of the respective metals in water, namely $Zn(NO_3)_2$, $Mn(NO_3)_2$ and $Fe(NO_3)_3$. Single step incipient impregnation was performed on the silica support to achieve metal oxide loading of 12-36% by varying the molarity of nitrate solutions. Upon incipient impregnation and drying, the samples were calcined in the flowing air at 350-550 ^oC; these are referred to as the "calcined" specimens. The specimens prepared as above, excepting the calcination step, are referred to as the "dried" sorbents. In the reference experiments, with the commercial H_2S sorbents (BASF SG-901 and Sud Chemie G-72E), they are crushed to the same particle size as that of the silica (100-200 microns) used to prepare the supported $Fe_xMn_yZnO_{1-x-y}/SiO_2$ sorbents.

II.1.1.2 Preparation of Mesoporous type silica (MCM)

The MCM-41 was procured from Sigma Aldrich and used as-received without any further purification. The MCM-48 was prepared as described by Schumacher and co-workers elsewhere [60], 10.4 g of cetyltrimethyl ammonium bromide (CTAB, Aldrich) was dissolved in 480 ml of water and 200 ml of absolute ethanol (99.5%, Aldrich). 48 ml of ammonia solution (32%, Aldrich) was added to the mixture and allowed to constantly stir for 15 min. Then, 13.6 g of tetraethoxysilane (TEOS, 98%, Aldrich) was added, and the whole mixture was constantly stirred at room temperature for 10 h. The obtained white suspension was then filtered, washed with hot distilled water and dried at 100 ^oC for 12 h. The white powder was then calcined at 550 ^oC in air for 10 h to obtain the MCM-48 as shown in Fig II.2.

Different types of supports including Alumina, Titania, ACP-carbon, MCM-41, MCM-48 silica and conventional silica gel were used in this study. The MCM-41 used in this study was procured from Sigma Aldrich and used as-received without any further purification.

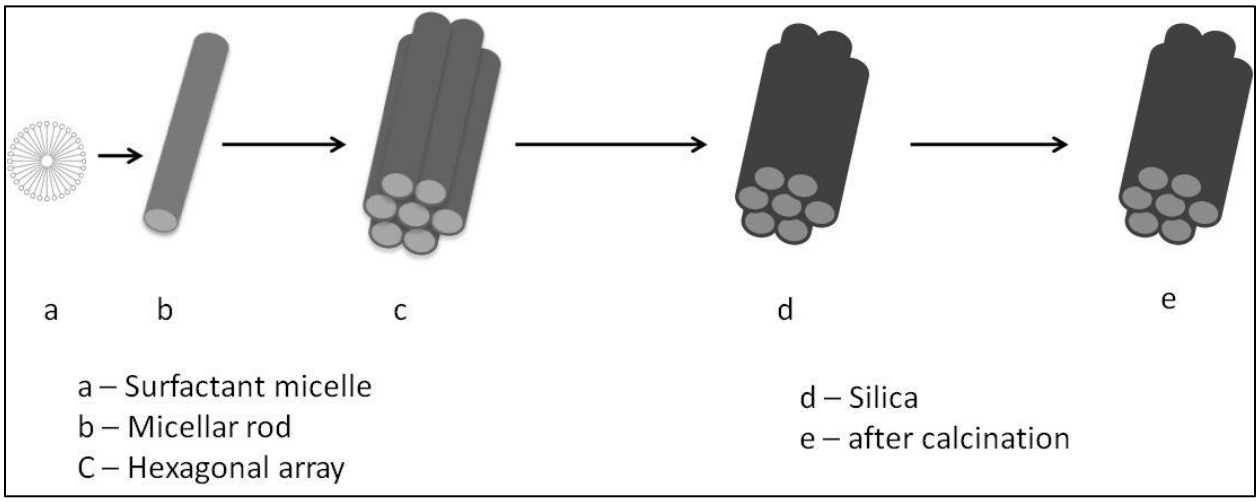

Figure II.1a: Preparation method of MCM- 48[40, 48, 60]

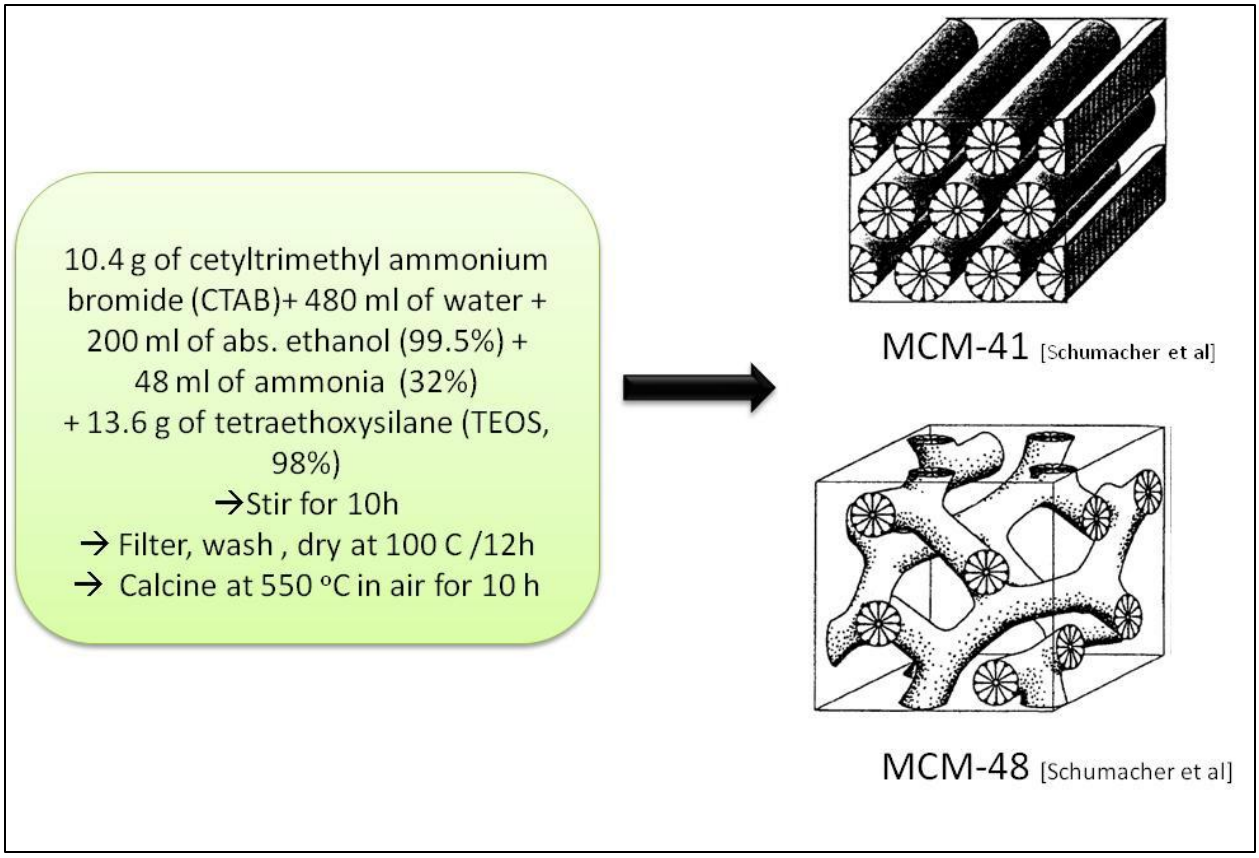

Figure II.1b: Preparation method of MCM- 48[40, 48, 60]

II.1.1.3 Preparation of Al_2O_3/Carbon

Activated PICA carbon of particle size 100-200 microns was dried in oven at 100 C. The dried Carbon was then impregnated with 2M Aluminum nitrate. The impregnated sample was then dried in air for 6hrs and then calcined at 300 C for 1h. The calcined sample Al_2O_3/C is ready to test after cooling it down to room temperature.

II.1.1.4 Glass fiber entrapped Sorbent preparation

Glass fiber entrapped sorbents were made by the wet-lay paper making procedure. Sintered microfibrous carrier was used to entrap 150-200 um diameter support particulates,

where SiO_2 was chosen as support and ZnO was then placed on the supports by incipient wetness impregnation. 6g of S2 glass fibers (8 microns diameter) and 2g cellulose were added in water and stirred vigorously to obtain uniform suspension. The suspension and 18g of silica particles were added into head box of $1ft^2$ M/K sheet former aeration. The preform ($1ft^2$) was then formed by filtration and drying. The glass fiber sheet was pre-oxidized in airflow for 30 min at 450^oC and then sintered for 1h at high temperature, ca, and 910^oC. The prepared microfibrous entrapped SiO_2 was immersed into zinc nitrate solution (2mol/L) for 15min, and then vacuum dried and naturally dried overnight and then calcined at 350^oC for 1h in air.

II.2 Pressure drop measurement set-up

To study the pressure drop effect, the setup as shown in the Fig.II.2 was used. It consisted of the differential pressure cell. The setup shown in Fig II.2 was used to measure the pressure drop across the reactor bed. Two sets of measurements were conducted on the microfibrous media as indicated in Chapter III (Section III.5). Effect of change in face velocity on the pressure drop and effect of change of media (change in solid loading) on pressure drop was studied.

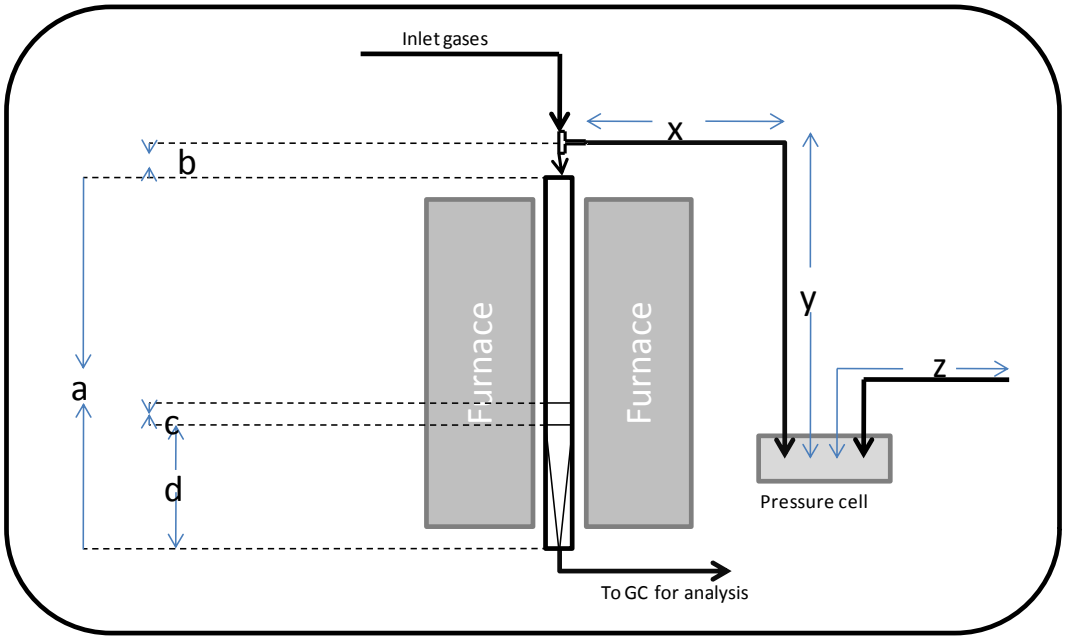

Figure II. 2: Schematic diagram of the pressure drop measurement

MOC – Material Of Construction

S.S – Stainless Steel

Reactor tube – Quartz – I.D – 0.45” O.D- 0.5”

To G.C for analyses/Inlet gases – 1/8” S.S

a- Length of reactor tube – 23”

b- Distance between reactor and inlet pressure tap (ultra torr fittings) – 2.5”

c- Length of bed + Glass wool – 1”

d- Length of glass beads – 9”

(x+y) – Length of inlet pressure tap- (MOS – ¼” S.S) – 37”

z- Length of outlet pressure tap – (MOC- ¼”S.S) -7”

II.3 Experimental Procedure

In the desulfurization experiments, the challenge gas was the model reformate with an inlet concentration of 1 or 2 vol. % H_2S, 33 vol. % CO or CO_2, balance H_2 (UHP grade from Airgas South, Inc.), at a face velocity of 1900 h^{-1} , corresponding to the volumetric gas flow rate of 0.1 slpm. The challenge gas was passed through the sorbent in the packed bed inside a vertically-mounted quartz tubular reactor (10 mm I.D. x 30 mm long), coaxially located inside a 200 mm long tubular furnace. In the reactor, sorbent weight was 0.5 g, bed size was 10 mm (dia.) × mm (thickness). The samples upon adsorption of H_2S are referred to as the "sulfided" samples. H_2S uptakes during the dynamic adsorption experiments were measured using a gas chromatography (GC) instrument (Varian CP3800) equipped with the thermal conductivity detector (TCD) and pulse flame photometric detector (PFPD).

II.4 .Adsorption experiment

The adsorption experiments for desulfurization were carried out at ambient conditions (20 ^{o}C, 1 atm) as shown in Fig II.3. It is comprised of three major sections gas supply section, Reactor system and analysis section. A vertical quartz made reactor (10 mm I.D. x 30 mm L) coaxially mounted in a 200 mm long tubular furnace. The temperature of the furnace during desorption experiments was controlled using a PID temperature controller. The gas flow rates were controlled by mass flow controllers (Omega FMA 2405, Alaborg GFC1718). The face velocity (GHSV) of the stream is 1900 h^{-1}, corresponding to volumetric gas flow rate of 0.1 slpm. An inlet concentration of 1 % (v/v) H_2S in H_2 (ultra high purity grade; from Airgas South, Inc.) was used as sulfur source at a face velocity of 2.12 cm/s, corresponding to the volumetric gas flowrate of 1900 h-1 GHSV (0.1 slpm). The desulfurization reactor contained 0.500 g

sorbent; the sorbent bed size was 9 mm in diameter and 10 mm thick. Gas supply system consists of two H_2S/H_2 gas cylinders of 2vol% and 321ppmv concentrations. UHP H_2 was utilized to dilute the H_2S gas concentration. COS/N_2 procured from Matheson Tri-gas was used in the experiments where COS was used as challenge gas. UHP N_2 was used to eliminate traces oxygen in the reactor during the experiment and to dilute COS concentration. UHP He was used as a inert gas to eliminate traces of Oxygen in the reactor. CO (99.5%) and UHP CO_2 were used as challenge gas to mimic the reformate streams composition, to investigate the COS formation and also to study their effect on the sorbent. H_2S uptakes during the dynamic adsorption experiments were measured using a gas chromatography (GC) instrument (Varian 3800) equipped with thermal conductivity detector (TCD) and pulse flame photometric detector (PFPD). . Varian GC 3800C equipped with three detectors TCD, PFPD and FID was used. TCD was utilized to analyze outlet gases, specification and details are mentioned in the appendix II.

A gas bubbler/ vaporizer was used to saturate the gas streams to study the effect of water or moisture on the system. There was also a provision to heat the bubbler to study the effect at the various moisture contents in the bed. Water was introduced in system by passing He or H_2 through the vaporizer with a temperature controller and was carried in a 1/8" stainless steel tubing wrapped with heating tape. This stream containing water was then mixed with H_2S stream before entering the reactor. In each adsorption run, 0.5 g sample was packed in the reactor. In this study, the breakthrough time was defined as the time from beginning of the desulfurization to the time when the H_2S concentration at the exit reached 100 ppmv. The specimens of the sorbents upon adsorption of H_2S are referred to as the "sulfided" samples.

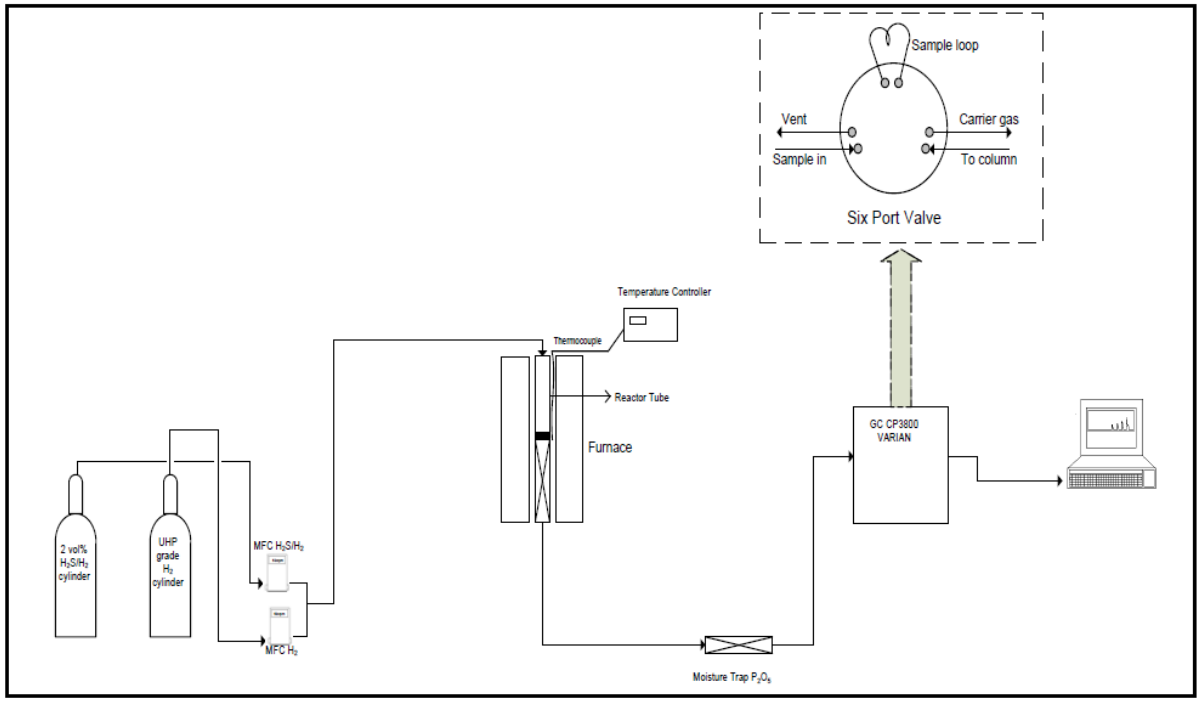

Figure II. 3: Schematic diagram of the experimental set-up

Regeneration of the "sulfided," i.e. "spent" sorbent was performed *in-situ* in the sulfidation reactor at 550 ^{o}C in air at a flow rate of 950 h^{-1}. Household air was used to regenerate the sorbent bed. The temperature of the furnace during the experiments was maintained using a PID temperature set point controller. The gas flow rates were controlled by mass flow controllers.

The Reactor system mainly consists of the quartz reactor tube, the dimensions and the structure is shown in the Fig.II.2. The dimensions of the reactor tube were 16-19" length and 0.5" I.D. The glass beads of size 4mm diameter from Fischer scientific were used to support the bed. The bed consisted of two layers of glass wool about 0.25cm length on the upstream and downstream ends of the sorbent bed as shown in the Fig II.4. These layers of glass wool ensured uniform gas flow through the sorbent bed and supported the particles in the sorbent bed from moving. The sorbent was loaded 9" from the bottom of the tube.

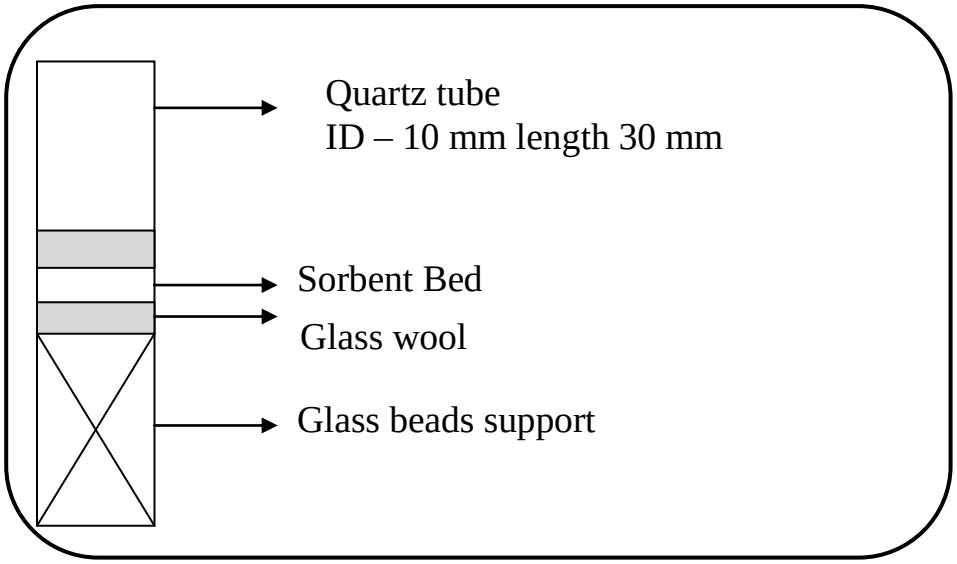

Figure II.4: Schematic Diagram of the Configuration of the Reactor Bed

Stainless steel tubing of ¼-1/8" was used in the set-up. The tubes and the fittings were replaced every 6 months to ensure no clogging has taken place. Leak detection was always performed using snoop - soap solution to ensure adequate and desired flow of the gases into the system.

II.4. Analytical/Characterization Techniques

N_2 Adsorption Desorption Isotherms

Nitrogen adsorption/desorption isotherms at 77 K were measured using the Autosorb 1-C instrument from Quantachrome Instrument Corp., USA. Prior to the measurement, all samples were degassed for 10 h at 200 °C. Specific surface area, S_{BET} was calculated using the BET

equation. The total pore volume, V_P was calculated at P/P_0 = 0.95. The pore width, P_w distribution over the range of ~2–80 nm was generated from the adsorption branches of the isotherms via the BJH method, and the calculations were performed using the Autosorb 1-C software for Windows from Quantachrome Instruments.

Scanning Electron Microscopy (SEM)

The surface morphology of the MCM samples before and after metal impregnation was investigated with Scanning Electron Microscopy (SEM). Prior to SEM (Zeiss Digital Scanning Microscope DSM940), the samples were vacuum coated with gold (Pelco SC-7 auto sputter coater).

X-Ray Diffraction(XRD)

XRD patterns were obtained using a Rigaku Miniflex diffractometer at room temperature. Diffraction patterns were obtained with the Ni-filtered Cu K_α radiation (λ = 0.15418 nm) using a scanning speed of 1 ^{o}/min. The resultant XRD patterns were compared with those from the standard commercial XRD database.

X-Ray Photoelectron Spectroscopy(XPS)

X-ray Photoelectron Spectroscopy (XPS) was performed using the Leybold-Heraeus LHS-10 instrument. The sample of the sorbent of ca. 200 mg was pressed into a pellet 16 mm dia. by a hydraulic press. The resultant pellet was loaded to the High Vacuum "loadlock" chamber (base pressure ~10^{-6} Torr), with the subsequent transfer to the high-vacuum (HV) XPS measurement chamber (10^{-8}-10^{-7} Torr). In XPS, the non-monochromated Mg Kα line with hv=1253.6 eV or Al Kα line with hv=1486.6 eV was used, and spectra were fitted by the XPSPEAK program. Sample charging effects were compensated by adjusting the XPS instrumental settings, until the Binding Energy (BE) of C 1s = 284.6 eV.

Electron Spin Resonance Spectroscopy (ESR)

The CW ESR spectra of the sorbent taken "as-is", either "calcined" or "sulfided", were recorded at the X-band on a Bruker EMX-6/1 EPR spectrometer composed of the EMX 1/3 console, an ER 041 X6 bridge with a built-in ER-0410-116 microwave frequency counter, an ER-070 magnet, and an ER-4102st standard universal rectangular cavity. Samples of the "sulfided" sorbent were transferred to the ESR test tube with a minimal exposure to ambient air. Samples were cooled to 77 K in a liquid nitrogen finger Dewar. All spectra were recorded with a field modulation frequency of 100 kHz, a modulation amplitude of 6 mT, a power incident to the cavity of 2 mW and a frequency of 9.37 GHz. Determination of the ESR spin concentrations were carried out under the nonsaturating conditions using 10 mM $CuSO_4$ solution in water as standard. ESR measurements with samples of the sorbent that were carefully outgassed in the High Vacuum (HV) of ~$1x10^{-6}$ Torr are consistent with those obtained upon the re-admission of air into the ESR test tubes. The BioEPR software was used for computer simulations of the ESR signals.

N_2 Adsorption and Desorption Isotherms:

Nitrogen adsorption/desorption isotherms at 77 K were measured by an Autosorb 1-C instrument

. Before measuring the total surface area, samples were outgassed for 3 h at 200 °C. The specific surface area, S_{BET} was calculated via the Brunauer-Emmett-Teller (BET) equation, and the total pore volume was calculated at $P/P_0 = 0.95$.

X-Ray Diffraction

XRD at room temperature was performed by a Rigaku Miniflex instrument and the diffraction patterns were obtained with the Ni-filtered $\underline{Cu\ K_{\alpha}}$ radiation (λ = 0.15418 nm), scanning speed of 1 ^{o}/min using commercial XRD libraries.

Chapter III: Wide Temperature Range H_2S Removal by Promoted ZnO/SiO_2 : Effect of Support, Entrapment in Microfibrous Media and Scale-up

Priyanka Dhage, Vivekanand Gaur[1], Hongyun Yang[2], Bruce J. Tatarchuk

Department of Chemical Engineering, Auburn University, Auburn, AL 36849, USA

[1]Filtrex Technologies Pvt Ltd. Bangalore - 560043, INDIA

[2]IntraMicron Inc. 368 Industry Dr. Auburn, AL, 36832, USA

Abstract

Promoted ZnO sorbents with formulation $M_{0.05}Zn_{0.95}O$ (M = Mn, Fe, Co, Ni, Cu) were supported on mesoporous silica gels such as MCM-41 and MCM-48. H_2S adsorption was conducted in temperatures ranging from room temperature to 400 ^oC in flowing 1%H_2S/H_2 at various moisture levels. The results of desulfurization tests on these sorbents at room temperature indicate that a copper doped ZnO (15% w/w)/MCM-41 sorbent ($Cu_{0.05}Zn_{0.95}O$/MCM-41) has the highest saturation sulfur capacity at 0.9 mol S/mol ($Cu_{0.05}Zn_{0.95}O$), which is approximately twice that of ZnO/SiO_2 sorbent at similar loadings. H_2S adsorption at elevated temperatures (ca. 400 ^oC), resulted in near total sulfidization of the available reactant regardless of dopant. At intermediate temperatures, the utilization of the reactant ($M_{0.05}Zn_{0.95}O$) toward H_2S removal depended on the support employed in the order MCM-41 > MCM-48 > silica gel. This dependence was investigated in terms of the support: surface area, pore volume, and pore size; using N_2 adsorption-desorption isotherms. With an

increase in ZnO loading on the silica support, the surface area, pore volume and pore size decreased. At equivalent levels of support surface area and pore size, higher pore volumes provided greater low temperature H_2S capacities, presumably as a result of the lower Zn $(NO_3)_2.6H_2O$ concentrations used during impregnation/drying and a diminution in $Zn_{0.95}M_{0.05}O$ crystallite size.

Keywords: H_2S removal; ZnO catalyst; Mesoporous silica; MCM-41; Breakthrough analysis

III.1. Introduction

High efficiency desulfurization is critical to maintain the activity of fuel processing catalysts and high-value membrane electrode assemblies in logistic fuel cell systems. On-board fuel processing of liquid hydrocarbon fuel is being investigated to supply hydrogen for fuel cell-based auxiliary power units. If sulfur is not removed from the liquid phase, the removal of sulfur as H_2S from the reformate is a key step since downstream catalysts and the fuel cell can be poisoned by a small amount of H_2S in the feed [3]. Depending on the fuel selection, additional ancillary components are required for processing the fuel to meet the fuel cell's requirement. Steam reforming catalysts, PEM anode catalysts and the shift catalysts are intolerant to sulfur, and the desulfurization step is very important to ensure adequate lifetime of fuel processors [61]. Hydrogen sulfide is present in many high temperature gas streams during extraction and processing of fossil fuels, natural gas and geothermal brines. H_2S is also found in many industrial process gases, particularly in the mineral and metallurgical process industries [62]. The sulfur compounds needs to be reduced to less than 1 ppmv for a clean environment because high concentration of sulfur compounds result in health hazards, air pollution, acid rain and corrosion of metallic materials. Hydrogen-rich fuel needs to be less than 100 ppb [63]. Metal oxides, in particular ZnO, are widely applied for gas desulfurization processes [64-66]. Westmoreland and

Harrison [13] have shown that the oxides of Fe, Mn, Zn, Ca, V, Cu, Co and W are the most suitable sorbents at temperatures above 300 ^{o}C. Among various metal oxides, the ZnO based sorbents have shown advantages of higher sulfur capacity and favorable sulfidation thermodynamics at moderate temperatures [67] . Silica supported with ZnO and/or doped with Cu is also a widely used catalyst for desulfurization [17, 20, 22]. In combination with high-temperature stability, low-temperature activity is highly desirable for a new catalyst. The removal of H_2S at high temperatures (ca. 350 ^{o}C) has been extensively studied, but little work has been reported in the literature for the development of low-temperature H_2S adsorbents [6]. Concerns about the removal of H_2S at low temperatures are growing because of its removal for fuel cell application and several other processes, including natural gas sweetening and the Claus process, wherein H_2S is by-product at low temperatures.

Mesoporous silica has been recently used as a support for metal catalysts, resulting in several cases in significant improvements when compared to commercial and conventional amorphous silica-alumina catalysts. Most of the literature on the mesoporous silica materials deals mainly with their synthesis and surface characterization. The mesoporous silica supports including MCM-41, MCM-48, SBA-15 are found to be the superior base matrix for various surface modifications with amines and their subsequent application in the low temperature removal of acidic gases like H_2S and CO_2 [36]-[37]. Very few studies are reported on the metal incorporation in mesoporous silica by incipient wetness impregnation. It is well-known that the surface area, porosity, and chemical nature of the oxide support can affect supported metal-catalyzed reactions. Therefore, it is interesting to compare adsorption capacity of metal oxide supported on mesoporous silica with conventional silica. Since ZnO has a high equilibrium constant for H_2S removal at ambient temperature, in the present work, mesoporous silica (MCM-

41 and MCM-48) supports are impregnated with ZnO by incipient wetness method. Additionally, the ZnO supported sorbents were doped with Cu and examined for desulfurization performance at room temperature. These materials were characterized by XRD, N_2 adsorption, and SEM to obtain detailed information in the development of new sorbents. The influence of moisture on H_2S removal was also discussed. After the adsorption tests, the catalysts were thermally regenerated for multiple adsorption-desorption cycles.

IV.2. Experimental Section

III.2.1 Silica support

Different types of silica supports including MCM-41, MCM-48 silica and conventional silica gel were used in this study. The MCM-41 used in this study was procured from Sigma Aldrich and used as-received without any further purification. The MCM-48 was prepared as described in Chapter II by Schumacher and co-workers [60].

III.2.2 Sorbent impregnation

The metal nitrate solutions of different transition metals were used as precursors for impregnating the MCM (-41 and -48) and silica support with different ZnO and doped ZnO loadings. The impregnated supports samples were dried at 100^{o}C for 6h and subsequently calcined at 350^{o}C for 1 h under air flow. All the samples were stored in desiccators for further use.

III.2.3 Adsorption experiment

The experimental set-up and procedure are described in Chapter II. The adsorption experiments for desulfurization were carried out at ambient conditions (20 ^{o}C, 1 atm). An inlet concentration of 1 % (v/v) H_2S in H_2 (ultra high purity grade; from Airgas South, Inc.) was used as sulfur source at a face velocity of 2.12 cm/s, corresponding to the volumetric gas flowrate of 1900 h-1 GHSV (0.1 slpm). H_2S uptakes during the dynamic adsorption experiments were measured using a gas chromatography (GC) instrument (Varian 3800) equipped with thermal conductivity detector (TCD). In each adsorption run, 0.5 g sample was packed in the reactor. In this study, the breakthrough time was defined as the time from beginning of the desulfurization to the time when the H_2S concentration at the exit reached 100 ppmv.

IV.3. Sorbent Characterization

Nitrogen adsorption/desorption isotherms at 77 K were measured using Autosorb 1-C model from Quantachrome Instrument Corporation. Prior to measurement, all samples were degassed for 10h at 200 °C. Specific surface area, S_{BET} was calculated using the BET equation. Total pore volume, V_P was calculated at $P/P_0 = 0.95$. The pore width, P_w distribution over the range of $\sim$(2–80 nm) was generated from the adsorption branches of the isotherms via the BJH method. Calculations were performed using Autosorb 1C software. XRD patterns were obtained using a Rigaku Miniflex diffractometer at room temperature using CuK_α radiation. Diffraction patterns were obtained with Ni-filtered CuK_α radiation (λ = 0.15418 nm) using a scanning speed of 1^{o}/min and an accelerating voltage of 30 kV. The resultant patterns matched with standard data for ZnO for the purpose of phase identification. The surface morphology of the MCM samples before and after metal impregnation was investigated with Scanning Electron Microscopy (SEM). Prior to SEM (Zeiss Digital Scanning Microscope DSM940), the samples were vacuum coated with gold (Pelco SC-7 auto sputter coater).

III.4 Results and discussion

III.4.1 Preparation and characterization of ZnO supported sorbents

XRD patterns of MCM-41 and MCM-48 are shown in Fig. III.1 (a-b).

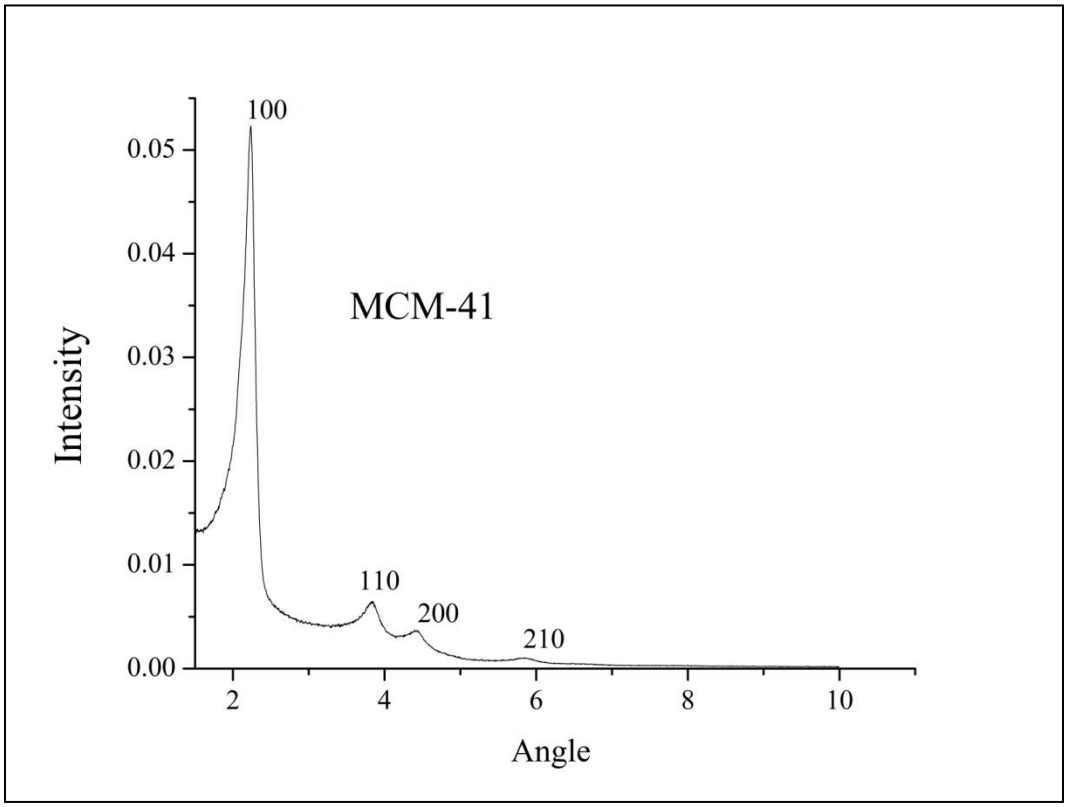

Figure III.1a: XRD Pattern of the MCM-41

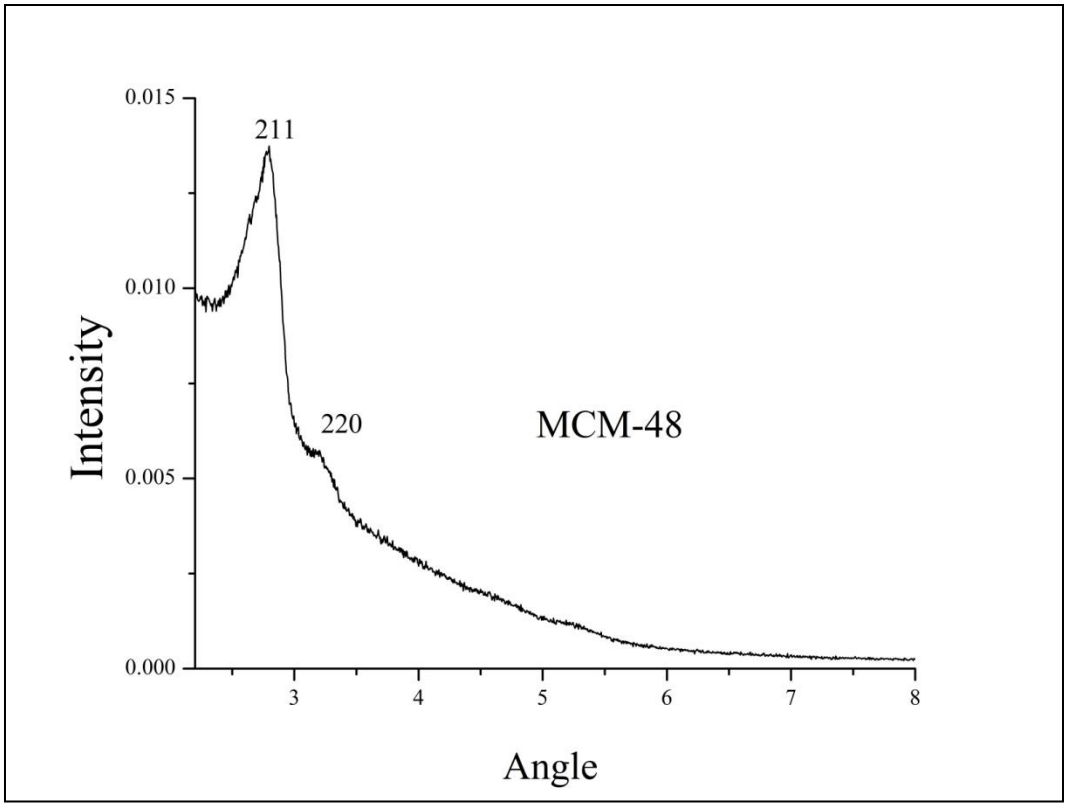

Figure III.1b: XRD Pattern of the Lab-made MCM-48

The MCM-48 was made in the lab and the XRD pattern was obtained to compare with the literature to ensure the ordered mesoporous structure. The diffraction peaks obtained at 2 angles of 1.8^{o}, 3.6^{o}, 4.5^{o}, 5.5^{o} for MCM-41 and 2.7^{o}, 3.2^{o} for MCM-48 confirmed the structure of the same as also reported elsewhere[68],[69]. The pore structure analysis obtained by nitrogen adsorption/desorption isotherms further confirmed the mesoporosity and that ZnO loading occurred inside the pore channels of the MCM-41 support. The degassed MCM samples showed a type IV isotherm as shown in Fig III.2(a-b).

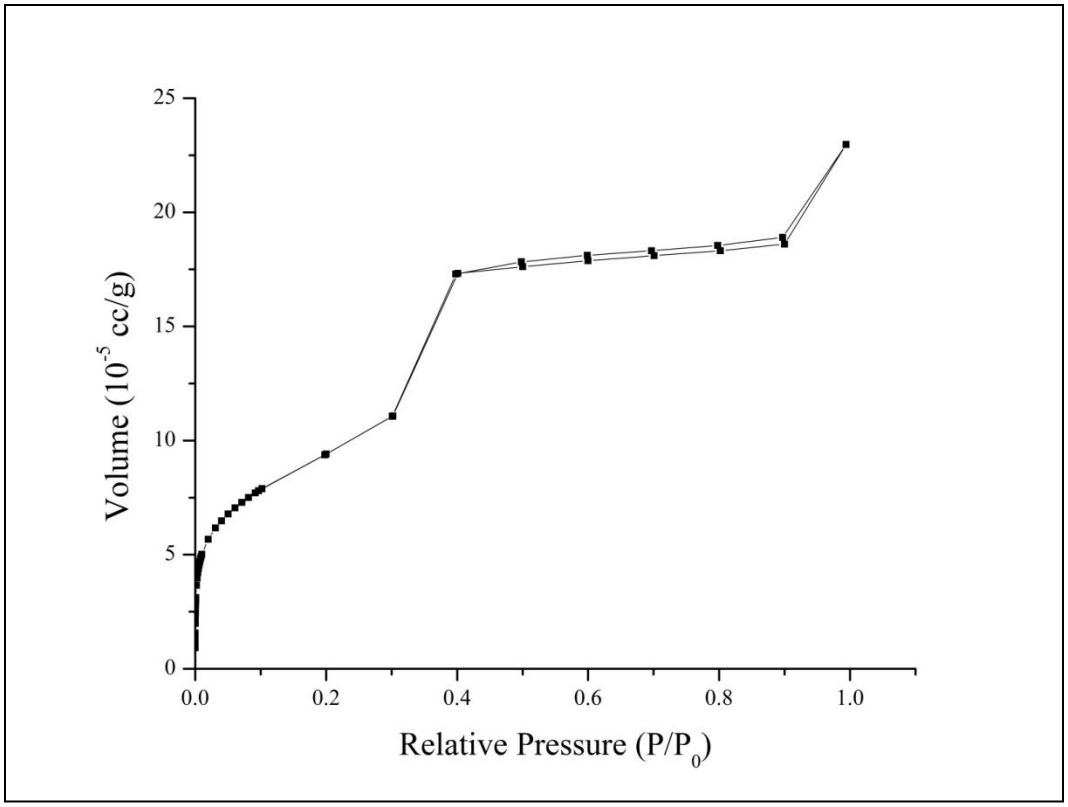

Figure III.2a : N_2 adsorption-desorption isotherm for MCM-41- Commercial

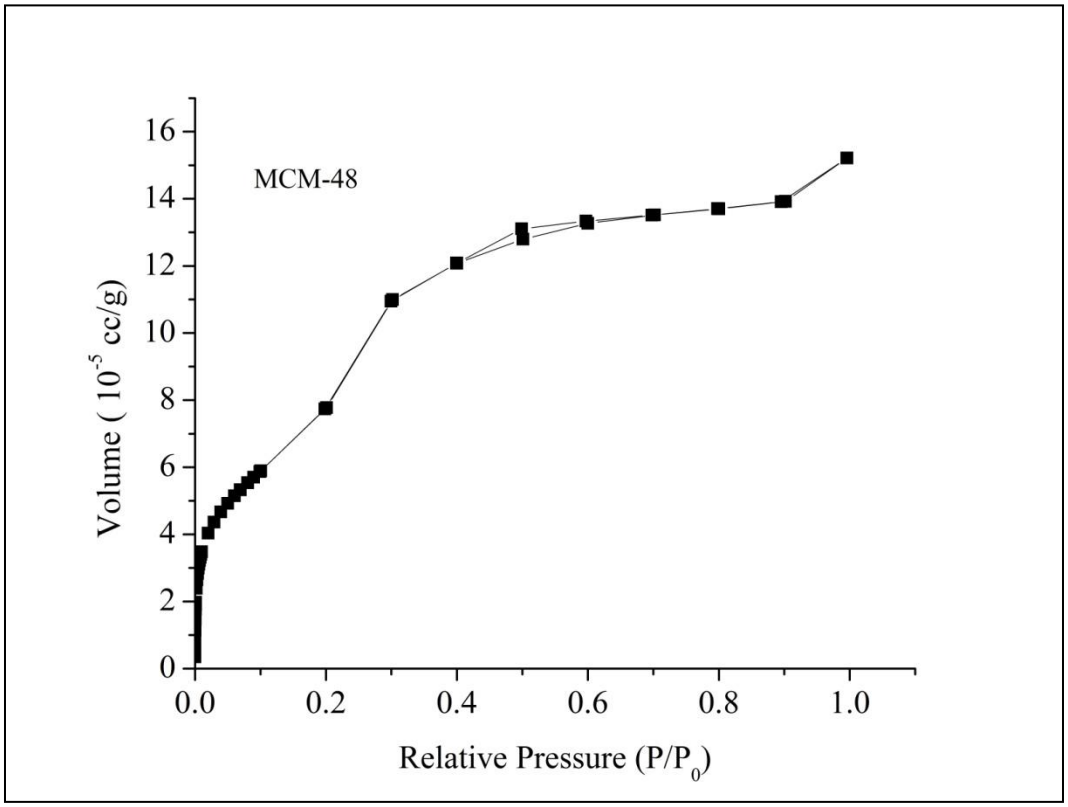

Figure III.2b : N_2 adsorption-desorption isotherm for MCM-48 – Lab made

The isotherms also confirm that after impregnation with ZnO and/or doped with CuO, the mesoporous pores were not completely filled or blocked, resulting in the preserved type IV isotherm, allowing liquid nitrogen to access the pores the pores. The surface area, pore volume, and pore size of MCM-41, MCM-48 and SiO_2 before and after impregnation with ZnO are shown in Table III.1.

Table III. 1. Structural characteristics of Silica sorbents determined by N_2 adsorption

Sample	**ZnO loading (w/w%)**	**S_g (m^2/g)**	**V_t (cc/g)**	**W_{avg} (nm)**	**Avg. Pore Size (nm)**

MCM-41	0	1260	1.30	2.45	4.1
ZnO/MCM-41	15	850	0.74	2.58	3.5
ZnO/MCM-41	25	672	0.71	2.25	3.5
Cu/ZnO/MCM-41	15	524	0.52	2.51	3.6
MCM-48	0	1420	1.10	2.53	3.1
ZnO/MCM-48	15	631	0.47	2.26	3.0
ZnO/MCM-48	25	592	0.45	2.26	3.0
Cu/ZnO/MCM-48	15	303	0.32	2.58	4.2

S_g: Specific surface area calculated from the BET equation; V_g: Total pore volume; V_{micro}: Micropore volume; W_{avg}: Average pore width determined from DR method

The BET area as well as the pore volume of all the support samples decreases on impregnation with the metal oxide. As metal loading increases, the surface area and pore volume decrease. SiO_2-supported catalysts have BET surface area between 200 and 300 m^2/g and large pore volumes. As the loading of ZnO was increased from 0 to 15% (w/w), the BET area, pore volume, and the average pore size decreased. The decrease in the BET area in MCM-41 and MCM-48 samples was observed to be from 1260 and 1420 m^2/g to 850 and 592 m^2/g, respectively. The

pore volumes were also decreased to almost half. Furthermore, on promoting the ZnO-based samples with 5 mol% CuO, the BET area and pore volume further decreased considerably. On the other hand, in the Cu-promoted samples, pore size was observed to increase significantly (in SiO_2) or marginally (in MCM). This indicates that impregnation of silica supports with metal oxides may result in an decrease in micro porosity and an increase in macro or meso porosity. In other words, it may be concluded that the metal oxides are preferentially dispersed in the interior of the porous texture of Silica, which results in the blocking of mainly the micropores and in the development of pores opening.

The pore size, surface area and pore volume of MCM-41 before and after ZnO loading were obtained from the nitrogen adsorption/desorption isotherms. Likewise, for the adsorption isotherms of Cu-promoted and unpromoted ZnO/MCM-41 shown in Figure III.3.

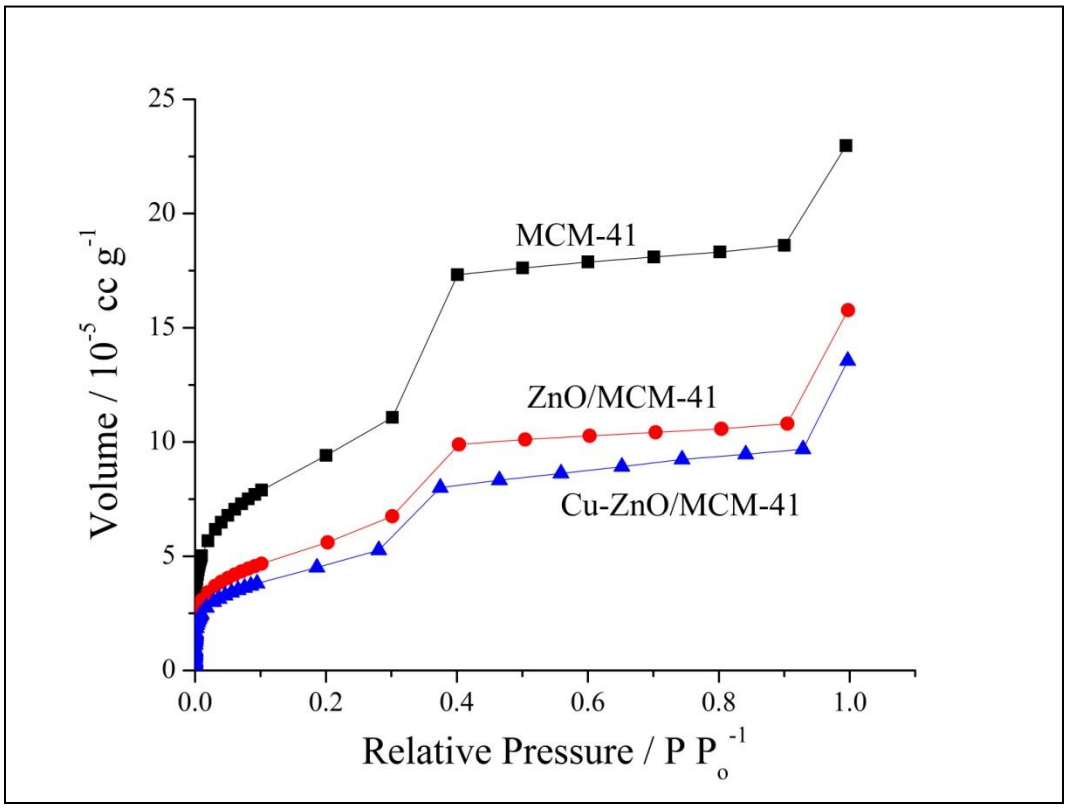

Figure III. 3a: N_2 adsorption isotherms for MCM-41, ZnO/MCM-41 and Cu-ZnO/MCM-41

The PSD of the MCM-41 and MCM-48 are shown in Fig III.3(b-c), it indicates the pore size in the range of 2-4 nm for both the MCM samples.

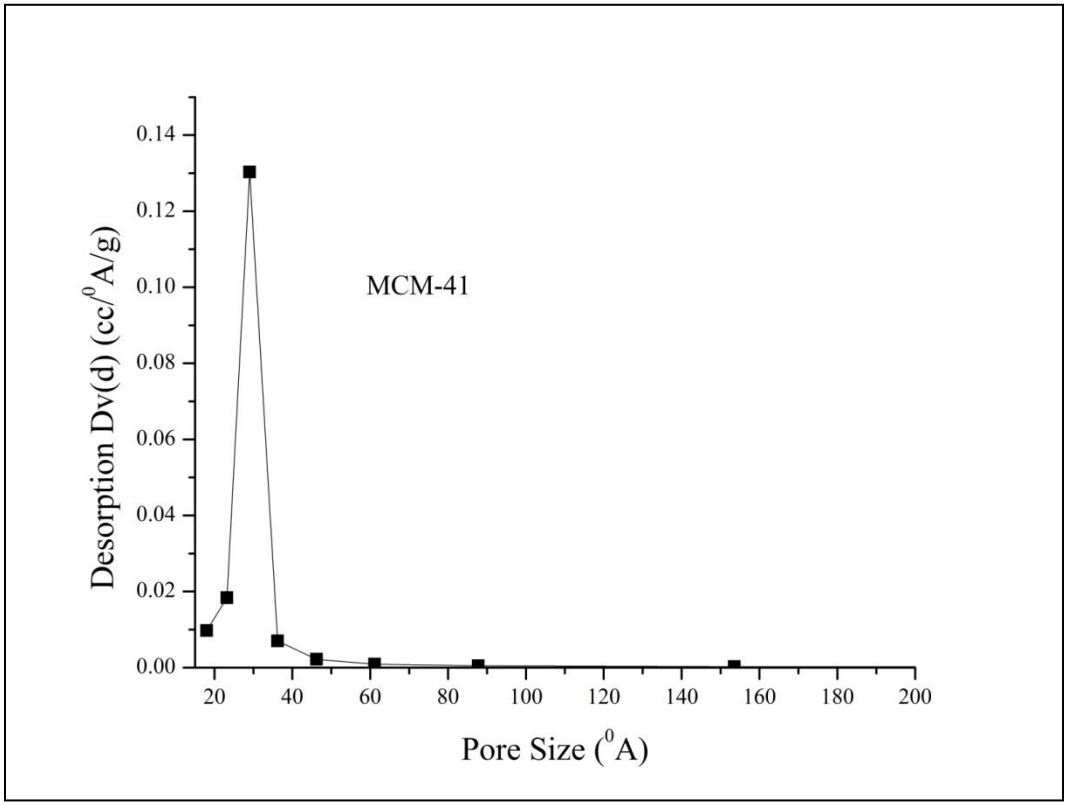

Figure III. 3b : Pore Size Distribution of MCM-41 (commercial)

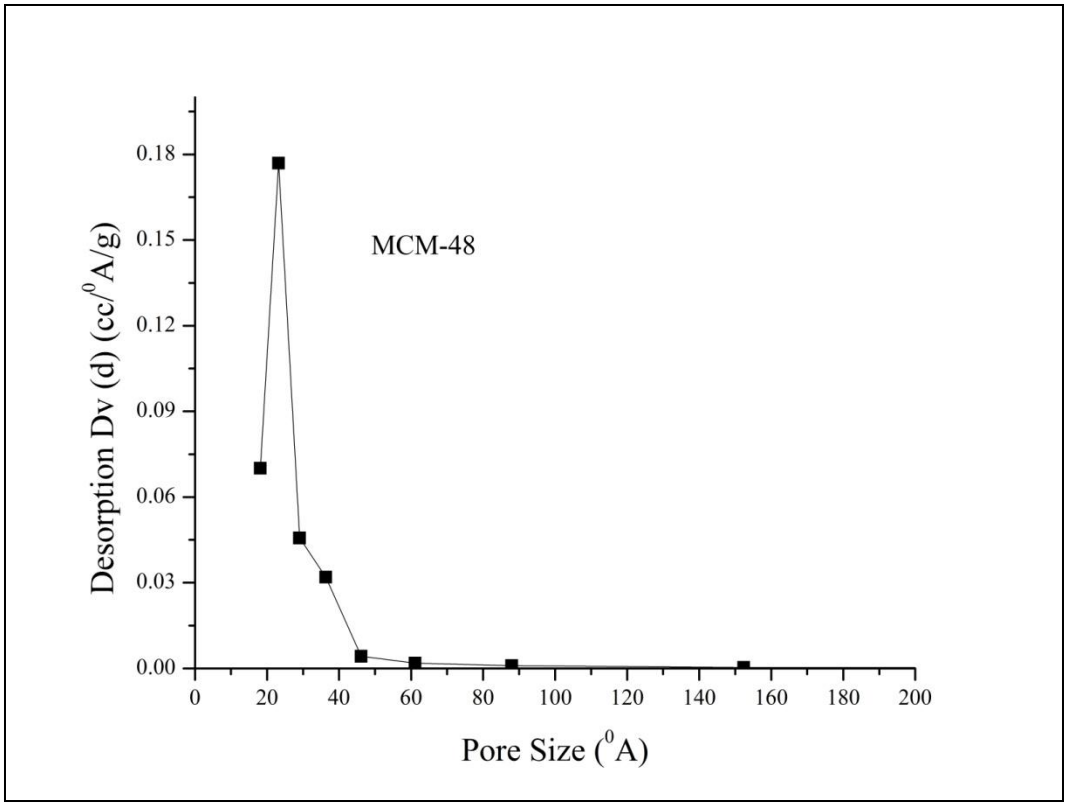

Figure III. 3c: Pore size distribution of MCM-48 (Lab made)

The PSD data is shown in Table III.1 and Fig III.3(b-c). The pore size of the MCM-41 support was 4.14 nm. After the ZnO was loaded into its channels, the pore size decreased. The pore size of ZnO (8%)/MCM was 3.5 nm, smaller than that of the MCM-41 support, which confirmed that ZnO was dispersed into the MCM-41 pore channels. With increasing ZnO loadings, the pore size further decreased, but only marginally. The pore sizes were 2.29 and 2.25 nm for ZnO (15%)/MCM-41 and ZnO (25%)/MCM-41, respectively. The surface area and the pore volume of MCM-41, after ZnO loading, exhibited the same trends as the pore size.

The morphology of MCM-41, MCM-48 and ZnO loaded MCM-41 and MCM-48 was viewed by SEM as shown in Fig III 4.

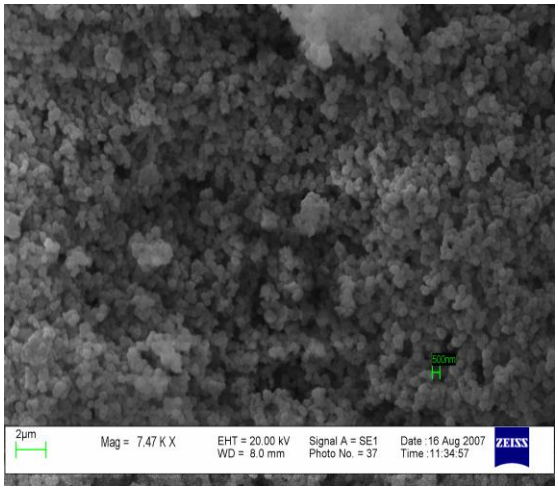

Figure III. 4a: SEM image of MCM-48 sample before impregnation - MCM-48 Blank

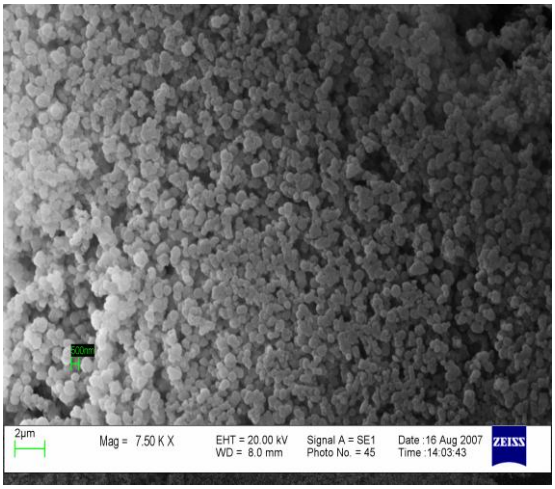

Figure III. 4b: SEM image of MCM-48 sample after impregnation - 15 % ZnO / MCM-48

The particle size of the MCM-41 and MCM-48 support was 5–10 µm. The MCM-41 particle was made of loosely packed small particles with submicron size. After impregnation with ZnO, the particle size of MCM-41 remained unchanged, this indicated that ZnO was dispersed into the support pores and was not deposited on the outer surface of the particles.

III.4.2 Effect of different types of metal oxides

In order to find an optimal sorbent for H_2S removal at ambient temperature, a number of adsorption experiments have been carried out on silica dispersed with different transition metal (Zn, Cu, Mn, Fe, Co and Ni) oxides. Fig. III.5a compares the breakthrough capacities of H_2S for various metals at room temperature. Different metal oxides supported on SiO_2 at almost identical loading of 21% (w/w) showed distinct performances. ZnO/SiO_2 showed the highest (~ 48 mg sulfur/g sorbent) capacity. On the other hand, iron, cobalt and nickel oxides supported silica samples are not effective candidate because they showed almost no capacity under identical operating conditions. *As a result, the H_2S adsorption performance of the supported metal oxides increased in the order: $Fe \cong Co \cong Ni < Mn < Cu < Zn$.*

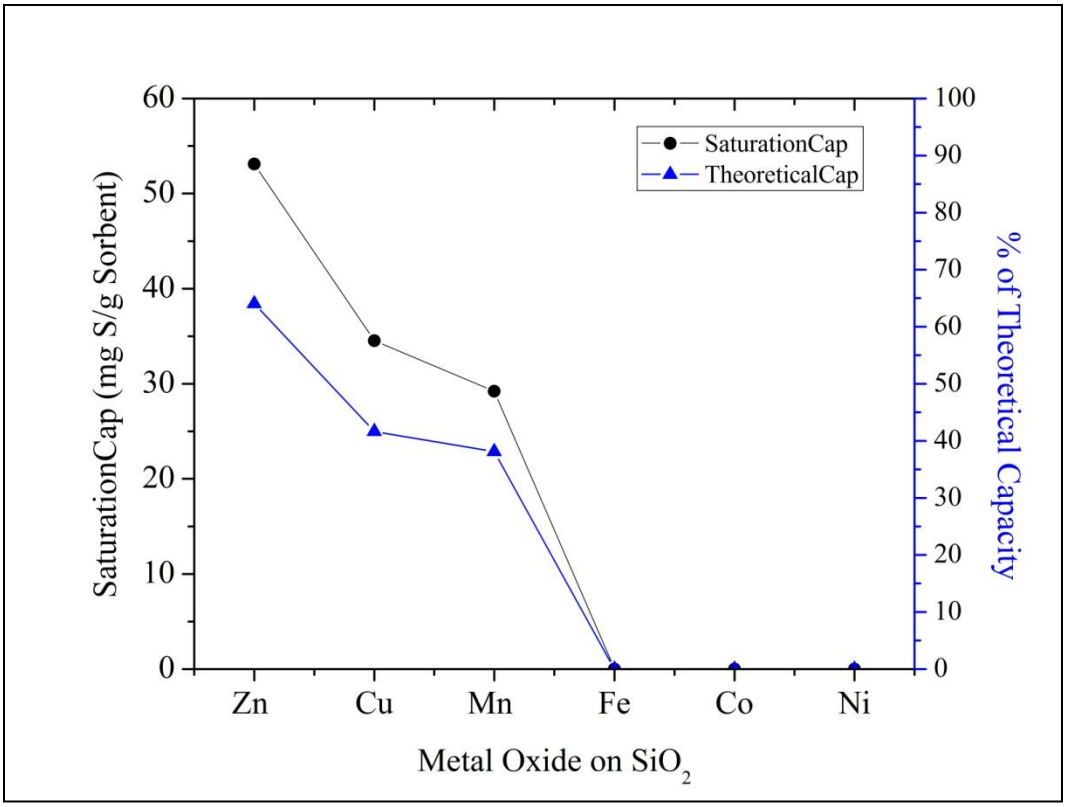

Figure III. 5a: Breakthrough capacity and % theoretical capacity valuesa for different metal oxides with same loading on silica tested at RT, Q= 100 cc/min, face velocity = 2.12 cm/s, Calcination condition = 350 C/1h, Wt. = 0.5 g.

The thermodynamic data of the reaction of the metal oxides with H_2S was obtained using the HSC software as shown in Fig III.5b. The formulae for saturation capacity and % theoretical capacity are given in appendix I. It shows that ZnO and CuO have favorable thermodynamics with lower outlet equilibrium concentrations (ppmv). This compliments the results obtained by the H_2S adsorption study conducted at room temperature on these metal oxides supported on silica with approximately similar metal oxide loadings. CuO showed better sulfidation thermodynamics than other oxides but CuO is unstable over the range of temperature.

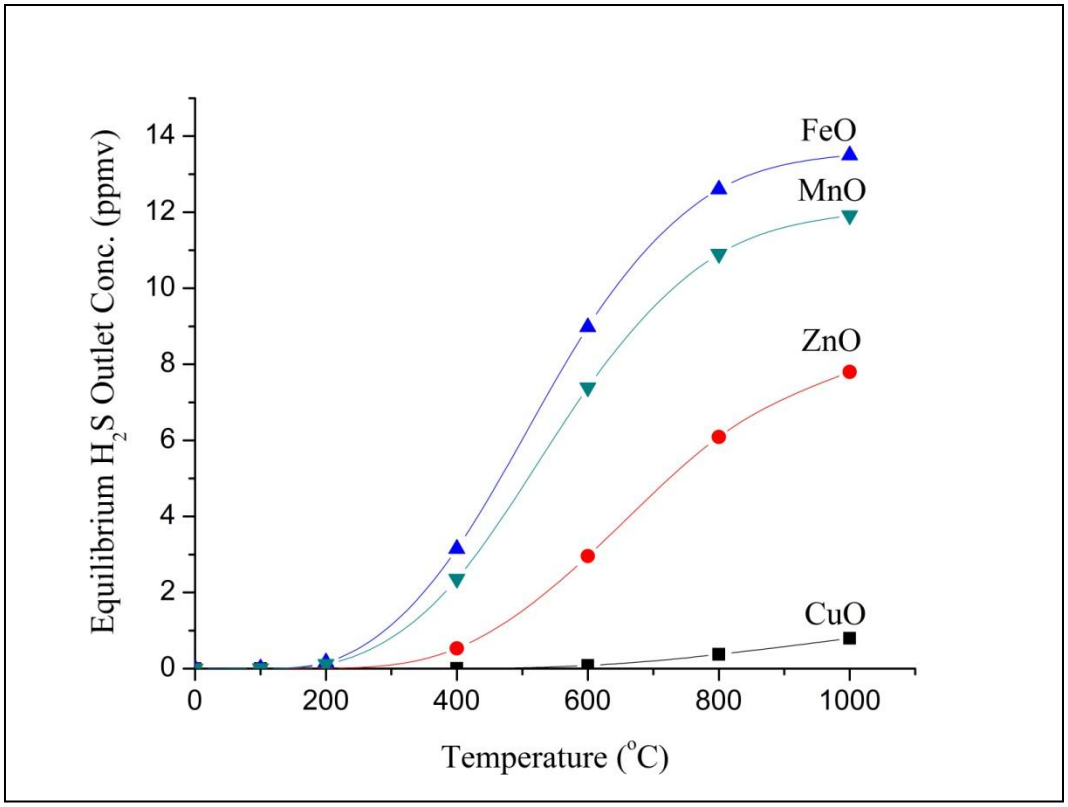

Figure III. 5b: Equilibrium H_2S concentration data generated using HSC software for various metal oxides

III.4.3 Comparison with the commercial ZnO

The H_2S adsorption of the ZnO/SiO_2 (21 wt%) was compared with the commercial ZnO samples obtained from Sud-Chemie (G-72E) and BASF (SG-901).The breakthrough performance of the three sorbents, tested at same conditions – V_f= 2.12 cm/s, sample wt = 0.5 gm, temperature = 20^{o}C, is shown in the Fig. III.6.The nature of the breakthrough curve differs for these sorbents indicating different diffusion mechanisms in each case due to the difference in the sample preparation. The commercial sorbents contain over 90% of pure ZnO with small amounts of binder whereas the ZnO/SiO_2 contains 21wt% impregnated on the silica and contains

uniform nanocrystals of the ZnO dispersed in the porous silica matrix. This leads to better ZnO utilization and adsorption capacity of the sorbent even at room temperature.

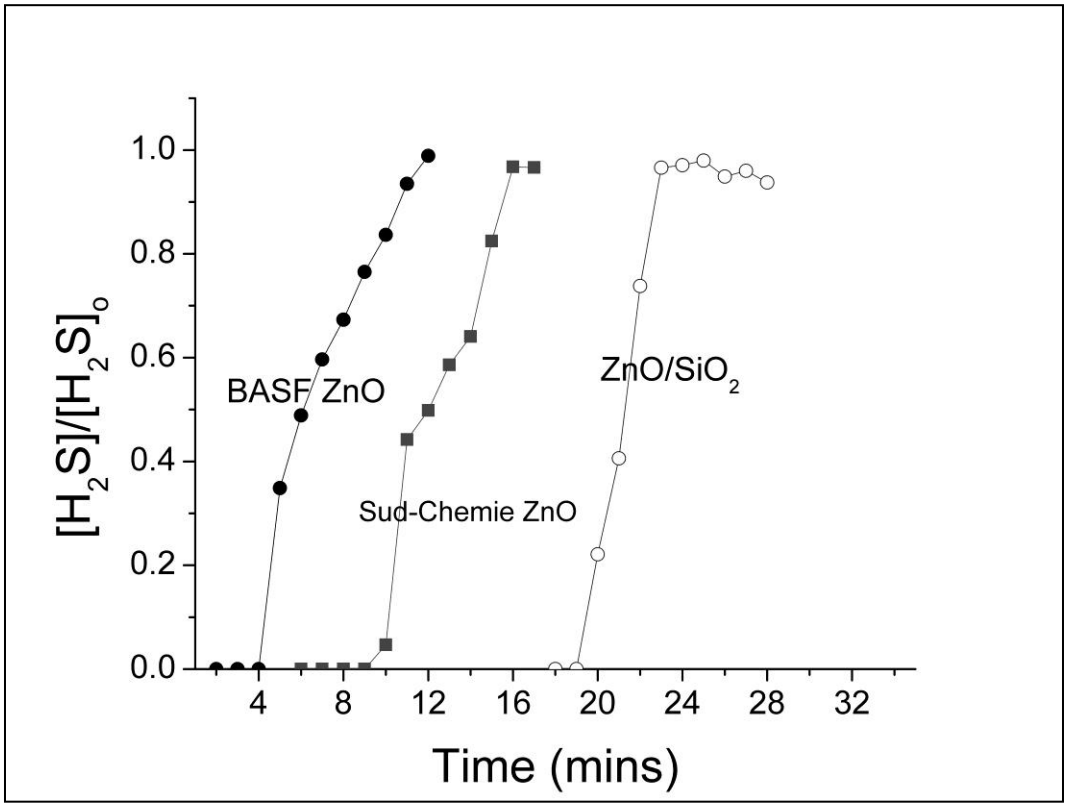

Figure III.6. Breakthrough curves for commercial ZnO and ZnO/SiO_2: T = 20 C, C_o = 1Vol% H_2S/H_2, Face Velocity = 2.12 cm/s, Wt. =0.5 gm

The shape of the breakthrough curve indicates that the adsorption (diffusion mechanism of the H_2S to ZnO) is different in all these cases. This is mainly due to the method of preparation of the sorbent. The lab-made ZnO/SiO_2 shows a desirable sharp breakthrough curve. The commercial ZnO were in the form of extrudates crushed to same size as SiO_2 (150-200 microns) for comparison. The extrudates contain approx. 90 % pure ZnO and rest is binder. The ZnO/SiO_2 (21 wt% loading) shows maximum H_2S capacity as compared to commercial extrudates with ~

90% ZnO loading. *The ZnO on the silica matrix is present in the form of nanocrystals with uniform dispersion, thus ensuring maximum accessibility to H_2S and this leads to higher capacity.* No XRD pattern was observed when the sample was tested indicating that the ZnO crystal size is < 4 nm.

III.4.4 Screening test for the metal oxide

Different metal oxides supported on SiO_2 at almost identical loading of 21% (w/w) showed distinct performances. ZnO/SiO_2 showed the highest (~53.12 mg sulfur/g sorbent) capacity. On the other hand, iron, cobalt and nickel oxides supported silica samples are not effective candidates because they showed almost no capacity under identical operating conditions. As a result, the H_2S adsorption performance of the supported metal oxides increased in this order: Fe ≅ Co ≅ Ni < Mn < Cu < Zn. The MCM materials exhibited a superior affinity to H_2S, and the desulfurization capacity is up to 0.9 mol S/mol sorbent at ~15% ZnO loading. Likewise, the capacity decreased with further increases in ZnO loading. This suggests that an optimum loading of metal oxides exists for every silica support depending on the support pore volume. An excess of 15% (w/w) ZnO loading on MCM-41 may result in the formation of relatively larger metal crystallites which may cause the blockage of micro and mesopores of the silica support. A similar explanation of the excess of ZnO loading is reported elsewhere [2]. During the desulfurization reaction, the reaction-product may plug the pores and limit the gas diffusion, resulting in a decrease in H_2S capture. The SEM images, as presented in Fig. III.4, showed spherical type morphology for the ZnO supported MCMs which is rather similar to their blank MCM-41 and MCM-48, and no zinc oxide aggregates were observed on the external surface of particles. Thus, the adopted method allowed the persistence of MCM-41 texture with

zinc oxide inserts in the MCM framework and/or forms finely divided zinc oxide nanoparticles in the pores of MCM samples.

III.4.5 Effect of promoter

To investigate the influence of the doped ZnO on the desulfurization activity, a series of metal (M) doped ZnO supported on silica (M-ZnO/SiO_2) with M/Zn atomic ratio of 5/95 were prepared by incipient wetness method. Here, M includes transition metals, including Mn, Fe, Co, Ni and Cu oxides. In all the promoted sorbent samples, the total (Zn + M) metal oxide loading was kept at 21% (w/w). Table III.2 shows the comparative desulfurization capacity of promoted and un-promoted ZnO-SiO_2 at room temperature.

The $CuO_{0.05}ZnO_{0.95}/SiO_2$ showed the highest saturation capacity followed by $FeO_{0.05}ZnO_{0.95}/SiO_2$. The decreasing order of H_2S removal at saturation level may be expressed as: $CuO_{0.05}ZnO_{0.95}/SiO_2$ > $FeO_{0.05}ZnO_{0.95}/SiO_2$ > $CoO_{0.05}ZnO_{0.95}/SiO_2$ > $NiO_{0.05}ZnO_{0.95}/SiO_2$ ≈ $MnO_{0.05}ZnO_{0.95}/SiO_2$. The saturation capacity of ZnO/SiO_2 increased by approximately 31% and 23% on Cu- and Fe-promotion, respectively. To compare the relative effect of doping on saturation capacity during desulfurization, theoretical utilization of metal (Zn + Cu) oxides was also calculated. Table III.2 shows the results obtained for M-ZnO/SiO_2. The percent metal utilization for H_2S sorption was highest for Cu and followed the same trend as for the saturation capacity. Interestingly, approximately 90% Zn/Cu was utilized at room temperature as shown in Fig.III.7 . Similar experiments were performed for Cu-ZnO/MCM-41 and Cu-ZnO/MCM-48, and the obtained results showed the same trend. It is proposed that Cu-promoted ZnO/SiO_2 may have increased defects on the ZnO surface and higher intra-particle diffusivity. The Cu doping may significantly change the crystallite size of ZnO.

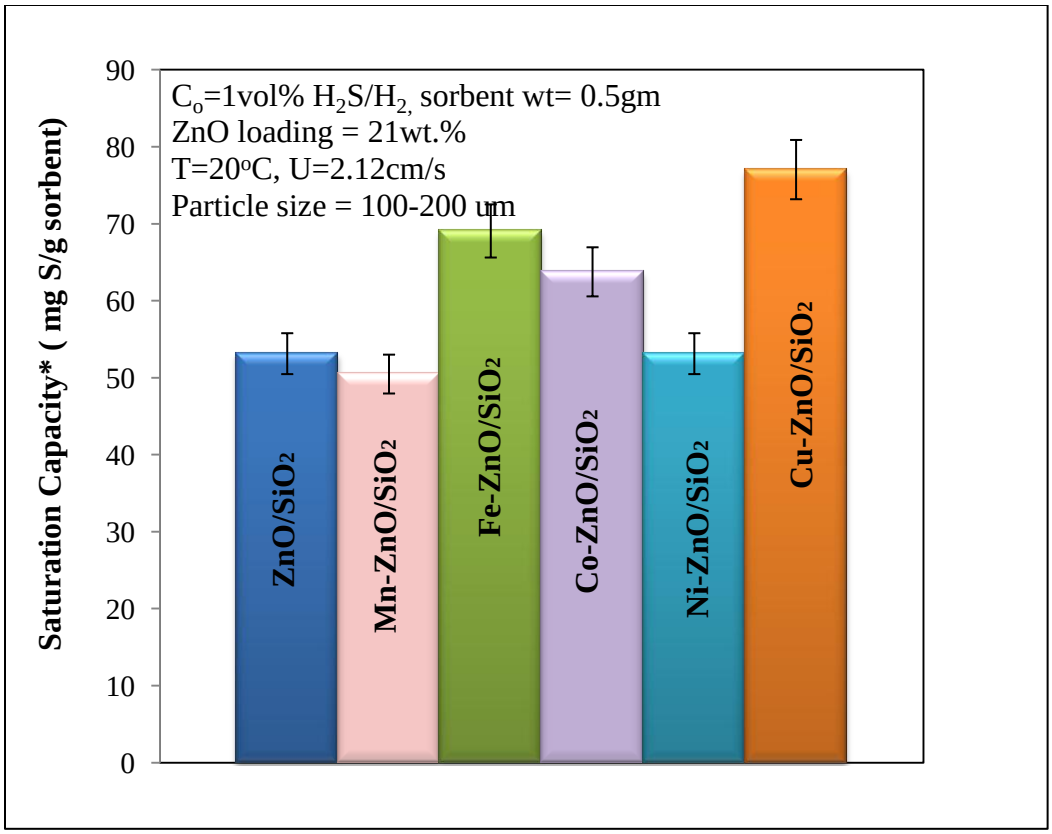

Figure III.7. Saturation capacity of the doped sorbents

Hypothesis:

The dopant (usually added in small quantities) serves to

- Reduce crystallite size
- Increase surface area
- Add defects to the structure (thus enhancing the accessibility of the H_2S to active metal for adsorption)

Table III.2. Saturation capacity values of the doped sorbents and commercial sorbents

Dopant@5mol% $M_{0.05}ZnO_{0.95}/SiO_2$	**Saturation Capacity (g S/g ZnO)**	**% of Theo. Capacity**
MnOx(1<x<1.5)	0.24	59.31
Fe_2O_3	0.33	81.25
Co Ox(1<x<1.5)	0.30	75.00
NiO	0.25	62.51
CuO	0.37	90.63
ZnO(un-doped)	0.25	62.51
ZnO (BASF SG-901)	0.02	4.96
ZnO (Sud-Chemie G-72E)	0.04	9.8

III.4.5.1 Effect of change in concentration of the promoter

Promoted ZnO sorbents, $M_xZnO_{(1-x)}/SiO_2$ where $0 \leq x \leq 1$ and (M, N = Cu, Ni, Mn, Fe, Co, Mg); were made by incipient impregnation method on SiO_2 with nitrates (2 M conc.) as precursors. The challenge gas was chosen as 1 vol% H_2S/H_2, outlet gases were analyzed by TCD-GC (Varian CP3800). The concentration of the dopant was varied from 0-100% for the Cu_x-$ZnO_{(1-x)}/SiO_2$, the sorbent shows highest adsorption at the $Cu_{0.2}ZnO_{0.8}/SiO_2$ indicating that the dopant concentration can be changed in the range of 5-20 atomic % with effective sulfur adsorption as shown in Fig.III.8.

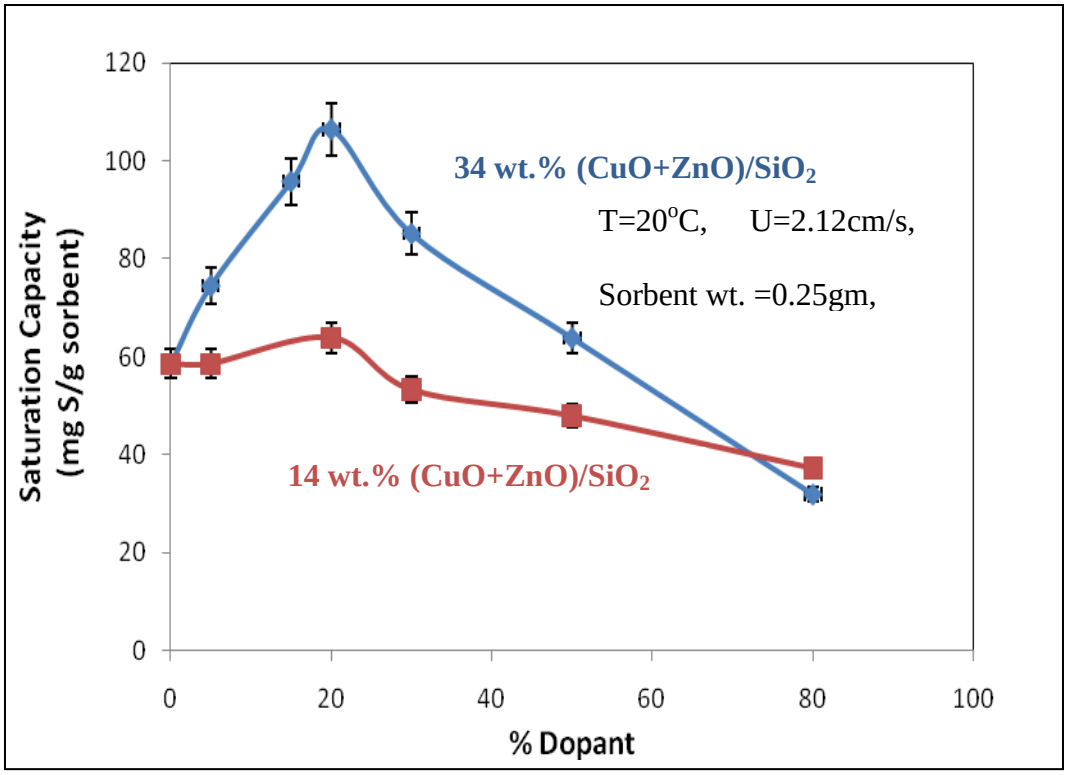

Figure III. 8. Saturation Capacity of the sorbents with varying Cu concentrations

Hypothesis: *When you have less dopant the dopant acts as adding more defects and hence adding this you are exposing more surface area , while if you keep adding a dopant that means you are replacing zinc with a less effective sorbent and hence after a certain optimum it keeps on dropping*

III.4.6 Effect of pore volume

To study the effect of pore volume, surface area of the support on the adsorption capacities of the sorbent silica (including mesoporous silica) of varying pore volume (0.6-2 cc/g), surface area (300-1200 m^2/g) were tested. ***Hypothesis**: The single step wetness impregnation metal loading*

increases as the pore volume of the support increases and this leads to increased sulfur adsorption capacity. Table III.3 shows silica of varying pore volume compared with MCM-41 and commercial ZnO. Higher the pore volume, higher is the ZnO that can be loaded in single step incipient wetness impregnation method and hence higher capacities are observed as shown Fig.III 9a [5].

Table III. 3. Capacity values of the silica with varying pore volumes and their adsorption capacities

Silica Pore volume (cc/g)	**Wt.% ZnO loaded**	**Expt. Saturation capacity (mg S/g sorbent)**	**Expt. Sat. Cap. % of theo. Cap. (392 mg S/g ZnO)**
0.8	11.50	18.65	41.4
1.15	15.80	31.87	51.4
1.65	21.20	50.46	60.7
1.8	22.66	53.21	59.9
0.23 (Sud-Chemie-G 72E)	90	34.58	9.8
1.0 (MCM-41)	14.00	55.77	94.8

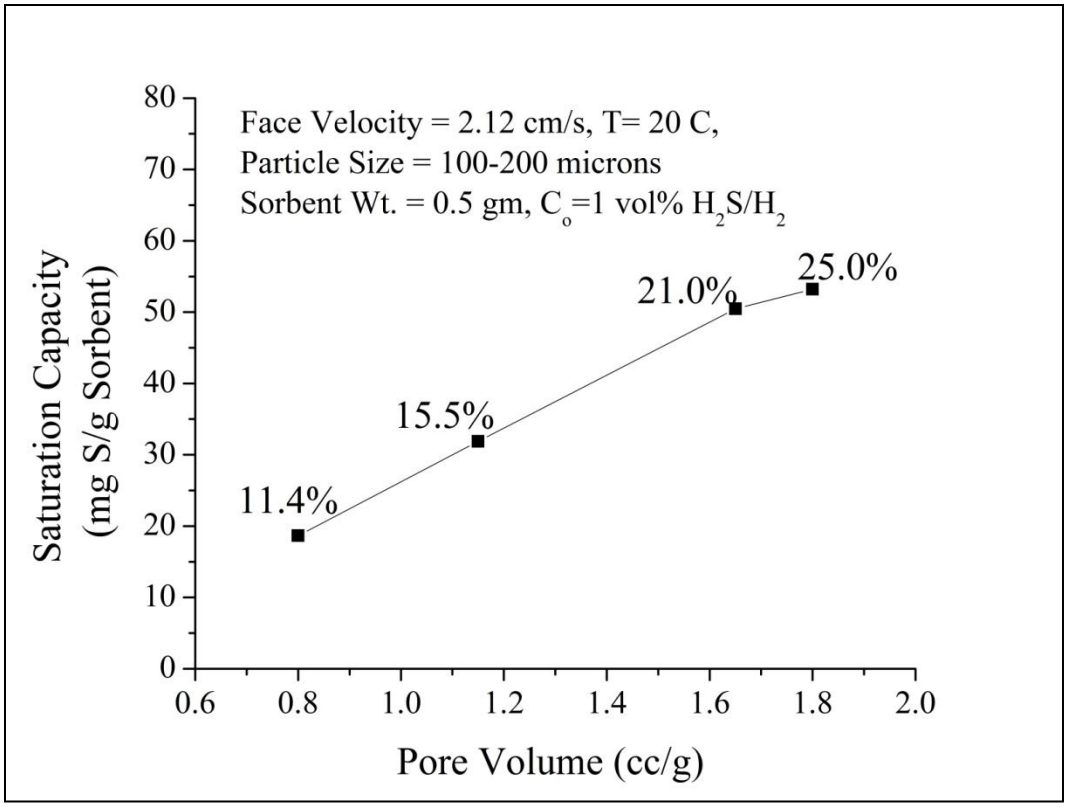

Figure III.9a. Saturation Capacities of the different silica with varying pore volume (i.e. varying ZnO loading)

Higher ZnO loadings lead to higher sulfur adsorption capacities but then for a given silica, how much of ZnO can be loaded that can still effectively remove per unit ZnO. This was studied in the next study as shown in Fig III.9b, where the type of silica support was kept same and varying amounts of ZnO were loaded by changing the concentration of the precursor. The Fig III.9b. shows that there an optimum loading for a given silica (pore volume and surface area), where the sorbent shows the maximum sulfur adsorption at a given operating condition. Single step impregnation ZnO loadings were varied on SiO_2 to obtain a series of ZnO/SiO_2 from 12 wt% - 36 wt% (Surface area: 300 m^2/g, Pore volume: 1.65 cc/g) by changing the concentration of the nitrate precursor from 0.5-3.5M. As the loading increases above 21wt% we expect the adsorption capacity to rise but after 21wt% loading the capacity goes down as indicated in Fig III.9b.

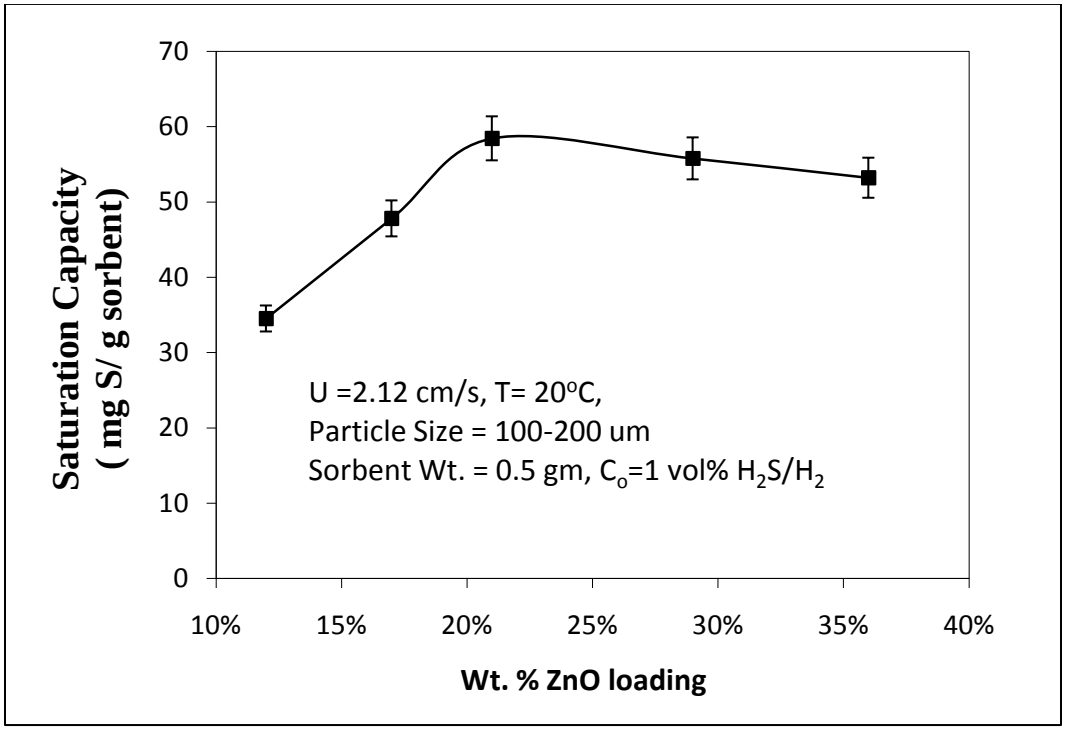

Figure III.9b. Saturation capacity of ZnO/SiO_2 with varying ZnO loading

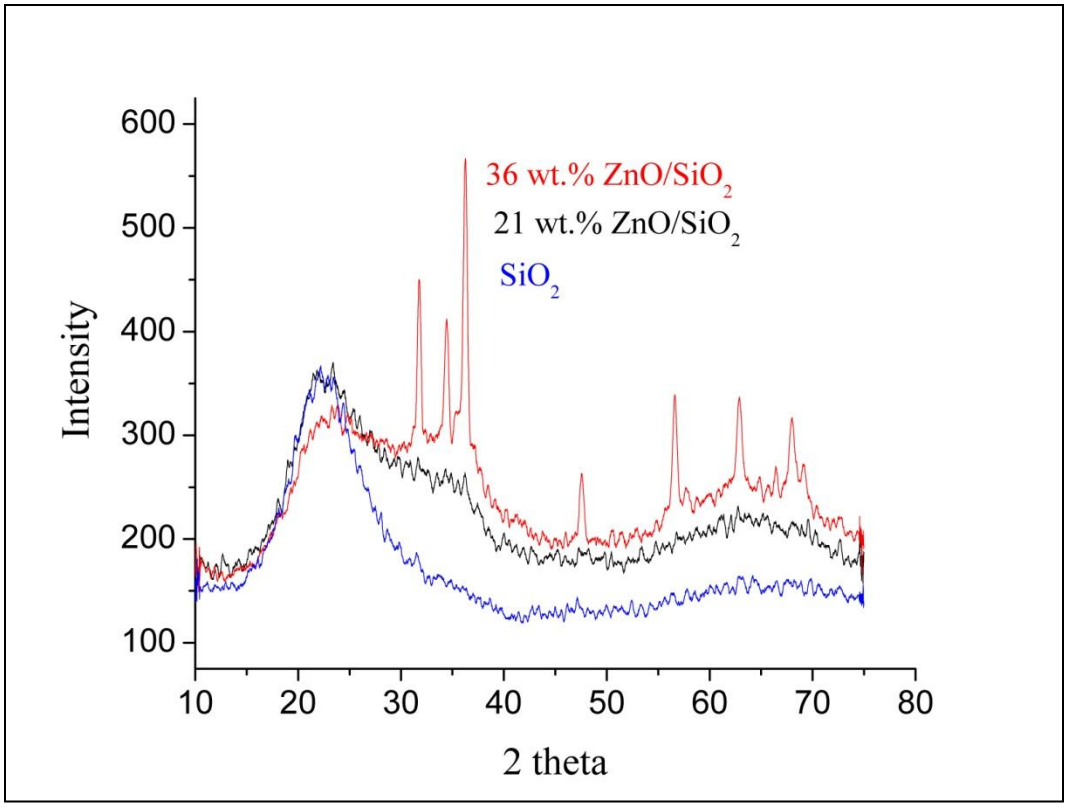

Figure III.9c. XRD patterns for silica and ZnO/SiO2 with varying ZnO loadings

***Hypothesis**: Use of higher concentration of the nitrate precursor leads to formation of larger ZnO crystallite size which can lead to blocking of the pores and hence limit the access of the gas to the complete pore.*

This was also verified by obtaining XRD of the samples, shown in Fig. III.9c. It was evident that until 21wt.% no XRD peaks were observed, indicating that small crystallite size which is probably uniformly distributed in the silica matrix but as the loading goes to 36wt. % significant ZnO peaks were observed by XRD. Fig III.9d. shows the effect of adding CuO into ZnO/SiO_2. Here 36 wt% ZnO/SiO_2 was used and this loading was kept constant only the concentration of the Cu was varied from 5-100%. The pattern shows that with 5% CuO in ZnO/SiO_2 the XRD pattern is similar to that of ZnO/SiO_2, indicating that CuO is still amorphous and is distributed

inside the matrix of ZnO/SiO_2. The 36wt.% CuO/SiO_2 shows clear peaks of existence of CuO. This can be compared to the XRD pattern obtained from pure $Cu_{0.05}Zn_{0.95}O$ and ZnO obtained from pure powders made by calcined the nitrates of respective solutions at 350 C/1h in air as shown in Fig. III. 9e.

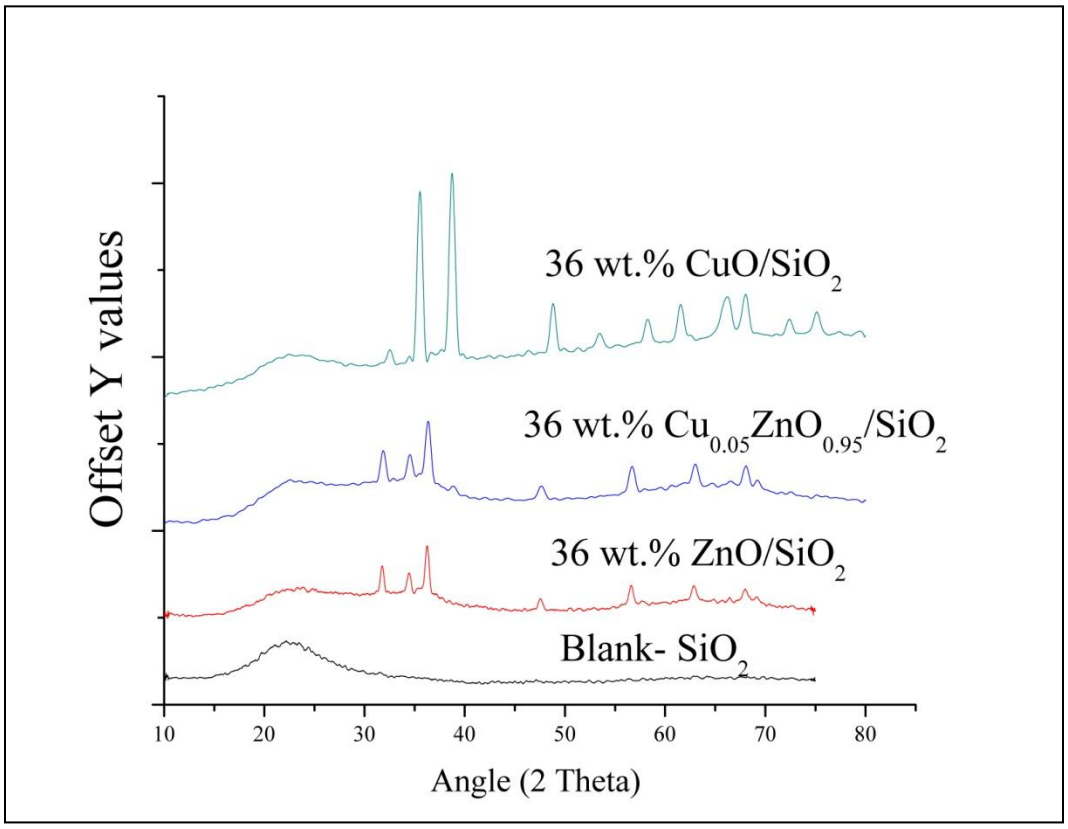

Figure III.9d. XRD Pattern showing effect of adding Cu (0.05-1) on ZnO/SiO_2

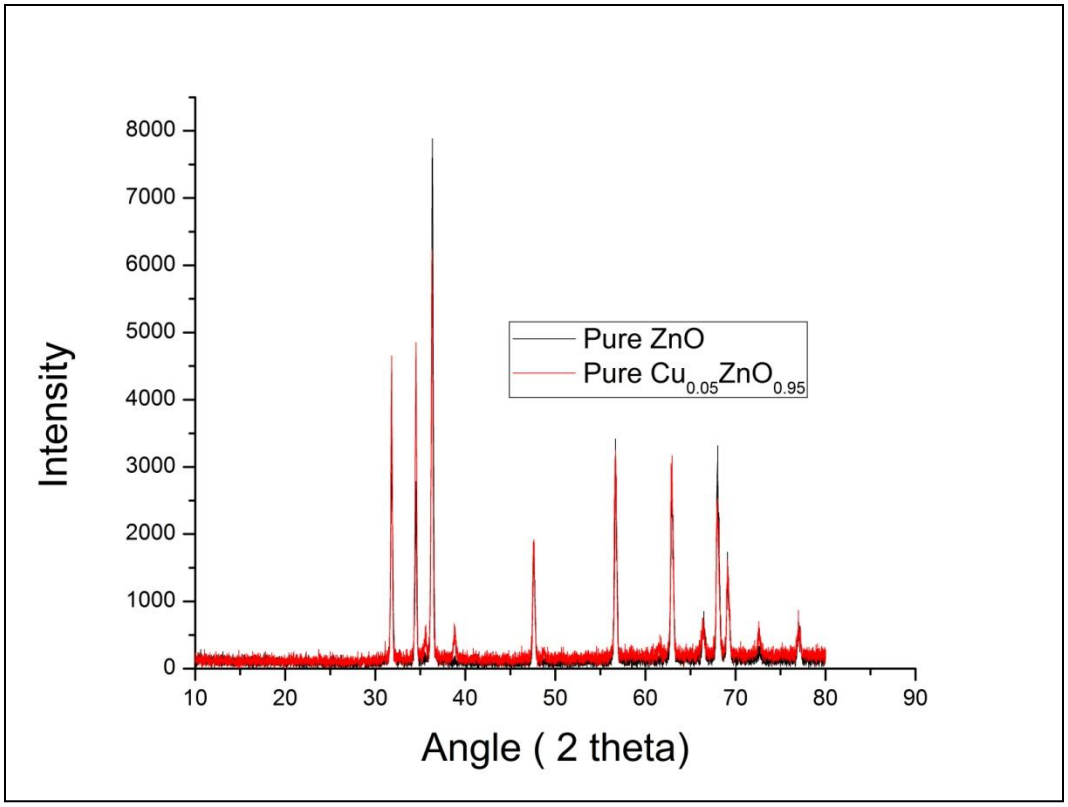

Figure III.9e. XRD Pattern of pure ZnO and $Cu_{0.05}Zn_{0.95}O$ made from the calcination (350 C/1h/air) from nitrate precursors.

III.4.7 Effect of calcination temperature

The impregnated samples, once dried in air for 6hrs were calcined. To study the effect of the calcination temperature the ZnO/SiO_2 (21wt %) samples were calcined at different temperatures in the range of 250-550 ^oC. The calcination is carried out to decompose the nitrates (used as precursor) to oxide. Fig.III.10a shows the saturation capacity of the samples tested for H_2S adsorption capacity with challenge concentration of 1 vol% H_2S/H_2 at room temperature. XRD of the samples calcined at different temperatures is shown in Fig. III.10a. The XRD shows that 250 ^oC is lower temperature for decomposition of nitrates to oxides and hence the capacity is high, because even thought the entire nitrate is not converted to metal oxide, the nitrates can

absorb additional sulfur. On the other hand, 550 ^{o}C is higher temperature which results in lower adsorption capacities, possibly due to increased crystallite size of the particles. 350 ^{o}C was chosen to be the calcination temperature for all the samples made henceforth. ***Hypothesis:*** *Lower calcination temperature can result in smaller more uniform and well dispersed crystals in the porous silica matrix.*

This was verified by obtaining the XRD patterns as shown in Fig. III.10b for these samples calcined at different temperatures. The XRD peak size increases as the calcination temperature went above 250 ^{o}C. At 250 ^{o}C we see a wider range of peaks (along with ZnO peaks) which are due to presence of nitrates in the sample. This also confirms that the temperature for calcination to ensure decomposition of nitrates to oxides should be above 250 ^{o}C and more precisely ~ 350 ^{o}C in air. The XRD patterns were obtained with samples of higher loading (~36 wt %) and the adsorption results in Fig. III.10a was carried out on ZnO/SiO_2 of 21wt%, since XRD patterns of ZnO (21wt %) /SiO_2 is not observable.

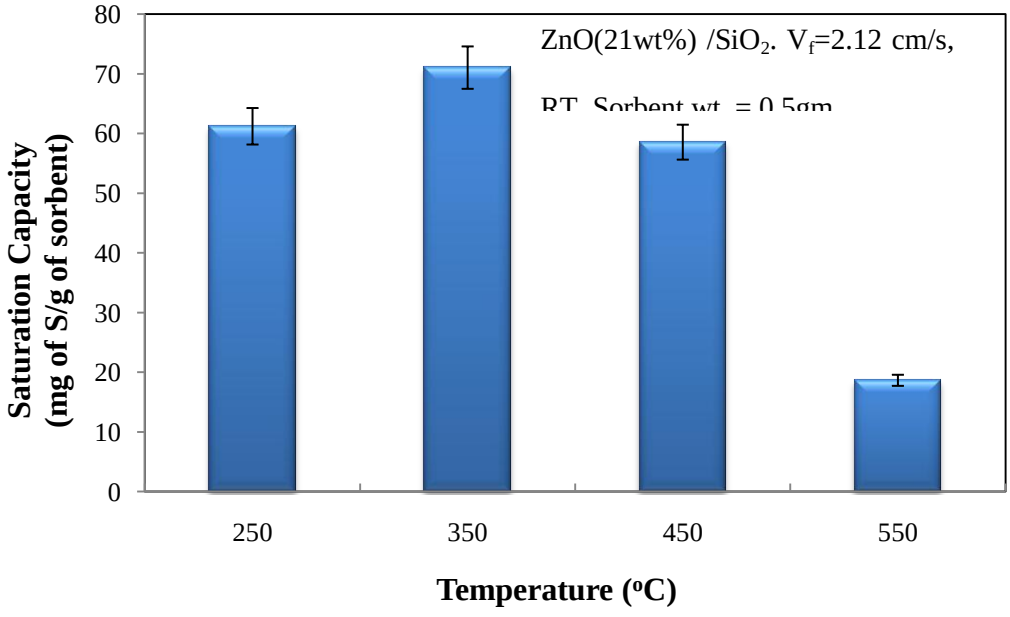

Figure III.10a. Saturation capacity of ZnO/SiO_2 calcined at different temperatures

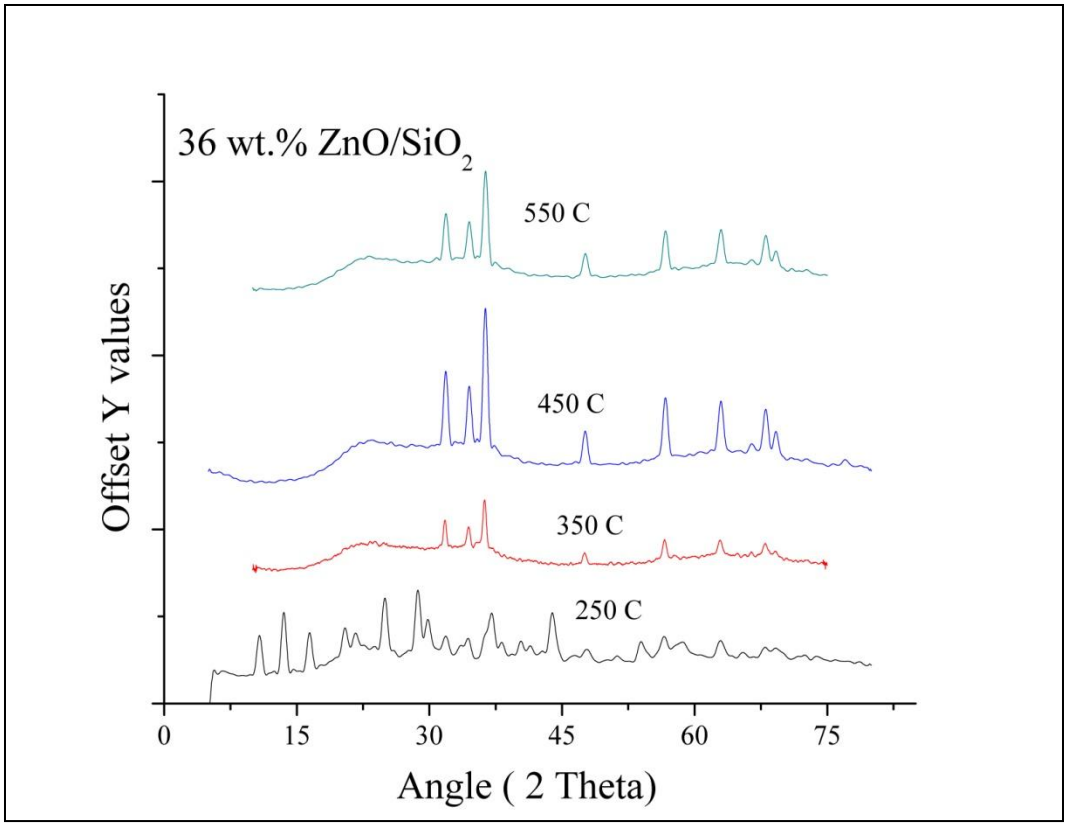

Figure III 10b.XRD patterns of the ZnO(36 wt.%) /SiO_2 calcined at different temperatures.

III.4.8 Effect of H_2S sorption temperature

To understand the effect of temperature on the adsorption of H_2S, ZnO supported silica was tested for its reactivity in the temperature range between 20 and 400 ^oC. Fig. III.11 compares the effect of sorption temperature on the H_2S adsorption capacity and saturation level for ZnO (15%)/SiO_2 and ZnO (15%)/MCM-41, when the inlet H_2S concentration (C_o) is 1% (v/v) in H_2 at a face velocity of 2.12 cm/s.

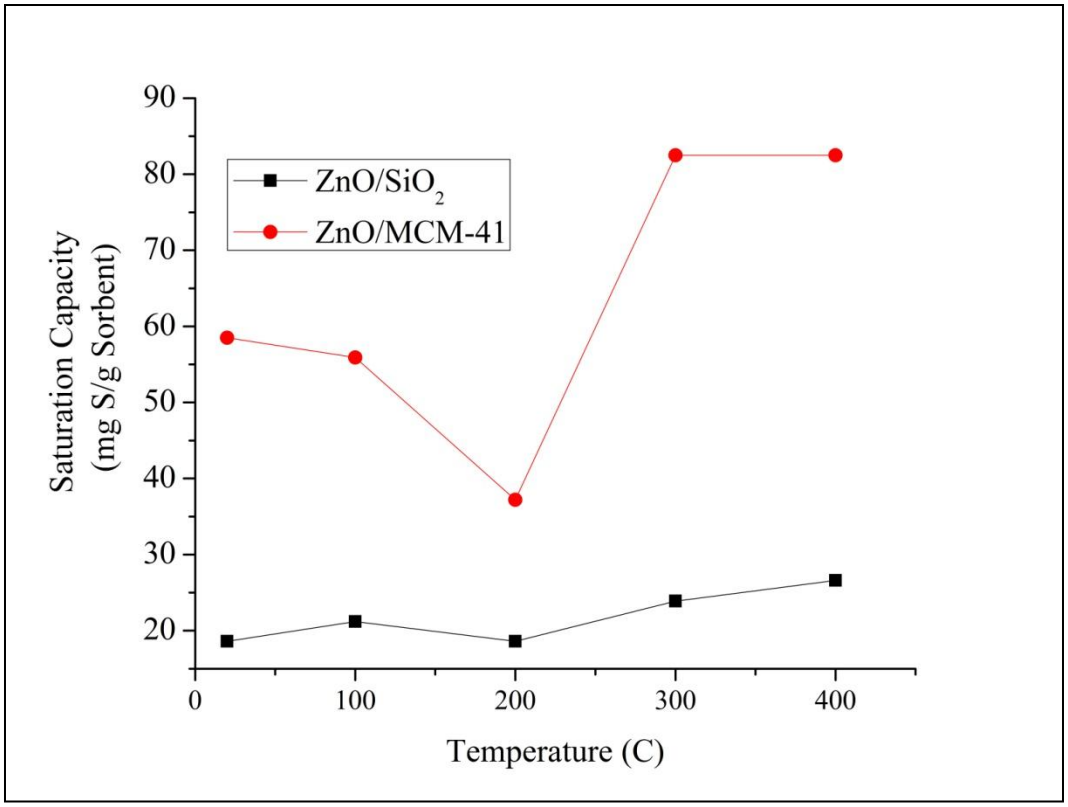

Figure. III.11 H_2S saturation capacity for ZnO/SiO_2 and ZnO/MCM-41 (15 wt% loading) tested from room temperature to 400 C, Q = 100 cc/min, Face velocity = 2.12 cm/s, Calcination condition = 350^{o}C/1h

The desulfurization capacity increased from 20 and 38 mgS/g sorbent to 33 and 65 mg S/g sorbent, respectively for ZnO/SiO_2 and ZnO/MCM-41 as the temperature is increased from 20 to 300 ^{o}C. The nature of the curves for both the sorbents (ZnO/SiO_2 and ZnO/MCM-41 can be explained as follows, at room temperature it is predominantly the physisorption and reaction that leads to higher capacities (attractive forces) as the temperature rises, there will be reduction in physisorption (attractive forces) as the kinetics of reaction starts taking over. At 200 C, a decrease in the capacity was observed for both sorbents, this is because attractive forces responsible for the Physisorption have dropped but the temperature is not sufficient to enhance

the kinetics of the reaction yet. A significant increase in capacity (~60 mg S/g sorbent) can be observed for ZnO/SiO_2 as the reaction temperature rises to 400 ^oC. However, the capacity remains unchanged for ZnO/MCM-41 as the temperature rises from 300 to 400 ^oC. As a result, the performance of ZnO supported on either support is significantly larger at a high operation temperature of 400 ^oC. The Cu-promoted ZnO/MCM-41 was also examined for its desulfurization capacity at 400 ^oC and room temperature. The result is shown in Fig III.12

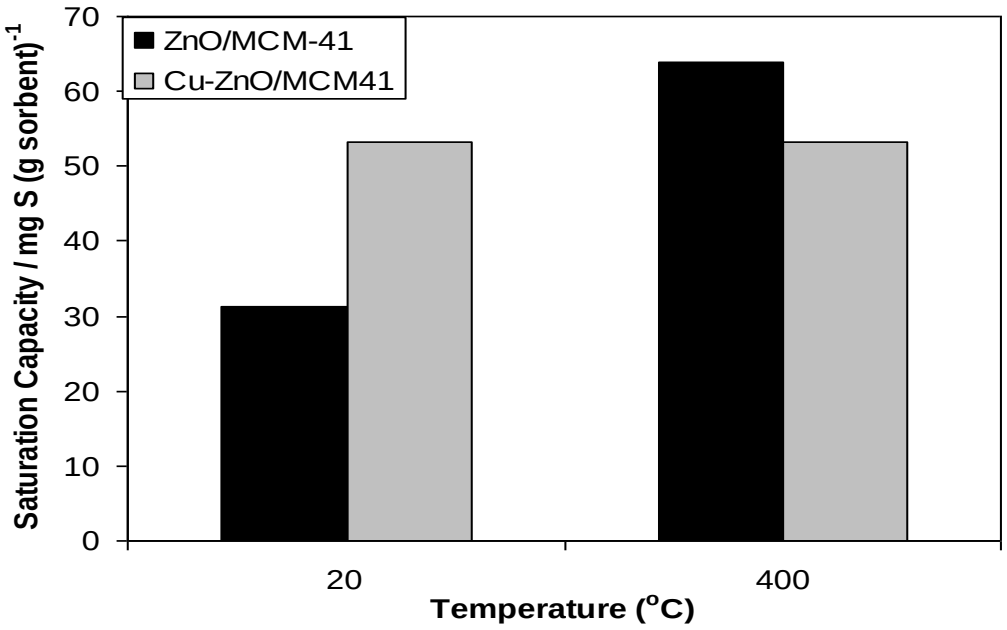

Figure III.12. H_2S saturation capacity for ZnO/MCM-41 and Cu0.05ZnO0.95/MCM-41 (15 wt% ZnO) tested at RT and 400 C, Q = 100 cc/min, Face velocity = 2.12 cm/s, Calcination condition = 350^oC/1h

At room temperature, an approximately 30% increase in capacity was observed by Cu-promotion of both ZnO/SiO_2 and ZnO/MCM-41. At 400 ^oC, the ZnO/SiO_2 showed almost 46% increase in

saturation capacity on promoting with Cu. The Cu-promoted ZnO/SiO_2 does not show improvement in capacity at 400^oC as compared to 20^oC indicating that the Cu dopant is only active at lower temperatures.

III.4.9 Comparative performance of different types of silica support

To determine the influence of support properties, in particular the structural properties, on the H_2S adsorption capacity, different types of silica materials, including the conventional and amorphous silica (SiO_2) and highly ordered mesoporous silica (MCM-41 and MCM-48) were chosen as support for ZnO and tested for their desulfurization performance. Unlike SiO_2, both MCM-41 and MCM-48 without any metal loading show some H_2S adsorption capacity at room temperature. This indicates a very weak interaction between H_2S and MCM-41/MCM-48 at room temperature. Both, the conventional silica gel and mesoporous silica were impregnated with ZnO at the identical loading of 15% (w/w). The desulfurization activity of these samples was examined using breakthrough capacity measurements described in previous section. Fig. III.13 shows the breakthrough curves obtained from the adsorption experiments on these ZnO-based silica samples under identical conditions.

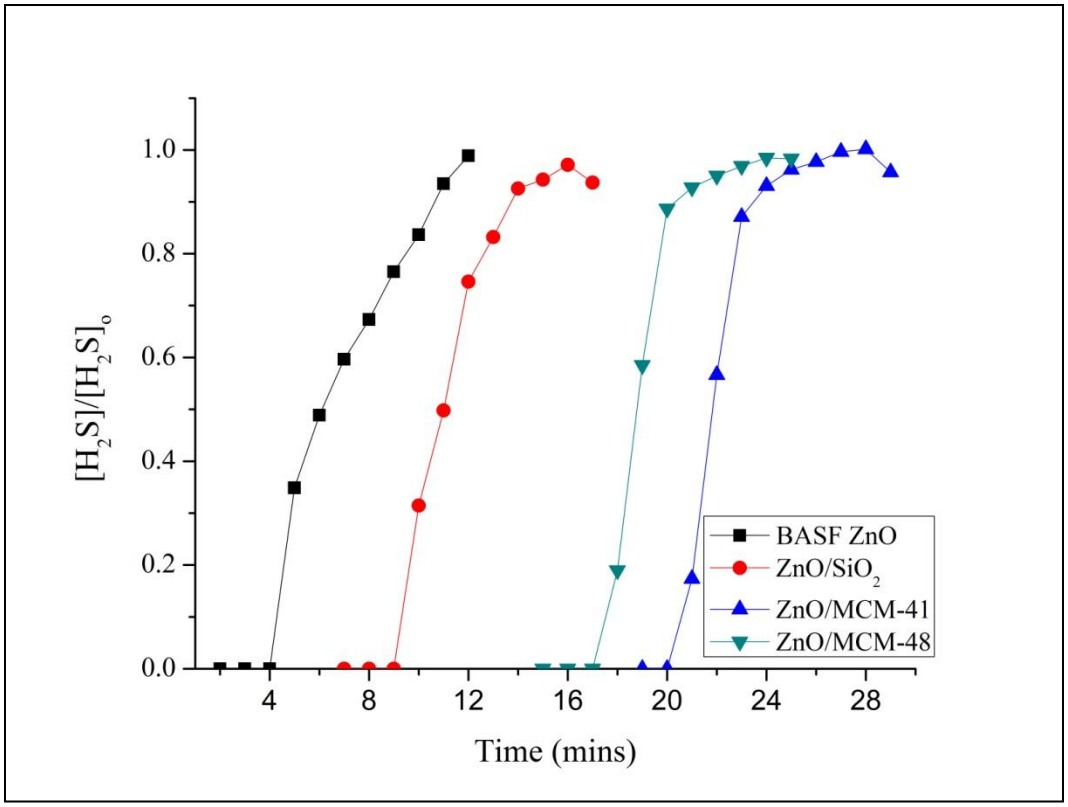

Figure III.13. H_2S Breakthrough curves for ZnO/SiO_2 and ZnO/MCM (15 wt% ZnO) compared with Commercial ZnO (~90% ZnO) tested at RT, Q = 100 cc/min, Face velocity = 2.12 cm/s, Calcination condition = 350^{o}C/1h

The adsorption behavior is almost similar for all three samples. The breakthrough of H_2S was observed to occur at 5, 17, and 20 minutes for the SiO_2, MCM-41 and MCM-48 samples. The longer breakthrough time and higher desulfurization capacity of MCM-sorbents suggests them to be superior candidates for H_2S removal over silica at ambient temperature. The enhanced adsorption capacity of MCM samples may be explained on the basis of their high surface area and well-structured pores, which may allow more uniform dispersion of ZnO crystallites. As can be seen in Table III.1, the BET surface area and total pore volume of MCM samples are significantly larger than those of SiO_2. Even after the loading of ZnO, MCM-41 and MCM-48

samples found to have significantly larger surface area as compared to that of the corresponding ZnO/SiO_2 sample. For example, after 15% (w/w) loading of ZnO, MCM-41 and MCM-48 samples have approximately four- and three- fold larger (850 and 631 m^2/g) surface area in comparison to that (248 m^2/g) for SiO_2 with equal ZnO loading. This suggests that the crystallites size of ZnO dispersed on larger surface (MCM-41 and MCM-48) may be smaller than that on the smaller surface of SiO_2. Further, the smaller pore size in MCM-41 (4.1 nm) and MCM-48 (3.1 nm) as compared with that in SiO_2 (25 nm) favor the possibility of smaller ZnO crystallite size dispersed inside their pores.

III.4.10 Effect of moisture content

The sorbents prepared by impregnation of silica and MCM-41 with Cu-doped ZnO were tested for their H_2S adsorption capacity in the presence of moisture. The moisture content in the inlet gaseous stream was varied from 1-10% (v/v). All the sorbent samples had a similar loading of Cu and ZnO and were tested under identical conditions. .Fig. III.14 shows that the capacity of $Cu\text{-}ZnO/SiO_2$ increased as the moisture content increased until 5% moisture level in the inlet stream. Indicating a maximum of 53 mg S/g sorbent breakthrough capacity in the stream and then the capacity was found to decrease. On the other hand, in the case of MCM-41 the capacity firstly decreased from 53.12 mg S/g sorbent to 17.67 mg S/g sorbent, respectively for moisture level from 0 to 2.5% and then remained constant until 10%.

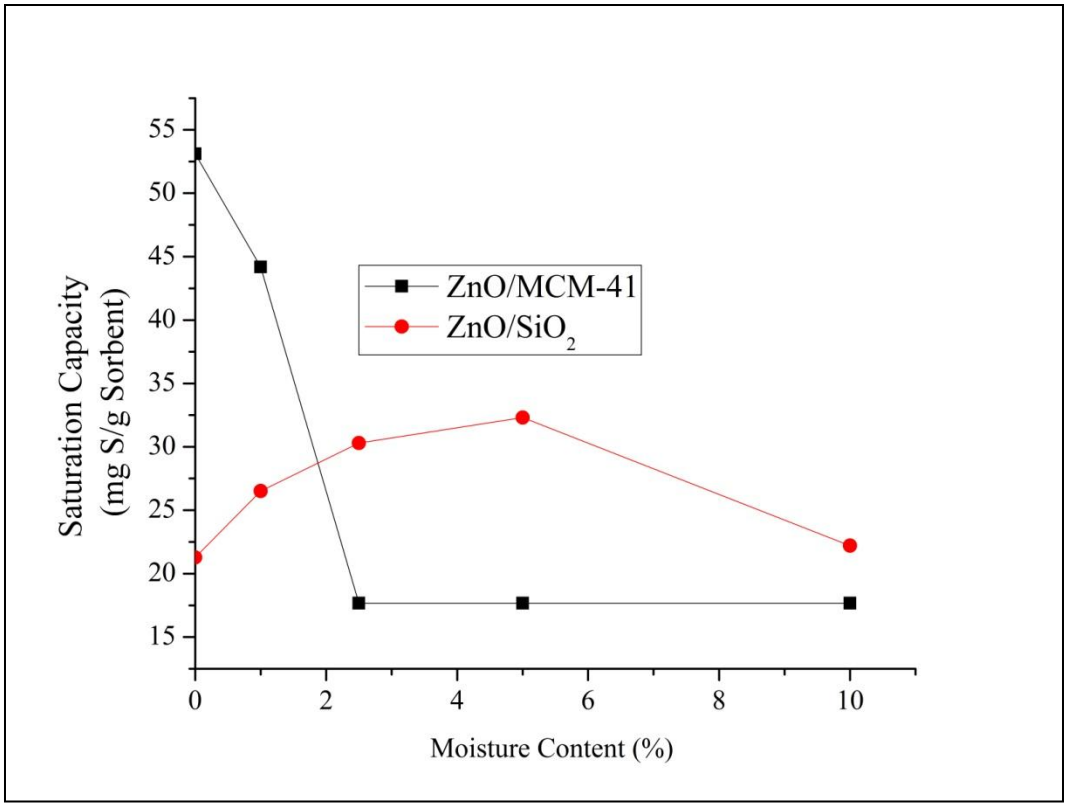

Figure III.14. H_2S saturation capacity for ZnO/SiO_2 and ZnO/MCM-41 (15wt. % ZnO) tested at varying moisture content (0-10%) at RT, Q = 100 cc/min, Face velocity = 2.12 cm/s, Calcination

This decrease in the capacity of the Cu-ZnO/MCM-41 may be due to the change in the structural integrity of MCM-41 support in the presence of moisture. In the case of silica, with the increase in moisture content above 5% the capacity drops due to competitive adsorption of H_2O and H_2S: the presence of moisture will block the pores of silica, thus reducing the saturation capacity.

III.4.11 Effect of regeneration temperature

The sorbents used in this study were also attempted to be regenerated after the sulfidation runs by thermal heating under an oxygen flow. The sorbents were tested for their repeated use over a number of adsorption-desorption cycles. The sulfided ZnO/SiO_2 samples were regenerated

at 600 ^{o}C in air for 1h (shown in Chapter IV). After regeneration the adsorption capacity of the ZnO/SiO_2 samples dropped almost 74% and then remained constant for the next cycles. It was observed that the Cu-promoted ZnO/SiO_2 showed similar behavior in regeneration. On the other hand, ZnO/MCM-41 and ZnO/MCM-48 showed no recovery of the H_2S adsorption capacity under identical regeneration at 600 ^{o}C. Based on a series of experiments on varying regeneration temperature and time, it was observed that the regeneration of ZnO/MCM-41 samples occurred at 400 ^{o}C, but the recovered adsorption capacity was lower (11%) than that (36%) of the ZnO/SiO_2.

III.4.11.1 Desorption test during regeneration

The reaction taking place

$$ZnS + 3/2\, O_2 \Leftrightarrow ZnO + SO_2$$

The desorption of the adsorbent bed was carried out to test the liberated gases using the PFPD detector. The desorbed gas was tested at equal interval of temperature (20-600^{o}C). The analysis showed lower levels of liberation of SO_2. This liberation of gases was more in the temperature range of 250-350^{o}C. It is important during the regeneration that presence of O_2 does not lead to formation of SO_2, if the regeneration gas contains more SO_2 then further removal of sulfur during regeneration should be adopted. The amount of SO_2 liberated in this case was less than 10% of the challenge sulfur concentration.

III.4.12 Effect of CO and CO_2

The reformate streams usually contains CO, CO_2, H_2O, H_2, N_2 and H_2S. Above mentioned tests confirmed the excellent performance of the prepared sorbents at room temperature over commercial sorbents in the presence of dry H_2S, therefore it was important to test the performance in the presence of CO and CO_2. The two best sorbents $Cu_{0.05}ZnO_{0.95}/SiO_2$ and $Mn_{0.025}Fe_{0.025}ZnO_{0.95}/SiO_2$ were tested in the presence of CO and CO_2. *No change in the capacity (both breakthrough and saturation) was observed for either of the sorbents in the presence of CO/CO_2, when tested at room temperature. as shown in Fig..III.15.* But similar study at high temperature indicated a loss in capacity at higher temperatures (T= 400C) as shown in Fig.III.16. This was due to the formation of the COS in the reformate streams due to the reaction between CO/CO_2 with H_2S. A detailed thermodynamic study to understand the formation of COS and strategies adopted to mitigate this issue of COS at high and low temperatures are described in Chapter VI.

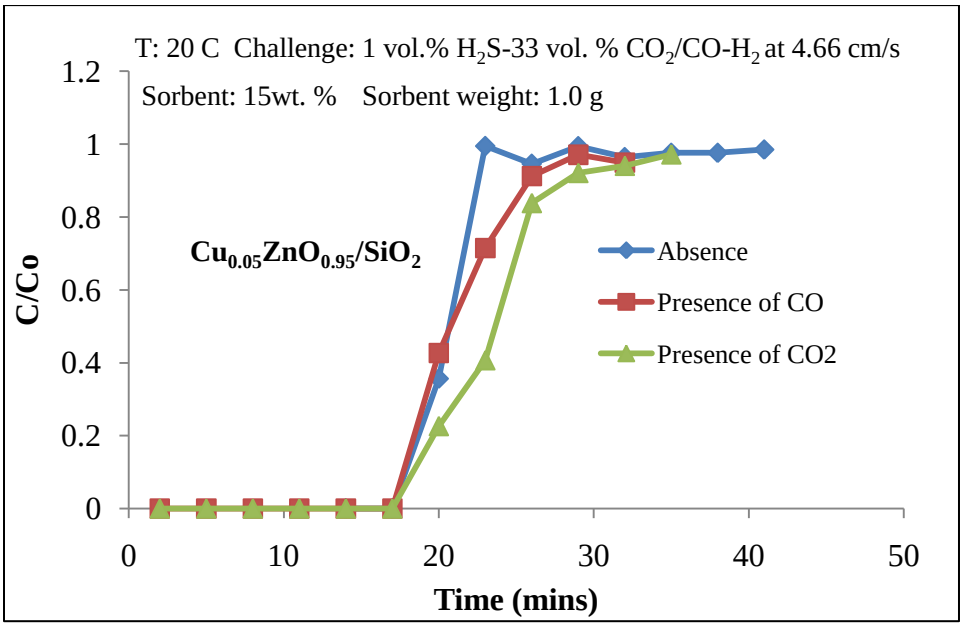

Figure III.15. Breakthrough curves for Cu doped ZnO/SiO_2 tested in the presence of CO and CO_2

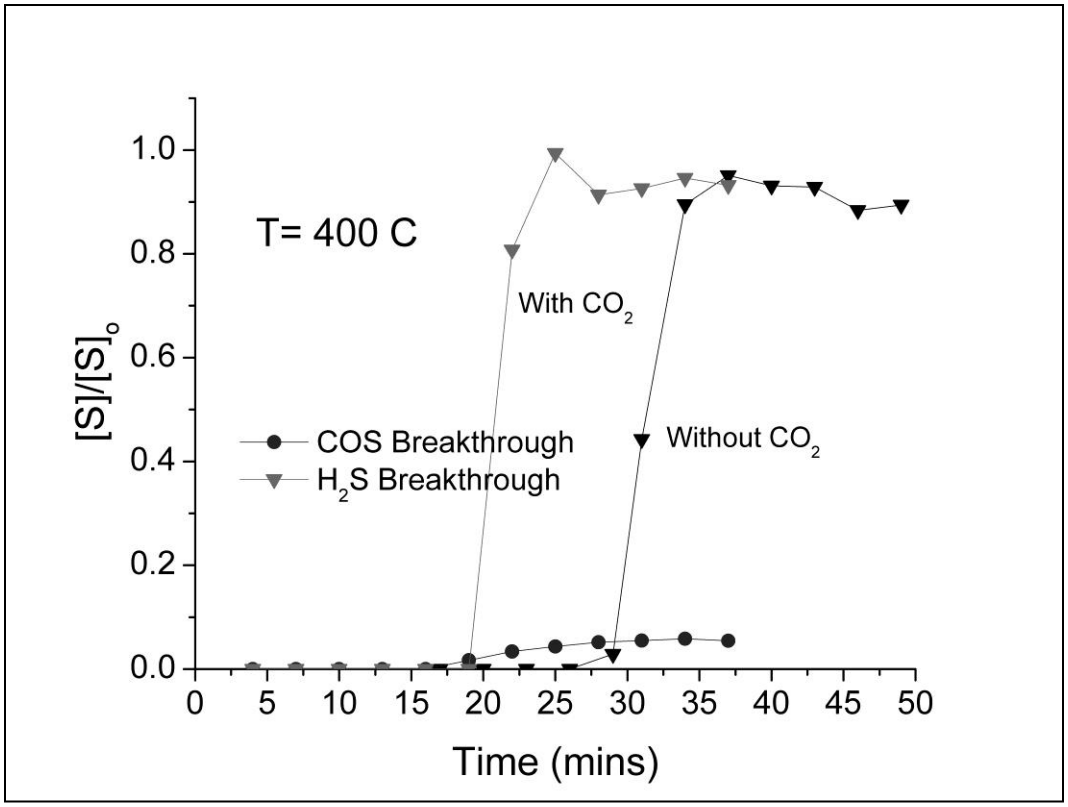

Figure III.16: Breakthrough performance of $Fe_{0.025}Mn_{0.025}ZnO_{0.95}/SiO_2$ with and without CO_2 at 400 C, Test conditions :Q ($2\%H_2S/H_2$) = 100 cc/min, Q(100% CO_2) = 100 cc/min, T = 400 C, GHSV = 8800 h^{-1} , Wt= 0.5 g

Cu in $Cu_{0.05}Zn_{0.95}OSiO_2$ is catalyst for the reaction between CO/CO_2 and H_2S and that is why there is significantly higher concentrations of COS formation at high temperature (T = 400 C). This led to a new set of novel bimetallic sorbents with higher sulfur adsorption capacities but a dopant other than Cu. Also, the capacity of the Cu sorbent dropped significantly in the presence of CO, CO_2 at high temperatures (T =400 C). There was therefore a need to develop a doped supported ZnO/SiO_2 sorbent with alternate dopant. It was shown in the previous study that among the single dopants, only showed higher adsorption capacity for sulfur removal and therefore bimetallic dopants were tested with various combinations.

III.4.13 Novel Bimetallic Sorbents for H_2S removal at room temperature

The aim of the study was to develop doped supported sorbents which can effectively remove in the reformate streams. The previous study focused on Cu as a dopant but Cu is a catalyst for the reaction between CO/CO_2 and H_2S at high temperatures and hence it was important to get rid of this dopant. A set of novel bimetallic dopant promoted ZnO/SiO_2 sorbents with formulation $M_{x/2}N_{x/2}ZnO_{(1-x)}/SiO_2$, where $0 \leq x \leq 1$, (M, N = Cu, Co, Ni, Fe, Mn) were prepared by wetness impregnation method. The nitrates (2M conc.) were used as precursors and the sorbent was dried for 6hrs followed by calcination. The sorbents showed better ZnO utilization and saturation capacity at room temperature in comparison to the single dopant promoted ZnO/SiO_2. The $Mn_{0.025}Fe_{0.025}ZnO_{0.95}/SiO_2$ showed highest saturation capacity as shown in Fig.III.17. Chapter V talks in details about this novel sorbent for H_2S removal and their performance over multiple cyles as well as the characterization of this sorbent to understand the role of the active sites.

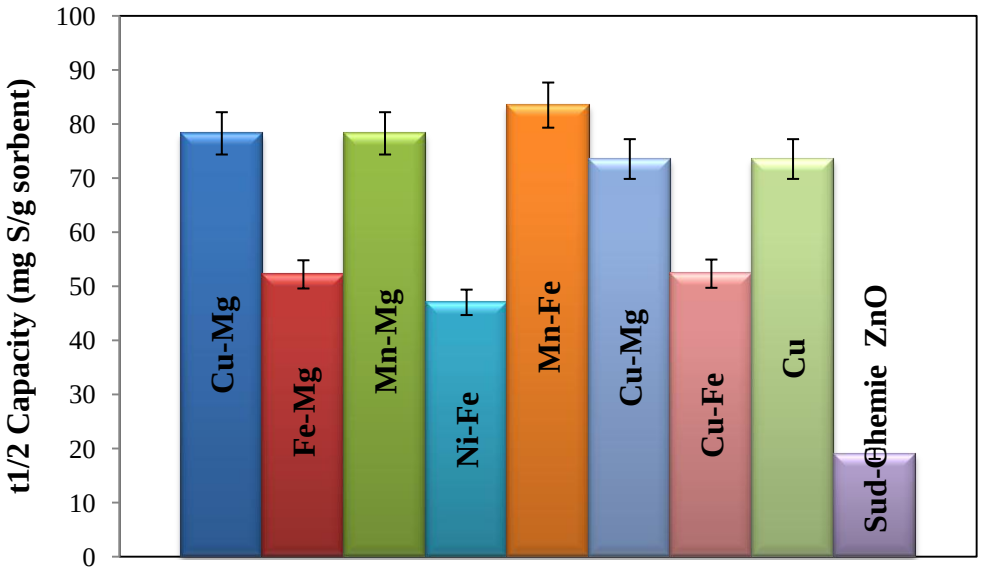

Figure III.17. Saturation Capacities of the novel bimetallic doped sorbents for H_2S removal

In Chapter VI. the results for this novel $Mn_{0.025}Fe_{0.025}Zn_{0.95}/SiO_2$ tested at higher temperatures (T=400 C) in the reformate stream are listed. The results indicate that the formation of COS was lower than in the presence of Cu, and the sorbent maintained higher capacities at T = 400 C in the presence of CO/CO_2.

III.4.14 Scale-up studies

The sorbents $Cu_{0.05}Zn_{0.95}O/SiO_2$ and $Mn_{0.025}Fe_{0.025}Zn_{0.95}/SiO_2$ were scaled up (1 kg batch) using the V-blender, shown in Fig.III.18 for the impregnation and it shows consistent performance as shown in Fig.III.19.

Table III.4.Theoretical utilization values for scale up of the sorbent

Batch number	Method	Batch size (gms)	% Theoretical Utilization
B1	Hand-made	20	82.65
B2	V-Blender	800	78.06
B3	V-Blender	800	82.65

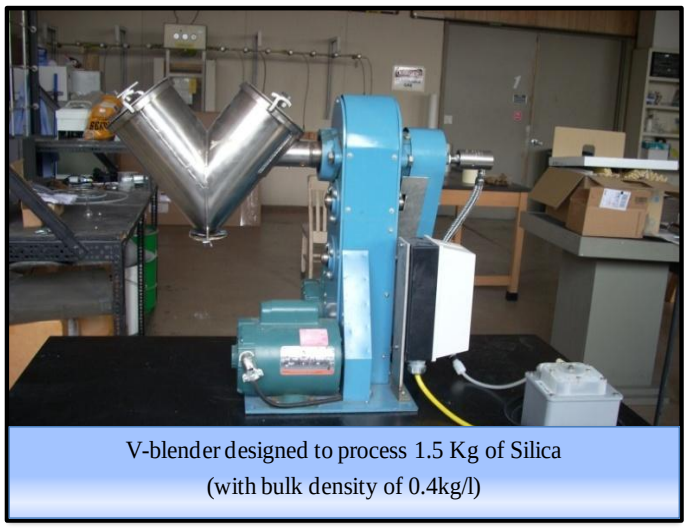

Figure III.18. V-blender used for impregnation of samples for scale-up studies

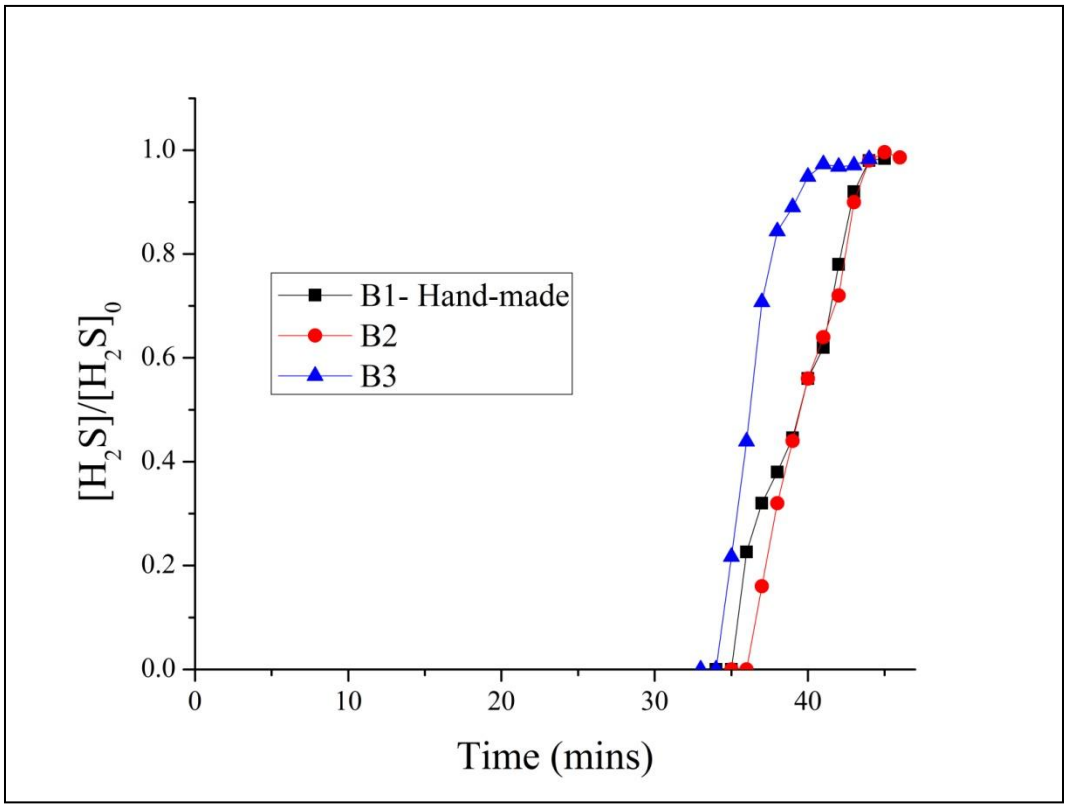

Figure III.19.Breakthrough curves for scale-up studies

III.5 Microfibrous Entrapped Sorbent

III.5.1 Kinetic effects due to microfibrous entrapped ZnO sorbents(MFES)

This work is done as a continuation of the work published in 2008 Chemical Engineering Science Journal [17], in collaboration with the Virginia Tech- Aerospace and Ocean Engineering department for CFD simulation study (VT-AOE), to better understand the purpose of microfibers in packed bed.

The basic relationships between breakthrough curves and the kinetic behaviors of fixed bed reactors were studied. Mecklenburg model[70], Wheeler model[71] and Yoon model[72] Mathematical models developed to predict the breakthrough time of adsorption processes taking place in packed beds. The bed depth service time equation (1) derived from Amundson equation[73]:

$$\ln\left(\frac{C_{Ao}}{C_A}-1\right)=K(\tau-t) \qquad (1)$$

Where lumped K is defined as:

$$K=k_a\phi\frac{C_{Ao}}{\rho_c} \qquad (2)$$

A sharp breakthrough curve always has a large lumped K. The breakthrough ZnO utilization (X) of packed bed increases with increase in lumped K value and the critical bed depth (Z_c)as shown in the rearranged equations (3) and (4) [17].

$$X=1-\frac{\ln\left(\frac{C_o}{C_b}\right)-1}{K\tau} \qquad (3)$$

$$Z_c = \ln\left(\frac{C_{Ao}}{C_b} - 1\right)\frac{UC_{Ao}}{K\rho_c} \qquad (4)$$

In the modified Amundson model[17], the lumped K is explicitly correlated to k_a as shown in equation (2). In this work, the equation (1) has been verified experimentally and is used to investigate the performance of packed beds and MFES.

III.5.2 Preparation of MFES

Microfibrous media with two different target fiber fractions were made using the method described in detail elsewhere [31]. The method is also described in the glass fiber entrapped sorbent preparation section of this document. Following compositions as shown in table were obtained by varying the fiber loading and sintering conditions.

Table III.5. Composition of the GFES

Loading	Material 1	Material 2
Solid Fiber %	2.9	4.35
Total Solid %	28	29.8
Void %	72	70.2

III.5.3 Model Evaluation

The GFES were tested at 400^{o}C in the presence of 0.5 vol% H_2S/H_2. The result shown in the Fig. III.20 is for material 1 tested at U=1.2 cm/s. K and τ were calculated from linear regression and the values obtained were 0.535 min^{-1} and 22 min respectively. Similar method was used for

calculations of all the K and τ values for varying face velocities (1.2-9.6 cm/s) and glass fiber volume fractions (3-4.5 vol %). Because of the symmetry of the breakthrough curve the τ and $t_{1/2}$ are equal. Ln (C_{Ao}/C_A-1) vs. t is linear for majority part of the breakthrough curve. The slope is indicative of the lumped K value and the intercept is the log reduction value for a given breakthrough curve.

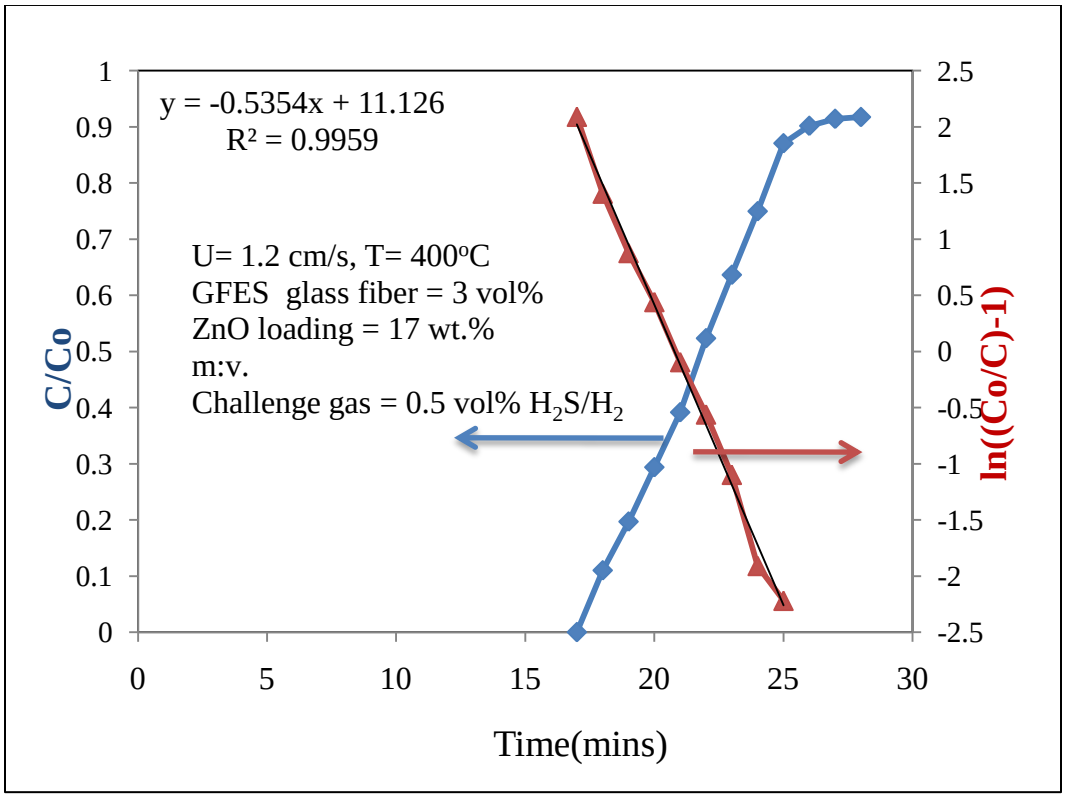

Figure III. 20. Evaluation of modified Amundson model

III.5.4 Effect of face velocity

The GFES with ~ 17 wt. % ZnO loading were tested at 400°C in the presence of 5000 ppmv of H_2S/H_2. In this experiment, the m: v (mass: volume) of the GFES was varied as the face velocity was doubled, in order to maintain the same τ.

Table III.6. Operating conditions: change in m: v with face velocity and length of bed

Ratio	**Face velocity U (cm/s)**	**Length of bed (inches)**
m:v	1.2	0.5
2m:2v	2.4	1.0
4m:4v	4.8	1.5
8m:8v	9.6	2.0

Lumped K values were obtained from the breakthrough curves and are shown in Fig III.21. A linear regression suggests that lumped K increases with $U^{0.56}$ for lower fiber (3 vol%) fraction in MFES and K increases with $U^{0.6}$ for higher (4.5 vol%) fiber fraction in MFES. The results are in agreement with the previous work done[17].

Material 1: Fiber vol= 3%

Table III.7a. Lumped K values for Material 1

U (cm/s)	Wt. (gms)	Lumped K (s^{-1})
1.2	1.86	0.0071
2.4	0.325	0.0101
4.8	0.613	0.0156
9.6	0.828	0.0216

Material 2: Fiber vol = 4.5 %

Table III.7b. Lumped K values for Material 2

(cm/s)	Wt. (gms)	Lumped K (s^{-1})
1.2	0.203	0.0089
2.4	0.425	0.0077
4.8	0.658	0.2005
9.6	0.838	0.0313

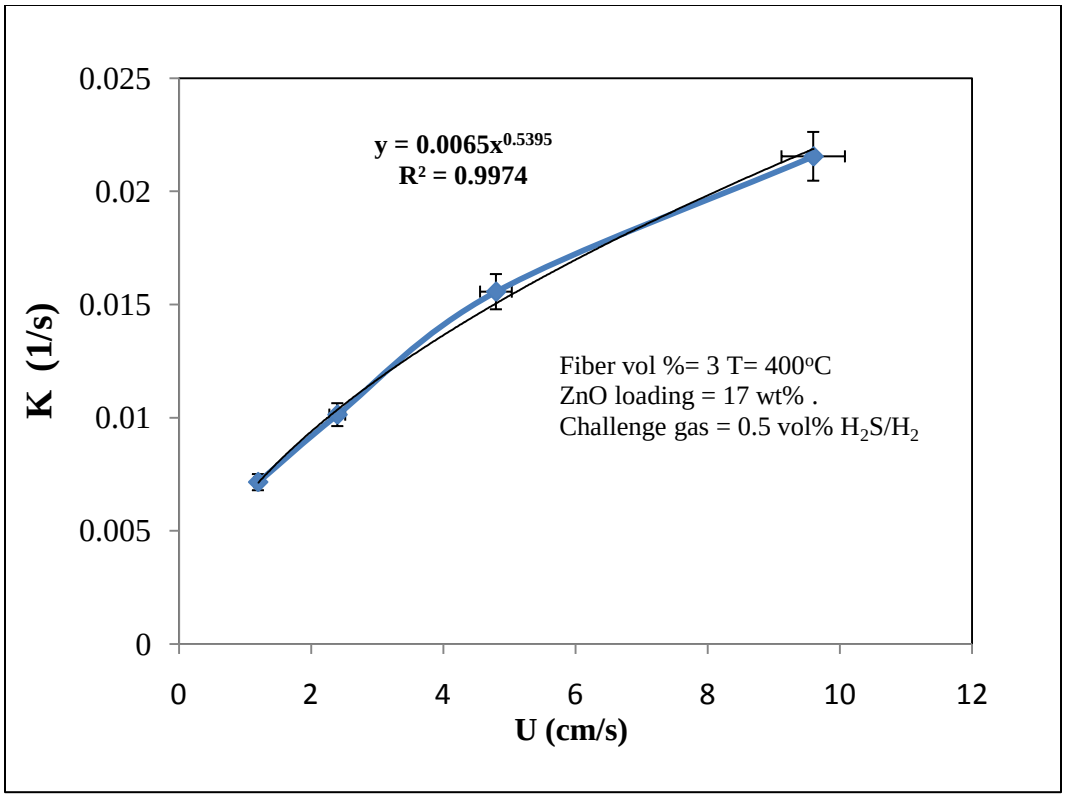

Figure III.21a. Relationship between lumped K and face velocity U for material 1 with glass fiber fraction = 3 vol%

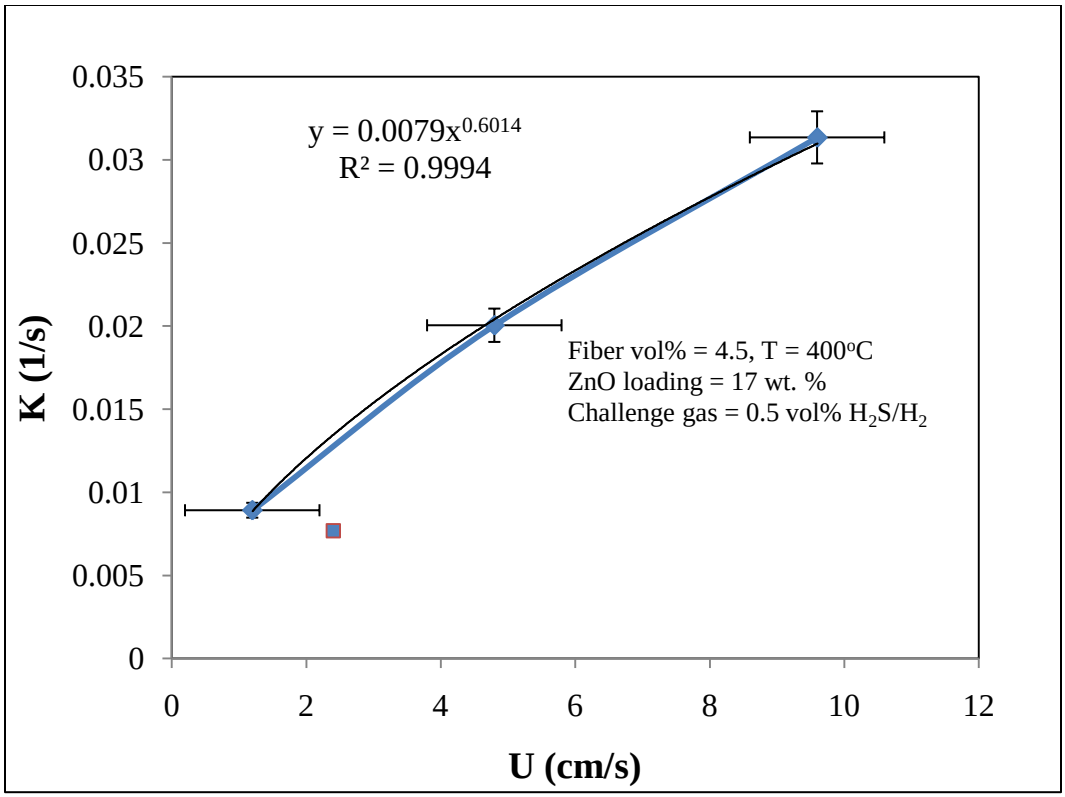

Figure III.21b. Relationship between lumped K and face velocity U for material 2 with glass fiber fraction = 4.5 vol%

III.5.5 Effect of Pressure:

The pressure drop data for the two materials under changing face velocities was obtained using a pressure cell. The set-up used for the measurement of the pressure drop at 400°C is described in the experimental section. The packed bed of small particle size (100-200 um) and large particle size (1-2mm) ZnO/SiO_2 with ~ 17wt. % loading were compared with the GFES. *The microfibrous entrapped sorbents give an advantage of the lower pressure drop for significantly high breakthrough times via enhanced contact efficiency and thus can be used very effectively for the miniaturized desulfurization units.* as shown in Fig.III.22

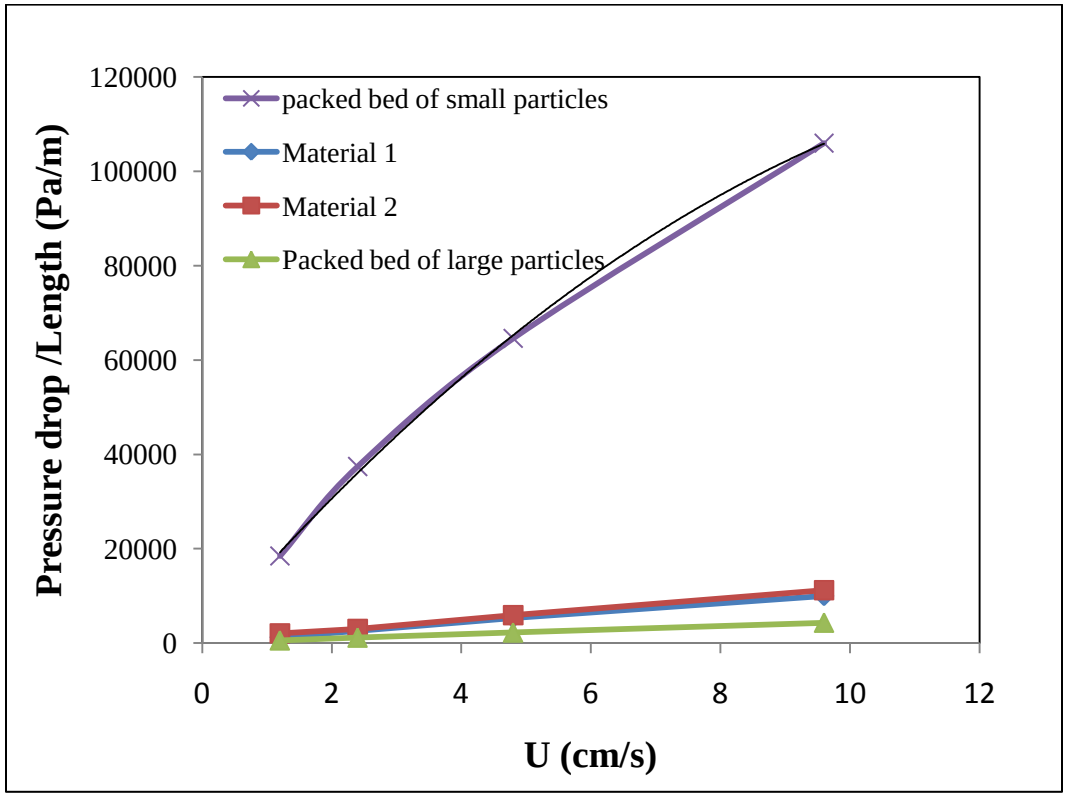

Figure III.22. Pressure drop data for the packed bed and GFES (Material 1 and 2) at 400oC

Table III.8a. Pressure gradient and log reduction for Material 1

Face Velocity (cm/s)	Pressure Gradient ΔP/L (Pa/m)	Log_{10} Reduction LR (t=0)	ΔP/LR
1.2	2022	4.83	418
2.4	2973	3.45	861
4.8	5917	8.62	1194
9.6	11213	11.19	1001

Table III.8b. Pressure Gradient and Log reduction values for Material 2

Face Velocity (cm/s)	Pressure Gradient ΔP/L (Pa/m)	Log_{10} Reduction LR (t=0)	ΔP/LR
1.2	1543	2.92	527
2.4	2579	4.81	536
4.8	5323	6.59	807
9.6	9997	9.46	1057

III.5.6 Composite bed design

With the enhanced mass transfer, Microfibrous Entrapped Sorbents (MFES) are targeted at high contacting efficiency, high ZnO utilization and high regenerability. It can be directly used in miniaturized desulfurizer with a thickness of several centimeters for applications, especially for those with low sulfur challenge concentrations. For desulfurization applications with high sulfur concentrations, MFES can be used as a polishing layer located at the downstream end of a conventional packed bed made of extrudates to form a composite bed.

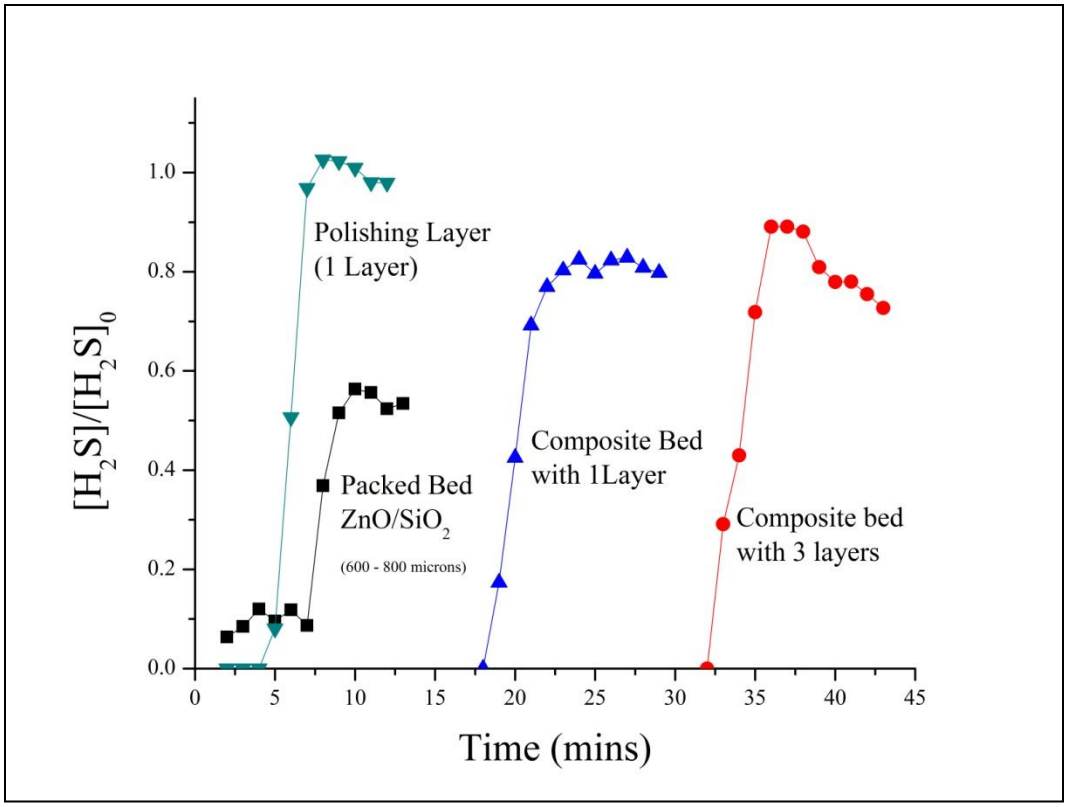
$[H_2S]/[H_2S]_0$
1.0
0.8
0.6
0.4
0.2
0.0
0
5
10
15
20
25
30
35
40
45
Time (mins)
Polishing Layer
(1 Layer)
Packed Bed
ZnO/SiO_2
(600 - 800 microns)
Composite Bed
with 1Layer
Composite bed
with 3 layers

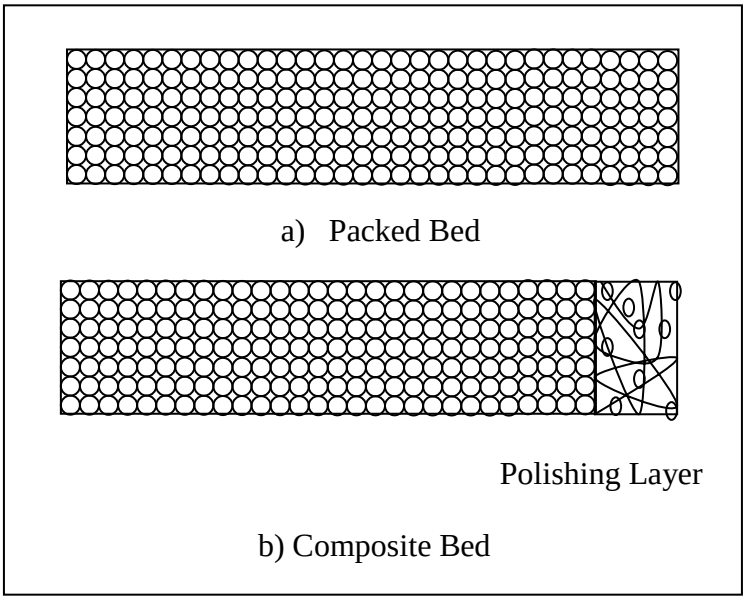
a) Packed Bed
Polishing Layer
b) Composite Bed

Figure III.23: a) Composite bed test using glass fiber entrapped sorbents as polishing layer**.** Performance of Polishing Sorbent and Packed Bed + Polishing Sorbent @ 1% H_2S in H_2, RT, 2.12 cm/s Breakthrough curves of a 2.5 cm thick packed bed of ZnO/SiO_2 extrudates and a composite bed (the packed bed followed with a 4mm polishing layer). b) Schematic diagram of the packed and composite bed.

Table III. 9: Composition of the packed bed and polishing layer

Polishing Layer	SiO_2 = 23%, Void = 75% and Fiber = 2.5% Particle Size = 100-200 microns, Bed Thickness = 4mm, ZnO loading = 19wt.%
Packed Bed	15 wt.% ZnO/SiO_2, Particle Size = 600-800 microns, Bed thickness = 2.5 cm

The composite bed test was carried out at RT using the Glass Fiber Entrapped Sorbent (GFES) as packed bed of larger particle size sorbent followed by the polishing layer of same sorbent of smaller particle size (100-200 μm) entrapped in the fibrous matrix of glass fibers. The Fig. 35 shows the breakthrough curve for packed bed and composite bed, the change in the breakthrough curve for composite bed can be attributed to the presence of the polishing layer at the downstream of the bed, since both the packed beds were tested at similar conditions. This

approach enhances the breakthrough time as much as ~ 3 times without adding extra pressure drop. The GFES is prepared by wet –lay paper making method with Silica particles (size: 150-200 um) entrapped in the mesh of glass fibers (8um dia.). The individual performances of only the polishing layer and the packed bed are presented in the Fig. III.23

III.6 Removal of SO_2:

Promoted ZnO/SiO_2 sorbents were tested for removal of 1vol%SO_2/Air at the ambient conditions. All the samples are made by incipient wetness impregnation method and calcined at 350 C/1h in air. The Table III.10 Shows the saturation capacity values for all the sorbents and Figure III. 24 shows the breakthrough performance.

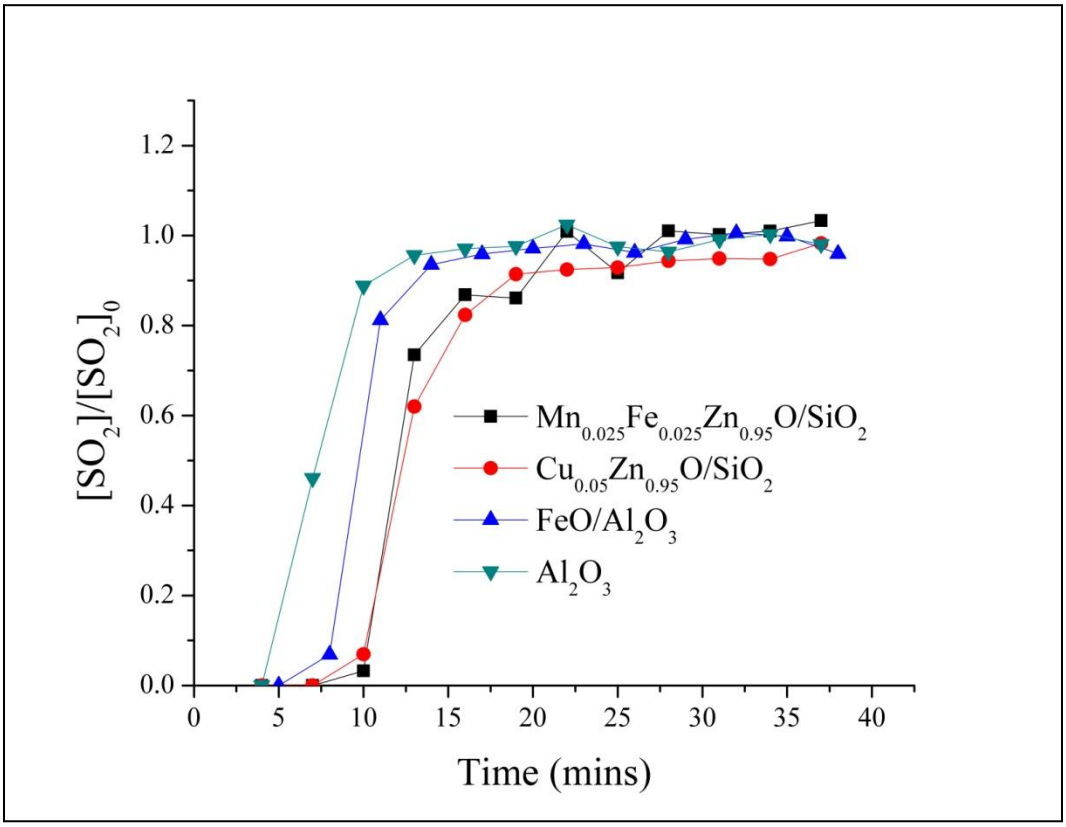

Figure III.24: Breakthrough performance of promoted ZnO/SiO_2 and FeO/Al_2O_3 (15wt.%). Test Conditions: T= 20 C, Co = 1vol% SO_2/Air, Face velocity = 0.53 cm/s

Table III.10 : Saturation capacity of the sorbents tested for SO_2 removal

Sample	Loading (wt.%)	Saturation Capacity (mg S/g sorbent)	Metal oxide utilization (%)
$Mn_{0.025}Fe_{0.025}Zn_{0.95}O/SiO_2$	15	32	58
$Cu_{0.05}Zn_{0.95}O/SiO_2$	15	32	58
FeO/Al_2O_3	15	19	42

III.7 Conclusions

Different types of silica materials, including the conventional silica gel (SiO_2) and highly ordered mesoporous silica (MCM-41 and MCM-48), were impregnated with ZnO and tested for desulfurization performance. The lab made ZnO based samples were compared with the commercial ZnO. These ZnO-based sorbents were doped with several transition metals including Mn, Fe, Co, Ni, and Cu. The Cu-dopant improved the desulfurization and regeneration performance of ZnO/SiO_2 significantly. Among the doped ZnO based sorbents, Cu-doped ZnO/MCM-41 ($Cu_{0.05}ZnO_{0.95}$/MCM-41) and ZnO/SiO_2 ($Cu_{0.05}Zn_{0.95}O/SiO_2$) are promising sorbents for low temperature H_2S removal for applications in PEMFCs. At room temperature, ZnO/MCM-41 demonstrated a high sulfur capacity (58.12 mg S/g sorbent), which is almost twice that of ZnO/SiO_2 at similar ZnO loadings. In the presence of moisture, the breakthrough capacity of Cu-ZnO/SiO_2 first increased up to a maximum of 53 mg S/g sorbent and then decreased, whereas, the breakthrough capacity of Cu-ZnO/MCM-41 decreased in the presence of moisture. It suggested that MCM-41 support is not suitable for moist gaseous streams. Due to the higher capacities achieved, the Cu promoted ZnO/SiO_2 can efficiently be used as a non-

regenerable inline filter before the reformate gases flow to PEMFC. $Cu_{0.05}ZnO_{0.95}$/MCM-41 are promising sorbents for room temperature H_2S removal for PEMFC application.

COS is formed in the reformate streams at high temperatures (T = 400 C). The effect of CO and CO_2 in the challenge was studied and $Cu_{0.05}Zn_{0.95}O/SiO_2$ showed significant drop in the capacity at high temperature (T= 400 C) due to COS formation and Cu is a catalyst for the reaction between CO/CO_2 and H_2S. Novel bimetallic doped sorbent $Mn_{0.025}Fe_{0.025}Zn_{0.95}O/SiO_2$ was developed to remove sulfur in the reformate streams with lower COS formations at T = 400 C. The pressure drop and kinetic parameters of the microfibrous entrapped ZnO/SiO_2 at three different face velocities and solid loadings were studied. The trends in lumped K with respect to fiber volume fraction in the microfibrous media were studied. The composite bed design give an advantage of lower pressure drop for higher breakthrough times via enhanced contacting efficiency.

Acknowledgements

This work was supported by the US Army under a U.S. Army contract at Auburn University (ARMY-W56HZV-05-C0686) administered through the US Army Tank-Automotive Research, Development and Engineering Center (TARDEC).

Chapter IV: Copper Promoted ZnO/SiO_2 Regenerable Sorbents for the Room Temperature Removal of H_2S from Reformate Gas Streams

Priyanka Dhage, Alexander Samokhvalov, Divya Repala, Evert C. Duin[1], and Bruce J. Tatarchuk

Department of Chemical Engineering, Auburn University, Auburn, AL 36849 (USA)

[1]Department of Chemistry and Biochemistry, Auburn University, Auburn, AL 36849

Abstract

The Cu-ZnO/SiO_2 sorbent for ultradeep adsorptive removal of H_2S from the reformate streams at room temperature was prepared, tested, and characterization of the active sites was performed. The Cu dopant significantly enhances desulfurization capacity of ZnO/SiO_2 sorbent at room temperature (up to 92 % utilization of ZnO), and maintains a high sulfur uptake capacity upon multiple cycles (up to 10) of regeneration by a simple thermal oxidation in air. The "as-prepared" ("calcined") sorbent contains Cu in the Cu^{2+} form, O, Si, Zn as ZnO at the coverage <0.2 of monolayer, while the "spent" ("sulfided") sorbent contains Cu, O, Si, S and Zn as ZnS form, as found by XPS. XRD suggests that both zinc and copper compounds of the CuO-ZnO/SiO_2 sorbent are nano-dispersed. The ESR spectroscopy found that the "calcined" and "sulfided" CuO-ZnO/SiO_2 sorbents contain Cu^{2+} in the single dispersion and coordination state. During H_2S adsorption, partial reduction of Cu^{2+} to Cu^{1+} occurs: the higher Cu concentration in the sorbent, the lower the reduction yield of Cu^{2+} to Cu^{1+} thus correlating with sulfur uptake capacity. The

"deactivated" sorbent (10-11 adsorption/regeneration cycles) is enriched with a different chemical form of Cu^{2+}, compared to the "as-prepared" sorbent.

Keywords: Desulfurization, H_2S, Dopant, ZnO, Cu, XPS, ESR

IV.1 Introduction

Electric power generation systems utilizing fuel cells, such as auxiliary power units (APUs) for diesel trucks and the military remote power supplies are the subjects of an intense research and development recently, due to their portability and high energy efficiency [74]. In these power-generating systems, the steam reformers, catalytic partial oxidation (CPO) or autothermal reformers (ATR) [75] are used that convert liquid hydrocarbon logistic fuels to H_2-enriched gaseous reformates. The major chemical components of the reformates are H_2, CO, CO_2, hydrocarbons with low molecular weight, water and sulfur-containing compounds (mainly H_2S and COS). The sulfur-containing gaseous reformates are known to be poisonous to the catalytic systems in fuel processing units (FPUs) and to electrolytes in fuel cells. Typically, to avoid poisoning, the feed to the fuel cell should contain less than 1 ppmv of sulfur; therefore, desulfurization systems need to be developed. In reformate streams, the most abundant sulfur-containing compound is H_2S. The modern adsorptive desulfurization technologies use the metal oxide-based sorbents that can reduce sulfur concentration from several thousand ppmv to the sub-ppmv levels [76, 77].

The most widely used sorbent for adsorptive removal of H_2S from the gas streams is zinc oxide ZnO. Key advantages of ZnO are its high sulfur capacity and the favorable sulfidization thermodynamics. The non-supported oxide sorbents operating at 500–800 ºC that are based on Zn and Ti oxides are known to work efficiently for only a small number of the sulfidization–regeneration cycles; as the number of cycles increases, the sorbent efficiency declines, and mechanical properties of the sorbent become unacceptable [78]. Based on the thermodynamics of sulfidization and phase separation [79], the choice of the regenerable sorbents has been often

directed towards copper oxides. The main advantage of the Cu-based sorbents is the highly favored sulfidization thermodynamics for copper in the oxidation states of +2 or +1, so that the equilibrium H_2S concentration in the outlet gas of the typical fixed-bed reactor can be lowered down to the sub-ppmv levels [1]. However, copper compounds (oxides and sulfides) have relatively low melting points, and they are prone to re-growth of the crystallites and to thermally-induced sintering that lowers the efficiency of the sorbent rapidly [1].

On the other hand, copper compounds are useful as dopants for the sorbents compared to other transition metal oxides. For instance, addition of the small amounts of copper oxide can significantly increase chemical reactivity of zinc ferrites [80], possibly due to copper migration from the "bulk" to the active surface at high temperatures [81]. Copper oxide was used as a dopant in a highly-dispersed state, impregnated into the porous supports, such as alumina [82], chromia [83] and others.

In earlier studies, it was shown that both surface and bulk dispersion and oxidation states of the Cu dopant are important factors in controlling the activity of the sorbent and its temporal stability upon multiple adsorption-regeneration cycles. There are few experimental techniques to study dispersion, oxidation and coordination state of the Cu dopant, such as ESR [84, 85] and XPS [85, 86]. To study the dopant that is the minority chemical component of the multi-component sorbent or catalyst, the experimental technique(s) needs to offer: i) a rather high sensitivity, ii) the ability to analyze both surface and the "bulk" of the specimen. Thus, ESR with its excellent sensitivity ($>10^{11}$ spins/sample) and the capability to measure in the "bulk" is the technique of choice. XPS can conveniently complement ESR, since it is the surface-sensitive technique. Moreover, upon introducing the Cu dopant ion into the lattice or onto the surface of

the ZnO crystallites, the formation of defects is reported, such as oxygen vacancies [87], and ESR is well-suited for detecting these [88].

It is known that, in part, deactivation of the sorbents is due to destruction of the 3D structure of the multi-component material due to thermal factors. Therefore, desulfurization sorbents that operate at room temperature are expected to show the increased temporal stability as compared to their high-temperature analogs, due to the lowered clustering, phase separation and diffusion of the dopant ions. Earlier, we prepared and tested the novel ZnO/SiO_2 sorbent for H_2S and carbonyl sulfide COS with the minimized mass transfer resistance [77, 89-92].

We report here preparation, desulfurization performance upon the multiple regeneration cycles, and experimental characterization of the Cu, Zn, O and S sites of the supported doped sorbent $Cu_xZn_{1-x}O/SiO_2$ for the ultradeep removal of H_2S that i) achieves >90% of the theoretical sulfur uptake capacity at room temperature, ii) reduces sulfur concentration from ~1000 ppm to < 1 ppm, iii) can be easily regenerated multiple times by simple heating in air without a significant loss of performance.

IV.2 Experimental

The doped ZnO-based sorbent with the formula $Cu_{0.05}Zn_{0.95}O/SiO_2$ was prepared by an incipient impregnation of the commercial high surface area silica (Fischer Scientific Inc., surface area ~550 m^2/g, powder 100-200 μm), with metal nitrates as the 2 M solutions in water used as precursors. Total metal loading was 15, 21 or 25 wt. %. After impregnation and drying, the samples were calcined in air at 350 ^oC; these are referred to as the "calcined" samples.

In the desulfurization experiments, the challenge gas was the model reformate with an inlet concentration of 1 or 2 vol. % H_2S, 33 vol. % CO or CO_2, balance H_2 (UHP grade from Airgas

South, Inc.), at a face velocity of 2.12 cm/s, corresponding to the volumetric gas flow rate of 0.1 slpm. The experimental setp-up and procedure are described in Chapter II. Regeneration of the "sulfided", i.e. "spent" sorbent was performed at 550 ^{o}C in the flowing air at a flow rate of 50 cc/min. The temperature of the furnace during the experiments was maintained using a PID temperature controller. The gas flow rates were controlled by mass flow controllers (Omega FMA 2405 Alaborg GFC1718). XRD, N2 adsorption-desorption isotherms, XPS and ESR are used to characterize the sorbents. The description of the techniques and conditions at which the equipments are operated is given in Chapter II.

IV.3. Results and Discussion

IV.3.1. Desulfurization Performance of the Sorbents

Figure IV.1 shows desulfurization performance of the undoped supported ZnO/SiO_2 sorbent prepared by us vs. the commercial ZnO extrudates (BASF and Sud-Chemie). Table IV.1 shows sulfur uptake capacity (g sulfur / g sorbent) and utilization of ZnO in the sulfidization reaction (% of the theoretical value for the ZnS stoichiometry).

Table IV.1: Sulfur capacities of the sorbents $M_{0.05}ZnO_{0.95}/SiO_2$

(at metal loading 21 wt. %).

M = dopant, $M_{0.05}ZnO_{0.95}/SiO_2$	Saturation Capacity, g S/g sorbent	ZnO Utilization at Saturation, %
Mn	0.050	60
Fe	0.069	83
Co	0.064	77

Ni	0.053	64
Cu	0.077	93
None	0.053	64

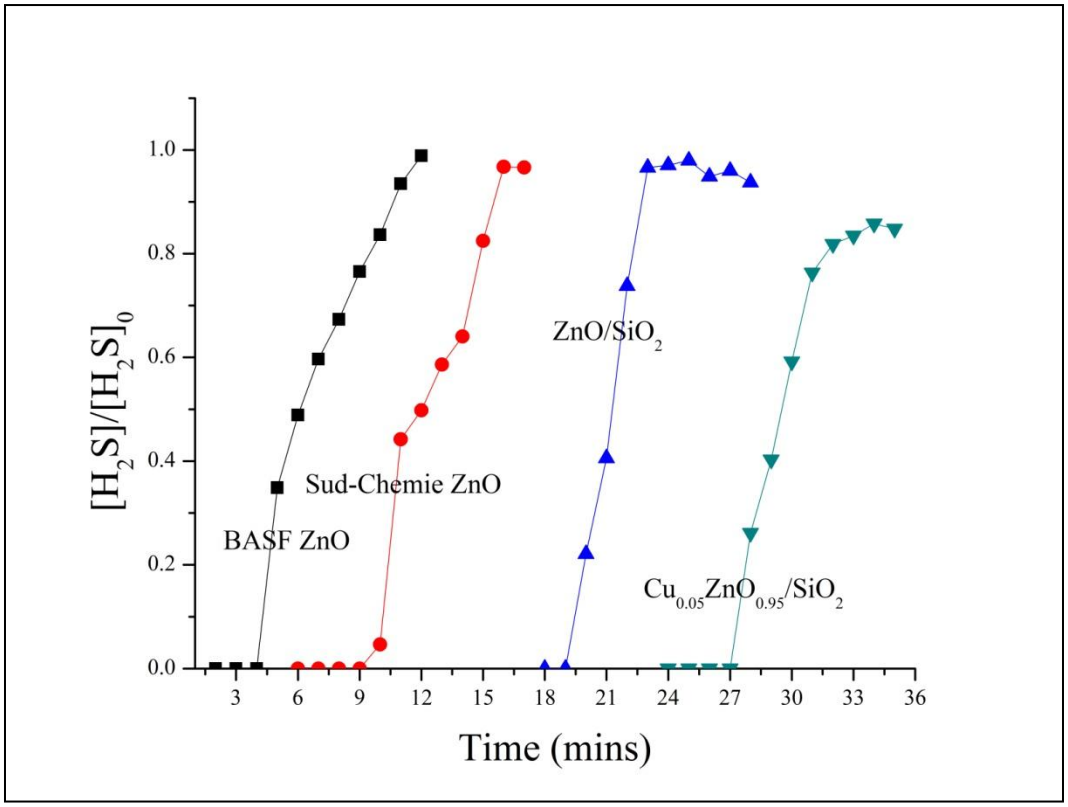

Figure IV.1: Breakthrough Curves for Commercial ZnO (BASF and Sud-Chemie) with 21 wt.% ZnO/SiO_2 and $Cu_{0.05}ZnO_{0.95}/SiO_2$. Test Conditions : Co = 1 vol%H_2S/H_2, T= 20C, Face velocity = 2.12 cm/s

The supported ZnO/SiO_2 sorbent showed better performance over both commercial ZnO-based sorbents. XRD of the ZnO/SiO_2 sorbent did not detect lines of neither zinc silicate Zn_2SiO_4 [93]

nor zinc oxide ZnO. These findings and the high sulfur capacity of the ZnO/SiO_2 sorbent indicate the nano-dispersed form of the supported ZnO, with a typical crystalline size of ~50 Å or less.

Table IV.2: Sulfur capacities and ZnO utilization of the doped sorbents $Cu_{0.05}ZnO_{0.95}/SiO_2$ vs. the un-doped ZnO/SiO_2 sorbent.

Sorbent	**ZnO Loading (w/w%)**	**Saturation Capacity (g S/g sorbent)**	**ZnO Utilization (%)**
BASF (SG-901)* ZnO	90	0.019	5.34
Sud-Chemie* (G-72E) ZnO	90	0.032	9.00
ZnO/SiO_2	21	0.053	63.88
ZnO/SiO_2	15	0.032	54.00
$Cu_{0.05}ZnO_{0.95}/SiO_2$	21	0.077	92.81
$Cu_{0.05}ZnO_{0.95}/SiO_2$	15	0.043	72.56
$Cu_{0.2}ZnO_{0.8}/SiO_2$	21	0.078	94.02
$Cu_{0.2}ZnO_{0.8}/SiO_2$	15	0.045	75.94

*Commercial ZnO is crushed to the same size 100-200 μm as the supported sorbent

The Cu-doped sorbent $Cu_{0.05}ZnO_{0.95}/SiO_2$ showed an enhanced sulfur adsorption capacity over all other sorbents (M = Mn, Fe, Co, Ni), over the un-doped ZnO/SiO_2 sorbent and over the un-supported commercial ZnO-based sorbents. Specifically, doped sorbent Cu-ZnO/SiO_2 shows a ~45 % improvement in the sulfur capacity over the undoped ZnO/SiO_2 sorbent. The XRD of the "calcined" doped $Cu_{0.05}ZnO_{0.95}/SiO_2$ sorbent was performed, and no lines due to any copper compound were found. This implies a high degree of dispersion of the Cu dopant in the $Cu_{0.05}ZnO_{0.95}/SiO_2$ sorbent. In the XRD of the "sulfided" sorbent, lines of CuS, Cu_2S and metallic Cu were not identified as well, that indicates the high dispersion of the Cu dopant in the "sulfided" sorbent and the absence of phase separation upon desulfurization.

IV.3.2. Performance of the Sorbents upon Multiple Regeneration Cycles

Figure IV.2 shows the breakthrough curves for the $Cu_{0.05}ZnO_{0.95}/SiO_2$ sorbent upon H_2S adsorption / regeneration cycles, as compared to the "fresh" sorbent. Upon multiple cycles of "desulfurization-regeneration", the sorbent retains up to 70 % of the initial sulfur capacity.

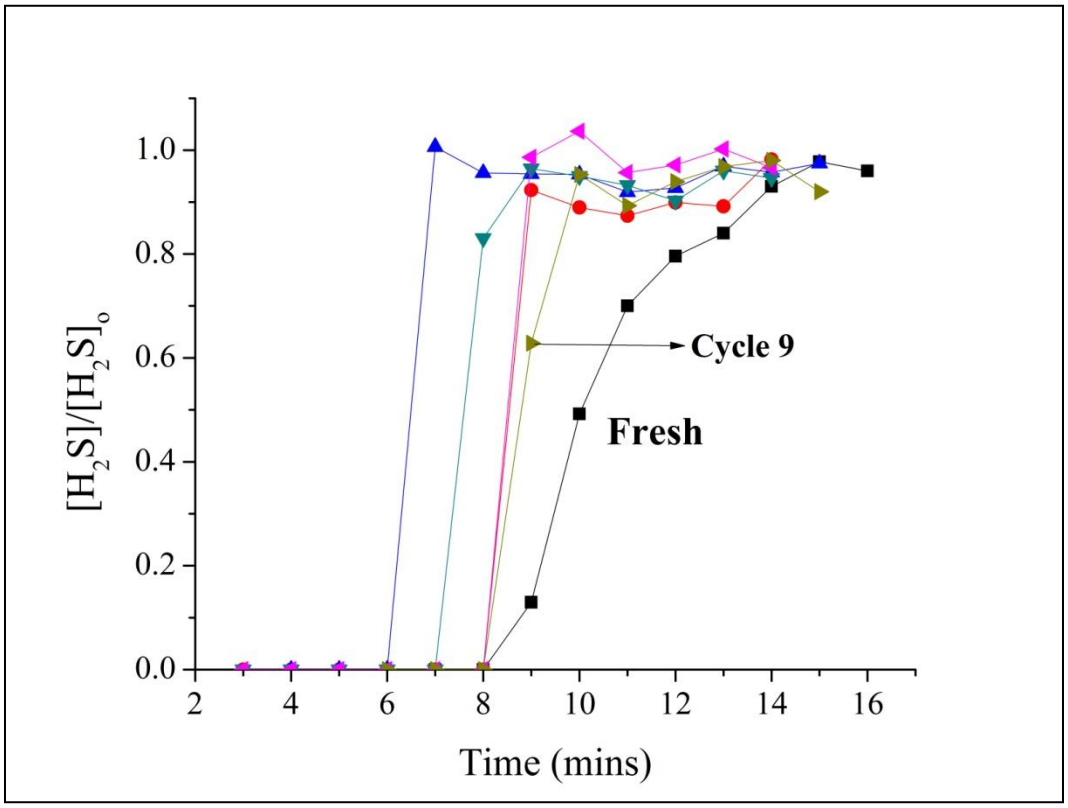

Figure IV.2 Breakthrough curves for Regeneration of $Cu_{0.05}ZnO_{0.95}/SiO_2$. Test Conditions: Calcination Temp = 350 C/Air/1h, Adsorption at 20 C, Co = 1vol% H_2S/H_2, Regeneration at : 550 C, Air/1h.

IV.3.3. Structural Characterization of the Sorbents

Table IV.3 shows surface area and pore volume of the sorbents. At ZnO loading on SiO_2 of 15 wt. %, there is ~16 % and 30 % reduction of surface area and pore volume respectively, as

compared to silica, and with the further increase of ZnO loading (at 25 wt. %), the surface area and pore volume are further reduced. On the other hand, upon doping the ZnO/SiO_2 sorbent (15 wt. % of ZnO) with Cu to obtain the $Cu_{0.05}$-$Zn_{0.95}/SiO_2$ sorbent, there is only a marginal change in surface area and pore volume. The latter finding indicates that structural characteristics of the ZnO/SiO_2 sorbent do not significantly change when Cu dopant is added.

Table IV.3: Surface Area and Pore Volume Data analyzed using N_2 Adsorption-Desorption Curves

Sample	ZnO Loading (w/w%)	S_g	V_g
		(m^2/g)	(cc/g)
SiO_2	0	550	0.792
ZnO/SiO_2	15	460	0.558
ZnO/SiO_2	25	330	0.486
Cu-ZnO/SiO_2	15	450	0.592
SiO_2	21	330	1.65
ZnO/SiO_2	21	244	1.04

IV.3.4. Characterization of the Sorbents by XPS

Figure IV.3 shows the XPS Zn 2p (Figure 3A), Zn $L_3M_{45}M_{45}$ (Figure 3B) and O 1s (Figure IV.3C) lines of the "calcined" sorbent $Cu_{0.2}Zn_{0.8}O/SiO_2$. The following elements are identified in the XPS survey spectrum (data not shown): Cu, Zn, Si, O, and spurious carbon as expected. No residual nitrogen was detected that indicates the complete decomposition of metal nitrate precursors used. The samples show a strong electrostatic charging (~5 eV), as expected for the electrically insulating silica support. The sorbent of the formula $Cu_{0.05}Zn_{0.95}O/SiO_2$ has the similar XPS spectrum, except that the XPS signal from the Cu dopant is too low to be reliably interpreted. The BE of the Zn 2p3/2 line is 1022.1 eV that is consistent with the reported BE of

1022.0-1022.1 eV for Zn^{2+} form [80] in zinc oxide catalyst [94] and of BE=1022.4 eV in pure ZnO [95]. The BE of the Zn $L_3M_{45}M_{45}$ peak is found by us to be 265.6 eV (with Mg anode). The Auger Parameter (AP) is useful for processing XPS spectra of the electrically insulating samples such as supported sorbents and catalysts, since its value is independent on the electrostatic charging of the specimens [96]. We calculated the AP_{Zn} to find the coordination state of Zn in the "calcined" sorbent, by using the formula AP_{Zn} = 1253.6 + BE(Zn 2p3/2) - BE(Zn $L_3M_{45}M_{45}$) = 2010.1 eV. This corresponds to ZnO as expected whose AP_{Zn} is 2010.25 eV [97]. On the other hand, for the ZnO-SiO_2 nano-composites that were prepared by the sol-gel technique and that were shown to contain ZnO nanoparticles embedded into the SiO_2 matrix with the significant concentration of Zn-O-Si bonds, AP_{Zn} is as low as 2009.1 eV [97]. We conclude that in the "calcined" Cu-ZnO/SiO_2 sorbent, Zn is present in the form of ZnO nanoparticles located on the SiO_2 surface, rather than included into the lattice of SiO_2.

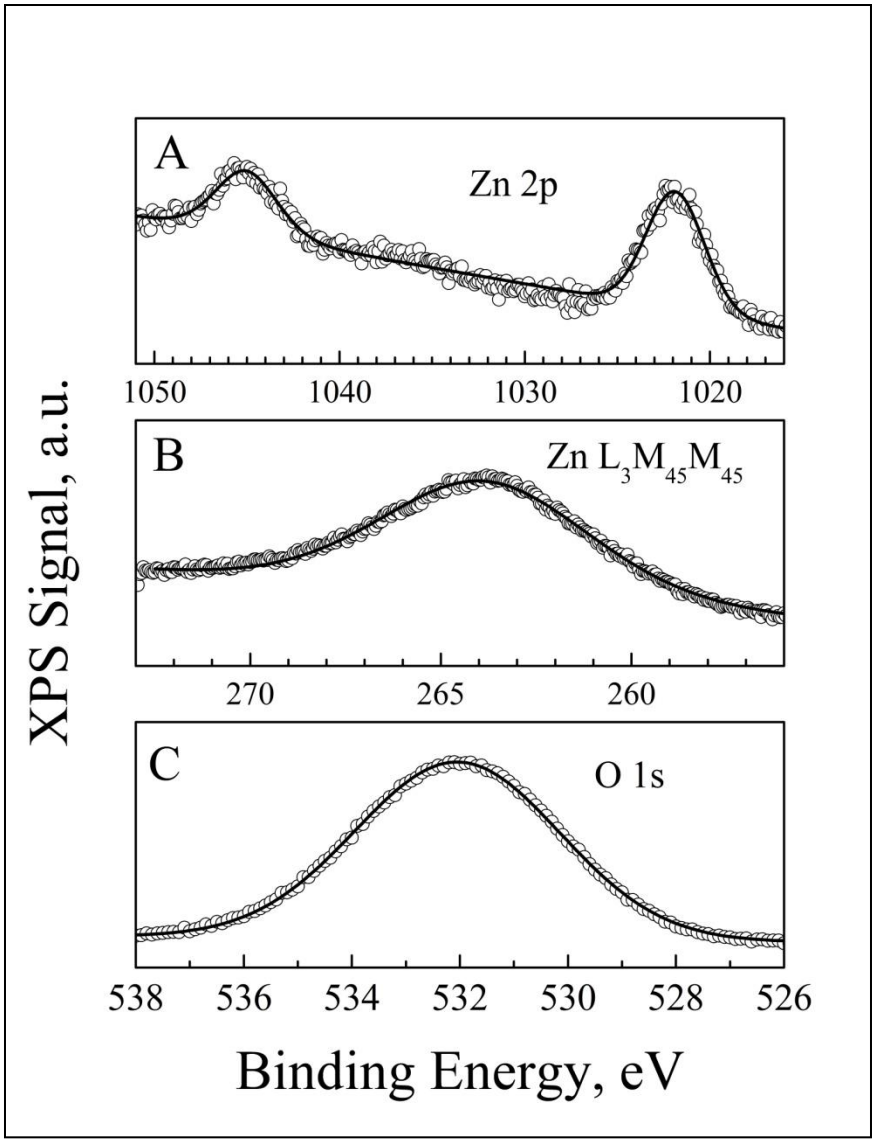

Figure IV.3: XPS Spectra of Calcined $Cu_{0.05}ZnO_{0.95}/SiO_2$

Figure IV.3C shows the O 1s peak that can be well fitted as the singlet (our attempts to fit it as spectral doublet were unsuccessful). The BE is 531.9 eV that is close to the reported value of 531.5 eV for silicon oxide SiO_2 [98]. It was reported that for the pure silica that was calcined with flowing oxygen at 673 K, the O 1s peak is the singlet [99], while for the SiO_2 thin films, both bridging oxygen atoms (Si-O-Si, BOs) at 531.5 eV and the non-bridging atoms (Si-O-, NBOs) at the lower BE are found as shoulders of the O 1s peak [98]. On the other hand, the BE

of O 1s in zinc oxide ZnO is as low as 529.7 eV [100]. From these data, we conclude that the O 1s peak in Figure IV.3C belongs mostly to the bridging oxygen of the silica support.

We have calculated the atomic ratios Cu/Zn, Zn/Si and O/Si from our XPS data, following the standard formula that includes the areas of the XPS peaks, the photoionization cross-sections σ and the photoelectron mean free paths (MFPs) [95]. The following ratios are found for the "calcined" sorbent of the nominal formula $Cu_{0.2}Zn_{0.8}O/SiO_2$: O/Si=2.00, Cu/Zn=0.30; Zn/Si=0.20. The atomic ratio O/Si=2.00 supports our conclusion above that the O 1s peak is mostly due to oxygen of the silica support. The atomic ratio Cu/Zn=0.30 is somewhat higher (by 20 %) than the theoretical atomic ratio of 0.25 for the sorbent $Cu_{0.2}Zn_{0.8}O/SiO_2$. The deviation of 20% must be attributed to the standard error bar of the XPS measurement of ~10% and the respectively larger error bars for the atomic ratio; the error bar may also include the systematic errors due to the values of σ and MFPs used. On the other hand, the measured atomic ratio of Zn/Si=0.20 is higher (by 53 %) than the nominal atomic ratio of Zn/Si=0.13 of the sorbent containing 15 wt. % ZnO supported on SiO_2. This deviation is significantly higher than the typical error of the XPS measurements, as mentioned above. Our explanation is that the atomic ratio determined by the surface sensitive XPS does not reflect the "bulk" atomic ratio Zn/Si=0.13. If Zn is located on the surface of silica as the nano-islands (or nano-particles), the Zn/Si ratio determined by XPS should be higher than the "bulk" ratio Zn/Si=0.13, due to the attenuation of the XPS signal of silicon support, consistently with our findings. However, only the small faction of the SiO_2 surface is covered by the ZnO, since the O 1s XPS peak mostly belongs to SiO_2, not to ZnO as shown by us above. From the combined XRD and XPS data is not possible to determine the exact coverage of the surface of SiO_2 with ZnO and the size of the nano-crystallites formed. Assuming 100 % dispersion of ZnO, the uniform dispersion of ZnO

over *all* available surface area of SiO_2 and the Zn-O bond length of 1.7 Å, the *nominal* coverage of ZnO is as low as 0.04 of a monolayer. The real coverage of ZnO is definitely higher, and is determined to be approximately 0.2 of a monolayer, as from our XPS data.

We have measured the XPS Cu 2p1/2 and 2p3/2 lines (data not shown) of the "calcined" sorbent $Cu_{0.2}Zn_{0.8}O/SiO_2$. There are the "shake-up" peaks in the spectra thus indicating the presence of Cu in the Cu^{2+} form. Based on the thermodynamic considerations and the "history" of calcination in air, all Cu is expected to be present in the Cu^{2+} state as CuO, rather than in the Cu^{1+} state. For the XPS spectra of CuO, the ratio of the area of the Cu shake-up peak at ~942 eV to the area of the Cu 2p3/2 peak at 933.6 eV is 0.53 [101]. However, in our XPS spectra, this ratio is less thus indicating the presence of both Cu^{1+} and Cu^{2+} forms. We conclude that artificial XPS-induced reduction of the Cu^{2+} form to Cu^{1+} form occurred. Indeed, XPS-induced reduction of Cu^{2+} in Cu-containing specimens due to the X-Rays, heat and secondary electrons was reported in the lietrature [102, 103]. Moreover, the conversion of the octahedral Cu^{2+} into the tetrahedral Cu^{2+} under the X-Rays radiation in the XPS experiments was reported in copper-exchanged X- and Y-type sodium zeolites [101]. Thus, a complementary non-destructive spectroscopic technique is needed to be used to learn about the speciation of the Cu dopant in the Cu-ZnO/SiO_2 sorbents.

Figure IV.4 shows the XPS Zn 2p (Figure 4A), Zn $L_3M_{45}M_{45}$ (Figure 4B) and O 1s (Figure 4C) lines of the "sulfided" sorbent of the formula $Cu_{0.2}Zn_{0.8}O/SiO_2$. The following elements are identified in the XPS survey spectrum (data not shown): Cu, Zn, S, Si, O and spurious carbon as expected. No nitrogen was detected as expected. The samples show a strong electrostatic charging (~5 eV), as expected for the electrically insulating material, therefore there is no significant amount of metallic copper in the samples. The binding energy (BE) of Zn 2p3/2 line

is measured to be 1021.9 eV. Binding energy (BE) of Zn 2p3/2 line is not very characteristic of coordination environment of zinc in ZnO vs. ZnS, with the difference being less than 0.5 eV [103]. The binding energy of the Auger $L_3M_{45}M_{45}$ line of zinc is 263.9 eV. We calculated the AP_{Zn} to find the coordination state of Zn in the "sulfided" samples, by using the formula AP_{Zn} = 1253.6 + BE(Zn 2p3/2) - BE(Zn $L_3M_{45}M_{45}$) = 2011.6 eV. This corresponds to ZnS whose AP_{Zn} is 2011.44 eV [104], while for ZnO, the AP_{Zn} is as low as 2010.25 eV [97]. Formation of ZnS is consistent with the high sulphur uptake capacity of the $Cu_xZn_{1-x}SiO_2$ sorbents upon sulfidization, ~92% of the theoretical value.

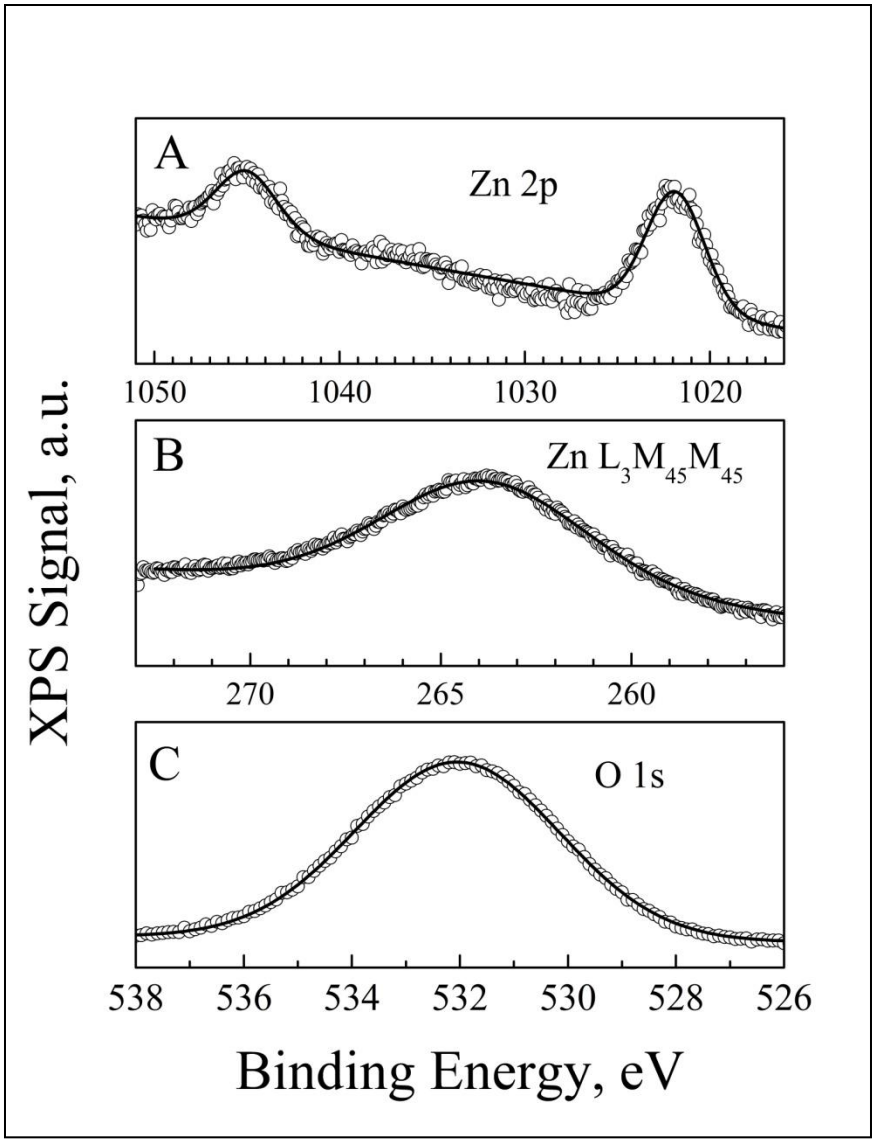

Figure IV.4: XPS Spectra of sulfided sorbents $Cu_{0.05}ZnO_{0.95}/SiO_2$

We have measured the XPS spectrum of the Cu 2p1/2 and 2p3/2 lines (data not shown) of the "sulfided" sorbent $Cu_{0.2}Zn_{0.8}O/SiO_2$. In the $Cu_{0.05}Zn_{0.95}O/SiO_2$ sorbent, the signal from Cu is too small to be reliably obtained. We have not found the XPS shake-up peaks of the Cu 2p lines in the spectra of the "sulfided" sorbent that indicates the absence of CuO. Further, the literature states that the expected sulfidization product CuS has no XPS shake-up peaks [105]. Using the

Auger $L_3M_{45}M_{45}$ line of Cu might be the choice, however, Auger lines are usually much broader that XPS lines, and fitting Auger line with the multiplet due to several components of Cu, from CuS, Cu_2S and Cu_2O is not reliable; in our measurements, the Cu Auger line was too small to be reliably interpreted. Moreover, the BE of the Cu 2p3/2 peak [106] in CuS (932.3 eV) is virtually identical to the one in Cu_2S [107], so that these forms of Cu cannot be distinguished by XPS. In addition, the XPS-induced sample damage of the Cu-containing specimens due to the X-Rays, heat and secondary electrons was reported [103] as manifested by the reduction of Cu^{2+} to Cu^{1+}. Thus, the complementary non-destructive spectroscopic technique was applied to learn more about the speciation of the Cu dopant.

IV.3.4. Characterization of the Sorbents by ESR

Figure IV.5 shows ESR spectra of the "calcined" sorbent $Cu_xZn_{1-x}O/SiO_2$. Figure IV.5A corresponds to the $Cu_{1.0}Zn_{0.0}O/SiO_2$, Figure IV.5B – $Cu_{0.1}Zn_{0.9}O/SiO_2$, Figure IV.5C - $Cu_{0.01}Zn_{0.99}O/SiO_2$ and Figure IV.5D - $Cu_{0.001}Zn_{0.999}O/SiO_2$. Silica support that was prepared similarly to the "calcined" sorbent, except that Cu^{2+} salt was not used, shows no ESR spectrum, as expected. No spectral lines due to the paramagnetic Cu^0 atoms are found in the spectra of the "calcined" sorbents $Cu_xZn_{1-x}O/SiO_2$, as expected. In addition, no spectral lines of any Reactive Oxygen Species (ROS) or oxygen vacancies [87] are present in the ESR spectra. The "calcined" sorbent of the formula $Cu_{0.0}Zn_{1.0}O/SiO_2$ shows no ESR spectrum, thus confirming that the spectral multiplet in Figure 5 belongs to Cu^{2+}.

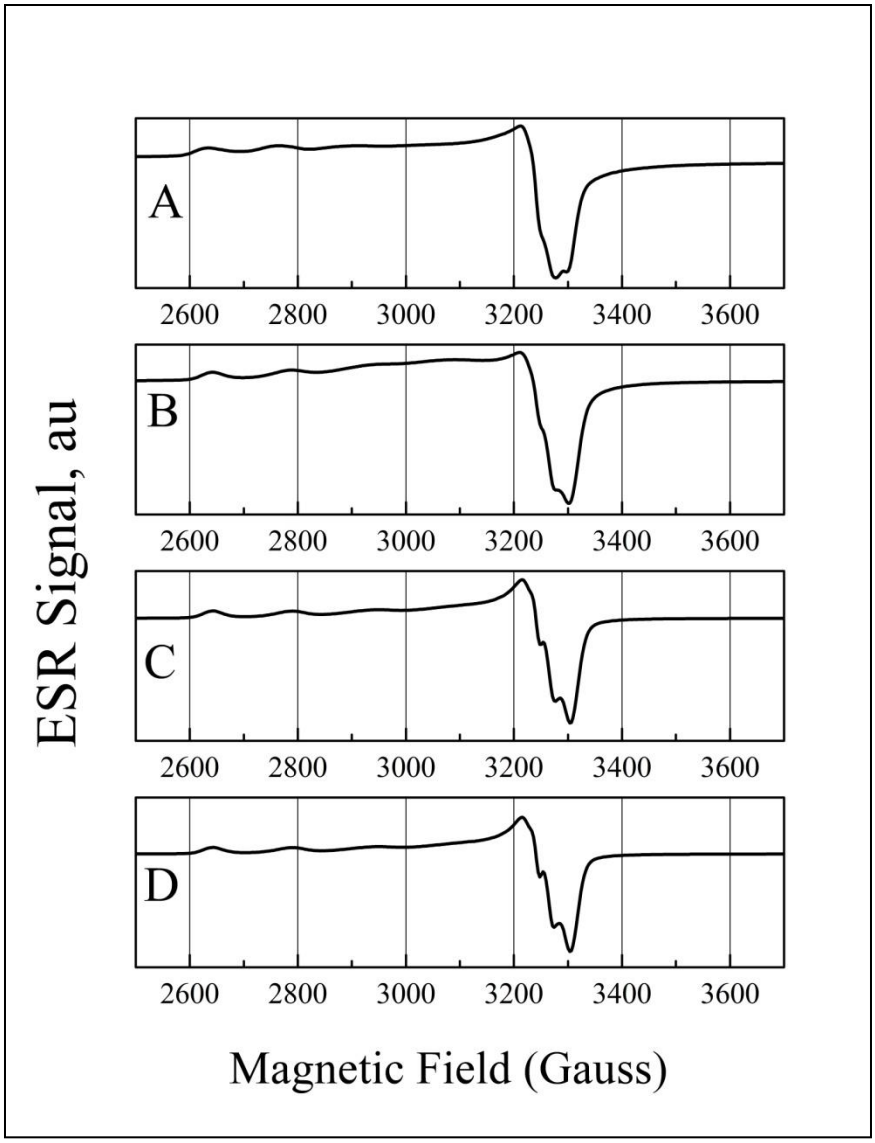

Figure IV.5: ESR spectra of the "calcined" sorbent $Cu_xZn_{1-x}O/SiO_2$ Figure 5A - $Cu_{1.0}Zn_{0.0}O/SiO_2$, Figure 5B – $Cu_{0.1}Zn_{0.9}O/SiO_2$, Figure 5C - $Cu_{0.01}Zn_{0.99}O/SiO_2$ and Figure 5D - $Cu_{0.001}Zn_{0.999}O/SiO_2$.

The ESR spectral pattern of Cu^{2+} is rather complicated, both due to hyperfine splitting [108] and presence of two major stable isotopes, ^{63}Cu (mole fraction 0.6915, nuclear spin 3/2) and ^{65}Cu (mole fraction 0.3085, nuclear spin 3/2) that both contribute to the multiplet observed. The ESR spectrum of Cu^{2+} in $Cu_{0.05}Zn_{0.95}O/SiO_2$ was simulated as the single kind of Cu^{2+} species (Figure

6), and was found to have g values of 2.077, 2.051 and 2.349, consistently with the literature reports of the copper-zinc oxide catalysts [84]. The ESR spectra of the "calcined" $Cu_xZn_{1-x}O/SiO_2$ sorbent show broadening of the spectral features of the Cu^{2+}, as concentration of Cu^{2+} increases (Figure IV.5). This behavior is well known [109], and it was attributed to interactions between isolated Cu^{2+} ions.

Various forms of Cu species are found to exist in both supported and unsupported copper-containing oxides: nanoclusters [110], isolated Cu^{2+} ions [110, 111], binuclear oxygen-bridged ion pairs [112] such as $[Cu\text{-}O\text{-}Cu]^{2+}$. The high probability of formation of the Cu^{2+}-OH-Cu^{1+} bridge structures was found by calculations [113]. Therefore, the straightforward interpretation of the ESR spectrum is difficult [111], thus some chemical tests needed to be performed in order to assign the spectrum to the certain Cu^{2+} species.

First, we have checked if evacuation of the "calcined" sorbent $Cu_{0.05}Zn_{0.95}O/SiO_2$ in the ESR test-tube down to 10^{-6} Torr with the subsequent readmission of air affects the ESR spectrum of Cu^{2+}. It was reported that Cu^{2+} ions present on surface of the Cu-Zn-Al mixed oxide catalysts cause the significant broadening of the ESR signal upon admission of air, due to interaction of Cu^{2+} with the adsorbate [84]. We have observed no line narrowing of the Cu^{2+} signal upon outgassing that indicates that the majority of Cu^{2+} ions in the "calcined" sorbents $Cu_xZn_{1-x}O/SiO_2$ are not on the surface of the sorbent. No other spectral lines appeared in the ESR spectrum of the sorbent upon evacuation and re-admission of air. The latter finding indicates that the ROS, including oxygen vacancies and superoxide radicals [114] are not present in the significant amounts in the "calcined" sorbents $Cu_xZn_{1-x}O/SiO_2$ and are unlikely to play a role in the surface chemistry of the subsequent H_2S adsorption.

Next, we have checked if reduction of Cu^{2+} ions with CO changes the ESR signal of the "calcined" sorbent $Cu_{0.05}Zn_{0.95}O/SiO_2$. It was reported [84] that CO exhibit a high reactivity towards the surface Cu^{2+} ions in the Cu-containing catalysts at room temperature, reducing Cu^{2+} to Cu^{1+} and even to Cu^0. We have not observed any changes in the ESR spectrum of Cu^{2+} after reduction of the "calcined" sorbent $Cu_{0.05}Zn_{0.95}O/ SiO_2$ with CO at room temperature. This finding is consistent with the conclusion that majority of Cu^{2+} ions are not on the surface. This excludes the possibility of the CuO-ZnO phase separation, formation of the "core-shell" supported nanoparticles or the islands of Cu oxides. This finding also indicates that no reduction of the Cu dopant in the "calcined" sorbent $Cu_xZn_{1-x}O/SiO_2$ occurs due to chemical reaction with the CO component of the H_2S containing reformates.

It was also reported that Cu^{2+} ions in the CuO-ZnO catalysts are not reduced by H_2 at room temperature if Cu^{2+} ions are well-dispersed in the binary oxide [84]. We have not observed any significant changes in the ESR spectrum of Cu^{2+} after reduction of the "calcined" sorbent $Cu_{0.05}Zn_{0.95}O/SiO_2$ with H_2 at room temperature. This finding indicates the following: i) The Cu^{2+} species present in the "calcined" sorbent are likely to be the isolated Cu^{2+} ions; ii) Cu^{2+} ions are not preferentially located on surface of the sorbent; iii) no reduction of Cu^{2+} with H_2 component of the model reformate occurs upon H_2S adsorption, iv) Cu_2O is unlikely to be present in the "sulfided" sorbent, and any Cu^{1+} found in the "sulfided" sorbent is formed upon chemical reaction with H_2S, not with H_2 component of the reformate. The latter finding allows to expect that variations of the H_2 concentration in the reformate would not affect the reactions of the Cu dopant in the $Cu_xZn_{1-x}O/SiO_2$ desulfurization sorbents.

The overall shape of the ESR signal of Cu^{2+} in the "calcined" $Cu_xZn_{1-x}O/SiO_2$ sorbent is similar to that of the polycrystalline sample containing isolated ions Cu^{2+} in a site with an axial

symmetry [114]. It is also similar to the ESR signal of Cu^{2+} ions in the site of octahedral symmetry with tetragonal distortions, namely, with axis lengthening and planar shortening [110]. We conclude that there is only one kind of Cu^{2+} ions in the "calcined" sorbent $Cu_xZn_{1-x}O/SiO_2$ that is Cu^{2+} ions well-dispersed in the "bulk" of the sorbent.

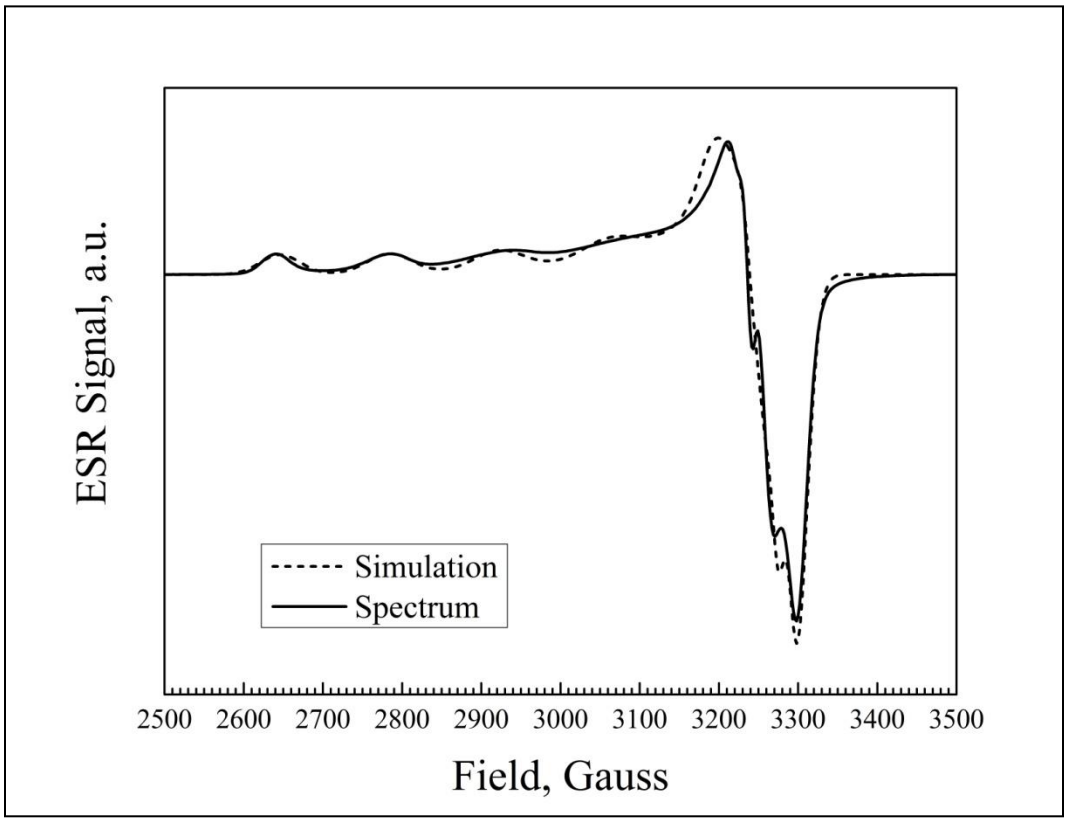

Figure IV.6: ESR spectrum of Cu^{2+} in $Cu_{0.05}Zn_{0.95}O/SiO_2$ simulated as the single kind of Cu^{2+} species.

The ESR spectra of the sulfide Cu (0,0.1,0.2 and 1) was also obtained. The spectral shapes of the signals of Cu^{2+} ions are similar to those of the "calcined" sorbents (Figure IV.5), although the ESR intensities are lower for the "sulfided" sorbents. We did not observe the ESR patterns of the Cu^0 atoms, the ROS species or oxygen vacancies. The findings indicate a partial reduction of the ESR-active Cu^{2+} form to the ESR-silent Cu^{1+} form upon the interaction of the "calcined" sorbent with the H_2S component of the reformate. In the ESR spectra of the "sulfided" sorbent, there was

an additional ESR triplet of the low intensity that was also found in the ESR spectrum of the silica support treated with H_2S in hydrogen. This ESR triplet is sensitive to admission of air to the ESR test-tube, and is tentatively assigned to the HS^- or S_2^- anion radical or similar species [115, 116], however, its exact structure is not known. Upon thermal oxidative regeneration of the "sulfided" sorbent, the ESR triplet disappears that supports its assignment to the reduced, rather than oxidized, form of radical species. In order to reliably determine the ESR signal of Cu^{2+} in the "sulfided" sorbent, the triplet was subtracted from the spectra, and the spectral reminder that belongs only to Cu^{2+} was doubly-integrated as usual.

Figure IV.7A shows the doubly integrated (DIN) ESR signal of Cu^{2+} that is proportional to molar concentration of Cu^{2+} in the "calcined" vs. "sulfided" sorbents $Cu_xZn_{1-x}O/SiO_2$ (x=0.001, 0.01, 0.05, 0.1 and 1). Figure 7B shows the yield Y of chemical reaction of the reduction of Cu^{2+} to Cu^{1+} upon the interaction with the H_2S component of the reformate.

$$Y = [Cu^{2+}_{calc.}] - [Cu^{2+}_{sulf.}] \ / \ [Cu^{2+}calc.] \qquad (1)$$

where $[Cu^{2+}_{calc}]$ is molar concentration of Cu^{2+} in the "calcined" sorbent; $[Cu^{2+}_{sulf.}]$ is molar concentration of Cu^{2+} in the "sulfided" sorbent. The Cu^{2+} reduction yield Y is dependent on concentration of copper in the "calcined" specimens: the higher the concentration of copper, the less efficient the reduction of Cu^{2+} into Cu^{1+}. This dependence correlates with the sulfur uptake capacity of the $Cu_xZn_{1-x}O/SiO_2$ sorbent, namely, sulfur capacity is significantly reduced for the samples with the high concentration of Cu, ~x>0.2. This correlation suggests that the highly dispersed Cu^{2+} ions in the $Cu_xZn_{1-x}O/SiO_2$ sorbent act as promoters of the adsorption of H_2S by the host material ZnO and are themselves converted to copper sulfides.

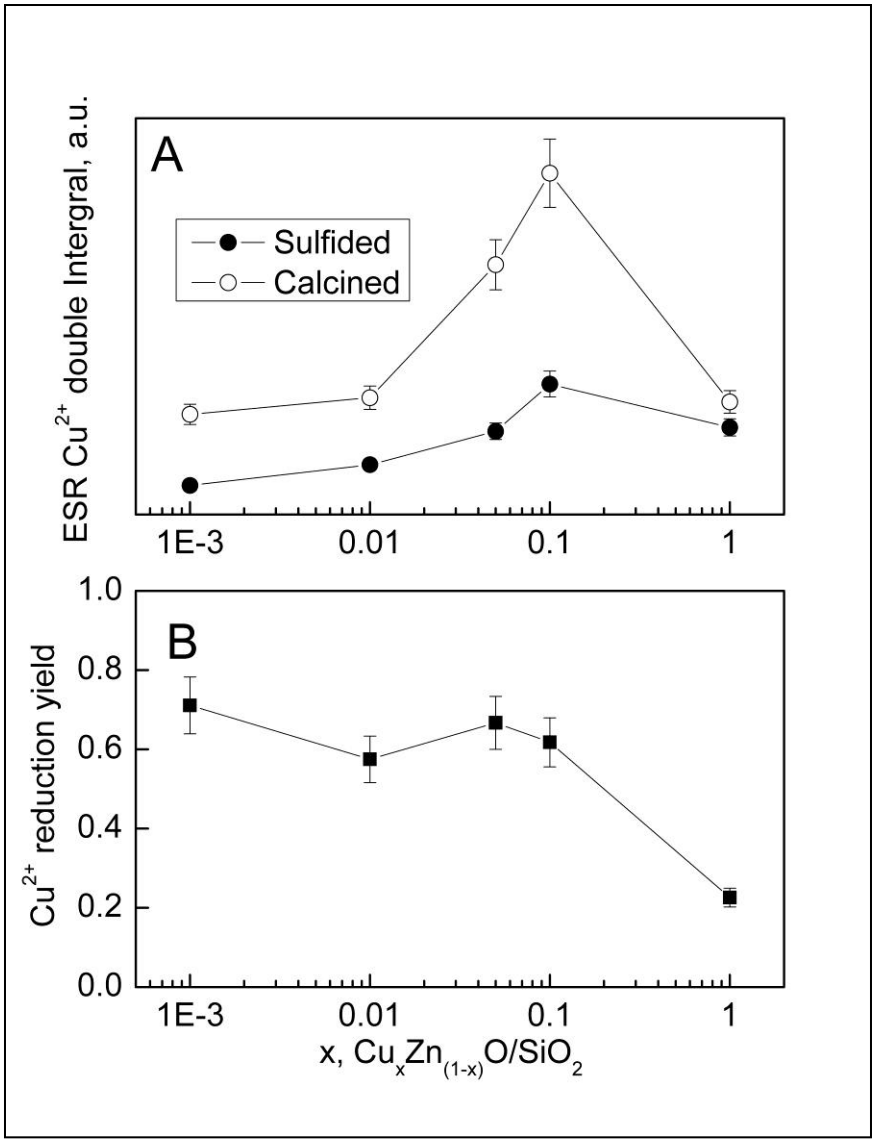

Figure IV.7: Figure 7A shows the relative signal intensity of Cu^{2+} proportional to molar concentration of Cu^{2+} in the "calcined" vs. "sulfided" sorbents $Cu_xZn_{1-x}O/SiO_2$ (x=0.001, 0.01, 0.05, 0.1 and 1). Figure 7B shows the yield Y of chemical reaction of the reduction of Cu^{2+} to Cu^{1+} upon the interaction with the H_2S component of the reformate

We have noted that upon the multiple desulfurization-regeneration cycles, there is a reduction of the sulfur uptake capacity (Figure IV.2). We have investigated if the reduction of the sulfur capacity upon multiple cycles is accompanied by the changes in the ESR signal of

Cu^{2+} dopant ions. Figure IV.8 shows ESR spectrum of Cu^{2+} in the sorbent $Cu_{0.05}$-$Zn_{0.95}O/SiO_2$, "calcined" *as-prepared* vs. "calcined" upon 10 cycles of desulfurization-regeneration. Several changes can be noted. First, the hyperfine structure of Cu^{2+} at 2600-3100 G is less pronounced for the multiply-regenerated sorbent. This suggests clustering of the isolated Cu^{2+} ions or the formation of a second kind of Cu^{2+}. Second, the peak at ~3300 G shows different shapes, namely, the low-field shoulder at ~3285 G is stronger for the multiply-regenerated "calcined" sorbent, and the high-field shoulder at ~3305 G is stronger for the "fresh calcined" sorbent. Those differences indicate that some changes occur to the Cu^{2+} dopant ion upon multiple adsorption-regeneration cycles. Specifically, spectral changes could occur due to 1) aggregation of Cu^{2+} ions into nano-clusters or islands (phase separation); 2) diffusion of Cu^{2+} ions towards the surface of the supported sorbent and formation of the surface Cu^{2+}; 3) diffusion towards the SiO_2 interface, forming some kind of the interfacial copper silicate.

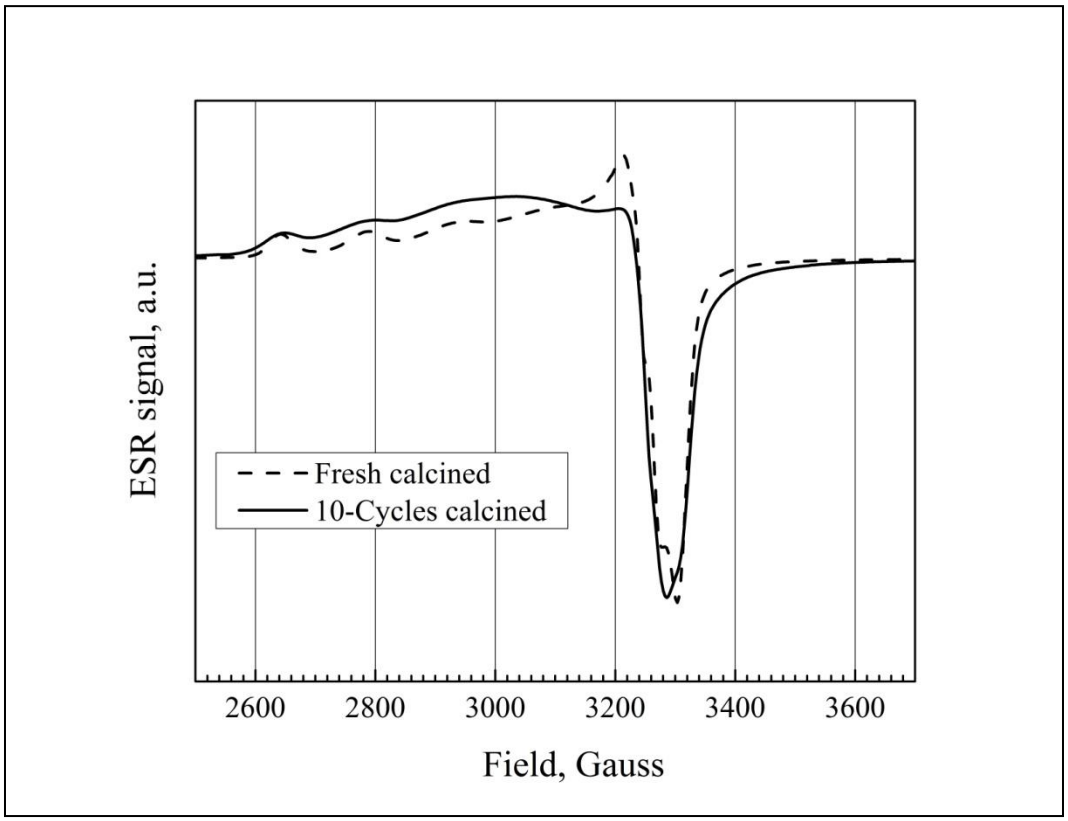

Figure IV.8: ESR spectrum of Cu^{2+} in the sorbent $Cu_{0.05}$-$Zn_{0.95}O/SiO_2$, "calcined" *as-prepared* vs. "calcined" upon 10 cycles of desulfurization-regeneration.

The surface complex with three Cu-O-Si bonds shows the largest shift of the ESR peak maximum towards the low field, compared to the surface complexes with two Cu-O-Si bonds. Moreover, the surface complex with three Cu-O-Si bonds shows the spectral shift compared to the Cu species that are not coordinated with surface of silicon oxide, i.e "bulk" form of Cu^{2+}. Based on the assignments from the literature [117], we propose that spectral change of the ESR signal of Cu^{2+} upon multiple desulfurization-regeneration (Figure IV.8) could be due to forming at least one Cu-O-Si bond, upon the thermally-induced diffusion of Cu^{2+} ions towards the interface with silica support. The alternative explanation originates, when we compare the spectral shape of the regenerated sorbent $Cu_{0.05}$-$Zn_{0.95}O/SiO_2$ (Figure 8) with ESR spectrum of the "calcined" sorbent that contains only copper and no zinc, i.e. $Cu_{1.00}$-$Zn_{0.00}O/SiO_2$, Figure 5A. Both spectra show the same pattern, namely, the stronger shoulder at the low field, ~3285 G and the weaker shoulder at the higher field, ~3305 G. Such similarity implies that in the multiply-regenerated sorbent, agglomeration of Cu^{2+} could also take place. Additional experiments are underway to determine in more detail the atomic level structure of the Cu^{2+} centers in the multiply-regenerated sorbent, as function of the "aging" of the sorbent. One of the complementary approaches is to use the well-designed model sorbents, such as thin films of binary oxides, CuO-ZnO on the oxidized silicon wafers, in their "calcined" vs. "sulfided" form, to learn in the systematic fashion about the thermally-induced sintering, diffusion and surface chemical reactions upon sulfidization and regeneration.

IV.4 Conclusions

The Cu dopant enhances utilization of the ZnO active phase of the novel ZnO/SiO_2 sorbent during adsorptive desulfurization of the reformate streams at room temperature, from 64 % to 92 %, and maintains a high sulfur uptake capacity upon multiple cycles of a simple thermal oxidative regeneration of the "spent" sorbent in air (up to 10 cycles). Both zinc and copper oxides are nano-dispersed in the $Cu\text{-}ZnO/SiO_2$ sorbent, and both the "calcined" and "sulfided" forms of the sorbent contain Cu^{2+} in the single dispersion and coordination state. The higher concentration of the Cu promoter in the $Cu\text{-}ZnO/SiO_2$ sorbent, the lower the reduction yield of Cu^{2+} to Cu^{1+} upon adsorption of H_2S that correlates with sulfur uptake capacity. The "deactivated" sorbent (upon 10 adsorption-regeneration cycles) is enriched with the different chemical form of Cu^{2+} dopant, as compared to the "as-prepared" sorbent.

Acknowledgement

Authors would like to thank the US Army (TARDEC Contract W56HZV-05-C-0686) for the financial support of this work.

Chapter V: Regenerable Fe-Mn-ZnO/SiO_2 sorbents for Room Temperature Removal of H_2S from Fuel Reformates: Performance, Active sites and Operando studies

Priyanka Dhage, Alexander Samokhvalov[1], Divya Repala, Evert C. Duin[2], and Bruce J. Tatarchuk[1]

Department of Chemical Engineering, Auburn University, Auburn, AL 36849

[1]Department of Chemistry, University of Rutgers, Camden, NJ 08102

[2]Department of Chemistry and Biochemistry, Auburn University, Auburn, AL 36849

Abstract

The Fe- and Mn-promoted H_2S sorbents Fe_x-Mn_y-$Zn_{1-x-y}O/SiO_2$ (x, y=0, 0.025) for the ultradeep desulfurization of model reformates at room temperature were prepared, tested and characterized. Their sulfur uptake capacity significantly exceeds that of both commercial unsupported ZnO sorbents (by 60 %) and of the un-promoted supported sorbent ZnO/SiO_2 (by 30 %). Sulfur sorption capacity and the breakthrough characteristics remain satisfactory after up to 10 cycles of adsorption/regeneration, with regeneration performed by a simple heating in air. XRD shows that both "calcined" and "spent" sorbents contain the nano-dispersed forms of ZnO, Fe and Mn and XPS confirms the conversion of the supported ZnO phase to ZnS. The "calcined" sorbent contains Fe^{3+} and Mn^{3+} ions, while upon H_2S adsorption, their reduction to Fe^{2+} and Mn^{2+} occurs. Fe^{3+} ions are believed to occupy the surface of the supported ZnO nanocrystallites, while Mn^{3+} ions are distributed uniformly within ZnO.

Keywords: Desulfurization, H_2S, Promoter, ZnO, Fe, Mn, XPS, ESR

V.1. Introduction

Fuel cell-based systems for electric power generation, such as auxiliary power units (APUs) for diesel trucks and remote power supplies for the military, offer both portability and high energy efficiency, and they have been intensively studied in the past decade [74]. Recently, high power fuel cells were developed for *non-transport* applications as well, ranging from kilowatt [118] to megawatt [119] power generating systems. Intensively developed fuel cell technologies constitute the basis of a potential energy-efficient and environmentally benign "hydrogen economy" [120]. The core components of the fuel cell-based power generation systems are: i) steam reformers, ii) catalytic partial oxidation (CPO) reformers and iii) autothermal reformers (ATR) [75] that convert liquid hydrocarbon logistic fuels to the H_2-enriched gaseous reformates. H_2S impurity in the reformates is known to be poisonous to the catalytic systems of fuel processing units (FPUs), fuel cell electrodes and electrolytes in the Poly Electrolyte Membrane fuel cells (PEMFCs). In order to avoid "sulfur poisoning," reformates should contain < 1 ppmv or even < 60 ppb sulfur as for the PEMFCs [121], and robust and inexpensive desulfurization materials and regimes need to be developed. Modern adsorptive desulfurization technologies that use metal oxide-based H_2S sorbents can reduce sulfur concentration in the gas phase from several thousand ppmw down to the sub-ppmv levels [76, 77]. However, the majority of such sorbents were developed for the hot-gas cleanup (HGC) of the streams of the integrated gasification combined cycle (IGCC); therefore, such sorbents operate at high temperatures, ~500-800 ºC [122].

The best material for adsorptive removal of H_2S is ZnO [123] because of its favorable sulfidation thermodynamics and high sulfur capacity (by weight). However, a serious problem of the high temperature (> 500 ºC) H_2S adsorbents is the reduction of ZnO by hydrogen into metallic zinc and evaporation of the latter [122]. Several oxides of other metals such as iron, vanadium, zinc, copper, manganese and molybdenum have been proposed as high-temperature desulfurization sorbents since the 1970s [124]. Chemical and structural transformations of those oxides upon desulfurization/regeneration were investigated; for instance, it is known that in the environment of the IGCC gasifier, Mn_3O_4 form is readily reduced to MnO and the latter reacts with H_2S at the high temperatures [122]. Iron oxides have also been extensively investigated since the 1970s; iron oxide-based H_2S sorbents have high sulfur capacity and reactivity towards H_2S. However the equilibrium concentration of H_2S is as high as 100 ppmw. In addition, a number of the degradation processes occur above ~ 500 ºC, most importantly reduction of Fe_3O_4 to FeO [122]. Mixed metal oxide sorbents for high temperature desulfurization of coal gases were extensively reviewed in the past [125, 126].

Recently, active research and development efforts have been directed towards "mid-temperature" H_2S adsorbents [123]. For instance, iron oxide sorbents supported on silica provide improved stability *vs.* unsupported iron oxides for adsorptive desulfurization at the "mid-temperature" range, ~400 ºC [122]. The major research objective of the studies of the "promoted" desulfurization sorbents is to provide better attrition resistance, higher sulfidization capacity, lower equilibrium concentrations of H_2S and COS and an ability to remove multiple gas contaminants at the same time [123].

It is known that, in part, temporal deactivation of the sorbents is due to the destruction of the unique 3D structure of the material due to thermal factors. Therefore, desulfurization sorbents

that operate at room or slightly elevated temperatures are expected to show increased temporal stability as compared to their high- and mid-temperature analogs. Recently, there is increased interest in the "low temperature" H_2S adsorbents that operate between room temperature and ~100 ºC [127-129]. For instance, we reported preparation and testing of novel ZnO/SiO_2 sorbents for H_2S and carbonyl sulfide COS with the minimized mass transfer resistance [77, 89-92] that operate at room temperature and retain their high desulfurization capacity after >10 desulfurization/regeneration cycles, with the regeneration performed by the inexpensive and robust calcination in the flowing air.

The typical desulfurization promoters of the ZnO-based H_2S sorbents are cations of transition metals (TMs). The multi-component desulfurization sorbents are expected to demonstrate either additive or synergetic effects, similar to those reported for the heterogeneous catalysis, as found, for instance, by a high throughput synthesis and screening routine [130]. Both surface and bulk dispersion and oxidation states of the promoter ions are important factors controlling both reactivity of the sorbent and its temporal stability upon the multiple adsorption-regeneration cycles. Therefore, mechanistic studies of the effects of the promoter ions are needed.

To study the desulfurization promoter, i.e. the *minority* chemical component of the multi-component sorbent (or catalyst), suitable experimental technique(s) needs to offer: i) a rather high sensitivity, ii) the ability to analyze both surface and the "bulk" of the specimen, iii) the ability to study the local structure of the promoter site. There are few experimental techniques available to study the dispersion, oxidation and coordination state of the TM promoters, namely Electron Spin Resonance (ESR) [84, 85] and X-Ray Photoelectron Spectroscopy (XPS) [85, 86]. ESR has an excellent sensitivity ($>10^{11}$ spins/sample), and it provides information on the oxidation and coordination state of the typical TM dopant ions [12-14]. ESR is the typical "bulk-

sampling" technique, due to the large penetration depth of the gigahertz radio-frequency used; however, it can be effectively used as well to study the surface-localized radicals and the radical ions in the solid materials [131, 132]. On the other hand, XPS can conveniently complement ESR as pertinent to the studies of heterogeneous chemical systems, such as sorbents and catalysts [133], since it is the surface-sensitive technique that analyzes the topmost ca. 10 nm of the material only. The main limitation of XPS is its relatively low sensitivity (> 5 % of the monolayer) [103].

We report here the preparation of $Fe_xMn_yZn_{1-x-y}O/SiO_2$ and measurements of H_2S uptake at room temperature and desulfurization performance upon the multiple regeneration cycles of tthese sorbents. The novel desulfurization sorbents $Fe_xMn_yZn_{1-x-y}O/SiO_2$ can i) achieve >90 % of theoretical sulfur uptake capacity at room temperature, ii) reduce sulfur concentration in the gaseous stream from ~1000 ppm to < 1 ppm, iii) and be easily regenerated > 10 times by simple heating in air without a significant loss of performance. We report the characterization of the Zn, Mn, Fe, S sites in those sorbents by ESR and XPS.

V.2. Experimental

The promoted ZnO-based desulfurization sorbents of the nominal formula $Fe_xMn_yZnO_{1-x-y}/SiO_2$ (x, y=0; 0.025) were prepared by incipient co-impregnation of high surface area (300-550 m^2/g) silica (Fischer Scientific Inc.) of grain size 100-200 μm with solutions of nitrates of the respective metals in water, namely $Zn(NO_3)_2$, $Mn(NO_3)_2$ and $Fe(NO_3)_3$. Single step incipient impregnation was performed on the silica support to achieve metal oxide loading of 12-36% by varying the molarity of nitrate solutions. Upon incipient impregnation and drying, the samples were calcined in the flowing air at 350-550 ^oC; these are referred to as the "calcined" specimens. The specimens prepared as above, excepting the calcination step, are referred to as the "dried" sorbents. In the reference experiments, with the commercial H_2S sorbents (BASF SG-901 and Sud Chemie G-72E), they are crushed to the same particle size as that of the silica (100-200 microns) used to prepare the supported $Fe_xMn_yZnO_{1-x-y}/SiO_2$ sorbents.

Breakthrough curves for both commercial sorbents and $Fe_xMn_yZnO_{1-x-y}/SiO_2$ sorbents were measured at 20 °C. In the desulfurization experiments, the challenge gas was the model reformate with an inlet concentration of 1 vol. % H_2S in H_2. Gases were purchased from Airgas Inc. The face velocity (GHSV) of the stream is 1900 h^{-1}, corresponding to volumetric gas flow rate of 0.1 slpm. The desulfurization reactor contained 0.500 g sorbent; the sorbent bed size was 9 mm in diameter and 10 mm thick. H_2S uptakes during adsorption experiments were measured using a gas chromatography (GC) instrument (Varian CP3800) equipped with the thermal conductivity detector (TCD) and pulse flame photometric detector (PFPD). The specimens of the sorbents upon adsorption of H_2S are referred to as the "sulfided" samples.

Regeneration of the "sulfided," i.e. "spent" sorbent was performed *in-situ* in the sulfidation reactor at 550 ^{o}C in air at a flow rate of 950 h^{-1}. The sorbent $Fe_xMn_yZnO_{1-x-y}/SiO_2$ of 15 wt. % loading of ZnO was regenerated for over 10 cycles, with the regeneration temperature being the same as that of the sample calcination before the 1-st desulfurization cycle. The temperature of the furnace during the experiments was maintained using a PID temperature setpoint controller.

The samples were characterized using the N_2 adsorption desorption isotherms to study the changes in surface area, pore volume and pore size before and after metal oxide loading. Also, XPS, ESR and XRD are used to characterize the sorbent. The techniques and the conditions at which the equipments were operated is described in Chapter II.

V.3. Results and Discussion

V.3.1 Performance of the $Fe_xMn_yZn_{1-x-y}O/SiO_2$ Sorbents

Figure V.1 shows the H_2S sorption performance of the commercial ZnO sorbents from Sud Chemie and BASF, of the supported sorbent ZnO/SiO_2 prepared in our lab (21 wt. % loading of ZnO) and of the promoted $Fe_{0.025}Mn_{0.025}ZnO_{0.975}/SiO_2$ sorbent (21 wt. % loading of ZnO). The $Fe_{0.025}Mn_{0.025}ZnO_{0.975}/SiO_2$ sorbent shows a superior H_2S uptake compared to the others.

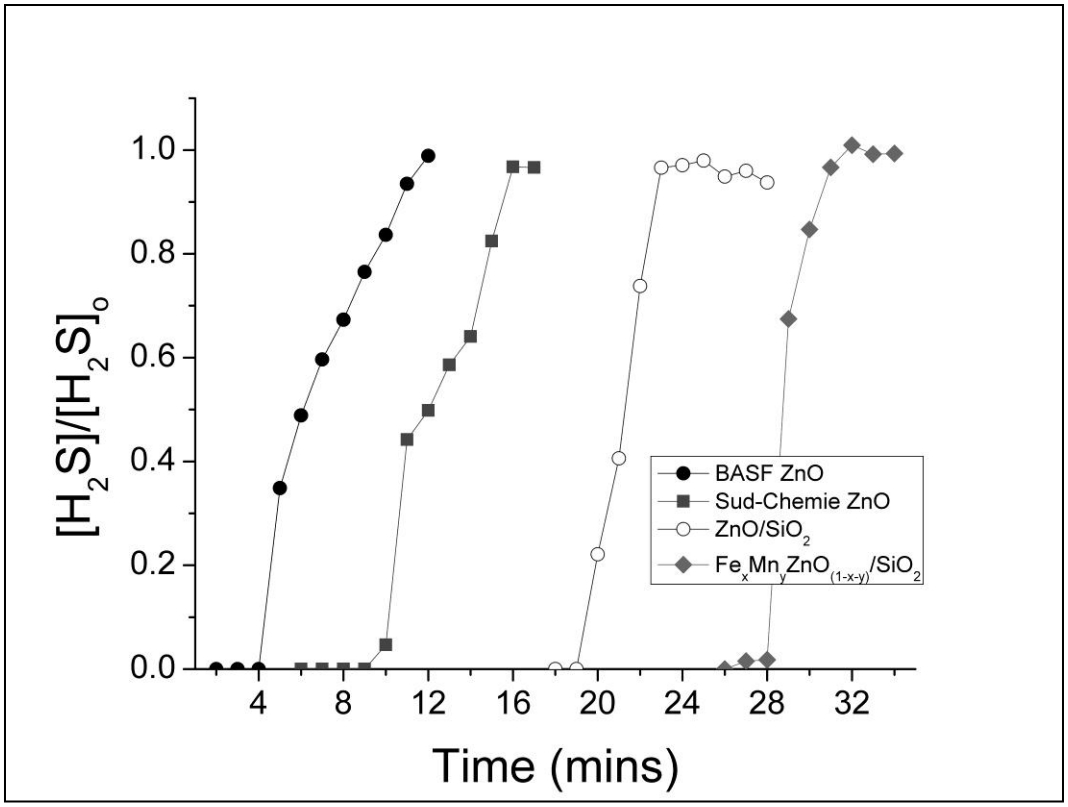

Figure V.1. H_2S Breakthrough curves of the commercial ZnO Sorbent from BASF (filled circles), Sud-Chemie (Squares), ZnO/SiO_2 (open Circles) and $Fe_{0.025}/Mn_{0.025}ZnO_{0.095}/SiO_2$ sorbent (diamonds)

Table V.1 shows the sulfur uptake capacity (g sulfur / g sorbent) and utilization of ZnO in the sulfidization reaction (% of the theoretical value for the ZnS stoichiometry) attained at the breakthrough and the saturation regimes. The breakthrough is defined as 2% of inlet concentration. The supported ZnO/SiO_2 sorbent has shown better performance over both commercial ZnO-based sorbents. XRD of the ZnO/SiO_2 sorbent at 15% wt. loading of ZnO did not detect lines of either zinc silicate Zn_2SiO_4 [93] nor zinc oxide ZnO. These findings and the

high sulfur capacity of the ZnO/SiO_2 sorbent indicate that the nano-dispersed form of ZnO is present in the supported sorbent, with the typical ZnO crystalline size ~40 Å or less.

Table V.1: Comparative breakthrough, saturation capacities and ZnO utilization data

Sorbent	**Loading**	**Sat Cap**	**ZnO Utilzation Sat. Cap**	**Breakthrough Cap**	**ZnO Utilization at Breakthrough**
BASF ZnO (SG-901)	90	0.019	5	0.011	3
Sud-Chemie (G-72E)	90	0.032	9	0.024	7
ZnO/SiO_2	15	0.032	54	0.026	45
$Fe_{0.025}ZnO_{0.975}/SiO_2$	15	0.043	72	0.035	58
$Mn_{0.025}ZnO_{0.975}/SiO_2$	15	0.043	72	0.037	62
$Fe_{0.025}Mn_{0.025}ZnO_{0.95}/SiO_2$	15	0.045	76	0.037	62
ZnO/SiO_2	21	0.053	64	0.051	61
$Fe_{0.025}Mn_{0.025}ZnO_{0.95}/SiO_2$	21	0.075	90	0.069	83

The adsorption capacity among the promoted sorbents of the formula $Fe_xMn_yZnO_{1-x-y}/SiO_2$ follows the trends: $Fe_{0.025}Mn_{0.025} \sim Mn_{0.025} > Fe_{0.025}$ and $Fe_{0.025}Mn_{0.025} > Mn_{0.05} > Fe_{0.05}$. XRD of the $Fe_{0.025}Mn_{0.025}ZnO_{0.975}/SiO_2$ sorbent in both "calcined" and "sulfided" forms was performed, and no lines due to any Fe or Mn compound were found that indicates a high degree of dispersion of the Fe and Mn promoters. Moreover, the observed promoter effects of Mn and Fe cations on the ZnO/SiO_2 sorbent are of the *synergetic*, rather than *additive* nature. Indeed, the increase of H_2S uptake of the promoted sorbent due to the additive effect would be insignificant

within the error bars of determining the outlet concentration of H_2S, given the low concentration of both Mn and Fe cations *vs*. concentration of ZnO in the promoted $Fe_{0.025}Mn_{0.025}ZnO_{0.975}/SiO_2$ sorbent. The synergetic mechanism of Mn and Fe H_2S sorption promoters implies that Fe and Mn cations are dispersed on top or within the ZnO supported nano-phase, rather than forming their own phases on the SiO_2 support.

V.3.2 Structural Characterization of the Sorbents

Figure V.2 shows the saturation capacity of the ZnO/SiO_2 sorbents and the total surface area vs. the wt. % loading of ZnO. It can be seen that the total surface area decreases linearly with the ZnO loading. On the other hand, saturation sulfur capacity is not linear *vs.* loading of ZnO within the whole range: it increases rather sharply at 0-25% loading and plateaus at the higher loadings. Similar phenomena were reported in the literature; for instance, H_2S uptake by Fe-Zn mixed metal oxides at room temperature is not proportional to their (active) surface area [134]. The non-linearity is due to the different chemical reactivity of the active sites of the sorbents of the different surface area.

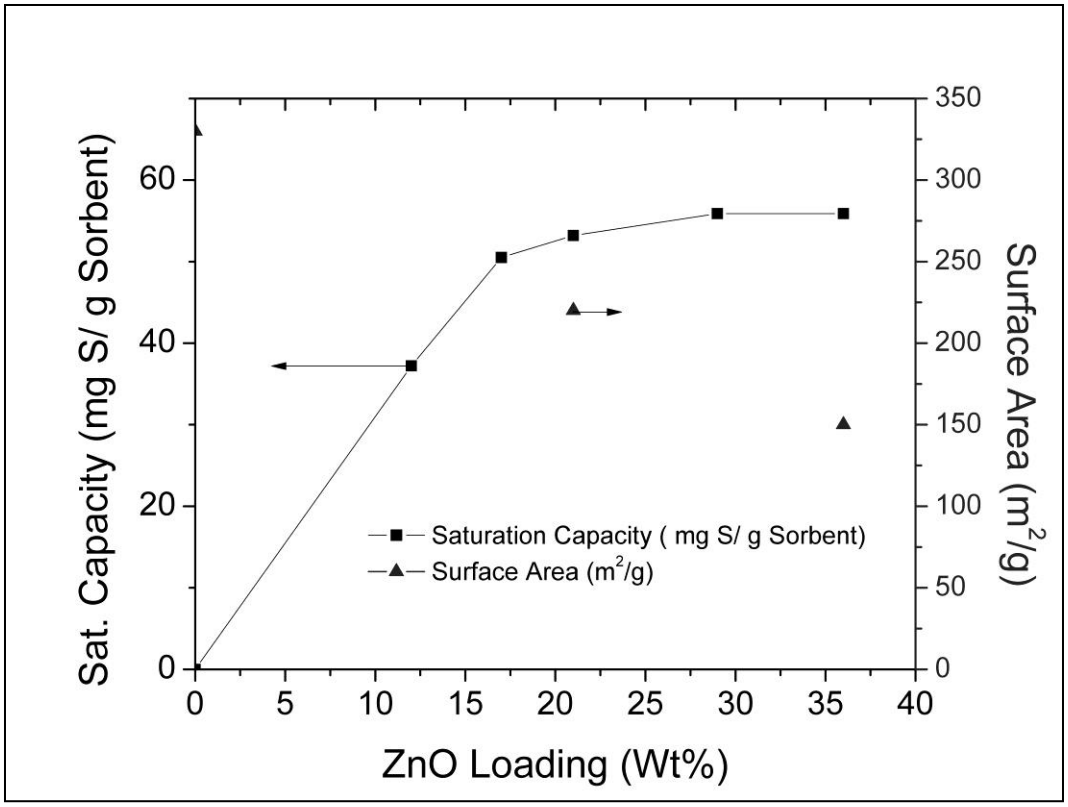

Figure V.2: H_2S Capacity (mg Sulfur/ g Sorbent) and the total surface area *vs.* the loading of ZnO (wt. %) in the ZnO/SiO_2 Sorbents.

Figure V.3 shows XRD of the ZnO/SiO2 sorbents at high loadings of ZnO (21 and 36 %). The pattern observed for the 36 % wt. loading of ZnO belongs to the XRD spectrum of ZnO of the wurtzite (hexagonal) structure [135]. Therefore, at such high loading of the supported ZnO, the latter is present as large crystallites whose desulfurization behavior corresponds to the plateau of the sulfur uptake (Figure 2). At the lower loading of ZnO of 21 %, there are no XRD lines except those of the silica support (Figure V.3). Therefore, an increase of ZnO loading beyond ca. 21 % when ZnO is of the large crystal size does not lead to an increase of the sulfur capacity. Therefore, the conclusion is that H_2S sorption occurs in the surface layer of the nano-dispersed ZnO, rather than proceeds within its "bulk." This conclusion is consistent with earlier reports that concluded that the surface reactivity of the ZnO-based H_2S sorbents as room temperature, when

only the outermost 0.6 nm of ZnO reacts with H_2S [134]. Indeed, for the ZnO crystallites at the limit of XRD detection (4 nm), as little as > 40% of the atoms are located on surface [136], while for the smaller ZnO crystallites (2 nm), as many as > 80% of all the atoms are on the surface.

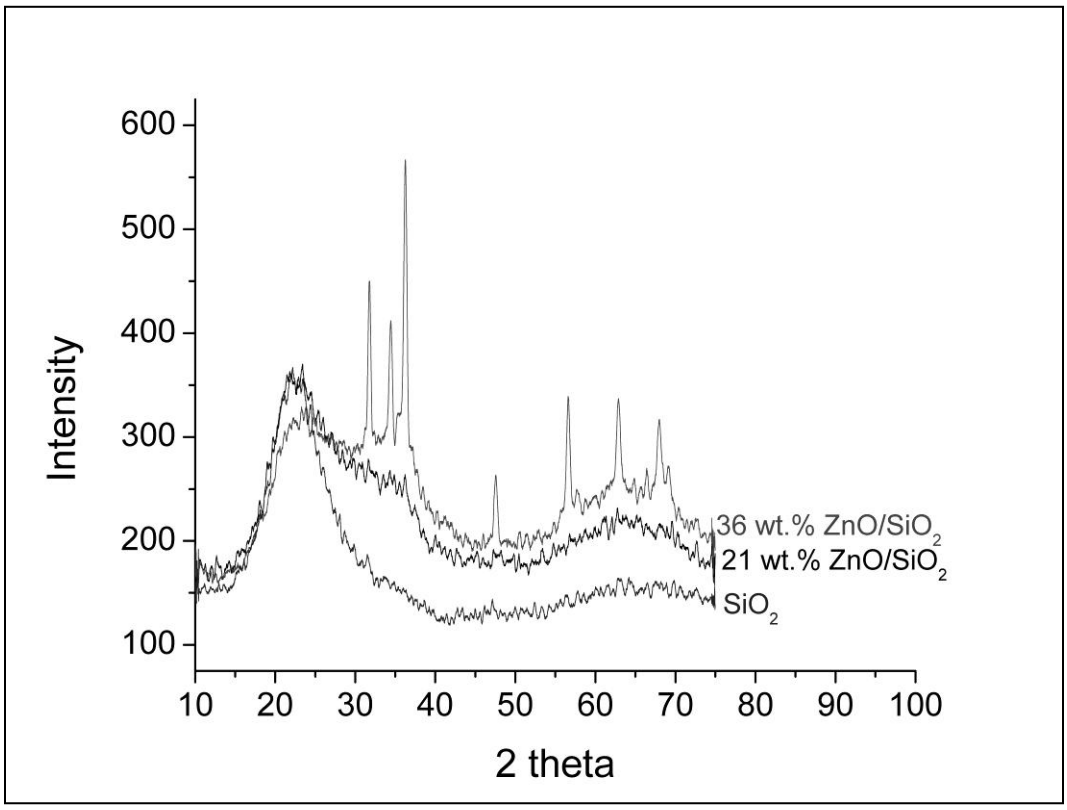

Figure V.3.: XRD Spectra of the ZnO/SiO_2 sorbents at 36 wt% of ZnO (solid line) and 21 wt. % (dashed dotted line) vs. SiO_2 support (dotted line)

Table V.2: Structural characterization of various H_2S sorbents

Sorbent	Loading	Surface Area	Pore Volume

		(m^2/g)	**(cc/g)**
SiO_2	0	550	0.79
ZnO/SiO_2	15	460	0.55
ZnO/SiO_2	25	330	0.48
$Fe_{0.025}ZnO_{0.975}/SiO_2$	15	325	0.52
$Mn_{0.025}ZnO_{0.975}/SiO_2$	15	314	0.53
$Fe_{0.025}Mn_{0.025}ZnO_{0.95}/SiO_2$	15	375	0.59
SiO_2	0	330	1.65
ZnO/SiO_2	21	244	1.04
$Fe_{0.025}Mn_{0.025}ZnO_{0.95}0/SiO_2$	21	160	1.02

The structural characteristics of the H_2S sorbents as determined by N_2 adsorption are shown in Table V.2. Upon promoting the ZnO/SiO_2 sorbent (15 wt. % of ZnO) with Fe and Mn to obtain the $Fe_xMn_yZnO_{1-x-y}/SiO_2$ sorbent, there is only a marginal change in surface area and pore volume. We have used the other silica support (with the pore volume of 1.65 cc/g) to prepare the sorbent with ZnO loading of 21 wt. %, and have obtained similar results. The latter finding indicates that structural characteristics of the ZnO/SiO_2 sorbent at those loadings do not significantly change when Mn and/or Fe promoter cations are added. Therefore, the promoted sorbents with ZnO loading of either 15 % or 21 % are the most effective, and the multiple-cycle adsorption/regeneration was conducted on the sorbent with ZnO loading of 15 %.

V.3.3 Performance of the Sorbents upon Multiple Regeneration Cycles

Figure V.4 shows the breakthrough curves for the $Fe_xMn_yZnO_{1-x-y}/SiO_2$ sorbents upon H_2S adsorption / regeneration cycles, as compared to the "fresh" sorbent (loading of ZnO is 15 wt %). The "fresh" sample is prepared at the calcination temperature of 550 ºC and the regeneration was performed at the same temperature. The sorption capacity fluctuates within the first 10 sulfidation/regeneration cycles; however, at the 10-th cycle, the capacity is as high as >80 of the "fresh" sorbent.

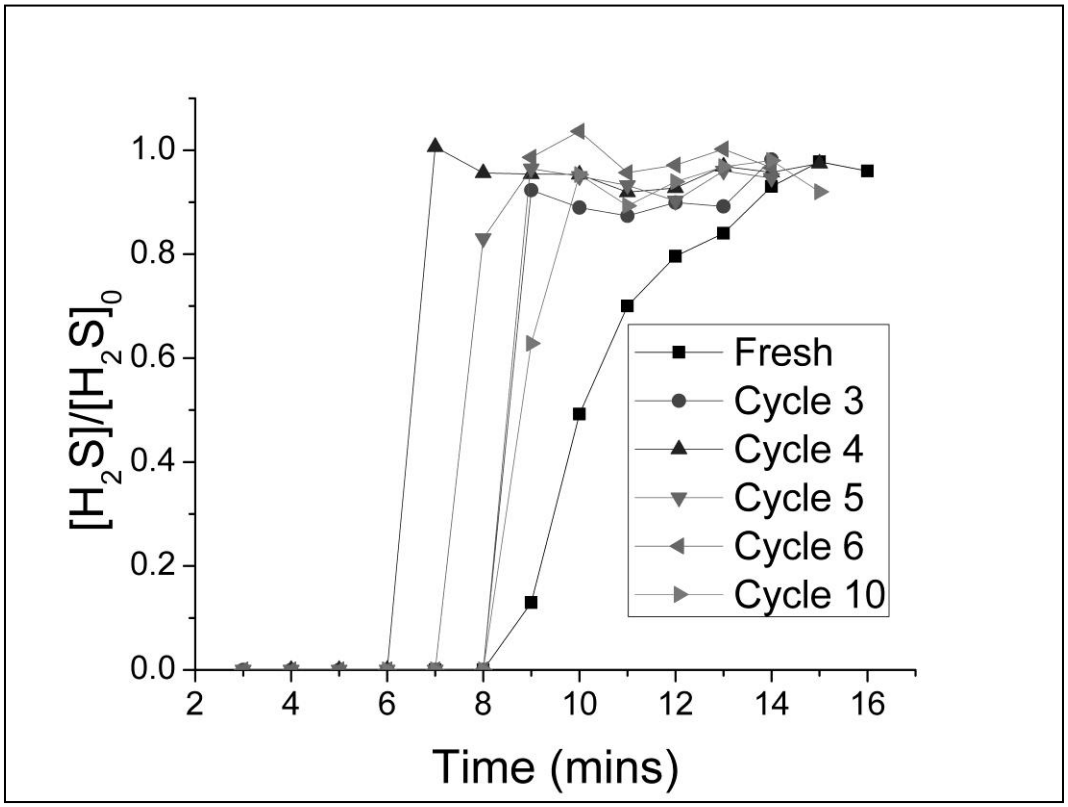

Figure V.4: H_2S breakthrough curves upon the multiple adsorption/regeneration of Fe_x-Mn_y-ZnO_{1-x-y}/SiO_2 sorbent

The loss of activity of the H_2S sorbents upon multiple sulfidation/regeneration cycles is well known; it is also known that the sulphur capacity does not always steadily decay *vs*. the number of cycles, but may undergo some fluctuations. For instance, in the multi-cycle study of H_2S

breakthrough curves obtained with the CuO/SiO_2 sorbent, the breakthrough capacity upon the 2-nd cycle is only ~50% as compared to the 1-st cycle. However, the capacity increases with the further cycles, with the occasional reduction of the breakthrough capacity on the 12-th cycle [137]. This type of behavior is likely to be due to the "hysteresis" effects, as the result of the dynamic changes in the materials system used under the non-equilibrium conditions of the repeated cycling of both temperature and the redox regime used (reductive conditions of the sulfidation *vs.* the oxidative conditions of the regeneration). The study investigating the sulfur breakthrough capacity within the multicycle (up to 100) tests were carried out for zinc titanate sorbents sulfided at the "middle-temperature" range of 480 °C [138]. The breakthrough capacity was shown to change following the complex pattern: increase of capacity up to the 3-rd cycle, then the fluctuating decaying trend of capacity.

V.3.4 Characterization of the Sorbents by XPS

Figure V.5 shows the XPS spectra of the calcined sorbent $Fe_{0.2}Zn_{0.8}O/SiO_2$. The strong electrostatic charging of up to 6 eV was observed, as expected for the electrically insulating specimen containing silica. Oxygen, silicon, iron, zinc and spurious carbon were detected in the survey spectra (not shown) as expected. The absence of the N 1s line in the XPS spectra indicates the complete decomposition of the nitrate precursors as expected. The sorbents with the *lower* concentration of Fe or Mn, such as $Fe_{0.05}Zn_{0.95}O/SiO_2$ and $Mn_{0.05}Zn_{0.95}O/SiO_2$ did not show the reliable XPS signals to determine Fe or Mn, consistently with the known limited sensitivity of XPS towards the species present at a small fraction of the monolayer. We note that the $Fe_{0.2}Zn_{0.8}O/SiO_2$ sorbent (Figure V.5) shows the satisfactory H_2S capacity, and the shape of its breakthrough curve reminds the one of the $Fe_{0.05}Zn_{0.95}O/SiO_2$ sorbent (data not shown).

Therefore, the structural and chemical information obtained from the analysis of the XPS data of the transition metal (TM) enriched XPS samples such as $Fe_{0.2}Zn_{0.8}O/SiO_2$ is relevant to the $Fe_xMn_yZn_{1-x-y}O/SiO_2$ (x,y=0, 0.05) sorbents that show the best desulfurization performance.

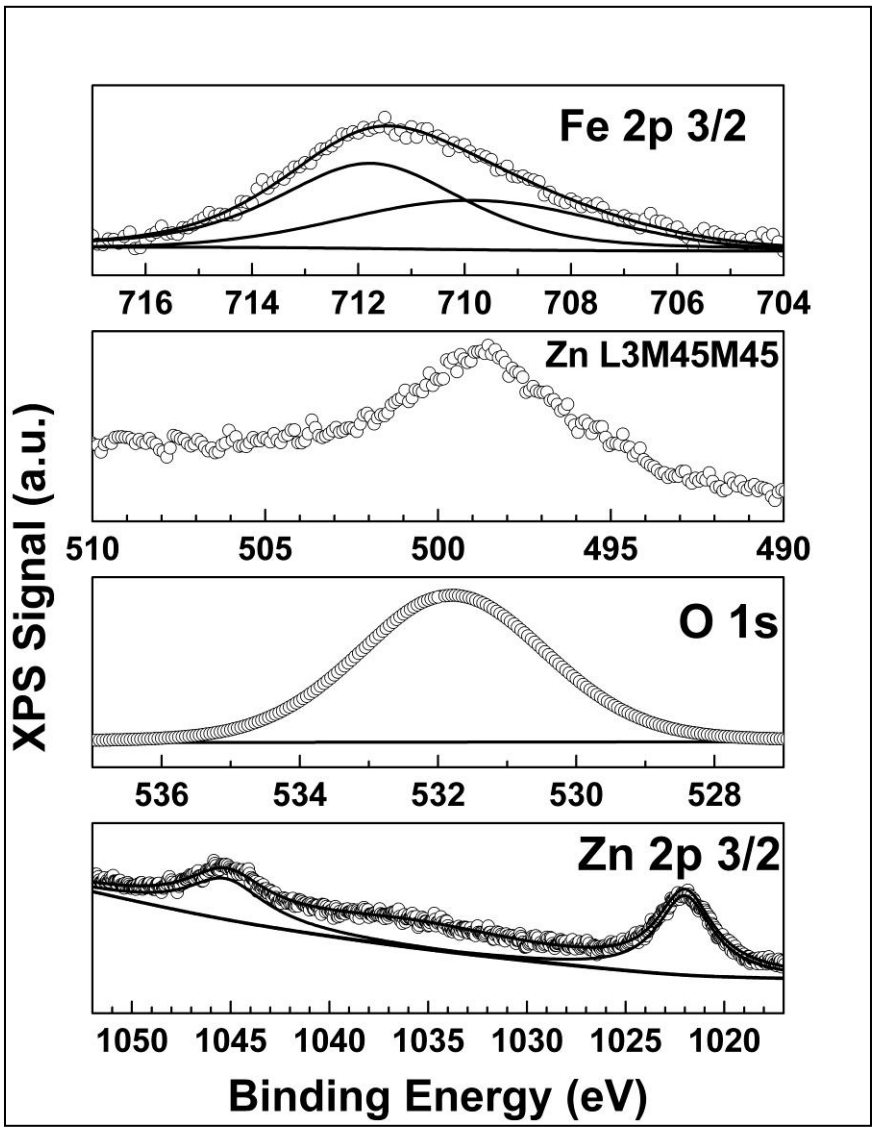

Figure V.5: The XPS lines of Fe 2p3/2 (Figure 5A), Zn Auger $L_3M_{45}M_{45}$ (Figure 5B), O 1s (Figure 5C) and Zn 2p (Figure 5D) of the "calcined" sorbent $Fe_{0.2}Zn_{0.8}O/SiO_2$.

The Binding Energy (BE) of the Zn 2p3/2 line (Figure V.5D) is 1022.1 eV that is consistent with the reported BE of 1022.0-1022.1 eV for the Zn^{2+} form in the zinc oxide catalyst [80]. The BE of the Zn $L_3M_{45}M_{45}$ peak (Figure V.5B) is 498.9 eV. The XPS Auger Parameter (AP) is more

useful than the BE for the determination of the oxidation state and coordination environment of atoms in the electrically insulating samples such as supported sorbents and catalysts, since its value is independent on the electrostatic charging [96]. The AP_{Zn} is calculated to find the oxidation and coordination state of Zn in the "calcined" sorbent, by using the formula AP_{Zn} = K.E.(Zn_{Auger}) + B.E.(Zn) = 2010 eV. As expected, this corresponds to ZnO whose AP_{Zn} is 2009.8 eV [97]. It must be further mentioned that atomic ratio of Zn/Si = 0.26 as measured by XPS is higher than the nominal value for the 21 % wt. loading of ZnO on silica. Hence, it should be concluded that in the "calcined" $Fe_{0.2}Zn_{0.8}O/SiO_2$ sorbent, Zn is present in the form of the ZnO nanoparticles located on the SiO_2 surface, rather than those included into the lattice of SiO_2.

Figure V.5C shows the O 1s peak that can be well fitted as the singlet, and its BE of 531.6 eV is close to the value [98] of 531.5 eV that was reported for O 1s line in silicon oxide SiO_2. For the pure silica that has been calcined in the flowing oxygen at 673 K, the O 1s peak is the singlet, while for the SiO_2 thin films, both bridging oxygen atoms (Si-O-Si, BOs) at 531.5 eV and the non-bridging atoms (Si-O-, NBOs) at the lower BE are found as shoulders of the O 1s peak [98]. On the other hand, the BE of O 1s in zinc oxide ZnO is as low as 529.7 eV [100]. From these data, we conclude that the O 1s peak in Figure V.5C belongs mostly to the bridging oxygen of the silica support, consistently with the low coverage of the ZnO as determined above by us.

Figure V.5A shows the Fe 2p3/2 XPS line that can be fitted with two spectral components. In the XPS studies of the Fe-containing sorbents and catalysts prepared or exploited in air, it was reported that Fe^{2+} and Fe^{3+} are the most typical oxidation states of iron [139]. Thus we conclude that Fe in the $Fe_{0.2}Zn_{0.8}O/SiO_2$ sorbent exists in both +2 and +3 oxidation states, with the BEs of the 2p3/2 line for Fe^{2+} and Fe^{3+}at 709.5 and 711.1 eV, respectively.

Atomic ratios in the calcined $Fe_{0.2}Zn_{0.8}O/SiO_2$ sorbent have been calculated from the XPS data. The ratio O/Si is found to be 2, as expected. The Fe/Zn ratio as determined by XPS is 0.6; that is significantly higher than the value of 0.25 as expected for the sorbent of the nominal formula $Fe_{0.2}Zn_{0.8}O/SiO_2$. This discrepancy should be attributed to the structure of the sorbent with its surface enriched with iron. Phase separation in the unsupported binary oxides of zinc and iron was reported earlier. For instance, upon the calcination of the binary oxide $ZnO\text{-}Fe_2O_3$ at 350 °C that was prepared by the co-precipitation from the solutions of metal salts, Fe_2O_3 was found by XRD as the separate phase [134]. These findings are consistent with our model of the partial exclusion of Fe^{3+} cations from the lattice of the nanocrystalline supported ZnO upon calcination.

On the other hand, in the XPS spectrum of the $Mn_{0.2}Zn_{0.8}O/SiO_2$ sorbent (data not shown), there are no XPS lines of manganese, apparently due to the too small concentration of manganese within the probing depth of XPS. Given the similar values of both photoemission cross-sections and the electron mean free paths (MFP) for the Mn2p and Fe 2p lines [140], we conclude that in the $M_xN_yZn_{1-x}O/SiO_2$ sorbents (M,N = Fe, Mn), the surface of the supported ZnO nano-crystallites is enriched with Fe, while Mn is dispersed relatively uniformly within the ZnO nanocrystallites.

Figure V.6 shows the XPS lines of the sulfided sorbent $Fe_{0.2}Zn_{0.8}O/SiO_2$. C, O, S, Si, Zn and Fe are found in the survey XPS spectrum. The Zn 2p3/2 line is found to be at 1021.6 eV, which can be attributed to ZnS. It is further confirmed by calculating the Auger parameter; namely, the A.P. of Zn in the sufided sorbent is calculated to be at 2011.5, which closely matches that of the ZnS form [104], as expected. The assignment of the XPS lines of sulphur is not possible, due to the their weak intensity, consistent with the smaller photoemission cross-section of the S 2p and S 2s lines, as compared with those for metals, such as Zn, Fe or Mn [140]. The XPS atomic ratio O/Si

is 2, as expected for the SiO2 being the majority chemical compound of the surface of the sorbent. Therefore, there is no significant changes of the morphology of the supported nanocrystalline ZnO upon sulfidization, as opposite to the re-crystallization and coarsening of the ZnO nanoparticles in the unsupported mixed metal oxides after the reaction with H_2S at room temperature [128].

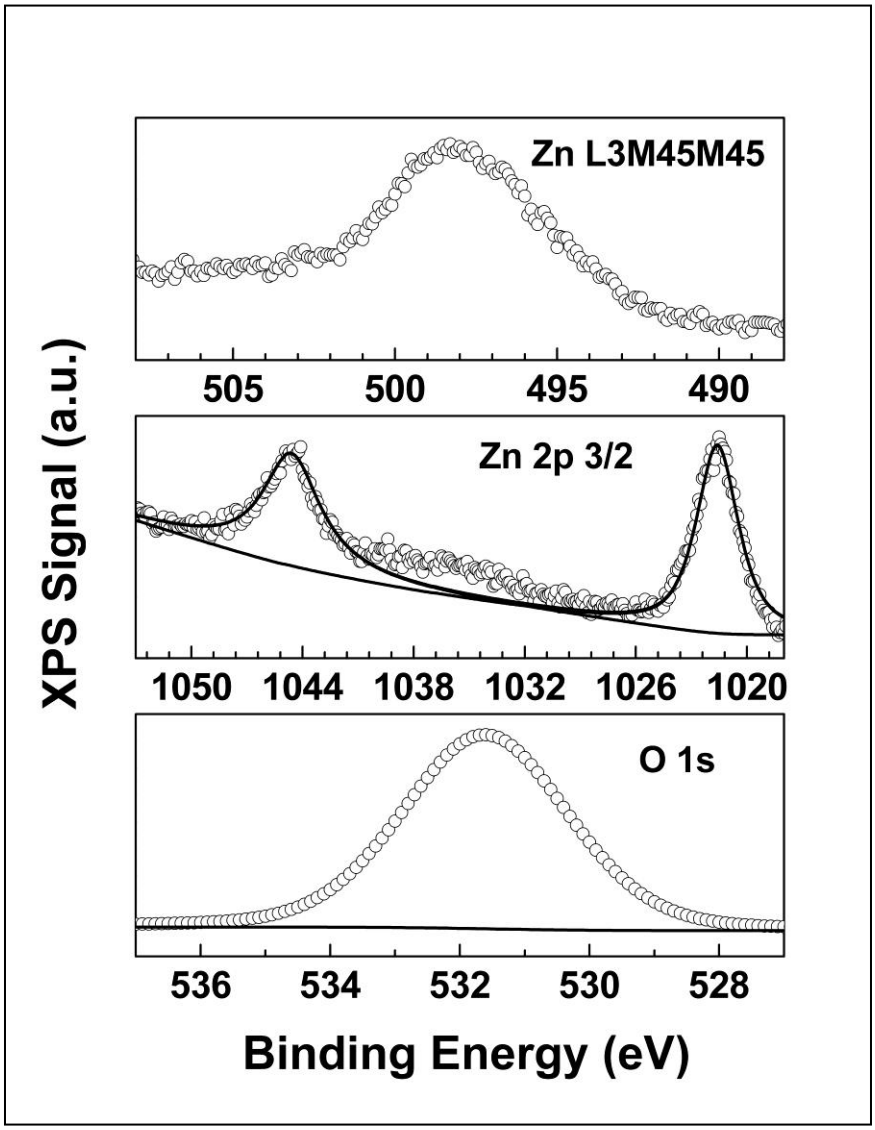

Figure V.6: The XPS lines of Zn Auger $L_3M_{45}M_{45}$ (Figure 6A), Zn 2p (Figure 6B) and O 1s (Figure 6C) of the sulfided sorbent $Fe_{0.2}Zn_{0.8}O/SiO_2$.

V.3.5 Characterization of the $Fe_xMn_yZn_{1-x-y}O/SiO_2$ Sorbents by ESR

Figure V.7A shows the ESR spectra of the "calcined" sorbents $Fe_{0.025}Zn_{0.975}O/SiO_2$ vs. $Fe_{0.025}Mn_{0.025}Zn_{0.950}O/SiO_2$, and Figure V.7B shows the spectra of the "sulfided" sorbents $Mn_{0.025}Zn_{0.975}O/SiO_2$ vs. $Fe_{0.025}Mn_{0.025}Zn_{0.950}O/SiO_2$. In the calcined sorbents, no ESR signal of Mn cations are seen that indicates the presence of Mn as the "ESR-silent" Mn^{3+} state only; even though Mn^{3+} with $3d^4$ electronic configuration is paramagnetic, but it is not ESR-detectable at room temperature due to the rapid spin-lattice relaxation [141]. The only ESR signal in the spectra of the calcined sorbent is the signal at g~4.28 (Figure V.7A) due to Fe^{3+} ions [142, 143]. According to the literature, the ESR signal at g~4.28 is due to the isolated Fe^{3+} cations in the tetrahedral coordination with rhombic distortion [143]. The ESR spectra of the "dried" sorbents of neither chemical composition could be recorded, likely due to the strong adsorption of the ESR radio-frequency by the water that is chemisorbed on the surface of the sorbents.

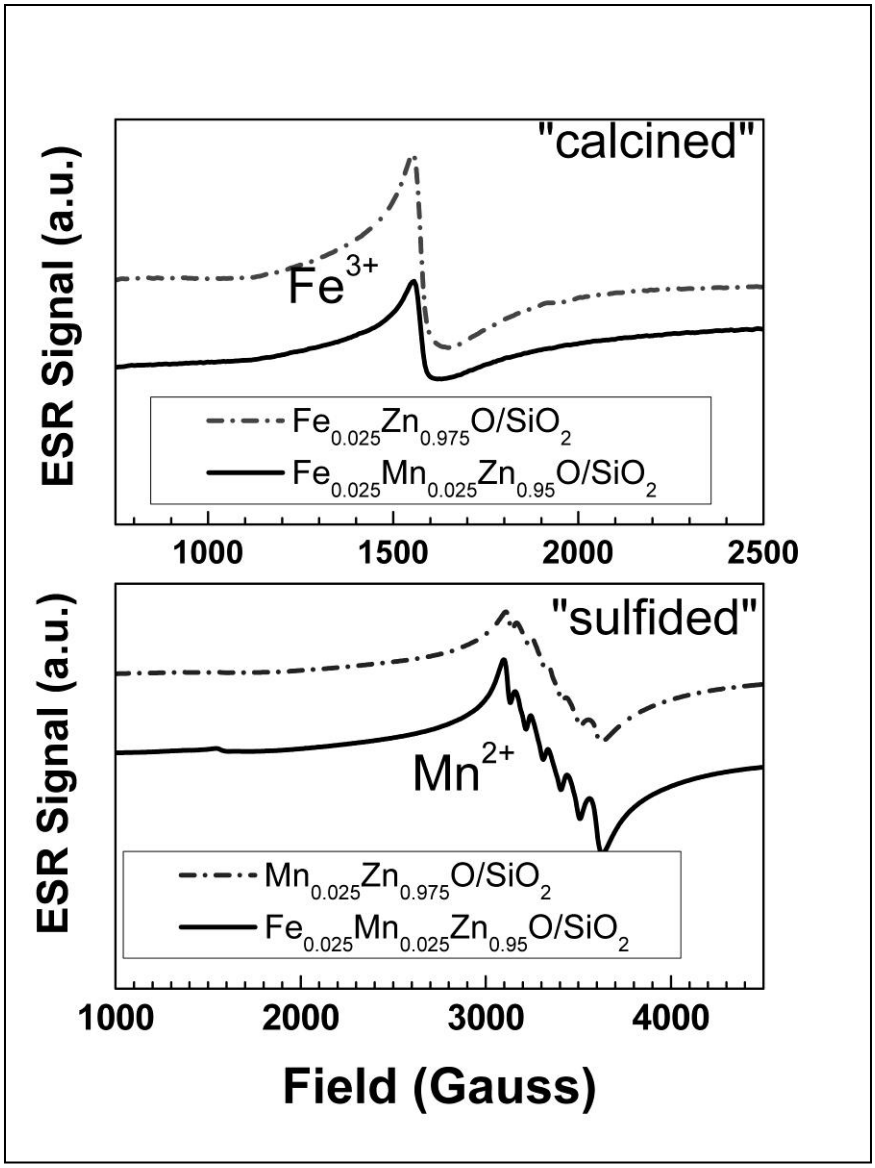

Figure V.7: ESR spectrum of the "calcined" sorbent $Fe_{0.025}Zn_{0.975}O/SiO_2$ (dotted solid line) vs. $Fe_{0.025}Mn_{0.025}Zn_{0.975}O/SiO_2$ (solid line), Figure 7A. ESR spectrum of the "sulfided" sorbent $Mn_{0.025}Zn_{0.975}O/SiO_2$ (dotted solid line) vs. $Mn_{0.025}Fe_{0.025}Zn_{0.975}O/SiO_2$ (thick solid line), Figure 7B.

In the spectra of the "sulfided" sorbents, the signal of Mn^{2+} appears (Figure V.7B), as the sharp sextuplet present on top of the broad spectral envelope at ~2500-4500 Gauss. The sixtuplet is

observed due to the hyperfine splitting (h.f.s.) of the isolated $^{55}Mn^{2+}$ ions in the tetrahedral or octahedral coordination geometry [144, 145]. For instance, Mn cations in the Mn-MCM-41 *vs.* Zn/Mn-MCM-41 zeolites were studied by ESR, and values of g-factor of about 2.002 and A values of ca. 90-95 Gauss were reported that correspond to the isolated Mn^{2+} centers [144]. Therefore, the reduction of Mn^{3+} cations to Mn^{2+} occurs upon reaction of the Mn-containing sorbent with H_2S in hydrogen. The broad spectral "envelope" is due to the interacting Mn^{2+} cations [145]. In the reference experiments with pure H_2, no spectral lines of Mn^{2+} appear in the ESR spectra; therefore, the reduction of Mn^{3+} to Mn^{2+} proceeds due to reduction by H_2S, not by the H_2 component of the challenge gas. The ESR signal of the isolated Fe^{3+} cations (Figure 5A) is much weaker (factor of 100) than the ESR signal of Mn^{2+} in the sulfided sorbent (Figure 5B), even though the stoichiometric amounts of the Fe and Mn are the same. Therefore, the Fe^{3+} isolated ions represent the minority form of iron. As a result, the quantitative or even semi-quantitative determination of various forms of Fe^{3+} by ESR cannot be performed.

The silica support that was prepared similarly to the "calcined" sorbent, except that Fe, Zn and Mn salts were not used, shows no ESR spectrum, as expected. The "calcined" sorbent of the formula $Fe_{0.000}Mn_{0.000}Zn_{1.000}O/SiO_2$ shows no ESR spectrum as well, thus confirming that the spectral multiplets in Figure V.5A and V.5B belong to Fe^{3+} and Mn^{2+}, respectively. In addition, no spectral lines of any Reactive Oxygen Species (ROS) or oxygen vacancies [87] are present in the ESR spectra of neither calcined nor sulfided sorbents.

It is known that when two paramagnetic ions are within the close distance, ~10 Å, the interaction of their spins can be observed in the ESR spectra. For instance, it was reported for the binuclear enzymes that the amplitude of the ESR signal of the Mn^{2+} cation was reduced when the extra Mn^{2+} cation was added within 8-11 Å distance [146]. We have compared the ESR spectra of

Mn^{2+} in the sorbent with and without Fe promoter present (Figure 5B). The differences are minor, and upon the processing of the spectra by the standard double-integration (DIN), the differences are within the accuracy of the quantitative ESR measurement (~5 %). Therefore, Mn cations do not interact with Fe cations in the $Fe_{0.025}Mn_{0.025}Zn_{0.950}O/SiO_2$ sorbent that indicates that those cations are, on average, >10 Å away from each other. The data of the structural characterization of the sorbents are consistent with their relative H_2S uptake capacity: $Fe_{0.025}Mn_{0.025} \sim Mn_{0.025} > Fe_{0.025}$ and $Fe_{0.025}Mn_{0.025} > Mn_{0.05} > Mn_{0.05}$.

The ESR spectra of the sorbent with the high content of Fe and Mn, namely, FeO/SiO_2 and MnO/SiO_2 are quite broad, consistently with the signal broadening due to the strongly interacting paramagnetic TM cations. ESR spectrum of Fe/SiO_2 has the broad peak with g value of about 2. This corresponds to the clustered form of the Fe^{3+} ions, and the spectrum is similar to the spectrum of the Fe_2O_3 phase in the Fe-containing zeolites [143] and to the Fe_xO_y clusters [142]. The spectrum of the MnO/SiO_2 is also very broad, consistently with the spectrum of the interacting Mn^{2+} ions [144]. Loss of the h.f.s. due to broadening is typical for the samples containing more than 4.5 wt % of Mn [145], consistent with our data . n-situ ESR tracking change in Mn relates to the breakthrough curve of the $Mn_{0.025}Fe_{0.025}Zn_{0.95}O/SiO_2$ tested at same conditions. This indicates that the MnO is probably in the solid solution with ZnO and the presence of Fe lines as shown in XPS, Fe ions and clusters are predominantly distributed on the surface. The Figure V.8 shows the schematic representation of the possible locations of the active sites Mn and Fe in the promoted ZnO/SiO_2 depending on all the characterization techniques. More work needs to be done to prove the mechanism shown in Fig V.8.

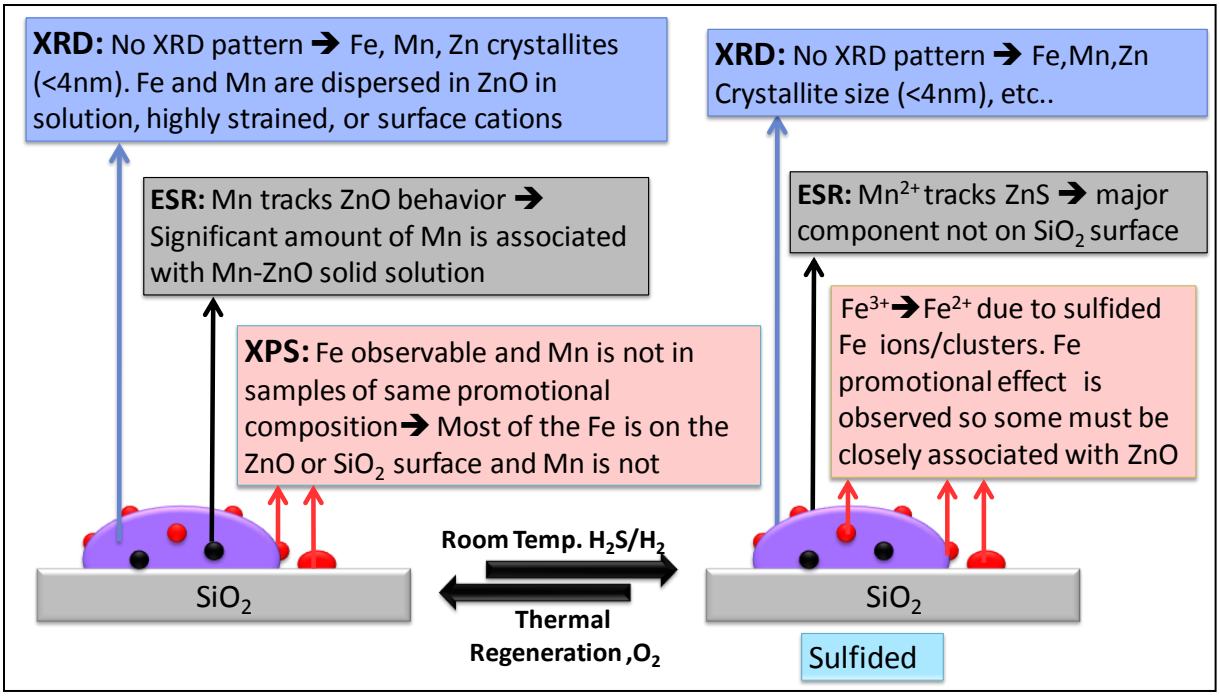

Figure V.8 Schematic diagram of the mechanism of distribution of the Mn, Fe active sites in ZnO/SiO_2

The important question is what are the mechanisms of the promoting effect of Fe and Mn cations on the desulfurization capacity of the Fe_x-Mn_y-$Zn_{1-x-y}O/SiO_2$ sorbents. In the literature, three mechanisms are discussed [127]: i) the enhancement of the active surface area of ZnO due to the presence of the TM oxide; ii) metal cation diffusion; iii) diffusion of HS^- and S^{2-} ions towards the bulk of the solid particles of ZnO. In the above referenced study of the unsupported Fe–Mn–Zn–Ti–O mixed metal oxides, the enhancement of H_2S uptake as explained due to the increase of ZnO active area is experimentally proven by the XRD and BET measurements. On the other hand, in the supported Fe_x-Mn_y-$Zn_{1-x-y}O/SiO_2$ sorbents studied by us, the changes of the surface area of the sorbent upon addition of the minor amounts of Fe or Mn promoters are too small to be measured by BET, and no XRD lines of any metal compound can be recorded for those nano-dispersed materials.

One has to note that both the Mn and Fe are the minor impurities in the $Fe_{0.025}Mn_{0.025}Zn_{0.95}O/SiO_2$ sorbents and they are the minor components of the supported nanophase of mixed metal oxides Fe- Mn-ZnO. Therefore, it is very challenging analytical and solid state chemistry task to study these sulfidation promoter sites. The promoter mechanisms of Mn and Fe cations could be proposed if the localization of those cations is determined or vice versa. From the XPS data, we conclude that the surface of Fe and Mn promoted ZnO/SiO_2 sorbents has an increased concentration of Fe, but decreased concentration of Mn. Therefore, Fe ions are likely to be located on the surface of ZnO, while Mn ions are likely to be located within ZnO crystallites. The mechanism of the promoter effect of Mn cations can be tentatively elaborated as follows. 1) If Mn cations were on the interface between ZnO and silica support, no or little promoter effects could be expected, due to the hindered diffusion of H_2S towards the $ZnO\text{-}SiO_2$ interface. Similarly, if Mn oxide formed its own nano-dispersed phase supported on silica, its effect on the H_2S uptake of ZnO would have been additive, i.e. negligibly small. The schematic representation for the proposed structure of $Fe_{0.025}Mn_{0.025}Zn_{0.95}O/SiO_2$ is as shown in Fig.V.9. Therefore, we propose that Mn cations are located within the nano-crystallites of the supported ZnO. The proposed localization of the Fe and Mn cations is consistent with our ESR data shat show no spin-spin interactions between Fe and Mn cations, *i.e*. their localization at least 10 Å from each other. This distance is of the same order of magnitude as the size of the ZnO nanocrystallites that are smaller than the XRD limit, i.e. < 40 Å. From the XPS data, we conclude that the surface of the $Fe_x\text{-}Mn_y\text{-}Zn_{1-x-y}O/SiO_2$ sorbent is enriched with Fe ions. We thus conclude that the surface of the $Fe_x\text{-}Mn_y\text{-}Zn_{1-x-y}O/SiO_2$ sorbent is enriched with Fe^{3+} ions, while Mn^{3+} ions are located within the ZnO supported nanocrystallites. Therefore, the promoter effect of Fe cations is likely to be the “local” enhancement of the reactivity of ZnO towards H_2S, while

the promoter effect of the Mn cations could be to decrease the size of the ZnO nanocrystallites [127].

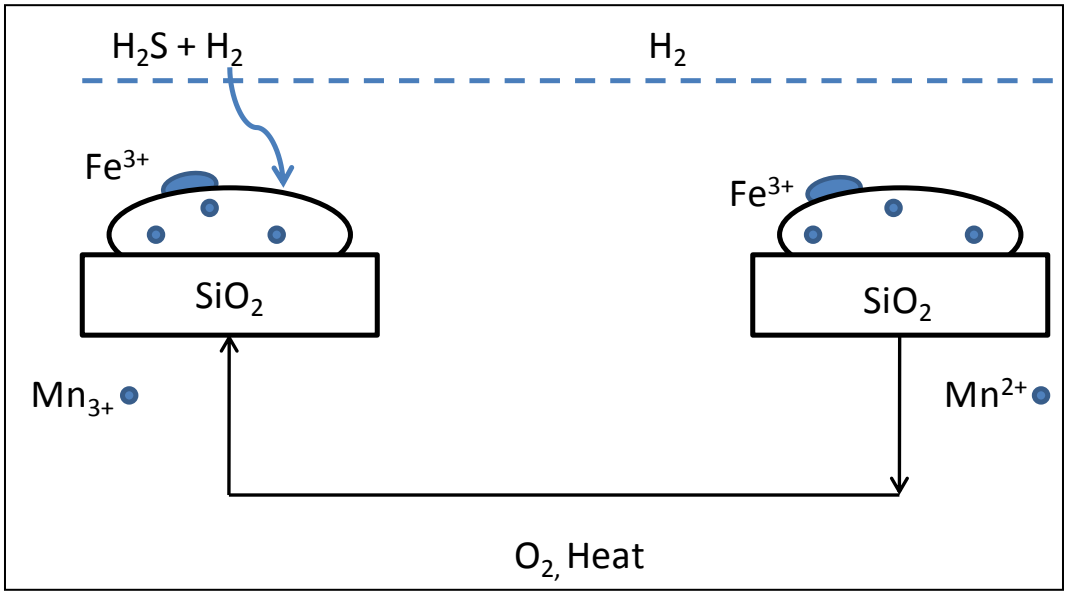

Figure V.9: Schematic representation of the structure of $Fe_{0.025}Mn_{0.025}Zn_{0.95}O/SiO_2$ sorbents and sulfidation/regeneration reactions.

The mechanisms of the promoter effects in the Fe_x-Mn_y-$Zn_{1-x-y}O/SiO_2$ sorbents cannot be directly determined from the structural or spectroscopic characterization, and they need to be understood from the complementary advanced spectroscopic studies, including the real-time Operando spectroscopy that is currently underway in our laboratory.

V.3 Conclusions

The Mn and Fe promoter cations significantly enhance the utilization of the ZnO active phase in reaction with H_2S of the novel sorbents Fe_x-Mn_y-$Zn_{1-x-y}O/SiO_2$ (x, y=0, 0.025), during desulfurization of the mixture of H_2S and H_2 at room temperature. The Mn- and Fe-promoted sorbents maintain a high sulfur uptake capacity upon the multiple cycles of a simple thermal oxidative regeneration of the "spent" sorbent in air (up to 10 cycles). ZnO and cations of Fe and Mn are nano-dispersed in the Fe_x-Mn_y-$Zn_{1-x-y}O/SiO_2$ sorbents, both the "calcined" and "sulfided" forms. As judged by XPS and ESR, the surface of the sorbent is enriched with Fe promoter cations, while Mn^{3+} promoter cations are located within the supported ZnO nanocrystallites.

Acknowledgement

The authors would like to thank the US Army (TARDEC Contract W56HZV-05-C-0686) for the financial support of this work. A.S. thanks Prof. Michael Bowman (Department of Chemistry of the University of Alabama at Tuscaloosa) for useful discussions.

Chapter VI: RT Hydrolysis and Removal of COS from Fuel Reformate Streams using Al_2O_3/Carbon & $Fe_{0.025}Mn_{0.025}ZnO_{0.95}/SiO_2$ Layered Beds

Priyanka Dhage, Hongyun Yang[1] and Bruce J. Tatarchuk

Department of Chemical Engineering, Auburn University, Auburn, AL 36849 (USA)

[1]Intramicron Inc. 368 Industrial Pkwy, Auburn AL 36830(USA)

Abstract

Removal of both H_2S and COS from reformate streams is critical for maintaining the activity of fuel processing catalysts. The objective of our work is developing sorbents for efficient, cost-effective and scalable removal of H_2S and COS over various temperatures, without significant activity loss upon multiple regeneration cycles. Bimetallic sorbents $M_{x/2}N_{x/2}Zn_{(1-x)}O$ supported on SiO_2/Al_2O_3 (M, N = Mn, Fe, Ni, Mg, Cu and $0 \leq x \leq 1$) prepared by impregnation/calcination were studied in packed bed, with model reformate gases (1 vol% H_2S, 33% CO/CO_2 inH_2, H_2O), room temperature to 400 C. Their sulfur uptake capacity at room temperature significantly exceeds that of both commercial unsupported ZnO sorbents (by 60 %) and of the un-promoted supported sorbent ZnO/SiO_2 (by 30 %), but showed no adsorption of COS. Sulfur sorption capacity and the breakthrough characteristics remain satisfactory after up to 10 cycles of adsorption/regeneration, with regeneration performed by a simple heating in air. At temperatures< 250^oC, COS formation is inhibited but significant amount of COS is formed in the

presence of CO_2/CO and H_2S. Al_2O_3/Carbon is a good catalyst for high temperature (T>100 C) COS hydrolysis. For room temperature COS hydrolysis, layered bed approach with COS hydrolysis on Al_2O_3/Carbon, followed by H_2S removal on $Fe_{0.025}Mn_{0.025}ZnO_{0.95}/SiO_2$ was adopted.

Keywords: COS hydrolysis, H_2S, Al_2O_3, ZnO, Fe, Mn, XPS

VI.1 Introduction

With the introduction of the strong legislation to reduce sulfur emissions, fresh impetus is being given to modifying improving existing desulfurization technology. However, dehydrodesulfurization does not remove or significantly affect sulfur containing compound, namely, carbonyl sulfide. Removal of sulfur containing compounds is one of the most important technologies for utilization of gasified products derived from various feedstocks such as biomass, waste and solid fossil fuels[147]. Especially, gaseous sulfur compounds of H_2S and COS are severe poisons against the following processing of steam reforming for hydrogen production or Fischer Tropsch synthesis [148]. Various researches for H_2S removal have been reported in details for the purification of gasified products derived from various feed stocks; however, removal of COS is not a big concern yet, because it is not the major sulfur compounds produced from gasification [12]. The absorption of H_2S by ZnO is stoichiometric above 350 ^oC but it falls rapidly at lower temperatures. The removal of COS has been reported to be more difficult at low temperatures in the range from room temperature to 200 ^oC than H_2S. ZnO is a preferred metal oxide because of favorable sulfidation thermodynamics, [13] but is not efficient to remove COS [7]. Gaseous sulfur compounds of H_2S and COS are severe catalyst poisons

against the following processes of steam reforming for hydrogen.COS can be formed by the conversion of H_2S and CO_2 in the absence of water. The conventional way to remove COS is hydrogenation and hydrolysis [149] COS is rather inactive compared to H_2S probably due to its neutrality and similarity to CO_2, COS is sometimes produced through the reaction of H_2S with CO_2, although the reaction can be reversible to produce again H_2S and CO_2 from the reaction of COS and H_2O depending upon the adsorption conditions[14, 149, 150].

The formation of COS is primarily governed by the reversible hydrolysis reaction and equilibrium conditions present:

$$COS + H_2O \Leftrightarrow H_2S + CO_2$$

Parallel to the necessity for safe operations, the removal of trace sulfur components, such as mercaptans or carbonyl sulphide (COS), is a major challenge in designing the gas conditioning process. The pros and cons of several design options for deep COS removal are discussed in a case study, where the results of a hybrid solvent are compared with the performance of a BASF solvent. These are compared to measurements from an operating plant. In a water-saturated reservoir, hydrogen sulphide (H_2S) and carbon dioxide (CO_2) are in thermodynamic equilibrium with COS. Thus a concentration of up to several hundred ppmv COS in the feed gas is not unusual. A relatively small volume of COS can combine with water to form H_2S if suitable equilibrium conditions exist [14]. Molecular Sieves (e.g. Zeolite A) present a new problem for H_2S removal because H_2S and CO_2 can react within the framework of the zeolite to produce COS and H_2O. The problem is amplified further by the ability of molecular sieves, such as zeolites A and X, to absorb water and force the reaction far to the right; increasing COS concentration[151]. Most of the studies are concentrated on COS removal at operation temperature in excess of 100 C and operational cost and energy consumption will be high[152] The studies on COS removal

and hydrolysis are divided in two parts: one part focuses on COS hydrolysis at low temperature and the other part on simultaneously removing both COS and H_2S. A mathematical model was developed for COS removal using coupling reactions on a bi-functional catalyst. The temperature favors the effectiveness of the reaction rate constant, H_2O adsorption equilibrium constant decrease in these conditions as expected [153]. The study of reaction mechanism for alumina as catalyst for COS hydrolysis in the temperature range 30-250 C was investigated [154]. Addition of Ni and Zn can efficiently promote COS hydrolysis on alumina at 30 C [155]. COS hydrolysis at low temperature (45-100 C) on alkali metal oxides and alkali earth metal oxides was studied[156].Single COS Removal process using an iron oxide catalyst around 50 C, where Fe_2O_3 was the catalysts for COS hydrolysis and the adsorbent for H_2S removal [157].

ZnO is reported to be best sorbent for sulfur adsorption [123] because of its favorable sulfidation thermodynamics and high sulfur capacity (by weight). However, a serious problem of the high temperature (> 500 ºC) H_2S adsorbents is the reduction of ZnO by hydrogen into metallic zinc and evaporation of the latter [122]. Several oxides of other metals such as iron, vanadium, zinc, copper, manganese and molybdenum have been proposed as high-temperature desulfurization sorbents since the 1970s [124]. Chemical and structural transformations of those oxides upon desulfurization/regeneration were investigated; for instance, it is known that in the environment of the IGCC gasifier, Mn_3O_4 form is readily reduced to MnO and the latter reacts with H_2S at the high temperatures [122]. Iron oxides have also been extensively investigated since the 1970s; iron oxide-based H_2S sorbents have high sulfur capacity and reactivity towards H_2S. However the equilibrium concentration of H_2S is as high as 100 ppmw. In addition, the number of the degradation processes occur above ~ 500 ºC, namely the reduction of Fe_3O_4 to

FeO [122]. Mixed metal oxide sorbents for the high temperature desulfurization of coal gases were extensively reviewed in the past [125, 126].

Recently, increasing interest has been paid to the "low temperature" H_2S adsorbents that operate between room temperature and ~100 ºC [127-129]. For instance, we reported preparation and testing of novel ZnO/SiO_2 sorbents for H_2S and carbonyl sulfide COS with the minimized mass transfer resistance [77, 89-92] that operate at room temperature and retain their high desulfurization capacity after >10 desulfurization/regeneration cycles, with the regeneration performed by the inexpensive and robust calcination in the flowing air.

To study the desulfurization promoter, i.e. the *minority* chemical component of the multi-component sorbent (or catalyst), suitable experimental technique(s) needs to offer: i) a rather high sensitivity, ii) the ability to analyze both surface and the "bulk" of the specimen, iii) the ability to study the local structure of the promoter site. The main limitation of XPS is its relatively low sensitivity (> 5 % of the monolayer) [103].

A previous study on the preparation of $Fe_xMn_yZn_{1-x-y}O/SiO_2$ and characterization of the active sites Zn, Mn, Fe, S sites in those sorbents by XRD and XPS has already been published [58] We report here the strategies to remove COS present/formed in the fuel reformate streams. And the preparation and performance of the novel Al_2O_3/Carbon for hydrolysis of COS and use of layered beds to remove both COS and H_2S. The measurements of H_2S uptake at room temperature, desulfurization performance upon the multiple regeneration cycles of the $Fe_xMn_yZn_{1-x-y}O/SiO_2$ sorbents are also discussed.

VI.2 Experimental

Activated PICA Carbon of particle size 100-200 microns was dried in oven at 100 C. The dried Carbon was then impregnated via incipient wetness impregnation method with 2M Aluminium nitrate. The impregnated sample was then dried in air for 6hrs and then calcined at 350 C for 30 mins. The calcined sample Al_2O_3/C is ready to test after cooling it down to room temperature. The ZnO/C and CuO/C were prepared by impregnating acetates as precursors and calcining at 120 C in air for 1 hr.

The promoted ZnO-based desulfurization sorbents of the nominal formula $Fe_xMn_yZnO_{1-x-y}/SiO_2$ (x, y=0; 0.025) were prepared by incipient co-impregnation of high surface area (300-550 m^2/g) silica (Fischer Scientific Inc.) of grain size 100-200 μm with solutions of nitrates of the respective metals in water, namely $Zn(NO_3)_2$, $Mn(NO_3)_2$ and $Fe(NO_3)_3$. Single step incipient impregnation was performed on the silica support to achieve metal oxide loading of 12-36% by varying the molarity of nitrate solutions. Upon incipient impregnation and drying, the samples were calcined in the flowing air at 350-550 ^oC; these are referred to as the "calcined" specimens. The specimens prepared as above, excepting the calcination step, are referred to as the "dried" sorbents. In the reference experiments, with the commercial H_2S sorbents (BASF SG-901 and Sud Chemie G-72E), they are crushed to the same particle size as that of the silica (100-200 microns) used to prepare the supported $Fe_xMn_yZnO_{1-x-y}/SiO_2$ sorbents.

Breakthrough curves for both commercial sorbents and $Fe_xMn_yZnO_{1-x-y}/SiO_2$ sorbents were measured at 20 °C. In the desulfurization experiments, the challenge gases were the model reformates with an inlet concentration of 1 vol. % H_2S in H_2 and 0.1% COS in N_2. Model Reformate streams composition was chosen CO_2 = 30 %, CO = 30%, H_2O= 1% and H_2S=1%

balance H_2. Gases were purchased from Airgas Inc and Matheson Tri-Gas. The face velocity (GHSV) of the stream is 2000-20000 h^{-1}. Challenge gas was passed through the sorbent in a vertically-mounted packed bed tubular reactor (10 mm I.D. x 30 mm long) made of quartz that was coaxially located inside a 200 mm long tubular furnace. The desulfurization reactor contained 0.5-1.0 g sorbent; the sorbent bed size was 9 mm in diameter and 10 mm thick. H_2S uptakes during adsorption experiments were measured using a gas chromatography (GC) instrument (Varian CP3800) equipped with the thermal conductivity detector (TCD) and pulse flame photometric detector (PFPD). The specimens of the sorbents upon adsorption of H_2S are referred to as the "sulfided" samples.

Regeneration of the "sulfided," i.e. "spent" sorbent was performed *in-situ* in the sulfidation reactor at 550 ^oC in air at a flow rate of 950 h^{-1}. The sorbent $Fe_xMn_yZnO_{1-x-y}/SiO_2$ of 15 wt. % loading of ZnO was regenerated for over 10 cycles, with the regeneration temperature being the same as that of the sample calcination before the 1-st desulfurization cycle. The temperature of the furnace during the experiments was maintained using a PID temperature setpoint controller. The gas flow rates were controlled by mass flow controllers (Omega FMA 2405 Alaborg GFC1718).

Nitrogen adsorption/desorption isotherms at 77 K were measured by an Autosorb 1-C instrument (Quantachrome Instrument Corp., USA). Before measuring the total surface area, samples were outgassed for 3 h at 200 °C. The specific surface area, S_{BET} was calculated via the Brunauer-Emmett-Teller (BET) equation, and the total pore volume (V_P) was calculated at P/P_0 = 0.95.

VI.3 Results and Discussions

VI.3.1 Desulfurization Performance of the Sorbents

Figure VI.1 shows the H_2S sorption performance of the commercial ZnO sorbents from Sud Chemie and BASF, of the supported sorbent ZnO/SiO_2 prepared in our lab (21 wt. % loading of ZnO) and of the promoted $Fe_{0.025}Mn_{0.025}ZnO_{0.95}/SiO_2$ sorbent (21 wt. % loading of ZnO). The $Fe_{0.025}Mn_{0.025}ZnO_{0.975}/SiO_2$ sorbent shows a superior H_2S uptake compared to the others.

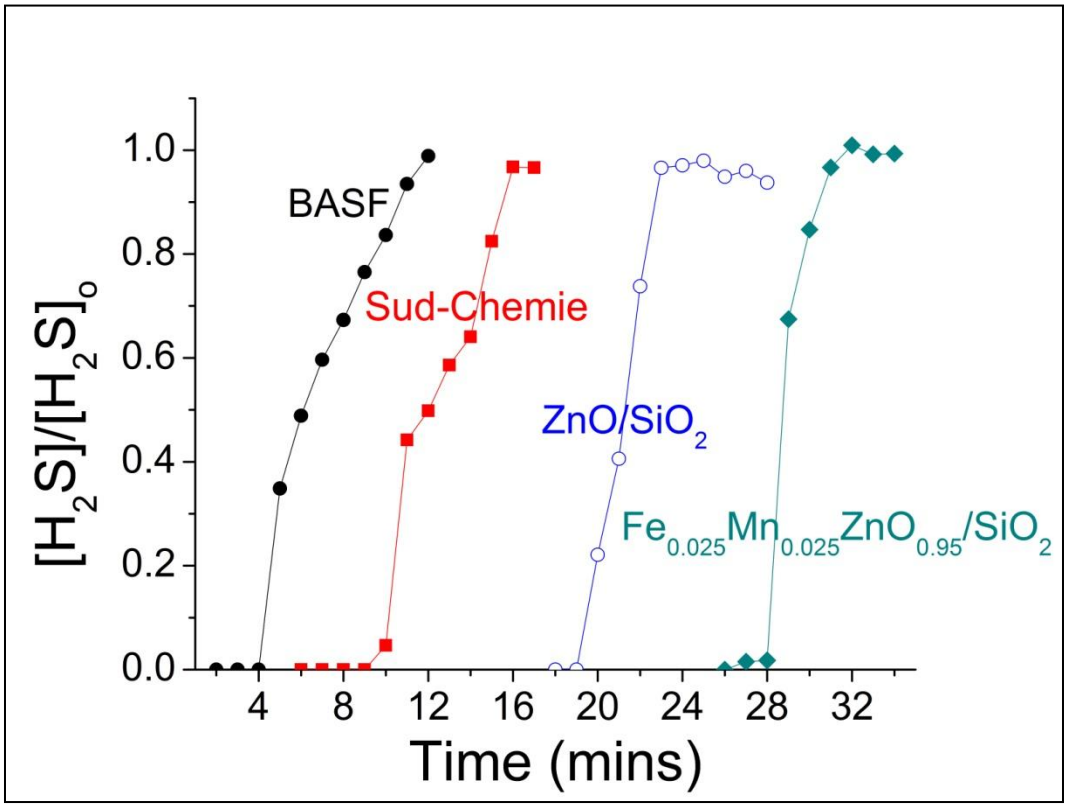

Figure VI.1. H_2S Breakthrough curves of the commercial ZnO Sorbent from BASF, Sud-Chemie ZnO/SiO_2 and $Fe_{0.025}/Mn_{0.025}ZnO_{0.095}/SiO_2$ sorbent. Test conditions: adsorption T= 20 C, Particle size = 100-200 microns, Co=1 vol5 H_2S/H_2

Table VI.1 shows the sulfur uptake capacity (g sulfur / g sorbent) and utilization of ZnO in the sulfidization reaction (% of the theoretical value for the ZnS stoichiometry) attained at the breakthrough and the saturation regimes. The breakthrough is defined as 2% of inlet

concentration. The supported ZnO/SiO_2 sorbent has shown better performance over both commercial ZnO-based sorbents. XRD of the $Fe_{0.025}Mn_{0.025}ZnO_{0.975}/SiO_2$ sorbent in both "calcined" and "sulfided" forms was performed, and no lines due to any Fe or Mn compound were found that indicates a high degree of dispersion of the Fe and Mn promoters.

Table VI.1: Breakthrough and Saturation H_2S Capacity and utilization of ZnO (%) for various sorbents

Sorbent	**Loading**	**Sat Cap**	**ZnO Utilization Sat. Cap**	**Breakthrough Cap**	**ZnO Utilization at Breakthrough(%)**
BASF ZnO (SG-901)	90	0.019	5	0.011	3
Sud-Chemie (G-72E)	90	0.032	9	0.024	7
ZnO/SiO_2	15	0.032	54	0.026	45
$Fe_{0.025}Mn_{0.025}ZnO_{0.95}/SiO_2$	15	0.045	76	0.037	62

Figure VI.2 shows the COS adsorption at 400 C on the SiO_2 and Al_2O_3 based samples, tested with inlet challenge gas varying from 500ppmv COS/N_2. The silica based samples include SiO_2, ZnO/SiO_2 and $Fe_{0.025}Mn_{0.025}ZnO_{0.95}/SiO_2$ and alumina based samples include commercial BASF ZnO (SG-901) and Al_2O_3 and FeO/Al_2O_3 (15wt% loading). Alumina is a catalyst for COS hydrolysis at high temperature. The result shows that catalytic activity of alumina did not degrade for 6 hrs at the specified test conditions but silica based sample didn't show any affinity or catalytic activity for COS hydrolysis.

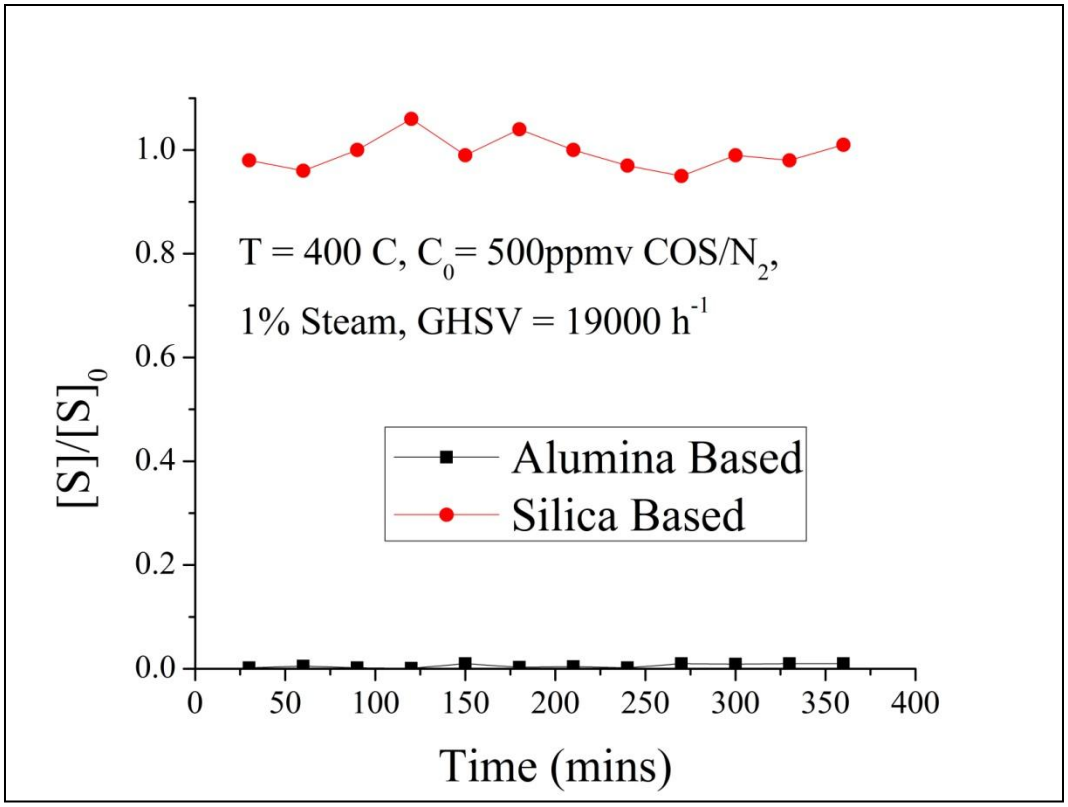

Figure VI.2: COS hydrolysis at 400 C using Al_2O_3 based and SiO_2 based sorbents. Inlet concentration: COS/N_2 = 500 ppmv, 1% Steam, GHSV = 19000h^{-1}

VI.3.2 COS Removal & Hydrolysis

Figure VI.3A shows the breakthrough performance of $Fe_{0.025}Mn_{0.025}ZnO_{0.95}/SiO_2$ tested at 400 C in the presence of CO_2 and H_2S. The result indicates that COS is formed in the presence of CO_2 and H_2S. The stream contains 50% CO_2 and 1%H_2S and rest H_2. At 400C, it is evident that COS is formed and because the sorbent has no reactivity for COS. The TCD detector was used to analyze the outlet gases. The chromatograph of the COS and H_2S was recorded in the same run as TCD can detect both the gases simultaneously. Keeping the test conditions same, the $Mn_{0.025}Fe_{0.025}Zn_{0.95}O/SiO_2$ was tested without CO_2, it showed almost 90% theoretical capacity without the formation of COS.

To understand how COS was formed, equilibrium COS concentrations for the reactions (1-3) running simultaneously were obtained using the HSC* software. The outlet COS concentrations are shown in Figure VI.3B and the outlet H_2S concentration for reaction (4) is shown in Figure VI.3C.

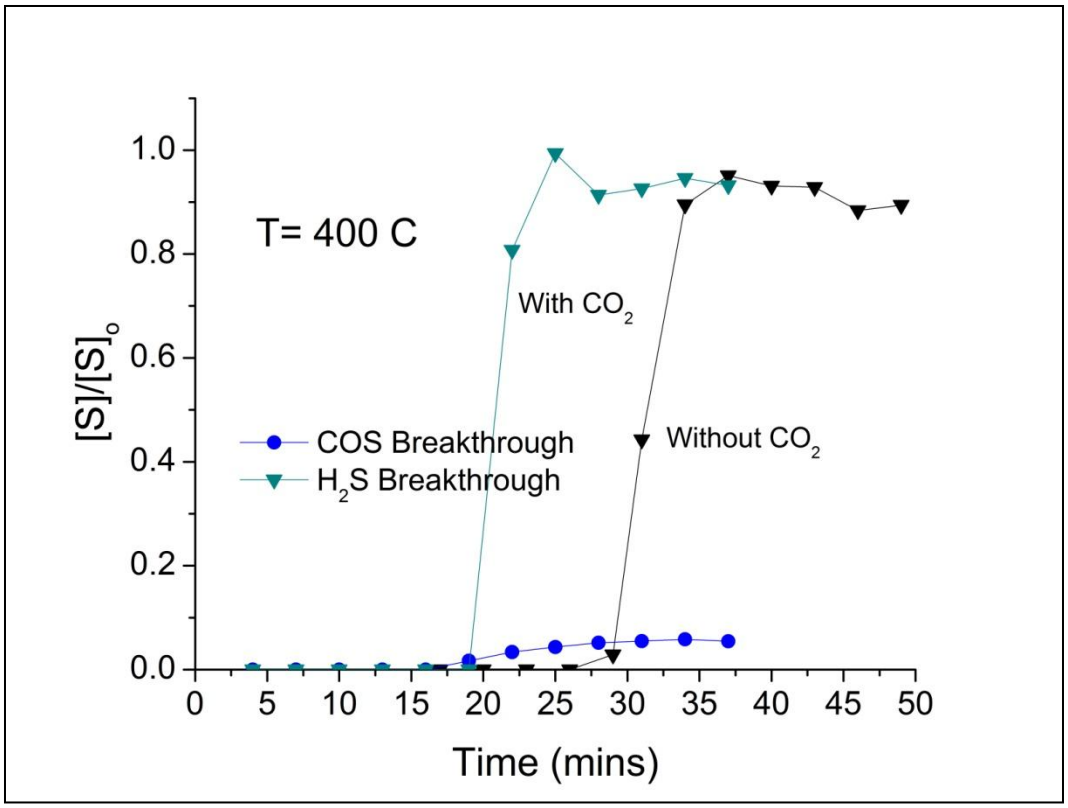

Figure VI. 3A: Breakthrough performance of $Fe_{0.025}Mn_{0.025}ZnO_{0.95}/SiO_2$ with and without CO_2 at 400 C, Test conditions :Q (2%H_2S/H_2) = 100 cc/min, Q(100% CO_2) = 100 cc/min, T = 400 C, GHSV = 8800 h^{-1} , Wt= 0.5 g

The graph shows that when CO_2 is present in the gas stream CO_2 reacts with H_2S to form COS.

$$CO_2+H_2S \Leftrightarrow COS+H_2O$$

The reaction is homogenous and leads to significant formation of COS at high temperatures (T> 250 C).

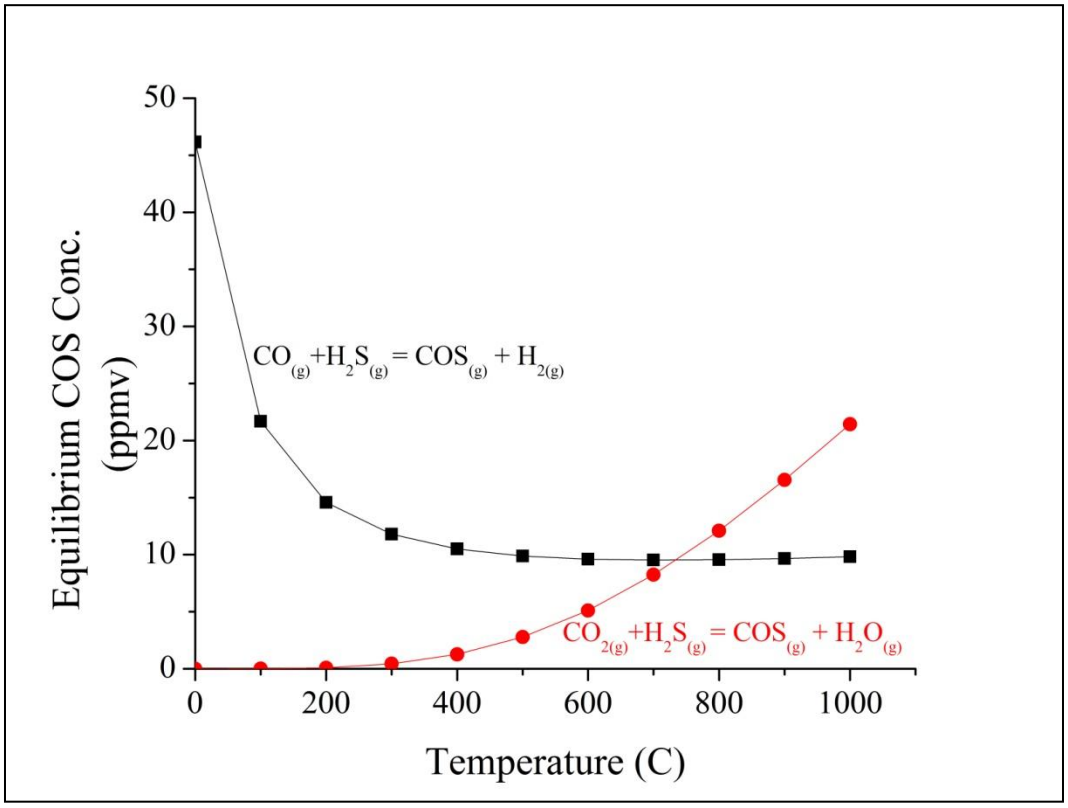

Figure VI.3B: Equilibrium COS Concentrations. Reformate Composition (vol %): CO = 25 %, CO_2 = 10%, N_2 = 33 %, H_2O = 7%, H_2 = 25 % and H_2S = 0.03%

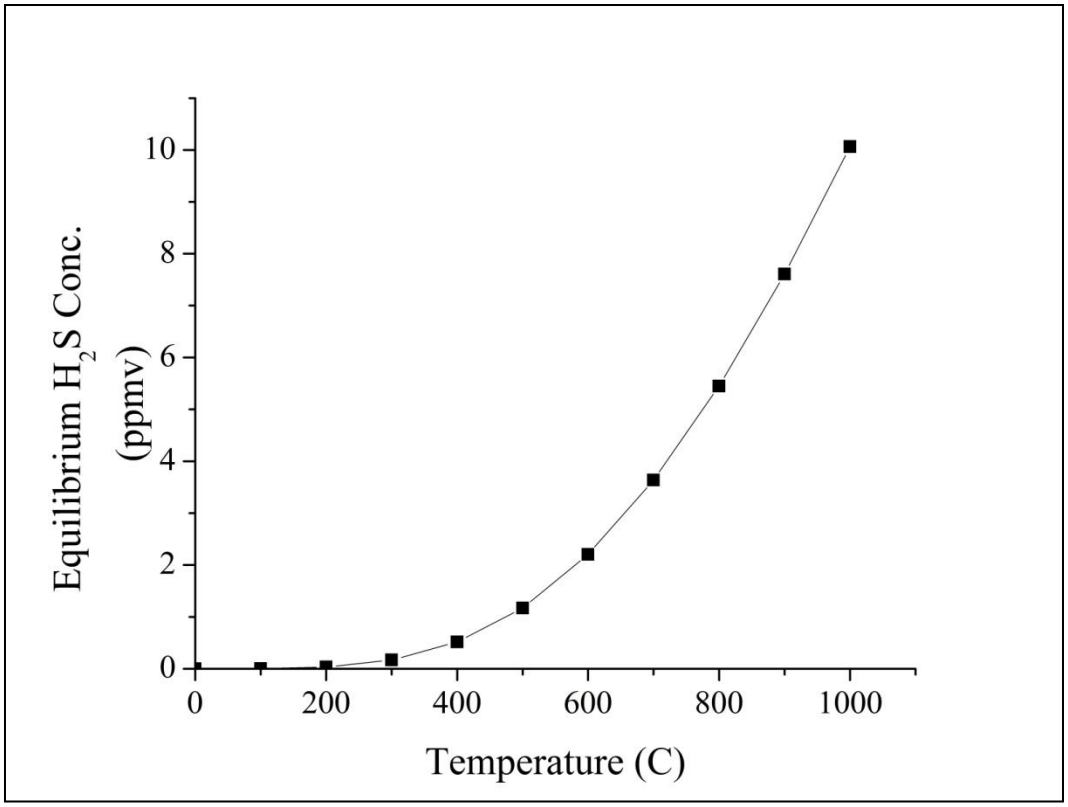

Figure VI.3C: Equilibrium H_2S Concentrations. Reformate Composition (vol %): CO = 25 %, CO_2 = 10%, N_2 = 33 %, H_2O = 7%, H_2 = 25 % and H_2S = 0.03%

The equilibrium concentrations of COS produced by CO and CO_2 on reacting with H_2S are shown in Figure VI.3B. This led to the hypothesis that COS formation in the reformate stream can be inhibited if the temperature is restricted to less than 250 C. Figure VI.3D shows the same test carried out at room temperature. This result shows that room temperature even in the presence of CO_2 along with H_2S, negligible amount of COS was formed. The Table VI.2 shows the comparison of the capacities at various temperatures, with and without CO_2.

1) $CO_{2(g)} + H_2S_{(g)} \Leftrightarrow COS_{(g)} + H_2O_{(g)}$ (Homogeneous)

2) $CO_{(g)} + H_2S_{(g)} \Leftrightarrow COS_{(g)} + H_{2(g)}$ (Heterogeneous)

3) $CO_{(g)} + H_2O_{(g)} \Leftrightarrow CO_{2(g)} + H_{2(g)}$ (WGS)

4) $ZnO_{(g)} + H_2S_{(g)} \Leftrightarrow ZnS_{(s)} + H_2O_{(g)}$

5)

Table VI.2: Saturation Capacity of $Fe_{0.025}Mn_{0.025}ZnO_{0.95}/SiO_2$ with and without CO_2 at room temperature and 400 C

T (^oC)	Composition of Stream (vol %)	Saturation Capacity (mol S/mol ZnO)
20	CO_2 =50, H_2S =1, H_2 = 49	89
400	CO_2 =50, H_2S =1, H_2 = 49	74
400	CO_2 = 0, H_2S =1, H_2 = 99	98

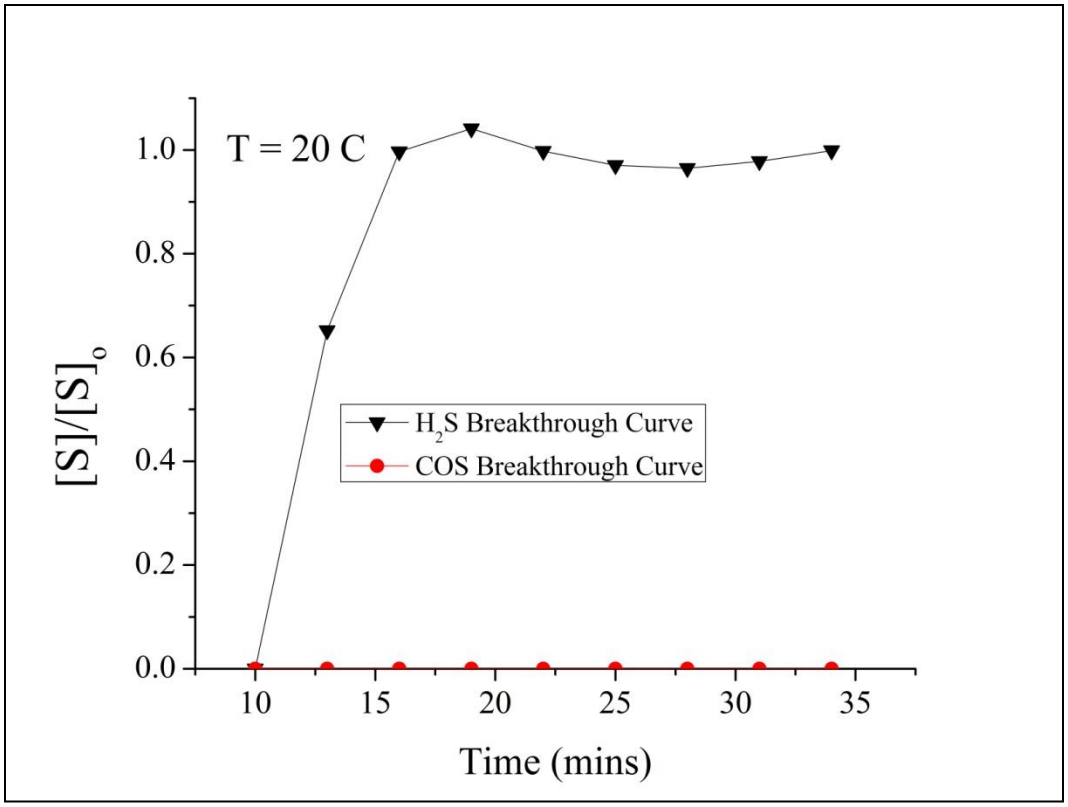

Figure VI. 3D. Breakthrough performance of $Fe_{0.025}Mn_{0.025}ZnO_{0.95}/SiO_2$ at 20 C Test conditions: Q (2%H_2S/H_2) = 100 cc/min, Q(100% CO_2) = 100 cc/min, T = 20 C, GHSV = 3800 h^{-1} , Wt= 0.5 g

Figure VI.4 shows the relative effect of adding CO/CO_2 to the bed at 400 C with inlet concentration of 300 ppmv. Initially the bed is operated with only H_2S/H_2 in the stream and after 40 minutes 10% CO was introduced into the bed, the PFPD detector shows an increase of about 3.3 ppmv. This steadily decreases upto 2 ppmv. At 175 minutes 7% CO_2 was introduced in the system and it shows about 0.2 ppmv increase in the outlet sulfur concentration. After 250 minutes both CO and CO_2 were removed from the stream and the concentration of sulfur goes

down to 0.2 ppmv. The rise in concentration after adding CO and CO_2 is due to formation of COS. The figure shows that addition of CO/CO_2 into the system leads to COS formation.

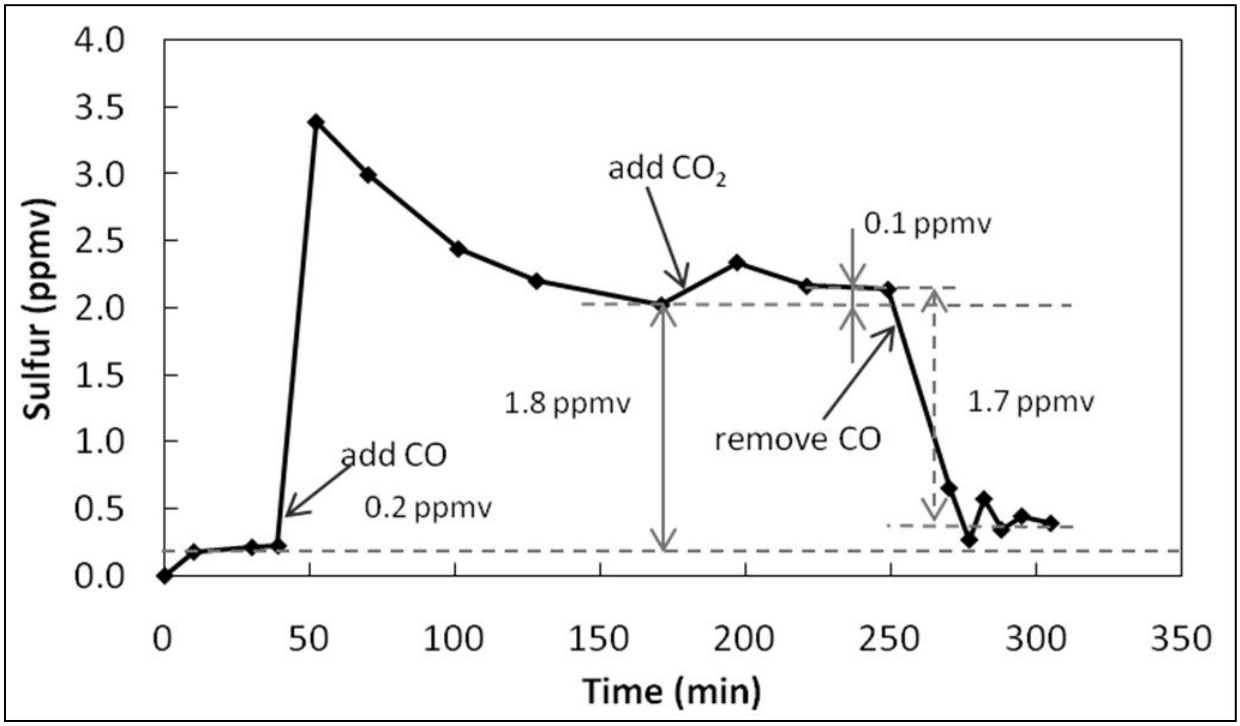

Figure VI.4: Breakthrough curves of layered beds tested with 300 ppmv H_2S-25% H_2-25% CO-10% CO_2-7% H_2O-33% N_2 at a face velocity=100 cm/s at 400 C. Bed length: 22 cm

Figure VI.5 shows breakthrough performance of Al_2O_3, FeO/Al_2O_3 and $Fe_{0.025}Mn_{0.025}ZnO_{0.95}/SiO_2$ tested at 400 C with CO_2 and H_2S in the inlet gas. At the test conditions, presence of CO_2 and H_2S at the given composition leads to formation of COS on $Fe_{0.025}Mn_{0.025}ZnO_{0.95}/SiO_2$ sorbent as shown by filled circles and H_2S breakthrough is shown by triangles. The FeO/Al_2O_3 shows no adsorption for H_2S as well as COS at these conditions.

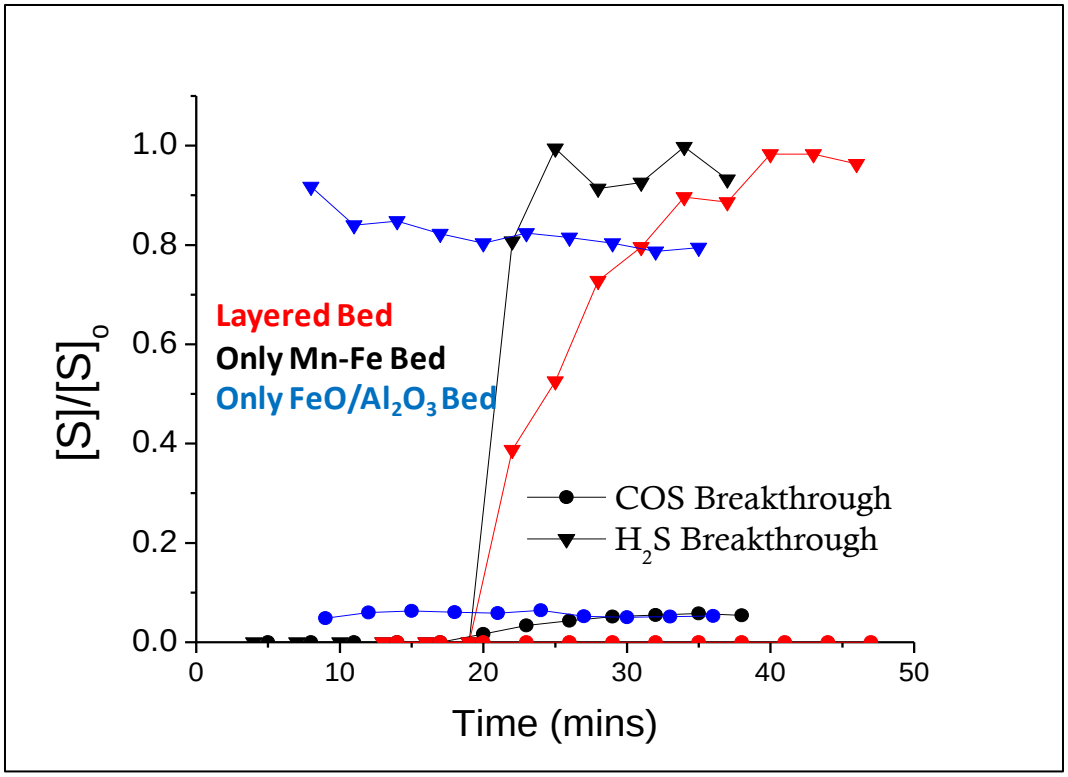

Figure VI.5: COS Removal using layered bed. Test conditions: T = 400 C, GHSV = 15000 h^{-1}, Wt. of each layer = 0.5g Metal oxide loading of each layer= 15%wt. Gas Composition (vol%) : CO_2 = 28%, H_2S = 0.5%, H_2O = 1%, H_2 = 70.5%

H_2S is more active than COS and therefore it reacts with the active sites of FeO/Al_2O_3 and hence the catalytic activity of Al_2O_3 were diminished, as opposed to the result in Figure VI.2 where COS is the challenge gas and Al_2O_3 works efficiently well as a catalyst. The layered bed in Figure VI.5 is the bed of $Fe_{0.025}Mn_{0.025}ZnO_{0.95}/SiO_2$ followed by a layer of 'guard bed' FeO/Al_2O_3. This design ensures adsorption of H_2S by $Fe_{0.025}Mn_{0.025}ZnO_{0.95}/SiO_2$ and the COS formed by reaction of CO_2 and H_2S is taken care by second layer FeO/Al_2O_3.As the result shows, there is no significant reduction in capacity in layered bed, also no detectable amounts of COS were seen in the outlet gas composition.

Figure VI.6 shows COS hydrolysis on carbon and Al_2O_3/carbon tested at room temperature with 1000 ppmv COS as challenge gas. The breakthrough curve for bare carbon shows that COS is adsorbed with breakthrough time of ~ 7 minutes. The breakthrough curve for Al_2O_3/C indicates that COS was adsorbed upto C/Co= 0.5 and it remains constant at that concentration, formation of H_2S was evident as shown in the figure. Part of COS is hydrolyzed to H_2S. This indicates that Al_2O_3/C can effectively hydrolyze COS even at room temperature with ambient moisture. In another study, commercial (a) Al_2O_3 (Fischer ~ 90% pure alumina), the (b)pure alumina made by calcination (350C/1h) of aluminium nitrate and (c) the physical mixture of this alumina with the carbon support were tested for COS hydrolysis to verify if the hydrolysis was due to Al_2O_3 or because of the unique method of preparation. Above mentioned (a-c) sorbents did not show hydrolysis of COS to H_2S at room temperature. Hence indicating that the alumina loaded via impregnation on carbon support hydrolyzes the COS at room temperature. In Figure VI. 7, layered bed of Al_2O_3/C followed by $Fe_{0.025}Mn_{0.025}ZnO_{0.95}/SiO_2$ was used. The composite bed design ensures that the H_2S formed by COS hydrolysis over Al_2O_3/C can be taken care by $Fe_{0.025}Mn_{0.025}ZnO_{0.95}/SiO_2$. As shown in the figure, the H_2S breakthrough curve goes through maxima, indicating the H_2S formed via COS hydrolysis is taken care by $Fe_{0.025}Mn_{0.025}ZnO_{0.95}/SiO_2$. The results indicated here are preliminary results and need further work to ascertain the role of alumina, carbon for COS hydrolysis. The authors recommend further work for characterization of the sorbent to understand the mechanism of hydrolysis. At this point it is speculated that the surface hydroxyls are responsible for the conversion of COS to H_2S.

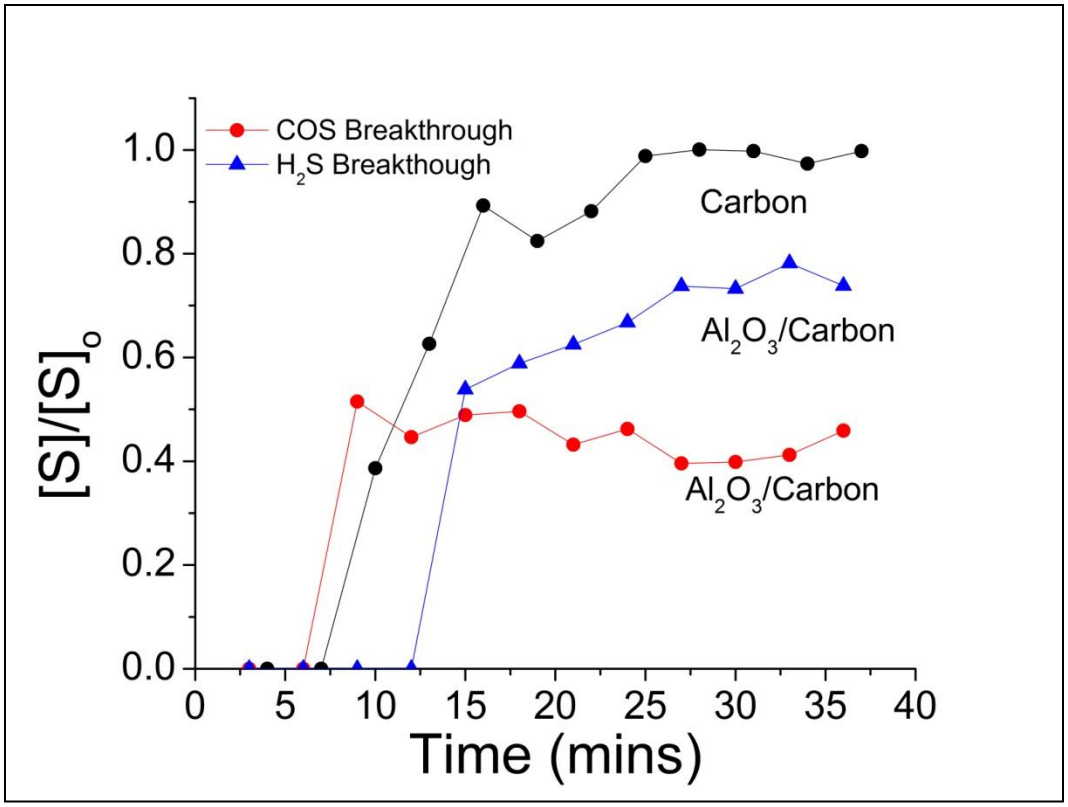

Figure VI.6: COS Hydrolysis using Al_2O_3/C, Test conditions: C_o = 1000 ppmv COS/N_2, T= 20C, Particle Size = 100-200 microns.

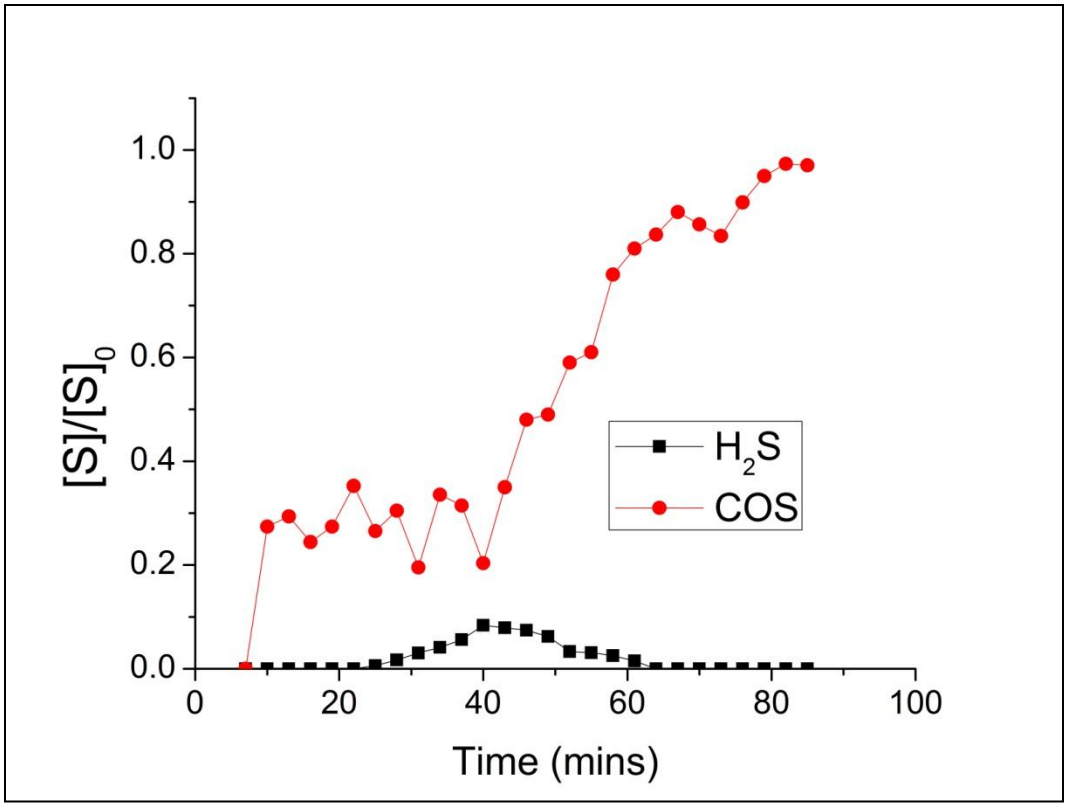

Figure VI.7. COS Hydrolysis for extended time on Al_2O_3/C. Test conditions: C_o = 1000 ppmv COS/N_2, T= 20C, Particle Size = 100-200 microns.

V.4. Conclusions

The removal of COS from the reformate streams via hydrolysis was the focus of this work. Promoted Carbon with alumina shows enhanced catalytic activity for conversion of COS at room temperature taking place via surface hydroxyl group. The Mn and Fe promoter cations significantly enhance the utilization of the ZnO active phase in reaction with H_2S of the novel sorbents Fe_x-Mn_y-$Zn_{1-x-y}O/SiO_2$ (x, y=0, 0.025), during desulfurization of the mixture of H_2S and H_2 at room temperature. The Mn- and Fe-promoted sorbents maintain a high sulfur uptake capacity upon the multiple cycles of a simple thermal oxidative regeneration of the "spent"

sorbent in air (up to 10 cycles). Thus, COS formation can be inhibited by restricting to low temperatures (T<250 C). Al_2O_3 based sorbents are good catalysts for COS hydrolysis at high temperature. COS formed at high temperatures (T=400C) by the presence of CO_2 and H_2S is taken care by the layered bed design.

Acknowledgement

The authors would like to thank the US Army (TARDEC Contract W56HZV-05-C-0686) for the financial support of this work. A.S. thanks Prof. Michael Bowman (Department of Chemistry of the University of Alabama at Tuscaloosa) for useful discussions.

Chapter VII: Conclusions and Recommendations for Future Work

VII.1. Conclusions

Conclusions for the work on sulfur removal using promoted ZnO/SiO_2 are presented at the end of the chapters (III-VI). An overview of all research activities conducted will be mentioned here. This study has led to development of novel materials, synthesis and analysis methods for effective sulfur removal over wide temperature range. Some of the notable achievements of this work are listed below:

1) Novel Cu promoted ZnO/MCM41 and MCM-48 (Mesoporous silica) was developed for H_2S removal over wide temperature range
2) The promoted ZnO/MCM-41 and ZnO/MCM-48 showed highest H_2S adsorption capacity at room temperature ever reported (~95% mol S/mol ZnO)
3) A study of effect of temperature, moisture content, metal oxide loading and support properties (surface area and pore volume) was performed
4) The composition of Cu promoted ZnO/SiO_2 was optimized (by varying Cu concentration 0-100%) $Cu_{0.2}ZnO_{0.8}/SiO_2$ showed highest H_2S adsorption capacity (~92% mol S/mol ZnO)
5) Novel Mn-Fe promoted ZnO/SiO_2 sorbent for removal of H_2S from the fuel reformate streams at ambient conditions developed

6) Characterization of the doped sorbents was carried out using XPS, XRD, ESR and N_2 adsorption and in-situ ESR studies to understand the role of the dopants
7) XRD suggests that both zinc and copper compounds of promoted ZnO/SiO_2 sorbents are nano-dispersed
8) The ESR spectroscopy found that the "calcined" and "sulfided" $CuO\text{-}ZnO/SiO_2$ sorbents contain Cu^{2+} in the single dispersion and coordination state. During H_2S adsorption, partial reduction of Cu^{2+} to Cu^{1+} occurs: the higher Cu concentration in the sorbent, the lower the reduction yield of Cu^{2+} to Cu^{1+} thus correlating with sulfur uptake capacity.
9) The "calcined" sorbent contains Fe^{3+} and Mn^{3+} ions, while upon H_2S adsorption, their reduction to Fe^{2+} and Mn^{2+} occurs. Fe^{3+} ions are believed to occupy the surface of the supported ZnO nanocrystallites, while Mn^{3+} ions are distributed uniformly within ZnO.
10) Thermal regeneration in air for the sorbent was established and use of promoted ZnO/SiO_2 over multiple regeneration cycles was demonstrated
11) The "deactivated" $Cu\text{-}ZnO/SiO_2$ sorbent (10-11 adsorption/regeneration cycles) is enriched with the different chemical form of Cu^{2+}, compared to the "as-prepared" sorbent.
12) The sorbents were scaled up (20g – 4kgs) and the batches showed consistency in the sulfur adsorption capacities
13) Formation of COS in the reformate streams was reported by understanding the thermodynamics of the reactions taking place
14) Methods to inhibit COS, removal COS and hydrolyze COS were demonstrated
15) COS can be inhibited by operating in the lower temperature regime in the fuel reformate streams

16) Activated Carbons can remove COS present in the fuel reformates at ambient conditions
17) FeO/Al_2O_3 catalyses hydrolysis of COS at higher temperatures (~400 C)
18) Novel Sorbent Al_2O_3/Carbon was developed to hydrolyze COS at ambient conditions
19) Room temperature hydrolysis and removal of sulfur (COS + H_2S) from fuel reformate streams was carried out using Al_2O_3/carbon and promoted ZnO/SiO_2 layered beds.

An effective desulfurization composition for fuel reformate streams was developed. Performance comparisons with other sorbents indicated high sulfur capacity. The sorbent composition was regenerable over multiple cycles. Characterization of these novel sorbents was studied. Routes to mitigate COS present/formed in the reformate streams were studied. Novel room temperature removal of gas phase sulfur (COS+H_2S) using layered beds of Al_2O_3/Carbon and $Mn_{0.025}Fe_{0.025}Zn_{0.95}O/SiO_2$ for COS hydrolysis and removal of H_2S respectively was demonstrated.

VII.2. Recommendations for Future Work

Scope of promoted ZnO/SiO_2

Most of the results in this study were focused on the fuel reformate gas compositions. It would be recommended to study if the sorbents work efficiently in different stream compositions like natural gas, syn-gas in the presence of different sulfur impurities like mercaptans, sulfides and aromatic sulfur to improve the scope of use of these sorbents.

Characterization of promoted ZnO/SiO_2

Although many characterization techniques were used to understand the exact role of the dopants in the ZnO/SiO_2, a clear picture of the mechanism is still not obtained. Use of some of the advanced techniques like EXAFS and Diffuse reflectance can help depict the defect structure of the ZnO/SiO_2 matrix. Because the dopant amount is significantly less, the techniques chosen should be highly sensitive.

Use of ESR and in-situ ESR has helped in more than many ways to realize the oxidations states of the Cu and Mn-Fe dopants because of its high sensitivity. Further studies might reveal more results.

Also use of chemisorption technique with an appropriate probe molecule should help know the dispersion and active surface area of the samples with and without dopants. This will give quantitative results change in crystallite size on addition of dopant. There is a speculation that addition of dopants adds defects into the structure and reduces the crystallite size hence leading to higher saturation capacities [64, 67, 158-162]. This can be verified using techniques like chemisorption.

Characterization of the Al_2O_3/Carbon sorbent is also essential to understand the mechanism of the hydrolysis of COS at room temperature. It is speculated that the surface hydroxyls[153] are the reason for this hydrolysis, but it is important to know the nature of the hydroxyls present, their role in hydrolysis, their concentration and thermal stability. Understanding these aspects would be important in order to develop a more stable and effective sorbent for COS hydrolysis.

References

1. Barbir, F. and S. Yazici, Status and development of PEM fuel cell technology. International Journal of Energy Research, 2008. 32(5): p. 369-378.

2. Barbir, F., PEM Fuel Cells: Theory and Practice: Elsevier Academic Press.

3. Song, C., An Overview of new approches to deep desulfurization or ultra-clean gasoline, diesel fuel and jet fuel. Catalysis Today, 2003. 86.

4. I.V. Babich, J.A.M., Science and Technology of novel processes for deep desulfurization of the oil refinery streams: a review. Fuel, 2003. 82.

5. Baird, T., Denny, P.J., Hoyle,R., McMonage, F., Stirling,D., Tweedy, J., Modified Zinc Oxide absorbents for Low-Temperature gas desulfurisation. J.Chem. Soc. Faraday Trans., 1992. 88(2).

6. Xue, M., et al., Screening of adsorbents for removal of H2S at room temperature. Green Chemistry, 2003. 5(5): p. 529-534.

7. Baird, T., et al., Modified Zinc-Oxide Absorbents for Low-Temperature Gas Desulfurization. Journal of the Chemical Society-Faraday Transactions, 1992. 88(22): p. 3375-3382.

8. Davidson, J.M., C.H. Lawrie, and K. Sohail, Kinetics of the Absorption of Hydrogen-Sulfide by High-Purity and Doped High-Surface-Area Zinc-Oxide. Industrial & Engineering Chemistry Research, 1995. 34(9): p. 2981-2989.

9. Yang, H.Y., et al., Breakthrough Characteristics of Reformate Desulfurization Using ZnO Sorbents for Logistic Fuel Cell Power Systems. Industrial & Engineering Chemistry Research, 2008. 47(24): p. 10064-10070.

10. Tatarchuk, B.J., Yang,H. and Dhage,P., Doped Zinc oxide sorbents for regenerable desulfurization applications US Patent WO 2008/137463 A2, 2008.

11. B.Tatarchuk, B.C., Y.Lu, L.Chen, E.Luna, D.Cahela, A. University, Editor. 2005: USA.

12. Sakanishi, K., et al., Simultaneous removal of H2S and COS using activated carbons and their supported catalysts. Catalysis Today, 2005. 104(1): p. 94-100.

13. Westermoreland P.R, H.D.P., Environmental Science and Technology, 1976. 10.

14. Watson, S., R. Kimmitt, and R.B. Rhinesmith, Study compares COS-removal processes. Oil & Gas Journal, 2003. 101(36): p. 66-+.

15. Husna Atakul, j.P.W., Albert W. Gerritsen and Pieter J.Van den Berg, Regeneration of MnO/Alumina used for high temperature desulfurization for fuel gases. Fuel, 1996. 75(3): p. 6.

16. Xuepeng Bu, Y.Y., Xuguo ji, and W.P. Cuiqing Zhang, New development of Zinc-based sorbents for hot gas desulfurization Fuel processing Technology 2007. 88: p. 5.

17. Yang, H.Y., D.R. Cahela, and B.J. Tatarchuk, A study of kinetic effects due to using microfibrous entrapped zinc oxide sorbents for hydrogen sulfide removal. Chemical Engineering Science, 2008. 63(10): p. 2707-2716.

18. Harris, D.K., D.R. Cahela, and B.J. Tatarchuk, Wet layup and sintering of metal-containing microfibrous composites for chemical processing opportunities. Composites Part a-Applied Science and Manufacturing, 2001. 32(8): p. 1117-1126.

19. Kalluri, R.R., D.R. Cahela, and B.J. Tatarchuk, Microfibrous entrapped small particle adsorbents for high efficiency heterogeneous contacting. Separation and Purification Technology, 2008. 62(2): p. 304-316.

20. Yang, H., Y. Lu, and B.J. Tatarchuk, Glass fiber entrapped sorbent for reformates desulfurization for logistic PEM fuel cell power systems. Journal of Power Sources, 2007. 174(1): p. 302-311.

21. Chang, B.K. and B.J. Tatarchuk, Microfibrous entrapment of small catalyst particulates for high contacting efficiency removal of trace CO from practical reformates for PEM H-2-O-2 fuel cells. Journal of Materials Engineering and Performance, 2006. 15(4): p. 453-456.

22. Chang, B.K., et al., Facile regeneration vitreous microfibrous entrapped supported ZnO sorbent with high contacting efficiency for bulk H2S removal from reformate streams in fuel cell applications. Journal of Materials Engineering and Performance, 2006. 15(4): p. 439-441.

23. Yang, H.Y., et al., Mass transfer study of hydrogen sulfide removal from reformats with microfiber entrapped ZnO/SiO2 sorbents for fuel cell application. Abstracts of Papers of the American Chemical Society, 2005. 230: p. U1655-U1656.

24. Lu, Y. and B.J. Tatarchuk, Microfibrous entrapped supported-ZNO sorbents with high contacting efficiency for trace H_2S removal in PEMFC applications. Abstracts of Papers of the American Chemical Society, 2003. 226: p. U48-U48.

25. Karanjikar, M.R., et al., Logistical fuel to hydrogen; An integrated processing approach augmented by microfibrous entrapped polishing catalysts and sorbents for PEM fuel cells. Abstracts of Papers of the American Chemical Society, 2004. 228: p. U683-U683.

26. Cahela, D.R. and B.J. Tatarchuk, Permeability of sintered microfibrous composites for heterogeneous catalysis and other chemical processing opportunities. Catalysis Today, 2001. 69(1-4): p. 33-39.

27. Twigg, M.V., Catayst Handbook Wolfe, London. 1989.

28. Ahn, S. and B.J. Tatarchuk, Fibrous metal-carbon composite structures as gas diffusion electrodes for use in alkaline electrolyte. Journal of Applied Electrochemistry, 1997. 27(1): p. 9-17.

29. Meffert, M.W., PhD Thesis, Auburn University. 1998.

30. Chang, B.K. and B.J. Tatarchuk, High contacting efficiency microfibrous entrapped PROX catalysts for reformate cleanup and PEM fuel cell applications. Abstracts of Papers of the American Chemical Society, 2004. 228: p. U686-U686.

31. Lu, Y., et al., Microfibrous entrapped ZnO-support sorbents for high contacting efficiency H2S removal from reformate streams in PEMFC applications. Microreactor Technology and Process Intensification, 2005. 914: p. 406-422.

32. M.A. Daley, C.L.M., J.A.D. Barr, S. Riha, A. Lizzio, G. Donnals, J. Economy, Adsorption of SO2 onto oxidized and heat treated activated carbon fibers (ACFs). Carbon, 1997. 35(3): p. 7.

33. M.N. Bae, M.K.S., Y. Kim, K. Seff, Crystal structure of Mn46Si100Al92O384. 89H2S, a hydrogen sulfide sorption complex of fully dehydrated Mn2þ-exchanged zeolite X. Microporous and Mesoporous Materials, 2003. 63: p. 10.

34. A. B. Bourlinos, M.A.K., and D. Petridis, Synthesis and Characterization of Iron-Containing MCM-41 Porous Silica by the Exchange Method of the Template. J. Phys. Chem. B, 2000. 104.

35. X-Y. Hao, Y.-Q.Z., J-W. Wang, W. Zhou, C. Zhang, S. Liu,, A novel approach to prepare MCM-41 supported CuO catalyst with high metal loading and dispersion. Microporous and Mesoporous Materials, 2005. 88(1-3).

36. Huang, H.Y., et al., Amine-grafted MCM-48 and silica xerogel as superior sorbents for acidic gas removal from natural gas. Industrial & Engineering Chemistry Research, 2003. 42(12): p. 2427-2433.

37. Xiaochun Xu, C.S., , Bruce G. Miller and Alan W. Scaroni, Adsorption separation of carbon dioxide from flue gas of natural gas-fired boiler by a novel nanoporous "molecular basket" adsorbent. Fuel Processing Technology, 2005. 86(14-15).

38. A. Corma, A.M.a.V.M.-S., Hydrogenation of Aromatics in Diesel Fuels on Pt/MCM-41 Catalysts. journal of Catalysis. 169(2).

39. Reddy, C.S.a.K.M., Mesoporous molecular sieve MCM-41 supported Co–Mo catalyst for hydrodesulfurization of dibenzothiophene in distillate fuels Applied Catalysis A: General, 1999. 176(1).

40. F. Schüth, A. Wingen and J. Sauer, Oxide loaded ordered mesoporous oxides for catalytic applications. Microporous and Mesoporous Materials, 2001. 44-45: p. 465-476.

41. Xiu S. Zhao, G.Q.M.L., and Graeme J. Millar, Advances in Mesoporous Molecular Sieve MCM-41. industrial & Engineering Chemistry Research, 1996. 35(7).

42. Pelrine B, P., Schmitt, K. D., Vartuli, J.C., Production of olefin oligomer. 1992.

43. Souza, M.J.B., et al., HDS of thiophene over CoMo/AlMCM-41 with different Si/Al ratios. Applied Catalysis a-General, 2007. 316(2): p. 212-218.

44. Kloetstra, K.R. and H. Vanbekkum, Base and Acid Catalysis by the Alkali-Containing Mcm-41 Mesoporous Molecular-Sieve. Journal of the Chemical Society-Chemical Communications, 1995(10): p. 1005-1006.

45. Kloetstra, K.R. and H. Vanbekkum, Catalysis of the Tetrahydropyranylation of Alcohols and Phenols by the H-Mcm-41 Mesoporous Molecular-Sieve. Journal of Chemical Research-S, 1995(1): p. 26-27.

46. Tanev, P.T., M. Chibwe, and T.J. Pinnavaia, Titanium-Containing Mesoporous Molecular-Sieves for Catalytic-Oxidation of Aromatic-Compounds. Nature, 1994. 368(6469): p. 321-323.

47. J. S. Beck, J.C.V., W. J. Roth, M. E. Leonowicz, C. T. Kresge, K. D. Schmitt, C. T. W. Chu, D. H. Olson, E. W. Sheppard, A new family of mesoporous molecular sieves prepared with liquid crystal templates. J. Am. Chem. Soc, 1992. 114(27).

48. Hao, X.Y., et al., A novel approach to prepare MCM-41 supported CuO catalyst with high metal loading and dispersion. Microporous and Mesoporous Materials, 2006. 88(1-3): p. 38-47.

49. Ozaydin, Z., S. Yasyerli, and G. Dogu, Synthesis and activity comparison of copper-incorporated MCM-41-type sorbents prepared by one-pot and impregnation procedures for H2S removal. Industrial & Engineering Chemistry Research, 2008. 47(4): p. 1035-1042.

50. Wingen, A., et al., Fe-MCM-41 as a catalyst for sulfur dioxide oxidation in highly concentrated gases. Journal of Catalysis, 2000. 193(2): p. 248-254.

51. Gac, W., et al., The influence of the preparation methods and pretreatment conditions on the properties of Ag-MCM-41 catalysts. Journal of Molecular Catalysis a-Chemical, 2007. 268(1-2): p. 15-23.

52. Lu, W.J., et al., A novel preparation method of ZnO/MCM-41 for hydrogenation of methyl benzoate. Journal of Molecular Catalysis a-Chemical, 2002. 188(1-2): p. 225-231.

53. Haber J., B.H.a.D.B., Manual of methods and procedures for catalyst characterization. Pure and applied Chemistry, 1995. 67.

54. Ilaria Rosso, C.G., Massimo Bizzi, Guido Saracco, and Vito Specchia, Zinc oxide sorbents for the removal of hydrogen sulfide from syngas. Industrial & Engineering Chemistry Research, 2003. 42.

55. Israelson, G., Results of testing various natural gas desulfurization sorbents Journal of Materials Engineering and Performance, 2007. 13(3).

56. P.Dhage, V.G., H.Yang and B. Tatarchuk Wide Temperature Range H2S Removal from Fuel Reformate streams using MCM-41 and MCM-48. Microporous and Mesoporous Materials, In Press.

57. Dhage, P., et al., Copper-Promoted ZnO/SiO2 Regenerable Sorbents for the Room Temperature Removal of H2S from Reformate Gas Streams. Industrial & Engineering Chemistry Research, 2010. 49(18): p. 8388-8396.

58. Dhage, P., et al., Regenerable Fe-Mn-ZnO/SiO2 sorbents for room temperature removal of H2S from fuel reformates: performance, active sites, Operando studies. Physical Chemistry Chemical Physics, 2011. 13(6): p. 2179-2187.

59. P.Dhage, H.Y.a.B.T., RT Hydrolysis and Removal of COS from Fuel Reformate Streams using Al_2O_3/Carbon+Fmn0.025Fe0.025Zn0.95O/SiO2 Layered Beds. In Press.

60. K. Schumacher, P.I.R., A.D. Chesne, A.V. Neimark, K.K. Unger, Characterization of MCM-48 Materials. Langmuir, 2000. 16(10).

61. James Larminie , A.D., Fuel cell systems explained. 2003.

62. Li, L.a.K., D., H2S Removal with ZnO during fuel Processing for PEM fuel cell applications. Catalysis Today, 2006. 116.

63. Song, C., Fuel processing for low-temperature and high-temeperature fuel cells Challenges and opportunitiesfor sustainable development in the 21st century. Catalysis Today, 2002. 77.

64. Baird, T., et al., Cobalt-zinc oxide absorbents for low temperature gas desulfurisation. Journal of Materials Chemistry, 1999. 9(2): p. 599-605.

65. Polychronopoulou, K., et al., Novel Fe-Mn-Zn-Ti-O mixed-metal oxides for the low-temperature removal of H2S from gas streams in the presence of H-2, CO2, and H2O. Journal of Catalysis, 2005. 236(2): p. 205-220.

66. Laperdrix, E., et al., Selective oxidation of H2S over CuO/Al2O3: Identification and role of the sulfurated species formed on the catalyst during the reaction. Journal of Catalysis, 2000. 189(1): p. 63-69.

67. Sasaoka, E., et al., Characterization of Reaction between Zinc-Oxide and Hydrogen-Sulfide. Energy & Fuels, 1994. 8(5): p. 1100-1105.

68. Quanchang Li, S.E.B., Linda J. Broadbelt, Jian-Guo Zheng and N. Q. Wu, Synthesis and characterization of MCM-41-supported Ba2SiO4 base catalyst. Microporous and Mesoporous Materials, 2003. 59(2-3).

69. Jae Wook Lee, D.L.C., Wang Geun Shim, and Hee Moon, Application of mesoporous MCM-48 and SBA-15 materials for the separation of biochemicals dissolved in aqueous solution. Korean Journal of Chemical Engineering, 2003. 21(1).

70. Klotz, I.M., The Adsorption Wave. Chemical Reviews, 1946. 39(2): p. 241-268.

71. Wheeler, A. and A.J. Robell, Performance of Fixed-Bed Catalytic Reactors with Poison in Feed. Journal of Catalysis, 1969. 13(3): p. 299-&.

72. Yoon, Y.H. and J.H. Nelson, Application of Gas-Adsorption Kinetics .1. A Theoretical-Model for Respirator Cartridge Service Life. American Industrial Hygiene Association Journal, 1984. 45(8): p. 509-516.

73. Amundson, N.R., A Note on the Mathematics of Adsorption in Beds. Journal of Physical and Colloid Chemistry, 1948. 52(7): p. 1153-1157.

74. A. Erzos, H. Olgun, and S. Ozdogan, Reforming Options for Hydrogen Production from Fossil Fuels for PEM Fuel Cells. J. Power Sources, 2006(154): p. 67.

75. A. Erzos, et al., Autothermal Reforming as a Hydrocarbon Fuel Processing Option for PEM Fuel Cell. Journal of Power Sources, 2003. 118: p. 384-392.

76. I. I. Novochinskii, et al., Low Temperature H2S Removal from Steam-Containing Gas Mixtures with ZnO for Fuel Cell Application. 1. ZnO Particles and Extrudates. Energy Fuels, 2004. 18: p. 576.

77. Y. Lu, et al. Microfibrous Entrapped ZnO-Supported Sorbent for High Contacting Efficiency H2S Removal from Reformate Streams in PEMFC Applications. in ACS Symposium Series 914. 2005. Washington, DC: American Chemical Society.

78. L. Alonso, et al., Characterization of Mn and Cu oxides as regenerable sorbents for hot coal gas desulfurization. Fuel Processing Technology, 2000. 62: p. 31-44.

79. J.H. Swisher and K. Schwerdtfeger, Review of metals and binary oxides as sorbents for removing sulfur from coal-derived gases. J. Mater. Eng. Perform., 1992. 1: p. 399.

80. E. Garcıa, et al., Thermogravimetric study of regenerable sulphur sorbents for H2S retention at high temperature. Thermochim. Acta, 1997. 306: p. 23.

81. R.V. Siriwardane and J. Poston, Characterization of copper oxides, iron oxides and zinc copper ferrite desulfurization sorbents by X-ray photoelectron spectroscopy and scanning electron microscopy. Appl. Surf. Sci., 1993. 68: p. 65.

82. S.S. Tamhankar, M. Bagajewicz, and G.R. Gavalas, Mixed-oxide sorbents for high-temperature of hydrogen sulfide. Ind. Eng. Chem. Process Des. Dev., 1986. 25: p. 429.

83. Z. Li and M. Flytzani-Stephanopoulos, Cu–Cr–O and Cu–Ce–O regenerable sorbents for hot gas desulfurization. Ind. Eng. Chem. Res., 1997. 36: p. 187.

84. E. Giamello, B. Fubini, and P. Lauro, Investigation of the State of Copper in Copper-Zinc Oxice Biphasic Catalyst by EPR and Adsorption Microcalorimetry. Applied Catalysis, 1986. 21: p. 133-147.

85. H.Y. Chen, et al., Synergism between Cu and Zn sites in Cu/Zn catalysts for methanol synthesis. Applied Surface Science, 1999. 152: p. 193-199.

86. Z. Wang, W. Wang, and G. Li, Studies on the active species and on dispersion of Cu in Cu/SiO2 and Cu/Zn/SiO2 for hydrogen production via methanol partial oxidation. International Journal of Hydrogen Energy, 2003. 28: p. 151-158.

87. J.-D. Grunwaldt, et al., In Situ Investigations of structural changes in Cu/ZnO Catalysts. Journal of Catalysis, 2000. 194: p. 452-460.

88. Isao Nakamura, et al., Role of oxygen vacancy in the plasma-treated TiO2 photocatalyst with visible light activity for NO removal. Journal of Molecular Catalysis A: Chemical, 2000. 161: p. 205–212.

89. B.J. Tatarchuk, H. Yang, and P. Dhage, Doped zinc oxide sorbents for regenerable desulfurization applications. US Patent WO 2008/137463 A2, 2008.

90. H. Yang, et al., Breakthrough Characteristics of Reformate Desulfurization Using ZnO Sorbents for Logistic Fuel Cell Power Systems. Ind. Eng. Chem. Res., 2008. 47: p. 10064–10070.

91. H. Yang, Y. Lu, and B.J. Tatarchuk, Glass fiber entrapped sorbent for reformates desulfurization for logistic PEM fuel cell power systems. Journal of Power Sources, 2007. 174(1): p. 302-311.

92. Y. Lu, et al., Microfibrous entrapped ZnO-support sorbents for high contacting efficiency H2S removal from reformate streams in PEMFC applications. Microreactor Technology and Process Intensification, 2005. 914: p. 406-422.

93. J. H. Zeng, et al., Precursor, base concentration and solvent behavior on the formation of zinc silicate. Materials Research Bulletin, 2009. 44: p. 1106–1110.

94. J.A. Lercher, H. Vinek, and H. Noller, TiO2/ZnO mixed oxide catalyst, characterization by X-ray photoelectron and infrared spectroscopy and reactions with propanol and butanol. Appl. Cat., 1984. 12: p. 293-307.

95. Md Nurul Islam, et al., XPS and X-ray diffraction studies of aluminum-doped zinc oxide transparent conducting films. Thin Solid Films, 1996. 280: p. 20-25.

96. D. Briggs and J.T. Grant, Surface Analysis by Auger and Electron Spectroscopy. 2003, Trowbridge: IM Publications and SurfaceSpectra Ltd.

97. Zhengping Fu, et al., An intense ultraviolet photoluminescence in sol–gel ZnO–SiO2 nanocomposites. J. Phys.: Condens. Matter, 2003. 15: p. 2867–2873.

98. S. Takeda and M. Fukawa, Surface OH groups governing surface chemical properties of SiO2 thin films deposited by RF magnetron sputtering. Thin Solid Films, 2003. 444: p. 153-157.

99. A. Bensalem, et al., Preparation and characterization of highly dispersed silica-supported ceria. Applied Catalysis A: General, 1995. 121: p. 81-93.

100. S. K. Nandi, et al., Structural and optical properties of ZnO films grown on silicon and their applications in MOS devices in conjunction with ZrO2 as a gate dielectric. Bull. Mater. Sci., 2007. 30(3): p. 247-254.

101. S. Contarini and L. Kevan, X-ray Photoelectron Spectroscopic Study of Copper-Exchanged X- and Y-Type Sodium Zeolites: Resolution of Two Cupric Ion Components and Dependence on Dehydration and X-Irradiation. J. Phys. Chem., 1986. 90(8): p. 1630-1632.

102. R. Schlesinger, H. Klewe-Nebenius, and M. Bruns, Characterization of Artificially Produced Copper and Bronze Patina by XPS. Surf. Interface Anal., 2000. 30: p. 135-139.

103. Handbook of Surface and Interface Analysis: Methods for Problem-Solving, ed. J. C. Riviere and S. Myhra. 1998, New York: Marcel Dekker, Inc.

104. J.W.L. Wong, et al., XPS studies of Auger parameter shift of ZnS Te alloys. Journal of Electron Spectroscopy and Related Phenomena, 2001. 113: p. 215–220.

105. Corrosion of Electronic and Magnetic Materials, ed. P.J. Peterson. 1992, Philadelphia: American Society for Testing and Materials.

106. Brion, D., Study by photoelectron-spectroscopy of surface degradation of FeS2, CuFeS2, ZnS and PbS exposed to air and water. Appl. Surf. Sci., 1980. 5: p. 133-152.

107. D.L. Perry and J.A. Taylor, X-Ray photoelectron and Auger spectroscopic studies of Cu_2S and CuS. Journal of Materials Science Letters, 1986. 5: p. 384-386.

108. J.-S. Yu and L. Kevan, Cu(II)-Adsorbate Interactions in Cu(II)-Exchanged K-L Zeolite. J. Phys. Chem., 1994. 98: p. 12436-12441.

109. M.G. Kalchev, A.A. Andreev, and N.S. Zotov, Water-Gas Shift Reaction on CuO-ZnO Catalysts. I. Structure and Catalytic Activity. Kinetics and Catalysis, 1995. 36(6): p. 821-827.

110. R.T. Figueriedo, et al., Spectroscopic Evidence of Cu-Al Interactions in Cu-Zn-Al Mixed Oxide Catalysts Used in CO Hydrogenation. Journal of Catalysis, 1998. 178: p. 146-152.

111. A. Martinez-Arias, et al., Effect of Copper-Ceria Interactions on Copper Reduction in a $Cu/CeO_2/Al_2O_3$ Catalyst Subjected to Thermal Treatments in CO. J. Phys. Chem. B, 1998. 102: p. 809-817.

112. Surface Chemistry and Physics, ed. A. F. Carley, et al. 2002, New York: Kluwer Academic/Plenum Publishers.

113. A. L. Yakovlev, et al., DFT Study of oxygen-bridged Zn2+ ion pairs in Zn/ZSM-5 zeolites. Catalysis Letters, 2000. 70: p. 175-181.

114. K. Hashimot and N. Toukai, Methanol decomposition over copper particles incorporated in the interlayer regions of zinc aluminum silicate hydroxide. Journal of Molecular Catalysis: A, 2002. 186: p. 79-88.

115. Kolosov, ESR Study of Adsorption of Hydrogen-sulfide, Propanethiol, and Thiophene on Molybdenum Oxide and Sulfide Deposited on Silica-gel. Kinetics and Catalysis, 1975. 16(1): p. 161-164.

116. A. A. Spozhakina, et al., The Interaction of Hydrogen Sulfide with Silica-Supported Phosphorus-Molybdenum Heteropolyacid. Kinetics and Catalysis, 1993. 34(6): p. 976-979.

117. L. Trouillet, et al., In situ characterization of the coordination sphere of Cu(II) complexes supported on silica during the preparation of Cu/SiO2 catalysts by cation exchange. Phys. Chem. Chem. Phys., 2000. 2: p. 2005-2014.

118. Sangho Yoon, et al., Self-sustained operation of a kWe-class kerosene-reforming processor for solid oxide fuel cells. Journal of Power Sources, 2009. 192: p. 360-366.

119. Loredana Magistri, et al., Design and Off-Design Analysis of a MW Hybrid System Based on Rolls-Royce Integrated Planar Solid Oxide Fuel Cells. Transactions of the ASME, 2007. 129: p. 792-797.

120. Song, C., Fuel Processing for Low-temperature and High-temperature Fuel Cells: Challenges, and Opportunities for Sustainable Development in the 21st Century. Catal. Today, 2002. 77(1-2): p. 17-49.

121. Ke Liu, Chushan Song, and V. Subramani, Hydrogen and Syngas Production and Purification Technologies. 2010, Hoboken, NJ: John Wiley & Sons, Inc. 545.

122. Lee D. Gasper-Galvin, Aysel T. Atimtay, and R.P. Gupta, Zeolite-Supported Metal Oxide Sorbents for Hot-Gas Desulfurization. Ind. Eng. Chem. Res., 1998. 37: p. 4157-4166.

123. Singfoong Cheah, Daniel L. Carpenter, and K.A. Magrini-Bair, Review of Mid- to High-Temperature Sulfur Sorbents for Desulfurization of Biomass- and Coal-derived Syngas. Energy Fuels, 2009. 23(11): p. 5291–5307.

124. P. R. Westmoreland and D.P. Harrison, Evaluation of Candidate Solids for High-Temperature Desulfurization of Low Btu Gases. Environ. Sci. Technol., 1976. 10: p. 659.

125. J. H. Swisher and K. Schwerdtfeger, Thermodynamic Analysis of Sorption Reactions for the Removal of Sulfur from Hot Gases. J. Mater. Eng. Perform., 1992. 1(4): p. 565-571.

126. J.H. Swisher and K. Schwerdtfeger, Review of Metals and Binary Oxides as Sorbents for Removing Sulfur from Coal-Derived Gases. Journal of Materials Engineering and Performance, 1992. 1(3): p. 399-407.

127. K. Polychronopoulou, et al., Novel Fe–Mn–Zn–Ti–O mixed-metal oxides for the low-temperature removal of H2S from gas streams in the presence of H2, CO2, and H2O. Journal of Catalysis, 2005. 236: p. 205–220.

128. K. Polychronopoulou, J.L.G. Fierro, and A.M. Efstathiou, Novel Zn–Ti-based mixed metal oxides for low-temperature adsorption of H2S from industrial gas streams. Applied Catalysis B: Environmental, 2005. 57: p. 125-137.

129. Kyriaki Polychronopoulou and A.M. Efstathiou, Effects of Sol-Gel Synthesis on 5Fe-15Mn-40Zn-40Ti-O Mixed Oxide Structure and its H2S Removal Efficiency from Industrial Gas Streams. Environ. Sci. Technol., 2009. 43: p. 4367-4372.

130. Sam Bergh, et al., Gas phase oxidation of ethane to acetic acid using high-throughput screening in a massively parallel microfluidic reactor system. Appl. Catal. A: General, 2003. 254: p. 67-76.

131. Mario Chiesa, Elio Giamello, and M. Che, EPR Characterization and Reactivity of Surface-Localized Inorganic Radicals and Radical Ions. Chem. Rev., 2010. 110: p. 1310-1347.

132. U.J. Katter, et al., Electron Spin-Resonance (ESR) Studies of Adsorbate Dynamics on Single Crustal Surfaces: Possibilities and Limitations. Ber. Bunsenges. Phys. Chem., 1993. 97(3): p. 341-353.

133. Venezia, A.M., X-ray photoelectron spectroscopy (XPS) for catalysts characterization. Catalysis Today, 2003. 77: p. 359–370.

134. Thomas Baird, et al., Modified Zinc Oxide Absorbents for Low-temperature Gas Desulf ur isat ion. J. Chem. Soc. Faraday Trans., 1992. 88(22): p. 3375-3382.

135. No-Kuk Park, et al., The preparation of a high surface area metal oxide prepared by a matrix-assisted method for hot gas desulphurization. Fuel Processing Technology, 2005. 84: p. 2165-2171.

136. Corrie L. Carnes and K.J. Klabunde, Unique Chemical Reactivities of Nanocrystalline Metal Oxides toward Hydrogen Sulfide. Chem. Mater., 2002. 14: p. 1806-1811.

137. Yi-Keun Song, et al., Reactivity of Copper Oxide-Based Sorbent in Coal Gas Desulfurization. Korean J. Chem. Eng., 2000. 17(6): p. 691-695.

138. Si Ok Ryu, et al., Multicyclic Study on Improved Zn/Ti-Based Desulfurization Sorbents in Mid-Temperature Conditions. Ind. Eng. Chem. Res., 2004. 43: p. 1466-1471.

139. Zhao-Tie Liu, et al., XPS Study of Iron Catalysts for Fischer-Tropsch Synthesis. Fuel Science and Technology Int'l., 1995. 13(5): p. 559-567.

140. Scofield, J.H., Hartree-Slater Subshell Photoionization Cross-Sections at 1254 and 1487 eV. Journal of Electron Spectroscopy and Related Phenomena, 1976. 8: p. 129-137.

141. Maasaki Yanagisawa, et al., Discoloration of Alumina Ceramics with Ultraviolet Radiation and Elucidation of its Mechanism. Journal of the Ceramic Society of Japan. 101(10): p. 1189-1191.

142. Reinhard Stoesser, et al., A Magnetic Resonance Investigation of the Process of Corundum Formation Starting from Sol-Gel Precursors. J. Amer. Ceram. Soc., 2005. 88(10): p. 2913-2922.

143. El-M. El-Malki, R. A. van Santen, and W.M.H. Sachtler, Introduction of Zn, Ga, and Fe into HZSM-5 Cavities by Sublimation: Identification of Acid Sites. J. Phys. Chem. B, 1999. 103(22): p. 4611–4622.

144. Blake J. Aronson, Christopher F. Blanford, and A. Stein, Synthesis, Characterization, and Ion-Exchange Properties of Zinc and Magnesium Manganese Oxides Confined within MCM-41 Channels. J. Phys. Chem. B, 2000. 104: p. 449-459.

145. W. Sjoerd Kijlstra, et al., Characterization of Al2O3-Supported Manganese Oxides by Electron Spin Resonance and Diffuse Reflectance Spectroscopy. J. Phys. Chem. B, 1997. 101: p. 309-316.

146. J. J. Villafranca, et al., Metal-Metal Interactions in Enzymes: EPR and NMR Investigations. Inorganica Chimica Acta, 1983. 79: p. 18.

147. Colin Rhodes, S.A.R., John West , B. Peter Williams , Graham J. Hutchings, The low-temperature hydrolysis of carbonyl sulfide

and carbon disulfide: a review. Catalysis Today, 2000. 59.

148. Hasler, P. and T. Nussbaumer, Gas cleaning for IC engine applications from fixed bed biomass gasification. Biomass and Bioenergy, 1999. 16(6): p. 385-395.

149. Bruno, P.D.N.S.a.T.J., Carbonyl Sulfide: A Review of Its Chemistry and Properties. Industrial & Engineering Chemistry Research, 2002. 41(22).

150. Liu, Z.-T., et al., Deactivation model of Fischer-Tropsch synthesis over an FeCuK commercial catalyst. Applied Catalysis A: General, 1997. 161(1-2): p. 137-151.

151. John D. Sherman, A.T.K., Suppression of COS formation in Molecular sieve purification of hydrocarbon gas streams. 1982, Union Carbide Corporation, Danbury , Conn. : United States.

152. Li, W., W. Shudong, and Y. Quan, Removal of carbonyl sulfide at low temperature: Experiment and modeling. Fuel processing Technology, 2010. 91(7): p. 777-782.

153. Li, W., W. Shudong, and Y. Quan, Removal of carbonyl sulfide at low temperature: Experiment and modeling. Fuel processing Technology, 2010 91(7): p. 777-782.

154. Williams, B.P., et al., Carbonyl sulphide hydrolysis using alumina catalysts. Catalysis Today, 1999. 49(1-3): p. 99-104.

155. West, J., et al., Ni- and Zn-promotion of [gamma]-Al2O3 for the hydrolysis of COS under mild conditions. Catalysis Communications, 2001. 2(3-4): p. 135-138.

156. Shishao, T., et al., Compensation effect in catalytic hydrolysis of carbonyl sulfide at lower temperature compensation effect in COS hydrolysis. Catalysis Letters, 1991. 8(2): p. 155-167.

157. Miura, K., et al., Simultaneous removal of carbonyl sulfide and hydrogen sulfide from coke oven gas at low temperature by iron oxide. Industrial & Engineering Chemistry Research, 1992. 31(1): p. 415-419.

158. Baird, T., et al., Mixed cobalt-iron oxide absorbents for low-temperature gas desulfurisation. Journal of Materials Chemistry, 2003. 13(9): p. 2341-2347.

159. Baird, T., et al., Structural and morphological studies of iron sulfide. Journal of the Chemical Society-Faraday Transactions, 1996. 92(3): p. 445-450.

160. Baird, T., et al., Characterisation of cobalt-zinc hydroxycarbonates and their products of decomposition. Journal of Materials Chemistry, 1997. 7(2): p. 319-330.

161. Baird, T., et al., Mixed Co-Zn-Al Oxides as Absorbents for Law-Temperature Gas Desulfurization. Journal of the Chemical Society-Faraday Transactions, 1995. 91(18): p. 3219-3230.

162. Baird, T., Characterization of Carbons Formed on Nickel Surfaces. Fuel, 1984. 63(8): p. 1081-1088.

Appendix I – Calculation formulae

Calculation of breakthrough capacity, saturation capacity and % theoretical capacity

1. **<u>Breakthrough capacity:</u>** Breakthrough is taken as 2% of C_O

$$= \frac{\left(volumetric flow rate of H_2S \left(\frac{m^3}{\min} \right) \times \left(\frac{P}{RT} \right) \left(\frac{mol}{m^3} \right) \times breakthrough time (\min) \times 32 \left(\frac{gmS}{mol} \right) \times 10^3 mg \right)}{Wt.sorbent\,(gm)}$$

2. **<u>Saturation Capacity:</u>**

The nature of the curve decides the method that can be used to calculate saturation capacity. In this work, we use the **$t_{1/2}$ method** since the breakthrough curves look very sharp and S-shaped. The time at which the C/C_o =0.5 is taken as $t_{1/2}$.

$$= \frac{\left(volumetric flow rate of H_2S \left(\frac{m^3}{\min} \right) \times \left(\frac{P}{RT} \right) \left(\frac{mol}{m^3} \right) \times t_{1/2} (\min) \times 32 \left(\frac{gmS}{mol} \right) \times 10^3 mg \right)}{Wt.sorbent\,(gm)}$$

3. % of Theoretical capacity:

The theoretical capacity for ZnO is ~ 392 g S/g sorbent. The % with the saturation capacity obtained is known as the % of theoretical capacity.

4. ZnO utilization:

$$= \frac{\left(volumetric flow rate of H_2S \left(\frac{m^3}{\min} \right) \times \left(\frac{P}{RT} \right) \left(\frac{mol}{m^3} \right) \times t_{1/2}(\min) \times 81 \left(\frac{gm ZnO}{mol} \right) \times 10^3 mg \right)}{Wt.sorbent\,(gm) \times ZnO loading\,(\%)}$$

Appendix II – GC Chromatography Analytic Methods

a. TCD Analysis Method

- Gas Chromatography Model — Varian CP3800
- Column type Packed Column — HayeSep Q, 80/100 8'× 1/8" SS
- Column Stabilization time — 2.00 min
- Oven Temperature — 80^{o}C
- Injector Temperature — 80^{o}C
- Detector Temperature — 175 ^{o}C
- Filament Temperature — 375 ^{o}C
- Carrier Gas — H_2
- Carrier Gas Flow Rate — 60mL/min
- 6 –port valve is switched to "inject" mode at the beginning of every minute and switched back to "fill" mode 2 seconds after injection

b. PFPD Analysis Method

- Gas Chromatography Model — Varian CP3800
- Column — Restek XTI (30mm×0.25mm×0.5μm)
- Oven Temperature Program: 60 ^{o}C for 1 min, Ramp to 90 ^{o}C at the rate of 20 ^{o}C/min and stay at 90 ^{o}C for 3.5 min. Total runtime is 6 minutes.
- Injector Temperature — 80^{o}C
- Capillary Flow Rate — 1.2 ^{o}C
- Air Flow Rate — 17 cm^3/min
- H_2 Flow Rate — 13 cm^3/min
- Split Ratio — 200
- Tube Voltage — 510 V
- Trigger level — 200 mA
- Sample Delay — 4 ms
- Sample Width — 10 ms
- Gain Factor — 2
- Syringe Size — 250 μL

Appendix III – Calibration of Gases

a. Carbon Dioxide

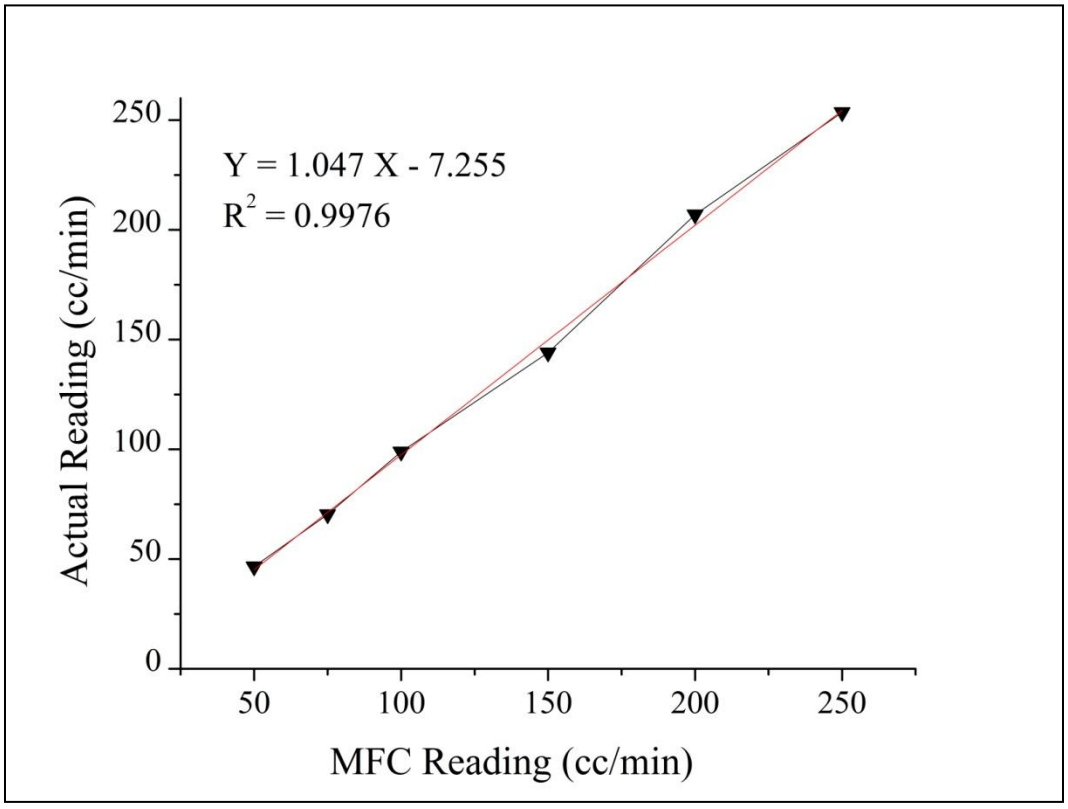

b. Nitrogen

= 0.9997

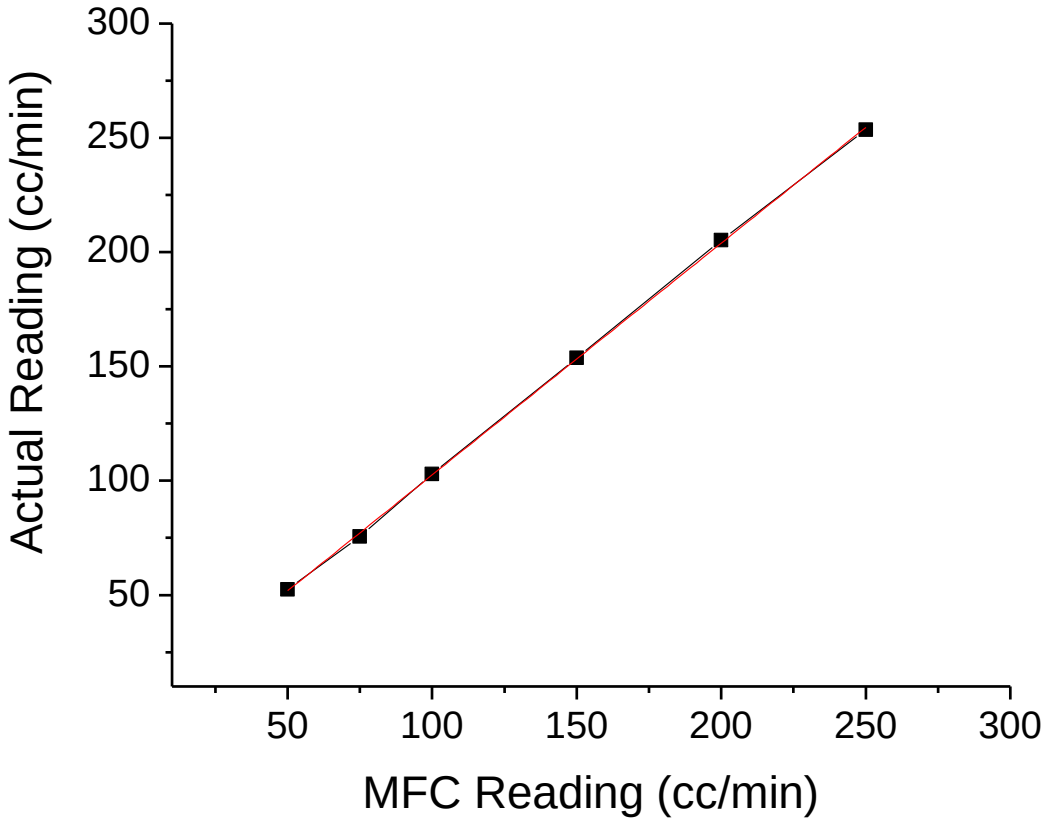

c. Carbon Monoxide

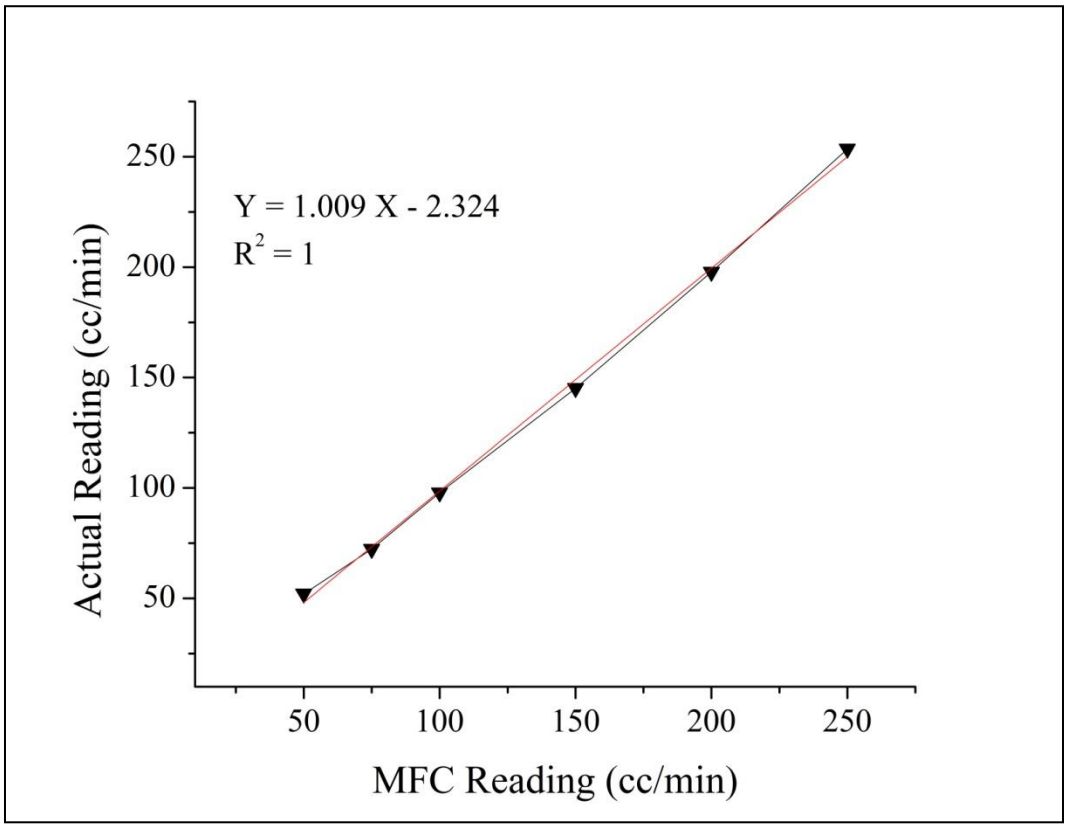

d. Hydrogen Sulfide

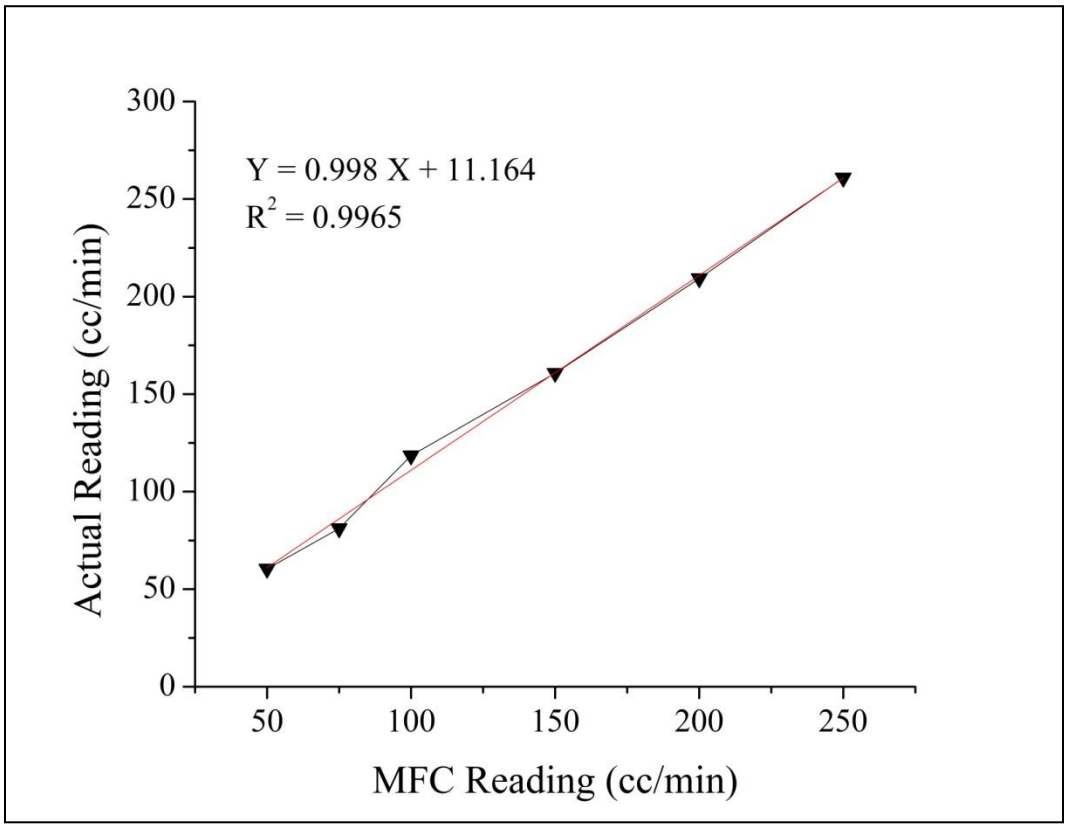

e. Carbonyl Sulfide

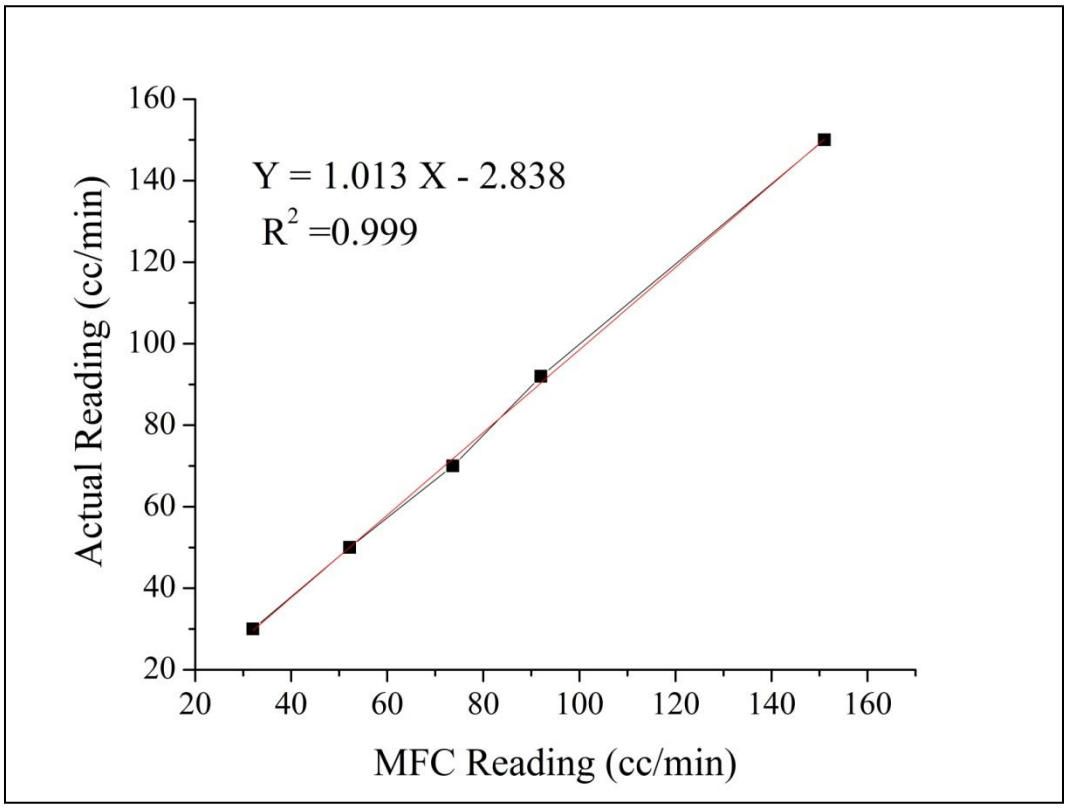

f. Furnace

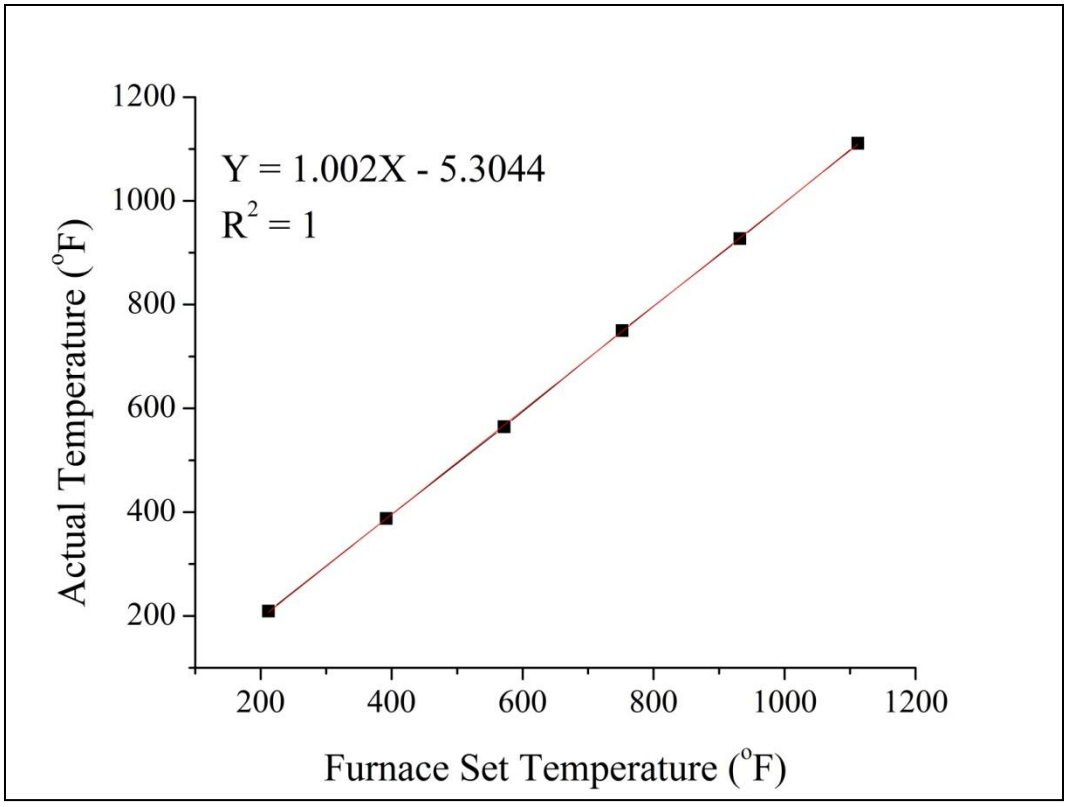
Y = 1.002X - 5.3044
R2 = 1
Actual Temperature (°F)
Furnace Set Temperature (°F)
200
400
600
800
1000
1200

Appendix IV – Inventory of Chemicals used

Chemical	**Vendor/Company**
Act.Carbon Centaur HSL	Calgon Carbon Corporation
Act.Carbon Minotaur OC	Calgon Carbon Corporation
Act.Carbon Centaur 4 x 6	Calgon Carbon Corporation
Act.Carbon BPL 4 x 6	Calgon Carbon Corporation
Selexsorb COS	BASF
ZnO SG9201	BASF
$Cr(NO_3)_3$	Aldrich
$Zn(NO_3)_2.6H_2O$	Aldrich
$Ni(NO_3)_2$	Aldrich
ZnO	Alfa
$Ag(NO_3)_2$	Alfa
$Fe(NO_3)_3.9H_2O$	Alfa
$Zn(NO_3)_2.6H_2O$	Fluka
$Cu(NO_3)_2.3H_2O$	Fluka
$Cs(NO_3)$	Alfa

$Fe(NO_3)_3.9H_2O$	Aldrich
$Zn(NO_3)_2.6H_2O$	Fischer
$Cu(NO_3)_2.3H_2O$	Fischer
$Mg(NO_3)_2.xH_2O$	Fischer
$Mn(NO_3)_2.xH_2O$	Adrich
$Cu(NO_3)_2.2.5H_2O$	Aldrich
$Al_2(NO_3)_3$	Aldrich
$Fe(NO_3)_3$	Aldrich
$ZrO(NO_3)_2.xH_2O$	Aldrich
$Ni(NO_3)_3$	Aldrich
$Cd(NO_3)_3$	Aldrich
$Ce(NO_3)_3$	Fluka /Alfa
$Co(NO_3)_2$	Aldrich
Mol. Sieves	Strem Chemicals
NaY Zeolite	Strem Chemicals/ Grace Davison
SiO_2 Grade 10181	Aldrich
Act. Al_2O_3	Aldrich
Silica 60A	Alfa
TiO_2	Alfa/Saint Gobain
Silica Grade 10184	Sigma
Silica	Strem Chemicals
Silica	Alfa
Zeolite	Zeolyst

Silica Grade 40	Aldrich
Mol. Sieves 13X	Aldrich
Silica 126724	Fischer
Selexorb CDX	BASF
PICA Carbon	PICA
Cu-ZnO Actisorb	Sud-Chemie
Silica	Grace Davison
TEOS	Aldrich
Mol. Sieves 3A	Aldrich
Mol. Sieves 4A	Aldrich
Mol. Sieves 5A	Aldrich
Glass Beads	Fischer – 11-312D 4mm